SWITCH

Sixth Framework Programme (2002-2006)

018530 - SWITCH

Sustainable Water Management in the City of the Future

Integrated Project

Global Change and Ecosystems

Deliverable reference number and title

D3.3.1–D3.3.6 EF–SF–UF–CW RESEARCH:

D3.3.1 Complete and ready EF–CW system

D3.3.2, D3.3.3 EF-SF study report. CW maturation report

D3.3.4, 3.3.5 EF–UF Study Report

D3.3.6 EF–SF–CW and EF–UF–CW configurations study reports.

Due date of deliverable: M60

Actual submission date: M60

Start date of project: 1 February 2006 Duration: 60 months

Organization name of lead contractor for this deliverable

THE HEBREW UNIVERSITY OF JERUSALEM

Integrating system of CW (Constructed Wetland) an EF (ElectroFlocculation process)–GF/MF/UF (Granulated/Micro/Ultra Filtration) study

Project co-funded by the European Commission within the Sixth Framework Programme		
Dissemination Level		
PU	Public	PU
PP	Restricted to other programme participants (including the Commission Services)	
RE	Restricted to a group specified by the consortium (including the Commission Services)	
CO	Confidential, only for members of the consortium (including the Commission Services)	

Summary D3.3.1-D3.3.6

EF (Electrofloculation) is an environmentally sustainable water treatment process, which involves the electrolytic addition of a coagulating metal from a sacrificial metal electrode such as aluminum or iron placed in the wastewater that hydrolyze and coagulates and flocculates with pollutants in the wastewater. The overall goal here is to develop and demonstrate an innovative model of integrated system of CW (Constructed Wetland) and EF for upgrading secondary effluent to the level that will permit their use for stream rehabilitation, park irrigation and other municipal uses that require high quality reclaimed wastewater. The work includes evaluation and comparison of the efficiencies of a constructed wetland and the electrochemical technology, in parallel and in series; Optimization of the design and operation of those technologies, including granular filtration (GF) or membrane filtration (UF/MF) particle separation steps, under site-specific conditions; Assessment of the ecological suitability of the polished effluent as a source of water for stream rehabilitation and downstream reuse.

The work concentrated on the coupling of Electroflocculation (EF) with constructed wetland (CW) for improved contaminants removal, phosphorous in particular, from secondary effluents. The work consisted of three phases: (i) electro-jar testing, (ii) continuous-flow EF-filtration (GF)–CW bench scale experimentation and (iii) field, half-industrial piloting. P, turbidity, TSS and TOC were particularly monitored. Laboratory experiments showed that EF-GF effectively removed phosphate (96%), while CW effectively removed organic matter (85%). Therefore, it seemed that the coupling of both unit processes would enhance the overall removal efficiencies. Field pilot results show that EF–GF removed up to 97% of total phosphorus, resulting in P concentrations of <0.4 mg/L, which are extraordinary results by any comparison. In addition to phosphorus removal, from the ecological point of view ammonia removal is as important as phosphorus. One of the advantages of the CW is efficient ammonia removal (over 90% in the first vertical cell with very low HRT). This is also important as the EF–CW hybrid consist of a vertical subsurface flow wetland which is the best for ammonia as well as low-medium concentrations of BOD and TSS. The system is capable of reducing some of the TOC (up to 53%) and most of the TSS up to 82%). The EF–CW hybrid action is explained by combining flocculation and adsorption mechanisms produced by the EF with filtration, sedimentation, sorption, and biodegradation processes in the CW beds.

In conclusion of this main part of the research, complementing CW treatment with a physicochemical process of electroflocculation can provide a tertiary treatment that effectively polishes secondary municipal effluent. While EF effectively reduces phosphate in both soluble and particulate forms CW treatment provides a transport-attachment trap to turbidity that escapes the electro-physico-chemical process and removes organic matter and N compounds. Laboratory tests showed that electroflocculation coupled with sand filtration effectively removed phosphate and suspended particles in contrary to the wetland gravel performance. The wetland gravel removed effectively organic matter, possibly by microbial degradation, as opposed to the EF-GF configuration. Field pilot results show that the EFector is capable of removing up to 97% of the total phosphorus, getting final concentrations smaller than 0.4 mg/l. Former electro-jar tests followed by continuous-flow, bench-scale results showed similar capabilities of up to 96% removal. The system is optimized for phosphorous removal by controlling current intensity, which represents coagulant dose and by controlling flow rate, which controls reactor residence time and turbulence. The hybrid process also enhances suspended solids (87%) and organics removal (53%) in addition to phosphorus removal. A well designed sand filtration following the EFector is highly recommended. Practically thinking, the EF unit (EFector) – constructed wetland hybrid system implies shorter residence time and better water quality, thus reduces land, construction and maintenance costs of the constructed wetlands as well as water loss. Overall, the different configuration has different advantages in contaminates removal from the wastewater. The combination of the two treatments (electroflocculation and constructed wetland) contributed to the removal of contaminates in every inspected aspect. Contaminants removal was at best when the constructed wetland preceded the electroflocculation unit, but a good sand filtration is needed in order to remove turbidity. A full scale system may be in use both for river and lake rehabilitation and tertiary wastewater purposes. It can be modular, with relative small footprint and automatically controlled according to pre-set currents and backwash sequence.

A future possibility that was examined was adding membrane ultrafiltration to the EF. Bench-scale study as firstly performed in the laboratory with artificially constituted water. It could be concluded, that EF can serve as an efficient pretreatment to membrane ultrafiltration of colloidal particles. Differences in critical flux can be attributed to cake properties, such as thickness and porosity, but also to amount of colloidal aluminum hydroxide present that can cause a degree of pore blocking. The effects of EF on the energy costs and fouling mechanisms of the membrane as a polishing treatment step and the optimal operation conditions (pH value, electric current

intensity) of the process were further investigated. It was demonstrated that pretreatment by EF is highly efficient in reducing fouling in microfiltration. At optimal condition (pH 6-6.5, 1 μg/liter of Al^{3+}) the energy that can be saved when using EF can be 10 times fold as compared to filtration without adding EF. Dealing with wastewater effluent treatment including membranes, membrane biofouling identification and ways to combat it have had to receive some special attention, due to its major potential economical impact. Alginate and Pseudomonas Aeruginosa bacteria have been identified as a dominant organic particle fouling component and as a dominant biofouling component. However, the use of hydraulic models to characterize a complex system including both has not been examined yet. In this work, different mixtures of those two components are filtered through a dead end laboratory UF membrane system and flux data is analyzed by means of hydraulic models. Short term preliminary experiments (60 min), in which components were examined alone and together, showed an excellent fit (R^2>0.99) to the linearized form of the 'Cake Filtration' model. This excellent fit allowed model extrapolations in which a partial 20 min database enabled forecasting the total 60 min flux verses time curve with good accuracy (max flux deviation <10%). Calculated Alginate specific cake resistance ($1.05–1.45\times10^{16}$ m/Kg) was found to fit with earlier work ($1.11\pm0.08\times10^{16}$ m/Kg). Long term preliminary experiments (Stage 1: 20 min filtration, Stage 2: 72 hr pressure relaxation, Stage 3: 40 min filtration), in which components were examined alone and together, showed an excellent fit (R^2>0.99) to the linearized form of the 'Cake Filtration' model for both Stage 1 and Stage 3. Long term preliminary experiments have also showed significant flux recovery (>40%). This was probably caused by the domination of pressure relaxation effect over biofouling formation effect, and will be further investigated as the work continues. While coping with biofouling it was hypothesized that metal in the form of nanoparticles (NPs) may improve its bactericidal performance in a water/wastewater suspension, which may help to minimize biofouling. The impact was evaluated by calculating log reduction. TEM microscopy was used to characterize the nanoparticles. The activity of the nanoparticles was found associated with concentration as well as with the numerical ratio between NPs and bacteria and NPs mean size. Electrostatic attraction or repulsion between the NPs and the negative charge components in the E.coli membrane were not found as a crucial mechanism for inactivation performance. To achieve a better understanding of the treatment processes, the particles in secondary effluents (Shifdan WWTP) were characterized, using automated image analysis. The capability to analyze and characterize particle shape and size by such advanced methodology can significantly assist in improving many process units, particle separation systems in particular. It was shown that filter removal efficiency can be

determined by various size and shape parameters, where different information is obtained for each analysis. During the field work, a necessity had arisen to further investigate the iron behavior. The oxidation processes of iron in electroflocculation cell were investigated for a pH range of 5–9 and a voltage of 3–25 V (corresponding to 0.05–0.4 Amperes). It was demonstrated and proven that, for all practical purposes, in all the pH and electric currents investigated, the form of iron that dissolved from the anode is Fe^{+2} (Ferrous). The gap between the amount of theoretical dissolution as calculate by Faraday's Law and the amount of dissolved iron ions that were observed can indicate two phenomena in electrochemical cells:

• With a lower pH, dissolution of the anode is possible even without the operation of an electric current. This leads to higher dissolution rates than the theoretical dissolution rates when the electric current is operated.

• The lower amounts of iron that were dissolved at a higher pH indicate that some of the electrons of the electric current participate in other reactions apart from the reaction of anode dissolution. Our results demonstrated that there is a probability that this second reaction is not the reaction of oxygen evolution; while a number of researchers have claimed that this reaction is the second major reaction near the anode.

The oxidation rates of the dissolved Fe^{2+} (ferrous) ions to Fe^{3+} (ferric) ions are almost similar to the known oxidation rates of iron in non electrochemical cells. Dissolved oxygen plays an important role in the EF process and has far-reaching influence on the following filtration. A dissolved oxygen exhaustion point (DOEP) can be determined. 1.3 mg/L DO concentration in this study could be regarded as the deflection point of ferrous accumulation in this study.

• Aeration-enhanced EF system could keep the DO level higher than DOEP, thus enabling the predominance of ferric hydroxide, rather than ferrous hydroxide, in the bulk water, which could provide better removal efficiency.

• EF combined with microfiltration could provide excellent results in residual iron and turbidity. It was not necessary to use ultrafiltration for their removal.

• Aeration-enhanced EF process hybrid with microfiltration exhibited the potential to provide better removal results of iron. The effluent could meet the stringent standard of unrestricted irrigation and directly river discharging.

LIST OF CONTENTS

LIST OF FIGURES

LIST OF TABLES

Chapter I. D3.3.1 Complete and ready EF-CW system

Due date of deliverable: M12

I.1 Objective

The aim of the study is to provide an optimal tertiary wastewater treatment by integrating two methods: a physicochemical process (Electroflocculation) and a natural process (Constructed Wetland).

Specific aims

- To evaluate the efficiency of EF-filtration in nutrients and particle removal in comparison with known abilities of constructed wetland
- To study the effect of EF on water quality as a pretreatment to the wetland system
- To examine the effect of EF on water quality as a post treatment to the wetland

I.2 Design and system modification

I.2.1 The Electrofloculation system

There are four main components in the system (Fig.1):

1. The Electrofloculation unit (EFector)
2. Sand filter
3. Holding tank
4. Control panel

The Electrofloculation unit is provided with secondary treated wastewater. It has a volume of 1.4 m^3 and is comprised of 12 pairs of perforated Iron electrodes, 1.25 m in diameter. The electric current passing through the electrodes releases iron ions that initiate the flocculation process.

After the water passes through the EFector, it continues through the sand filter that has a bedding of about 1m depth of sand grains built from two layers. The filter is 60% filled by sand bedding, allowing 40% floatation.

From there, the treated water accumulates in a 4 m^3 tank that supplies water to the constructed wetland and for backwashing the EFector and the filter.

The system is also equipped with an air compressor and a pump in order to backwash the filter and the EFector. The backwash is automatically activated when a pre-set time/turbidity/ΔP on the sand filter is reached.

Throughout the system there are 13 electric valves automatically controlled by a control panel that receives continuous turbidity values from a turbidimeter located after the sand filter.

After the water passes through the EFector, it continues through the granular filter and accumulates in a 4 m^3 tank that supplies water to the constructed wetland and for backwashing the EFector and the filter (Fig.2). The backwash is automatically activated when a pre-set time/turbidity/ΔP on the sand filter is reached.

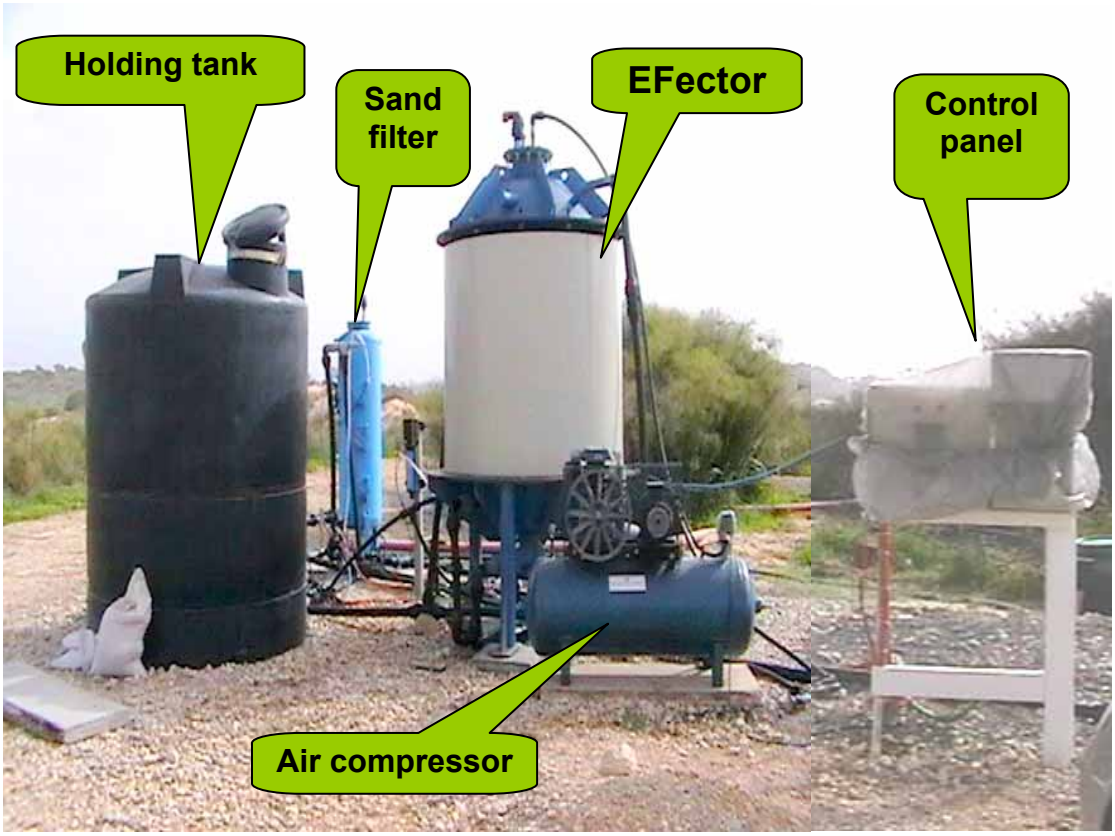

Fig. 1 The Electroflocculation system

I.2.1.1 Operation

The system is now fully operational where the Electroflocculation unit acts as a pretreatment to the wetland system.

The EFector performs flocculation at several current intensities, which actually represent coagulant dose, ranging 10A-60A. After the system has been optimized for phosphorous removal, by controlling current intensity, a pipe connection to the constructed wetland is operational and the Electrofloculation system provides continuous flow of treated wastewater to a constructed wetland pond.

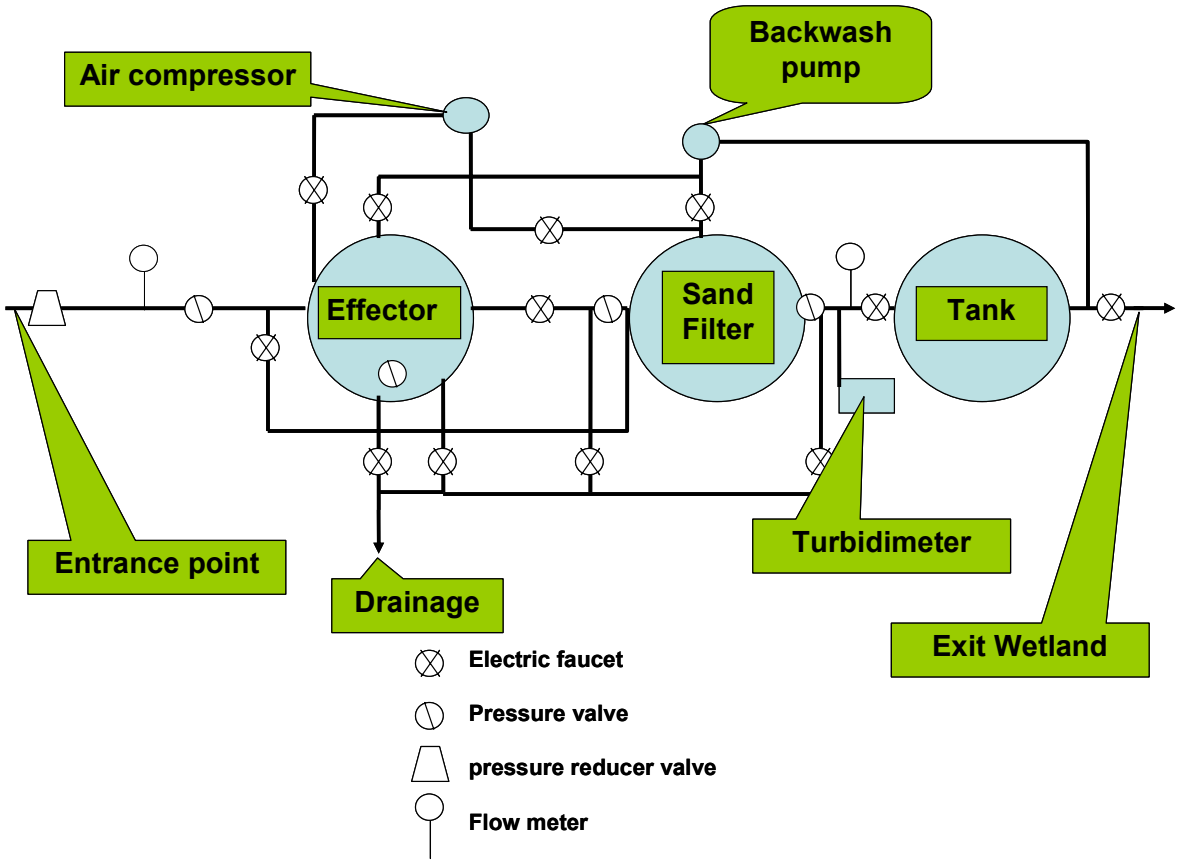

Fig. 2 EF-GF-CW system scheme.

I.2.1.2 Sampling and analysis program is as follows:

Parameter	Influent to EF/CW	Effluent from EF/CW system
pH	daily	daily
Temp	weekly	daily
EC	daily	daily
I	continuously	
V	continuously	
Flow rate	hourly	hourly
Filter pressure	hourly	hourly
Iron	daily	daily
Turbidity	continuously	continuously
TSS	daily	daily (if measurable)
COD/UV254	2/week	2/week
TOC/DOC	2/week	2/week
ICP (metals & TP)	1/week	1/week
PSD	1/week	1/week
TKN	1/week	1/week
BOD	1/week	1/week

I.2.1.3 Results

The field results agree with the bench scale unit experiments that preceded it, achieving over 95% of P removal to a level of <0.1 ppm. Organic matter removal is around 20-30%, depending on coagulant dose and TSS removal is up to 30%. Turbidity removal has not yet been optimized by the system alone but preliminary results show that when the Electroflocculation unit is followed by the CW system the TSS & turbidity removal is significantly improved.

Future work will continue evaluating the EF-GF-CW configuration in nutrients and particle removal and examine the effect of EF-GF on water quality as a post treatment to the wetland.

I.2.2 CW system (This part of the research was done in cooperation with Prof. Avital Gazith and Dana Milstein (Ph.D. student) from Tel-Aviv University)

At this project the secondary effluents of the Shafdan wastewater plant enters the wetland system after coarse filtration (400 μm) for removal of gross particulate matter that may interfere with the distribution of the effluents into the ponds. The effluent are then distributes to each of the pond series by a controlled distribution system (Fig.3).

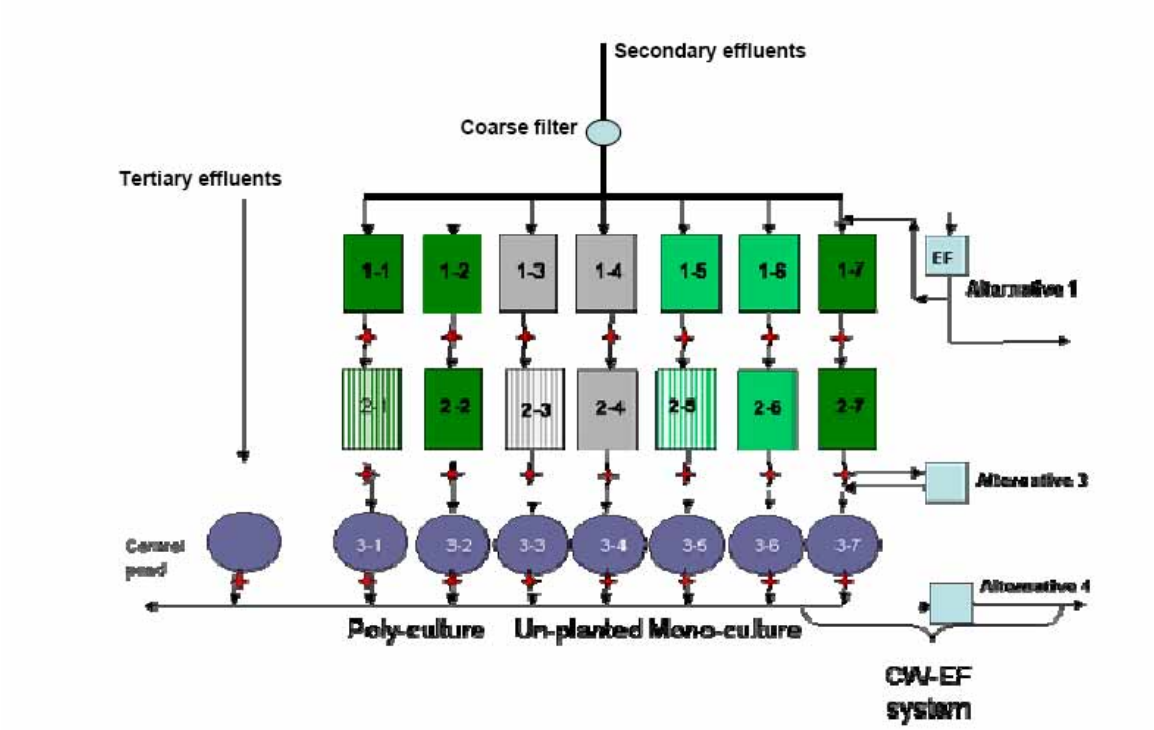

Fig. 3 CW controlled distribution system

CHAPTER II. D3.3.2, D3.3.3 EF-SF study report. CW maturation report

Due date of deliverable: M18-M24

Integrated system of constructed wetland and electro-flocculation: Bench-scale; and EF-sand filter combination

ABSTRACT

Electrocoagulation/electroflocculation offers a "green" alternative to the use of metal salts and it has been increasingly used in Europe and North America and for treatment of industrial wastewater. Based on literature, one of the major advantages of coagulation-flocculation process is phosphorus removal. Constructed wetland is normally incapable of effectively removing it. The major aim of the current work was therefore phosphorous removal, expecting that an electroflocculation unit would remove both soluble and particulate phosphorus and reduce load on the wetland.

In order to imitate the field pilot plant, laboratory experiments have been performed in a continuous flow cell followed by granular filtration (GF) for EF and a laboratory scale horizontal flow constructed wetland (CW). Preceding laboratory studies showed that Alum was more efficient in the removal of phosphate and particles then ferric chloride, within the natural pH range of the wastewater, 7-8. In addition, despite of a dominant dependency of phosphate removal ability on pH in both coagulants, the alum was favorable as it improved water turbidity. The electrocoagulation Jar tests have significantly widened the pH range suitable for phosphate removal and lowered the coagulants dose.

In the reported field study, iron electrodes were chosen for the EF-GF-CW tests, due to the health risk and financial costs involved with aluminum. Especially as continuous flow tests, by switching to sand filtering, enhanced the removals of turbidity and phosphate simultaneously.

The laboratory tests showed that EF-GF effectively removed phosphate and suspended particles in contrary to the wetland gravel performance. It was also found that the wetland removed effectively organic matter in opposed to the EF-GF configuration. Therefore, it seemed that the combination of both units would multiply their treating abilities.

First field pilot results show that the EFector (EF – electroflocculation unit) is able of removing up to 97% of total phosphorus. Further experiments obtained phosphorus removal in the range of

83-97%, reducing phosphorus concentrations to <0.1-0.51 mg/L. **These are extraordinary results by any comparison.** The system can be optimized for phosphorous removal primarily by controlling (a) current intensity, which stands for coagulant dose and (b) flow rate, which manipulate reactor residence time.

In addition to phosphorus removal, the system is capable of reducing some of the Total organic carbon (TOC) from the effluent and most of the total suspended solids (TSS). Removal of these parameters as well as turbidity might improve in combination with constructed wetland, to be investigated in the next phase of the research.

II.1 Scientific background

Electroflocculation offers an alternative to the use of metal salts and it has been increasingly used in North America for treatment to treat industrial wastewater from pulp and paper industries, mining and metal processing industries, foodstuff wastes, oil wastes, dyes, suspended particles, chemical and mechanical polishing waste, organic matter from landfill leachates, deofluorination of water, synthetic detergent effluents, mine wastes and heavy metal- containing solution (Mollah et al., 2001).

Two mechanisms may explain the coagulation process (Amirtharajah & Mills 1982):

a) Adsorption and charge neutralization–addition of positively charged hydrolytes causes charge neutralization that leads to less repulsive forces and aggregation under low pH ranges of 3–5.

b) Sweep coagulation- at high concentrations of hydrolytes (20–50 mg/l) and higher pH ranges of 6.8–8.2 aluminum and iron can settle as the hydroxide salts. When they are close to their iso-electric point, adsorption of colloidal particles happens. While settling, the hydroxide salts sweep colloids with them.

The presence of organic anionic macromolecules (humic and fulvic acids) and soluble organics in secondary effluent affects the flocculation process by raising the flocculant demand appreciably and hence affects the final water quality. In conventional coagulation studies, extraction and elimination of the organics from natural suspended solids, and removal of soluble organics from effluents reduced considerably the flocculant demand (Narkis & Rebhun 1997).

The optimum pH for turbidity and phosphate removal is around 5–9 in electroflocculation-electrofloatation by using aluminum and titanium electrodes. In that range the hydrolysis and polymerization of Al^{+3} give rise to the formation of such species as $Al(OH)^{+2}$, $Al_2(OH)_2^{+4}$, $Al(OH)_3$ and charged hydroxo-cationic complexes such as $Al_{13}(OH)_{32}^{+7}$, which are efficient for coagulation (Ge et al., 2004)

Current density can influence on electroflocculation treatment efficiency because it determines the removal rate of phosphate in dependency with initial concentration. When initial concentrations are low (10–50 mg/l) maximal removal happens already under low current density values (5mA/cm^2, duration 7 minutes). For high initial concentrations (100–200 mg/l) the current density is much higher (7.5 mA/nm^2) in order to achieve 90% phosphate removal (Bektas et al., 2004).

Phosphorus removal by wetland depends mostly on substrate capacity and wastewater residence time. It has been variable at best because substrates are often selected based on local availability and particle size for reduced clogging, without consideration for their capacity for P removal. Such specialized substrates are pumice, sand, and fly ash (Brooks et al., 2000). The adsorption and chemical precipitation of phosphorus towards the sediment is much more vigorous at the initial operation stage because the process has finite capacity (EPA, 2000).

Removal of organic matter through wetland involves several mechanisms: sedimentation, biological degradation and microbial uptake. Oxygen availability determines the proportion of aerobic to anaerobic degradation. During aerobic respiration, oxygen is used as an electron acceptor and the process is very efficient in converting the organic matter into gases, biomass and mineral products. During anaerobic respiration nitrate, carbonate and sulphate serves as electron acceptors and reduced to gases such as N_2, N_2O, each yielding successively less energy for the organism mediating the reaction. Therefore, anaerobic degradation of organic matter is slower than aerobic process (EPA, 2000).

II.2 The goal and objectives of the study

The overall goal of the research is to examine the potential of coupling a physicochemical process as Electrocoagulation, with natural process as constructed wetland for upgrading secondary effluent to the level that will comply with stringent standards for river rehabilitation.

The specific objectives of the 5-years investigation are as follows:

- To evaluate and compare the efficiency of an Electrocoagulation (EF) – granular filtration (GF) treatment to constructed wetland (CW) treatment, in nutrients and suspended solids removal.

- To study the effect of Electrocoagulation on effluent quality while proceeding constructed wetland plots (**EF-GF-CW**).

- To study the effect of Electrocoagulation on effluent quality as a polishing process following constructed wetland units (**CW-EF-GF**).

THE CURRENT REPORT RELATES TO EF-SF COMBINATION AND TO THE PRECEDING EF-GF-CW BENCH-SCALE SYSTEM

II.3 Methodology

The research work consisted of three successive steps, two in the laboratory and one at constructed wetland field site:

(a) Jar testing, including development of EF–jar testing batch system.

(b) Continuous-flow, bench/semi-pilot scale experiments, and

(c) Field, pilot plant experiments.

II.3.1 Laboratory stage (batch and continuous systems)

At the first stage, a bench scale unit was built and studied in the lab. Conventional (chemical) jar tests were conducted on 800 ml containers filled with Shafdan secondary effluent while using aluminum sulphate (alum) or ferric chloride as coagulant. Rapid mix at 120 rpm for one minute was followed by a 20 minutes flocculation period at 30 rpm and a gravity-settling period of 2 hours. In the modified jar tests the sample was withdrawn from the jars, immediately after flocculation period, and filtered through a paper filter (Whatman 545).

In the Electroflocculation (EF) test, an experimental cell has been built (Fig.4), where various values of electric current were applied during different time cycles while rapid mixing 800 ml of secondary effluent. The treatment followed by 10 minutes of slow mixing and filtration through a paper filter. 12-cm^2 aluminum or iron strip has been used as anode.

The continuous flow experiments were conducted on 1-liter cell that contains two perforated iron electrodes with an area of 114.22 cm^2. The height of the filter bed is 39 cm with 1 mm grain diameter. The artificial wastewater was prepared as described elsewhere (Egozy,1996) with additional phosphate stock solution consists of 2.865 g/l KH_2PO_4. Since the wastewater flow rate was set on 130 ml/min – the contamination injection flow rate was 0.65 ml/min for a dilution ratio of 1:200.

The laboratory scale horizontal flow constructed wetland (CW) was consisted of two units (basalt and dolomite beds) with a total area of 0.216m^2 (Fig.5). The pH was adjusted with 1N NaOH, H_2SO_4 and measured by digital pH meter model 201 Orion research.

II.3.2 Field pilot stage:

As a second stage in the research, a pilot electrofloculation system was built at the Shafdan wastewater treatment plant. The EF pilot plant has been constructed by TreaTec21 Industries Ltd.

(Israel). Design for this specific project is based on the lab experimental results and the Shafdan effluents characteristics (Appendix) which are (annual average): turbidity 6.4 NTU, phosphate, as P 2.7 mg/l, BOD 12 mg/l, COD 51 mg/l, nitrogen 9.2 mg/l, pH 7.35. The configuration, location and hydraulic and electrical connections have been coordinated with the wetland designer on one hand and the Shafdan operators on the other hand.

The Electrofloculation system (Fig.1)

There are four main components in the system:

1. The Electrofloculation unit (EFector)
2. Sand filter
3. Holding tank
4. Control panel

The Electrofloculation unit is provided with pre-screened secondary treated wastewater. It has a volume of 1.4 m^3 and is comprised of 12 pairs of perforated Iron electrodes, 1.25 m in diameter. The electric current passing through the electrodes releases iron ions that initiate the flocculation process.

After the water passes through the EFector, it continues through the granular filter and accumulates in a 4 m^3 tank that supplies water to the constructed wetland and for backwashing the EFector and the filter (Fig.2). The backwash is automatically activated when a pre-set time/turbidity/ΔP on the sand filter is reached.

Fig. 4 Laboratory Electroflocculation cell.

II.3.2 Methods

Turbidity measurements were conducted with 2100N Turbidimeter by HACH. The particle count was determined using Liquid Particle Counting System Model 9703 by HIAC/Royco. TOC and DOC were measured using a TOC-V CPN Shimadzu corporation. For DOC determination samples were filtered through a 0.45 µm filter. Phosphate, aluminum and iron were analyzed with ICP (OPTIMA 3000XL, Perkin Elmer).

II.4. Results and interpretation

II.4.1 Laboratory stage:

II. 4.1.1 Jar tests:

The initial purpose of the jar tests was to compare the efficiency of alum to that of ferric chloride. Alum was found efficient in the removal of phosphate (Fig. 6) and particles then iron (Fig. 7), within the natural pH range of the wastewater, 7–8. In addition, despite of a dominant dependency of phosphate removal ability on pH in both coagulants, the alum improved water turbidity, in contrast to ferric chloride. The electrocoagulation jar tests have significantly widened the pH range suitable for phosphate removal and lowered the coagulants dose.

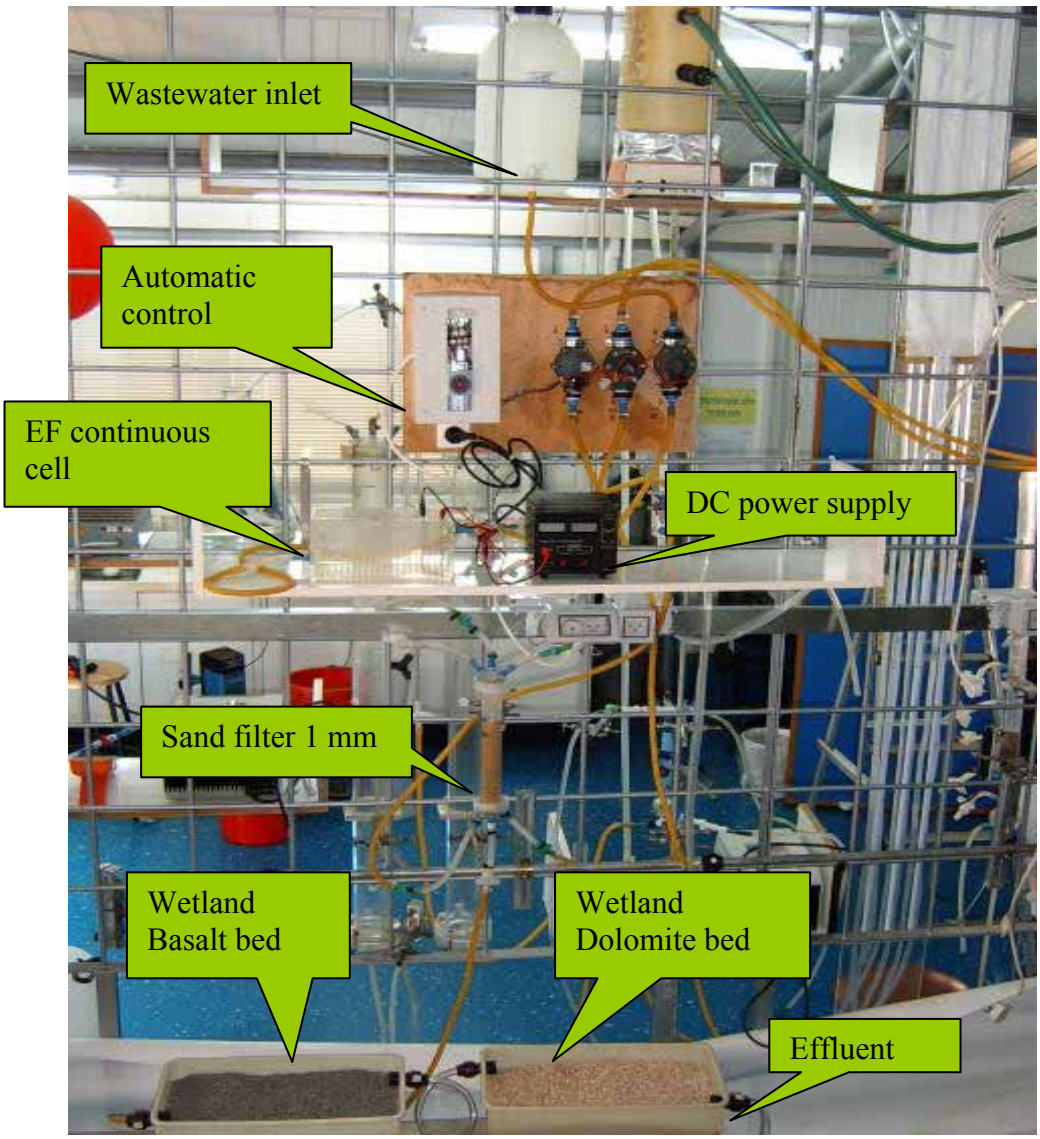

Fig. 5 EF-CW continuous-flow laboratory unit scheme.

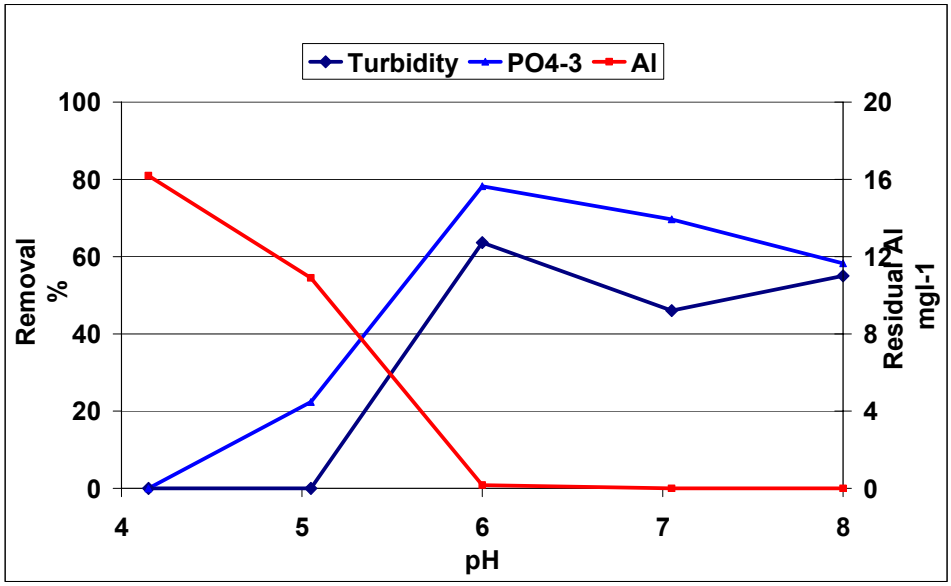

Fig. 6 PO_4^{-3} removal by a modified jar test of "Shafdan" secondary effluents.

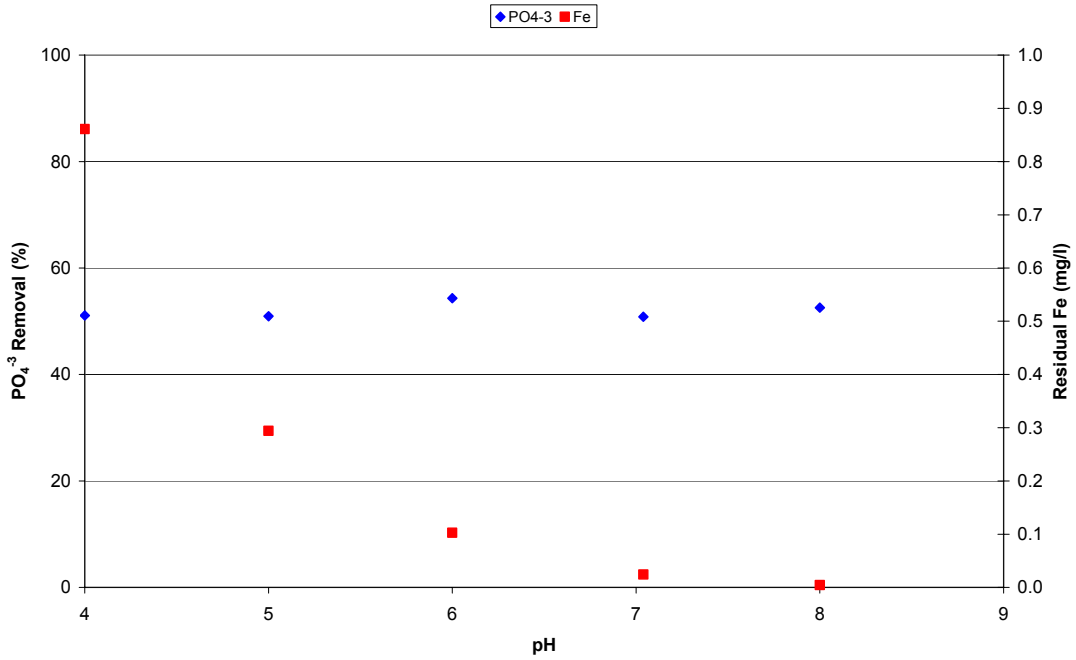

Fig. 7 PO_4^{-3} removal by modified jar test of "Shafdan" secondary effluents.

Despite of these findings, iron electrodes were chosen for the EF-GF-CW tests, due to the health risk and financial costs involved with aluminum. Especially as continuous flow tests, by switching to sand filtering, enhanced the removals of turbidity and phosphate simultaneously. In order to imitate the field pilot plant the subsequent laboratory experiments have been performed

in a continuous flow cell followed by granular filtration (GF) for EF and a laboratory scale horizontal flow constructed wetland (CW).

II.4.1.2 Constructed wetland (lab):

Separate operation of each unit revealed that the wetland was most beneficial in organic matter removal, within the range of 25-85% (Table 1), dependently of the concentration and time. In addition, it reduced residual iron by an order of magnitude and even more and lowered turbidity to remarkably low values, of 0.3-0.6 NTU.

At the beginning of the wetland operation (first 20 days), it managed to reduce 20– 72% of the turbidity and 57–74% of the oxygen from initial values of 2–6.9 NTU, 6.6–5.7 mg/l respectively. Beyond that period, the wetland added up to 27% of the turbidity and diminished less oxygen, only 26–46% of the initial concentration. The pH ranged between 6.7–6.95 (it usually escalates down stream) at the beginning to 7–7.2 afterward.

Table 1 Table 1 Laboratory constructed wetland performances as a function of operation period of artificial wastewater.

Operation period (day)	Inlet TOC concentration (mg/l)	TOC % Removal	Inlet DOC, mg/l	DOC % Removal	Inlet PO_4^{-3} (mg/l)	PO_4^{-3} % Removal
10	31.67	86			5.94	9
18	18.32	59			6.21	13
26	21.3	46			6.10	-2
35	15.87	69	12.41	85	4.50	5
43			9.77	50		
50			11.04	25		

II.4.1.3 EF-GF (lab):

Electrocoagulation treatment was found efficient in particles and phosphate removal (Table 2) since it rose from 50% to 90% and more, by raising the $i \cdot t$ value (which determines the concentrations of the disengaged Fe^{+3} ions in the bulk solution) from *23.5* to *84.6*. Reduction of

90% in particle number >2 µm from various concentration of 1500-30000 particles/ml, was attained while using the lowest iron dose.

II.4.1.4 Laboratory scale coupled unit

Based on the EF treatment results the *i·t* was kept at a constant value of 61.1 (A=0.13) and the granular filter was backwashed every 5 hours since the influent turbidity of electrocoagulated water was 21-51 NTU. The turbidity breakthrough correlates with high residual iron concentrations, probably due to over dose when raw turbidity was even lower-0.5 NTU or inadequate back washing which caused to accumulation of iron in the filter bed along with time. The wetland reduced filtered water turbidity between 25-75%.

The combined treatment was extremely effective in turbidity and iron elimination, provided that the wetland serves as polishing process (Fig.8) being their treating abilities complementary.

Table 2 Continuous flow EF-GF laboratory unit performances as a function of the *i·t* of artificial wastewater.

i·t (A·sec)	Inlet PO_4^{-3} concentration (mg/l)	PO_4^{-3} % Removal	Inlet turbidity (NTU)	Turbidity% Removal	Inlet TOC, mg/l	TOC % Removal	Residual Fe, mg/l
0 (filtering)	2.85	6	3	83	22.52	22.2	
	5.51	18	1.3	31			
	6.24	8	1.8	74			
	4.61	6	0.76	21			
	10.12	15	4.4	85			
	4.33	7	3.28	27			
23.5	4.61	81	0.49	26			0.035
	4.74	62	1	50			0.095
	6.08	51	2.62	83	11.08	10	0.035
42.3	6.38	76	3.7	86	16.25	9	0.036
61.1	6.38	94	3.7	87	16.25	4	0.184
84.6	4.61	91	0.58	-55			0.141
	8.94	96	1.26	83	7.64	-52	0.547
89.3	4.63	91	0.67	25			0.314

When considering reverse flow, the combined treatment looses its advantages. Filtrate turbidity deteriorated so much, despite of considerable reduction in coagulant dose, until the filter bed has been replaced with finer one. It showed better turbidity removal efficiency, while the coarse grain showed a moderate head loss development.

The DOC removal abilities varied between 12-85% by EF-GF treatment while the wetland abilities are divided: the first cell removed 12-40% of DOC, the second cell, which developed green algae in it, added organic matter especially when initial concentration was low. Since the EF continuously removed phosphate below detection limit (0.4 mg/l) the wetland abilities through that period are unidentified (Fig. 9).

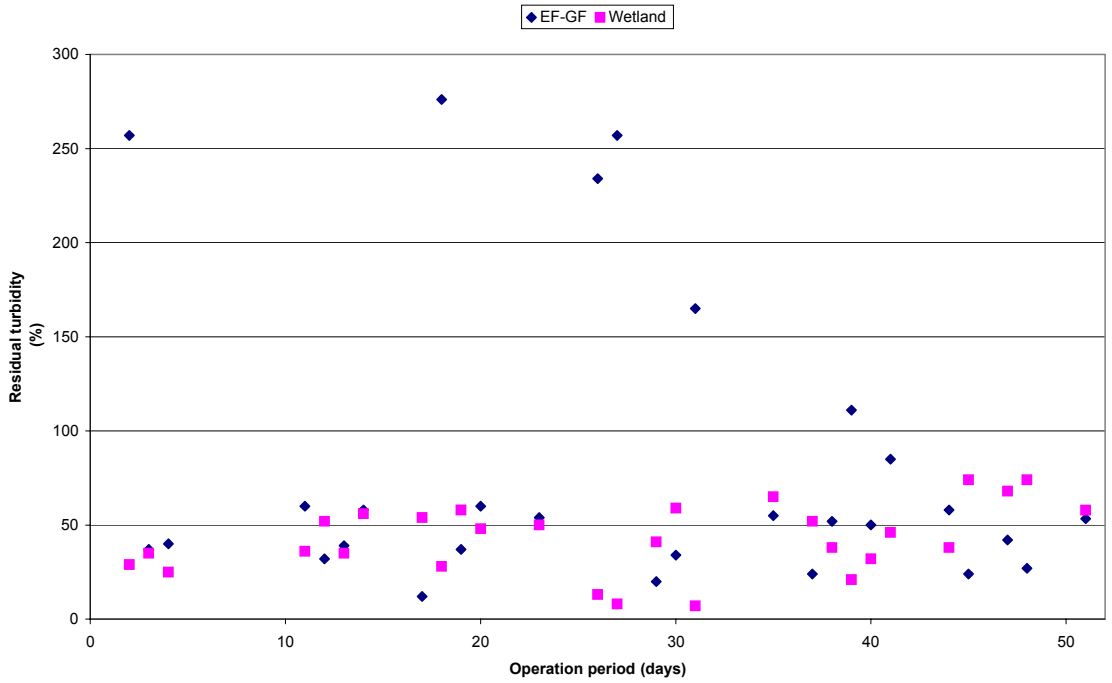

Fig. 8 Turbidity removal by laboratory coupled unit of EF-GF-CW

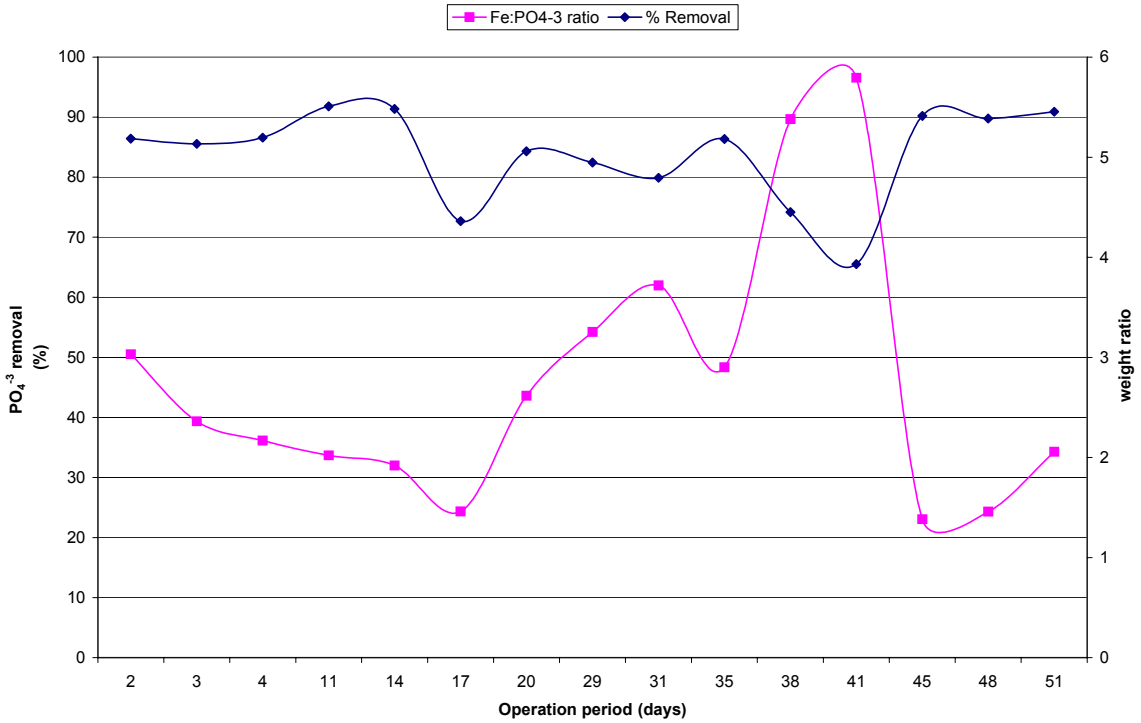

Fig. 9 Phosphate removal efficiency and the Fe: PO_4^{-3} ratio by weight during EF-GF treatment

Tables 3and 4 summarize the main findings of the laboratory stage.

Table 3. Laboratory results of bench scale constructed wetland.

CW	Inlet concentration	Outlet concentration	%Removal
Turbidity, NTU	2-6.9	1-2	20-70
Phosphate, mg/l	4.5-6.2	3-5	Up to18
Organic matter	9.8-21.3	2-11	25-85
Particles (2-17 µm diameter) , part./ml	5500-27000	1000-7000	13-98

Table 4 Laboratory results of bench scale electrofloculation –granular filtration unit.

EF-GF	Inlet concentration	Outlet concentration	%Removal
Turbidity, NTU	0.5-4.4	0.4-1	25-86
Phosphate, mg/l	2.8-10.1	0.4-4.95	51-96
Organic matter	7.6-16.2	10-17	4-10
Particles (2-17 µm diameter) , part./ml	5800-29000	300-2000	93-99

II.4.2 Field pilot stage

Electro-flocculation system investigation at Shafdan – EF-SF

II.4.2.1 Results and interpretation

As previously mentioned, one of the main objectives of this project is to evaluate the efficiency of removal of selected nutrients by Electrofloculation (EF) followed by filtration. It is hypothesized, that one of the major advantages of the electro-physical system over the natural system in contaminant removal would be expressed in phosphorous removal. The EF research focused at the reported period on phosphorous removal by the EF-GF (granular filtration) electrophysical system..

First field pilot results (Fig.10) showed that the EFector has the ability of removing up to 97% of total phosphorus.

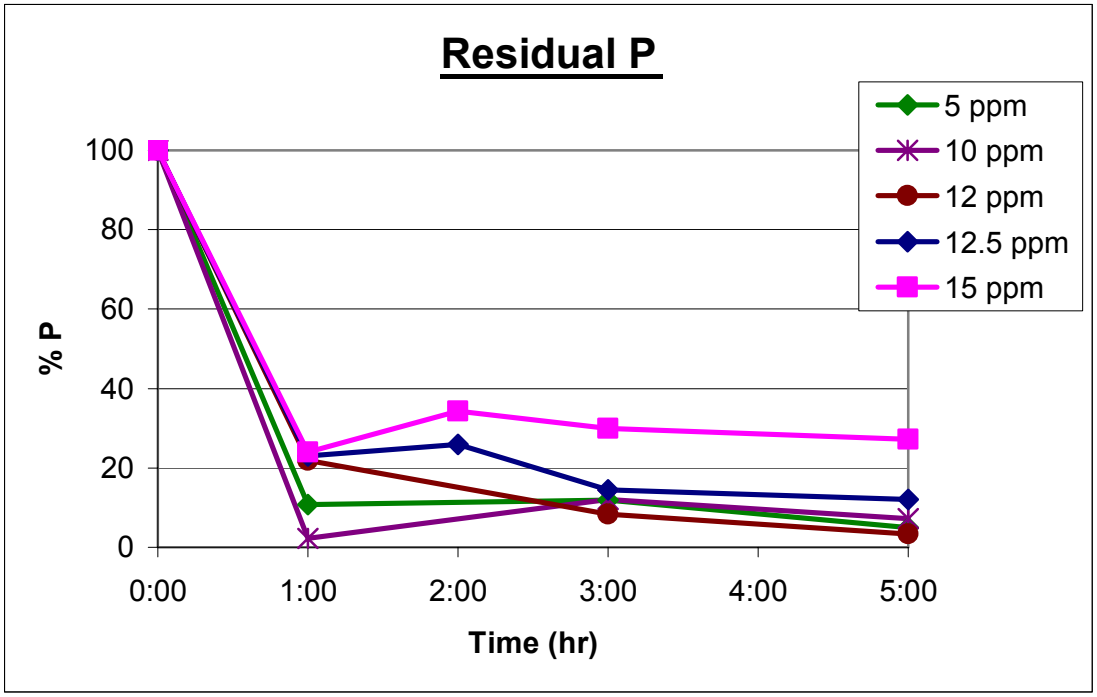

Fig. 10 Changes in total phosphorus concentration with time. Initials P levels: 0.5-2 mg/l. The average flow rate: around 1.5 m^3/hr

Preliminary results of carbon load removal showed that the EFector is capable of reducing some of the Total Organic Carbon (TOC) in the system (Fig. 11). As shown in the bench scale study,

where TOC concentration are around 12 mg/L, the electroflocculation was able to remove about 10% of TOC.

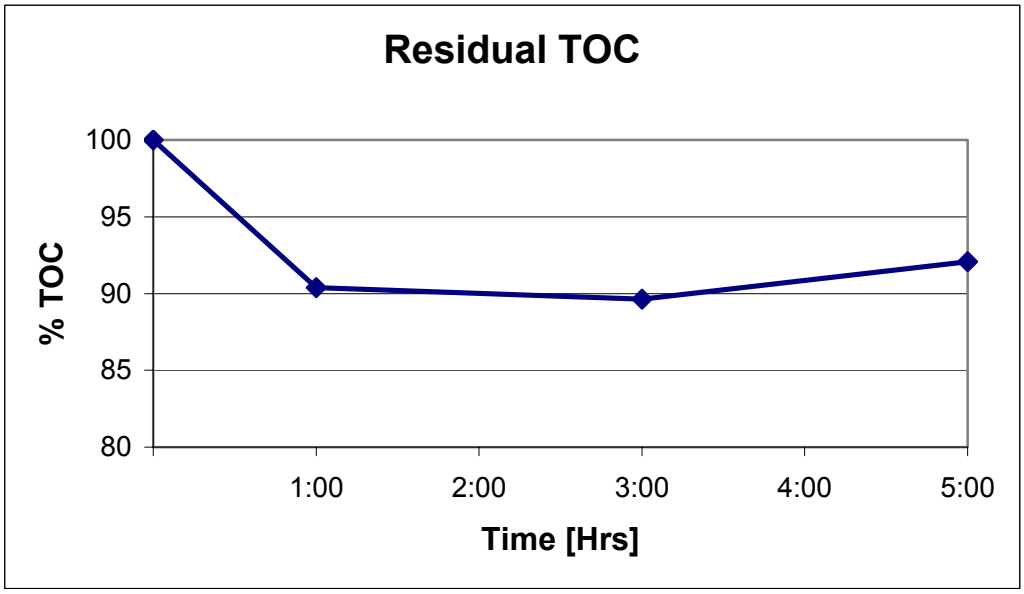

Fig. 11 Changes in Total Organic Carbon (TOC) concentration with time. Initials TOC level: 12.7 mg/l. The average flow rate: 1.5 m^3/hr and coagulant dose: 12 ppm Fe.

EF-SF field experimental results for turbidity, phosphorus, TOC and TSS are summarized in Table 5.

Table 5 EF-SF field pilot results

	Inlet concentration	Outlet EF-GF	% Removal EF-GF
Turbidity [NTU]	2-4.5	1.31- 6.6	0-30
Phosphorous [mg/L]	1-3	<0.1-0.51	83-97
Organic matter [mg/L]	10-15	9-12.56	11-24
TSS [mg/L]	2-10	2.22-8.25	18-22

The phosphorus removals shown in the table **are extraordinary results by any comparison.** Former electro-jar tests followed by continuous-flow, bench-scale results showed similar capabilities of up to 96% removal (see previous reports). The system can be optimized for phosphorous removal primarily by controlling (a) current intensity, which actually represents

coagulant dose and (b) flowrate, which changes the effect of reactor residence time. Based on the optimization results, the EF unit will soon operate continuously and its performance in comparison to the wetland set-up will be monitored.

One of the objectives of this study is to evaluate the efficiency of removal of selected nutrients by Electrofloculation (EF) followed by filtration. It seems very likely now, that one of the major advantages of the electro-physical system over the natural system in contaminant removal would be expressed in phosphorous removal.

The overall turbidity removal results, up to 30% – do not seem satisfactory. However, that was not the sand filter to blame. Actually the filter by itself worked in efficiencies greater than 80% in removing the flocs formed by the EFector and interacted with the phosphorous and with the primary colloids originated in the system's influent (Shafdan's secondary effluent). It is hypothesized, that part of the residual turbidity is constituted by dissolved iron species formed in the EFector, and perhaps needed more residence time and further media surface area to be further removed. A following CW unit could possibly do the job – to be experimented in a later phase of the Project.

II.4.2.2 Future work

The potential of the EF unit (EFector) to be integrated in the constructed wetland system will serve in shorter residence time and better water quality and therefore reduce investment costs of the constructed wetlands (CW). It is expected that the EF unit will remove both soluble and particulate phosphorus and reduce load on the wetland while the CW will work on the other contaminants that may be found.

In addition to the phosphorus removal, the EFector may have additional abilities in removing turbidity with partial removal of associated pathogens; heavy metals, and possibly endocrine disruptors. These capabilities are an important improvement over conventional or modified CW systems. During the following research period, we plan to add further analyses to the system in order to monitor and estimate its capability in reducing suspended solids and carbon load.

In a few weeks time the connection of the Electroflocculation unit to the first set of the CW ponds will be operational and continues flow experiments will be held. By that time, turbidity removal of the overall system will be optimized so that it would be later compared to its removal by the wetland.

It is expected, that this investigation will end up with the ability to scale-up the optimized pilot system to full scale for application in various locations, both for river rehabilitation and tertiary wastewater purposes. The full system can be modular, with relative small footprint and automatically controlled according to pre-set current intensities and backwash sequence to be concluded from this research.

II.5. Discussion

Based on literature, one of the major advantages of coagulation-flocculation over the natural system in contaminant removal is expresses in phosphorous removal. It was therefore expected that the EF unit would remove both soluble and particulate phosphorus and reduce load on the wetland.

The laboratory tests showed that EF-GF effectively removed phosphate and suspended particles in contrary to the wetland gravel performance. It was also found that the wetland removed effectively organic matter (perhaps the aerobic environment enhances the microbial degradation) as opposed to the EF–GF configuration. Therefore, it seemed that the combination of both units would multiply their treating abilities.

Results of suspended solids and carbon load removal demonstrate that the EFector is capable of reducing some of the Total Organic Carbon (TOC) in the system and most of the TSS. Thus, in addition to Phosphorus removal, the system is capable of reducing suspended solids and carbon load.

Turbidity and color are enhanced in the system by the ferrous/ferric addition. It could be that the extra turbidity is a result of a delayed oxidation of bivalent to trivalent iron. That mechanism still has to be investigated; the turbidity removal should be further optimized.

The wetland constantly reduced residual Fe concentration by an order of magnitude and more.

Other investigations indicate that the EFector may have additional abilities in removing pathogens; heavy metals, and possibly endocrine disruptors. These capabilities can provide a considerable improvement over conventional or modified CW systems, further research in those directions is highly recommended.

EF unit (EFector) - constructed wetland hybrid system implies shorter residence time and better water quality, thus reduces land, construction and maintenance costs of the constructed wetlands as well as water loss.

II.6. Practical implication

This investigation results enable now the further investigation according to the objectives above mentioned. It is expected now that at the end of this project, scaling-up of the optimized pilot system to full scale will be possible for application in Israel as well in other locations, both for river and lake rehabilitation and tertiary wastewater purposes. The system can be modular, with relative small footprint and automatically controlled according to pre-set current intensities and backwash sequence.

II.7. CW maturation report

This part of the research was done in cooperation with Prof. Avital Gazith and Dana Milstein (Ph.D. student) from Tel-Aviv University

In the maturation period the wetland was operated under intermittent flow regime at a rate of ca. 14.3 m^3 per day. In the mature stage the wetland is operated at a constant flow regime that varies (ca 20 m^3/day, except for 1.1 and 1.7 that receive ca 10 m^3 due to clogging).

Limnological conditions (temperature, dissolved oxygen, conductivity) were measured on site. Water samples for nutrients and pollutant analyses were collected both at the effluents entering and leaving the wetland ponds, transferred chilled to the laboratory, and analyzed on the same day. The wetland conditions and performance were tested during the maturation period.

II.7.1 Results:

pH

pH in the constructed wetland system varied between values of 6 to 8, reflecting hypoxic and high oxygen level, respectively. The lowest pH values were recorded in the third stage ponds which are relatively rich in organic matter (sloughed from the vegetation).

Electrical conductivity

At maturation period the electric conductivity was similar in all ponds and laid in range 1130 – 2340 μS/cm^2 at 25°C. There was no evidence for effect of loss of water via evapotranspiration on conductivity.

Temperature

The temperature was recorded during morning hours (6:00–10:00). There is evidence that the temperature of the effluent leaving the ponds is lower than that entering the system. The temperature range varies from ca. 15ºC (winter) to ca 30°C which were recorded during the summer (August).

TSS

The secondary effluent entering the wetland system was rather low in total suspended solids (TSS). During the maturation period the average concentration was 6 mg/l (±60%). The removal efficiency of TSS in the first stage treatment was ca 70% and in the second stage it reached 86%.

Oxygenation condition

During maturation period the dissolved oxygen saturation of the inflowing water was about 38% and remained above 30% throughout the different treatments at the ponds of the first stage

Total nitrogen

Ammonia and nitrate are interrelated via oxidation of the former and thus usually exhibit negative correlation. Analysis of total nitrogen can reveal the ultimate fate of this element in the system. In the first stage treatment there is practically no change in the total nitrogen concentration in the system during the maturation period (average total nitrogen concentration in the secondary effluent and in the treatment ponds 5.4 and 4.6 mg/l, respectively. In the second treatment stage there is evidence for some removal of total nitrogen with no apparent difference of pond structure and flow pattern. The removal efficiency is ca 34% (5.4 and 3.6 mg/l average concentration in the secondary effluent and treatment ponds, respectively). In the third stage the cumulative efficiency of removal of total nitrogen reaches 61%. There is no apparent effect of pond structure and flow pattern.

Appendix.

Shifdan secondary effluent quality (Shifdan's data)

Parameter	Units	No. of monthly data	2003 Arithmetic monthly means[1]												Annual average	Sd. Dev.
			1	2	3	4	5	6	7	8	9	10	11	12		
Arsenic	µg/l	1	<1	<1	<1	<1	<1	<1	<1	<1	<1	<1	<1	<1	<1	
Cadmiun	µg/l	1	<0.2	<0.2	<0.2	<0.2	<0.2	<0.2	<0.2	<0.2	<0.2	<0.2	<0.2	<0.2	<0.2	
Cyanide	µg/l	1	5	6	11	11	10	35	8	8	11	11	13	24	13	8.8
Lead	µg/l	1	<2	2	5	4	<2	<2	2	<2	<2	<2	2	<2	<2	1.4
Mercury	µg/l	0–1	<0.1	<0.1	<0.1	0.5	<0.1	<0.1	<0.1	<0.1	<0.1	0.2	<0.1	<0.1	.2	0.12
Selenium	µg/l	1	1	<1	<1	<1	<1	<1	<1	<1	<1	<1	<1	<1	<1	
Chromium	µg/l	1	4	3	5	5	8	3	4	3	4	3	4	4	4	1.4
Barium	µg/l	1	54	45	50	49	47	45	47	48	37	38	42	216	60	49.5
Silver	µg/l	1	<1	<1	<1	<1	<1	<1	<1	<1	<1	<1	<1	<1	<1	
Cooper	µg/l	1	38	41	63	68	66	45	72	23	50	56	104	4	53	26.2
Iron	µg/l	1	67	101	143	107	149	167	171	150	139	117	122	103	128	30.6
Manganese	µg/l	1	34	9	15	30	34	40	35	35	29	22	26	37	29	9.4
Zink	µg/l	1	71	84	192	161	63	42	47	33	74	46	71	118	84	49.4
Sodium	mg/l	1	195	165	195	177	201	213	216	218	227	215	219	222	205	19.1
Potassium	mg/l	1			19.6		19.2		20.7		25.8		17.8		20.6	3.1
Boron	µg/l	1	0.35	0.19	0.24	0.20	0.18	0.18	0.22	0.23	0.22	0.17	0.24	0.16	<0.22	0.05
Cobalt	µg/l	1	<3	<3	<3	<3	<3	<3	<3	<3	<3	<3	<3	<3	<3	
Nickel	µg/l	1	10	9	10	11	20	10	16	12	10	7	27	15	13	5.6
Strontium	µg/l	1	582	558	656	632	652	655	714	742	625	598	694	620	644	53.8
Molybdenum	µg/l	1	3	5	3	<3	3	3	3	3	3	<3	<3	3	<3	0.7
Tin		1	<5	<5	5	<5	<5	<5	<5	<5	<5	<5	6	<5	<5	
Silicon	mg/l	1			8.9						7.5		7.5		7.9	0.8
Lithium	µg/l	1	11	8	13	13	21	21	24	26	21	19	21	18	18	5.5
Aluminum	µg/l	1	31	75	68	116	53		85	61	58	61	83	119	74	26.3
Total bacteria	No./1 ml	0–1	1.1E+06	2.5E+06	1.4E+06	8.4E+05	4.4E+05	4.6E+05	5.1E+05	4.6E+05	4.9E+05	9.6E+05	1.1E+06	4.0E+05	7.5E+05	6.1E+05
Coliforms	MPN/100ml	0–1	6.4E+05	4.6E+05	1.6E+06	1.5E+05	8.0E+04	1.5E+05	2.3E+05	4.6E+05	1.6E+05	8.0E+05	1.8E+05	2.5E+05	3.6E+05	5.4E+05
Faecal Coliforms	MPN/100ml	0–1	1.4E+05	5.1E+04	1.7E+05	3.2E+03	5.8E+03	1.0E+04	1.0E+03	5.8E+04	2.0E+05	1.0E+05	1.8 +04	1.6E+04	2.5E+04	7.1E+04
Strept. Faecalis	MPN/100ml	0–1	1.8E+04	2.2E+04	1.7E+05	2.9E+03	2.4E+03	2.3E+03	3.2E+03	1.4E+04	9.0E+03	1.1E+04	2.2E+03	9.0E+03	8.2E+03	4.7E+03
Enteroviruses	PFU/400L	0–1			4[2]		1[3]						0[4]		2	0.5
SAR		1	4.7	4.1	4.9	4.3	4.9	5.2	5.3	5.2	5.6	5.3	5.4		5.0	

[1] Except for bacteriological analyses, where geometric monthly means are given
[2] PFU/70L
[3] PFU/40L
[4] PFU/30L

Chapter III. D3.3.4, 3.3.5 –EF–UF Study Report

Due date of deliverable: M24-48

This report is a part of Tali Harif Ph.D. thesis

Abstract

Electroflocculation (EF) is gaining popularity and becoming recognized an alternative process to conventional coagulation/flocculation (CF), although both are somewhat different. Research into this alternative technology has focused on efficiency and performance rather than on the fundamental basics which is the core of understanding the mechanisms of EF and ultimately will lead to better system design and process control.

In EF the active coagulant species are generated in situ by electrolytic oxidation of an appropriate anode material, thus differing from CF in which chemical coagulants such as metal salts or polymers and polyelectrolytes are used. The electrical current applied in EF creates a unique chemical/physical environment which affects coagulation mechanisms and subsequent aggregate/floc formation. This is due to competing redox reactions within the system, the first and foremost being hydrolysis. Coagulation mechanisms depend primarily on factors such as pH and coagulant dosage, which govern speciation of the active mononuclear species, hence the current has an additional affect as it both governs the dissolution of the metal coagulant into the system and also causes the pH to rise, as hydroxyl is simultaneously formed at the cathode. In addition, the dosing regime is an additive process over time in which negative counter ions are not introduced, and microbubbles are formed as hydrogen and oxygen are also products of the hydrolysis. It is also possible that the electrical field imposed could affect ion and particle transport.

The aim of this research is to gain a better understanding of the EF process, primarily on a theoretical level, but also to evaluate the applicability of the process as a viable alternative to conventional coagulation. The mechanisms of coagulation and flocculation in EF are elucidated, while connecting changes in suspension characteristics, floc growth patterns, structural evolution and floc morphology to operational parameters. A comparison with CF was performed, with regard to destabilization mechanisms and floc structural evolution. Finally, the applicability of the process was examined, as a viable alternative pretreatment process in membrane ultrafiltration.

All experiments were conducted using a model kaolin suspension of 15-60mg/l, prepared in distilled water, conductivity increased and pH corrected to 5, 6.5 or 8. Various EF cells were designed, depending on the requirements of each section of research. All cells were operated in

batch mode, and comprised two electrodes – a stainless steel cathode and an aluminum anode. The electrodes were connected to a DC external power source. The cell was operated in galvanostatic mode: the current was set and the potential found its own value at a predetermined rate, defined by Faraday's law.

Changes in ζ potential and pH were monitored. Fractal analysis was used in conjunction with image analysis and particle size distributions to gain a comprehensive analysis of the aggregates/flocs formed in the EF process. Size and structural evolution measurements were performed utilizing static light scattering techniques.

The membrane unit used was a stirred cell type, and the membranes were flat sheet hydrophilic polyethersulfone ultrafiltration membranes. The effect of suspension pretreatment on membrane fouling was measured by flux decline at constant pressure.

This study has identified key mechanisms dictating coagulation and flocculation behavior in EF, and gained an understanding of differences in these mechanisms compared to those in CF. The pH of the suspension is a vital parameter dictating coagulation and flocculation behavior and in EF, unlike CF, its final value will always be higher than its initial value. This rise is continuous and results in the shifting of coagulation mechanisms while the current is applied. The degree of pH change, however, can be controlled by adequate mixing conditions, and standard velocity gradient values were found to be sufficient for this.

The passage of current was found to affect particle transport. This could be due to the electrical field induced as enhanced aggregation of primary particles was observed without applying a velocity gradient for suspensions with high conductivity suspensions in which the diffusion barrier between primary particles was lowered.

In EF the sweep floc range is wider than in CF. Thus, EF is able to produce flocs over a wide range of doses and pH values. This versatility produces a range of floc "types", depending on conditions of operation.

The growth patterns of floc in EF were of sigmoidal behavior, and unlike CF were attained for all currents applied. This behavior was observed in CF only within optimal dose limits.

Floc growth in EF is quicker than in CF which EF shows a dependency of growth rate on current (dose), with higher growth rates obtained at higher currents. This dependency also depends on the initial pH, and a higher dependency exists for enhanced precipitation zones (pH 6.5).

Differences in structural evolution patterns between the two processes have also been identified. For adequate flocculation conditions (i.e sufficient growth) in CF the growth is into a more porous structure. In EF, however, the evolution is generally from a less compact structure into a more compact one. EF produces flocs which initially are more porous than those formed in CF, but are more fragile and more susceptible to shear forces. Thus they undergo compaction and in some cases structural fluctuation.

It appears that the flocculation mechanism in EF is of a diffusion limited type, whereas in CF it is more of a reaction limited nature. This can explain differences in floc growth rate and floc structural evolution between the two processes.

Floc size growth was found to be independent of current density, although these were found to be correlated to current application times.

EF was found to serve as an efficient pretreatment to membrane ultrafiltration with enhanced flux observed at pH 6.5 for higher currents, where sweep floc dominates and more porous floc structures are obtained. The major fouling factor is cake formation although results indicate that a degree of pore blocking occurs. The differences in critical flux can be attributed to cake properties, such as thickness and porosity, which are a function of the quantity of precipitate in solution and floc structure, respectively.

This thesis has provided conceptual development and experimental justification which unravel the mechanisms of EF. Thus EF is shown to be a versatile and reliable technology, which can serve as an alternative to conventional processes and has considerable potential for water treatment and reuse.

III.1. Introduction

One of the major challenges facing all countries today is to provide clean water to their expanding populations. Due to population growth, urbanization and climatic changes, even highly developed countries, such as the U.S, are realizing the importance of improving existing water supply networks by utilizing all potential water resources. These resources include recycled wastewater as well as raw water, which in the past might have been neglected due to its poor quality. There is, therefore, a need to develop innovative, more effective and less expensive techniques for treatment of water and wastewater. A wide range of water and wastewater treatment techniques are known which the application of varies depending on the quality of the raw water and the intended use of the treated water. Electroflocculation (EF) is gaining popularity and is becoming recognized as an alternative to conventional coagulation/flocculation processes. Despite treatment of wastewater by electrochemical processes for most of the 20th century, even more so in recent years, limited scientific research has explored the efficiency of the technology as an alternative process for water treatment. No substantial research has been conducted on the mechanisms of coagulation and flocculation in the EF process which are directly affected by the unique conditions the process creates, caused by imposing an electrical current to produce the active coagulant species – and are yet to be understood.

The aim of this research is to gain a better understanding of the EF process, primarily on a theoretical level, but also to evaluate the applicability of the process as a viable alternative to conventional coagulation. As such, the specific objectives are:

- Elucidate the mechanisms of coagulation and flocculation in EF while connecting changes in suspension characteristics and floc evolution and floc morphology to operational parameters.
- Compare EF with conventional flocculation (CF) with regard to destabilization mechanisms and floc structural evolution.
- Examine the applicability of the process as a viable alternative pretreatment to membrane ultrafiltration.

III.2 Materials and Methods

Different experimental procedures were used for research sections. Thus the methods are specified according to research section.

III.2.1 Characterizing solution changes and floc morphology

Colloidal suspension

0.3gr of kaolin ($AlSi_2O_5(OH)_4$, *Aldrich Chemical Company Inc. USA*) was suspended in 20 liters of distilled water (15mg/l final concentration) and homogenized using an *Ultraturax 2000, Ganke and Kunkel, GMBH*. 1.66gr of $NaHCO_3$ (*BDH Laboratory Suppliers, England*) was added (final concentration 83mg/l), the pH was corrected to 5 and 6.5 with NaOH or H_2SO_4, and conductivity was increased with $NaNO_3$ (*Riedel-Dehaen, GMBH*)**.**

EF unit

An EF unit which can be operated as a batch or continuous unit was designed (fig.12). It consisted of a cylindrical plexyglass shell, with a volume dimension of 77.64cm^3 (H=6.5cm, D=3.9cm) and two concentric electrodes, inserted one inside the other, creating a space into which water could flow to be treated. The outer electrode (H=6.5cm, D=3.8cm) was stainless steel and served as the cathode. The inner electrode was aluminum, which was the anode (H=6.5cm, D=1.8cm). The anode was perforated with 28 holes, each with a diameter of 0.5cm, leaving an effective anode area of 31.27cm^2. Through the anode a baffle was fitted, which was connected to a motor, powered by an external power source. Adequate mixing conditions were created within the cell due to the holes perforated through the anode. The electrodes were connected to a DC external power source .The cell was used in all experiments as a batch cell.

Particle size analysis

Particle size distribution (PSD) measurements were performed over a range of 2μm-300μm, using a *HIAC Royco Liquid Particle Counting System*.

Aggregate morphology/fractal dimension

The aggregates resulting from the process were photographed using an *Olympus digital camera DP70* (12.0 mega pixel resolution) which was mounted on a *Reichart* microscope. Morphological characterization of suspended aggregates is a microscopic technique which is

complementary to macroscopic methods for characterizing flocculated suspensions. Microscopy allows individual particles to be viewed, scrutinized and analyzed at high magnification, however sample extraction and preparation should be conducted with utmost care, so to not disrupt the structure. In this case, a drop of the sample was put onto a microscopic slide, *without* using a cover slip. Image analysis was used to morphologically characterize the resulting aggregates (i.e primary kaolin particles vs. aluminum hydroxide floc) and for quantifying their structure using a two-dimensional fractal dimension (D_2). To calculate D_2, the images were processed using standard software (photoshop), and then were analyzed using NIH-Image software which uses the box counting method. The fractal dimension measured by this technique is:

$$D = \lim_{L \to 0} - \log(N)/\log(L) \qquad (2.1\text{-}1)$$

N is the number of squares required to cover the object, and L is the resolution or size of the square. Plotting the number of squares against the resolution on a log-log plot returns the fractal dimension of the aggregate. One image (one aggregate) was used for each analysis, following application of thresholding. Several images were acquired for each measurement and the fractal dimensions obtained are based on an average of 7-8 aggregates.

ζ potential

The ζ potential of the post electroflocculated suspension was measured using a *Malvern Zetamaster S*. Each result was an average of three readings.

Experimental procedure

The cell was filled with the kaolin suspension, a velocity gradient (G) was set ($0sec^{-1}$, $10sec^{-1}$ or $30sec^{-1}$), and a current was applied for 1min. The G values were chosen according to typical values used for slow mixing in lab apparatus and larger scale systems.

The suspension underwent an additional 5 min mixing, after which a sample of the effluent was taken for analysis. The mixing time was set so floc size obtained would be adequate for microscopic analysis. The cell was operated in galvanostatic mode: the current was set and the potential found its own value dependent on the system's overall resistance. This ensured coagulant production at a predetermined rate, defined by Faraday's law. The currents used for the experiments were 0.05A, 0.1A, 0.2A, 0.3A producing $1.6mA/cm^2$, $3.2mA/cm^2$, $6.4mA/cm^2$, $9.6mA/cm^2$ respectively. The current densities are in good accordance with

figures reported in the literature (Mameri et al, 1998; Holt et al, 2002). The respective aluminum doses obtained were: 4mg/l, 8mg/l, 16mg/l, 24mg/l, for a dosing time of 1 min. Some experiments explored the effect of current density on the resulting aggregates, and these were carried out using 1/2 the current densities, and a dosing time of 2 min.

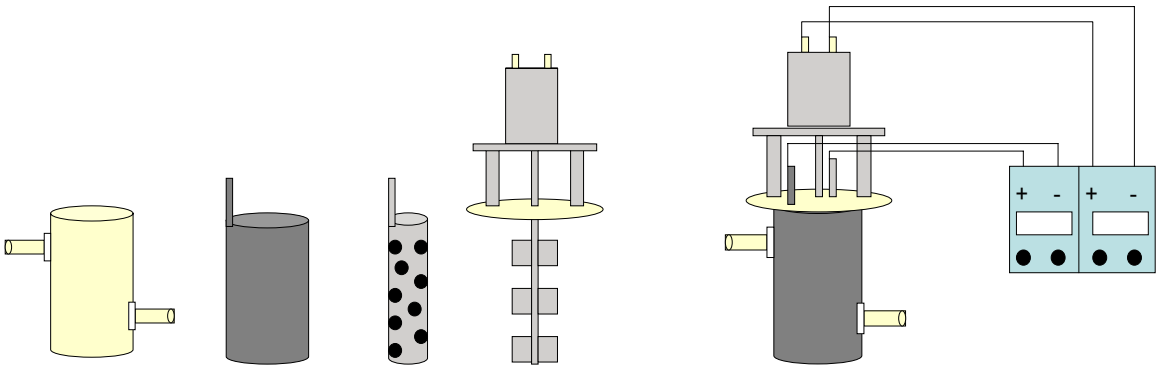

Fig. 12 Left: EF cell components: (from left to right) outer cell, outer electrode (stainless steel cathode), inner electrode (aluminum anode, perforated), mechanical baffle. Right: Components combined into EF cell and connected to DC power supply.

III.2.2 Monitoring size and structural evolution of flocs in EF and CF using static light scattering

Colloidal suspension

1.2gr of kaolin ($AlSi_2O_5(OH)_4$, *Aldrich Chemical Company Inc. USA*) was suspended in 20 liters of distilled water (60mg/l final concentration) and homogenized using an *Ultraturax 2000, Ganke and Kunkel, GMBH.* 1.66gr of $NaHCO_3$ (*BDH Laboratory Suppliers, England*) was added (final concentration 83mg/l), the pH was corrected to 5, 6.5 and 8 with NaOH or H_2SO_4, and conductivity was increased to 1mS/cm with $NaNO_3$ (*Riedel-Dehaen, GMBH*).

EF unit

An EF batch unit was designed (fig. 13). It consisted of a plexyglass cap, which could be fitted onto a 1 L chemical glass and to which the electrodes were attached. The inner electrode, the cathode, was made from stainless steel and concentric in form (H=10cm, D=2.5cm). It was fitted onto the arm of a magnetic stirrer, and stationary throughout all the experiments. The outer electrode, the anode, was made from aluminum and could be used in

two sizes, for applying different current densities: a concentric electrode (H=10cm, D=9.5cm) and two separate electrodes, with a total effective area of 1/4 of the former electrode. The electrodes were connected to a DC external power source. Mixing conditions within the cell were achieved with the magnetic stirrer and a constant mixing speed of 145 rpm was used for all experiments.

Floc size and structure analysis

Size distributions and structural information of kaolin-$Al(OH)_3$ flocs were determined as a function of time using a *Malvern Mastersizer Microplus*, which ascertains size by analysis of forward scattered light. The size distribution data given by the instrument covers the size range of 50nm to 500μm.A He-Ne laser light (λ = 633nm) was passed through a 2.0mm-width measurement cell in which the sample flowed. The beam was converged by a 300mm focusing lens and 42 detectors enabling the collection of light scattered from 0.03^o to 46.4^o. The plane of polarization of the laser beam is parallel to the detector axis (vertical). Size distribution information was obtained using supplied software which uses Mie theory to develop a scattering pattern that matches the scattering pattern of the sample being measured. Information on distribution size is presented in this study as the volume mean diameter:

$$D(V, 0.5) = \Sigma_i (V_i d_i)/\Sigma_i V_i \qquad (2.2\text{-}1)$$

Where V_i is the relative volume in size class i with mean class diameter d_i.

Information on floc structure was obtained by measuring the intensity of light (I) at all detectors and plotting log I versus log q (eq. 1.3.1.1.2-1). Information regarding the angles of the detectors and intensity correction data, based on the geometric configuration of the detectors, was supplied by Malvern Instruments.

Image analysis

Image analysis was used in conjunction with scattering measurements as a complementary analysis to ascertain floc properties over time. The aggregates resulting from the process were photographed using an *Olympus digital camera DP11* (3.0 mega pixel resolution) which was mounted on an *Olympus Stereoscope SZX12*. All photographs were taken at magnification x 50. The images here were not used for structure quantification by fractal analysis due to the relatively low resolution of the images obtained, as in this case particles may be incorrectly sized due to a blurred boundary between the particles and background (Chakraborti, et al., 2003).

ζ potential

As specified in section III.2.1.

Experimental procedure

The EF apparatus was fixed onto a 1L chemical glass containing 800ml of kaolin suspension, the electrodes submerged in the suspension. A current was applied for various time intervals (3, 6 and 10 minutes) at the end of which samples were analyzed (for pH, size distribution, ζ potential and image analysis). The complete dose of aluminum was achieved at 10 minutes, for each applied current, after which additional aluminum was not introduced into solution. At this stage samples underwent continuous mixing and measurements were taken at two more time intervals: 15 and 20 minutes. For all size distribution measurements, the Malvern Microplus was operated at a gentle pump speed of 400, so to minimize disruption of floc structure. The EF cell was operated in galvanostatic mode: the current was set and the potential found its own value dependent on the system's overall resistance. This ensured coagulant production at a predetermined rate, defined by Faraday's law. The currents used for the experiments were 0.042A, 0.11A and 0.22A, yielding aluminum doses of 2.43mg/l, 6.48mg/l and 12.96mg/l respectively. These doses are equivalent to aluminum content in 30mg/l, 80 mg/l and 160 mg/l commercial alum (8.1% of the total molecule). Current densities were altered by using different anode sizes. These are summarized in table 6.

Table 6 Current densities used for experiments.

Current applied	Current density (full anode)	Current density (1/4 anode)
0.042A	0.197mA/cm^{2}a	0.788mA/cm^2
0.11A	0.516mA/cm^2	2.062mA/cm^2
0.22A	1.031mA/cm^2	4.125mA/cm^2

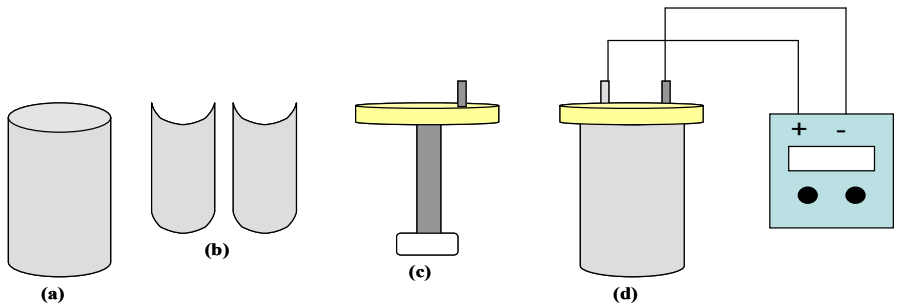

Fig. 13 Components of the EF batch cell: a. Full aluminum anode (213.3cm^2) b. 2 aluminum anodes, 1/4 total area of full anode (53.33cm^2) c. Stainless steel cathode fitted onto magnetic stirrer arm and attached to plexyglass cap d. Complete EF apparatus fixed onto a 1L chemical glass and connected to DC power supply.

Alum dosing

To create conditions in which alum dosing could be compared to the dosing regime in EF, alum was added to the suspension for identical time intervals as current operation in the EF unit (3, 6 and 10 minutes) at the end of which samples were analyzed (for pH, size distribution, ζ potential and image analysis). The complete alum dose was achieved at 10 minutes, and from this stage onwards samples underwent continuous mixing and measurements were taken at two more time intervals: 15 and 20 minutes.

A stock solution of 10,000ppm commercial alum ($Al_2(SO_4)_3 \cdot 18H_2O$) was prepared, and additive dosing was performed using a syringe pump (*74900 series, Cole- Parmer*). The preset dosing rates used were 0.24ml/min, 0.64ml/min and 1.28ml/min to achieve final doses of 30mg/l, 80mg/l and 160mg/l respectively.

III.2.3 EF as pretreatment to membrane ultrafiltration

Colloidal suspension

0.3gr of kaolin ($AlSi_2O_5(OH)_4$, *Aldrich Chemical Company Inc. USA*) was suspended in 20 liters of distilled water (15mg/l final concentration) and homogenized using an *Ultraturax 2000, Ganke and Kunkel, GMBH*. 1.66gr of $NaHCO_3$ (*BDH Laboratory Suppliers, England*) was added (final concentration 83mg/l), the pH was corrected to 5, 6.5 and 8, with NaOH or H_2SO_4, and conductivity was increased to 1mS/cm with $NaNO_3$ (*Riedel-Dehaen*, *GMBH*).

EF unit

The EF unit was a batch cell comprised of two flat sheet electrodes (an aluminum anode and stainless steel cathode), with an active area of 9cm^2, which were immersed in the treated suspension, and connected to an external DC power supply. The cell was run at constant current (range used was 0.06A-0.2A), for a fixed 7 minutes dosing period, and the doses were equivalent to 2.43mg/l, 6.48mg/l and 12.96mg/l aluminum, respectively.

Membranes

The ultrafiltration membranes used in this study were hydrophilic Polyethersulfone flat sheet membranes manufactured by *Microdyn-Nadir* (Germany), with a nominal molecular weight cut-off of 50kDa, and pure water flux > 250l/m^{2}h. Prior to use the membranes were soaked for 12 hours in distilled water purified with reverse osmosis.

Ultrafiltration test unit

A schematic diagram of the laboratory-scale membrane test unit is shown in figure 14. The membrane filtration unit was comprised of a nitrogen gas cylinder, which maintained a

constant pressure of 3 bars throughout the unit. A polypropylene feed reservoir, with a volume of 1250ml, held the colloidal suspension prior to the membrane module. The membrane module, made from polypropylene, was operated as a stirred cell. It contained an internal magnetic stirrer bar suspended close to the upper surface of the membrane with motion induced by a magnetic stirrer table placed beneath it. A flat disc membrane with an area of 11.3cm^2 was held in place with an O-ring. The permeate was collected in a chemical glass mounted onto an electronic balance (*Sartorius max 3100gr*), which was connected to a computer containing software that calculated the permeate flux from permeate weight accumulation.

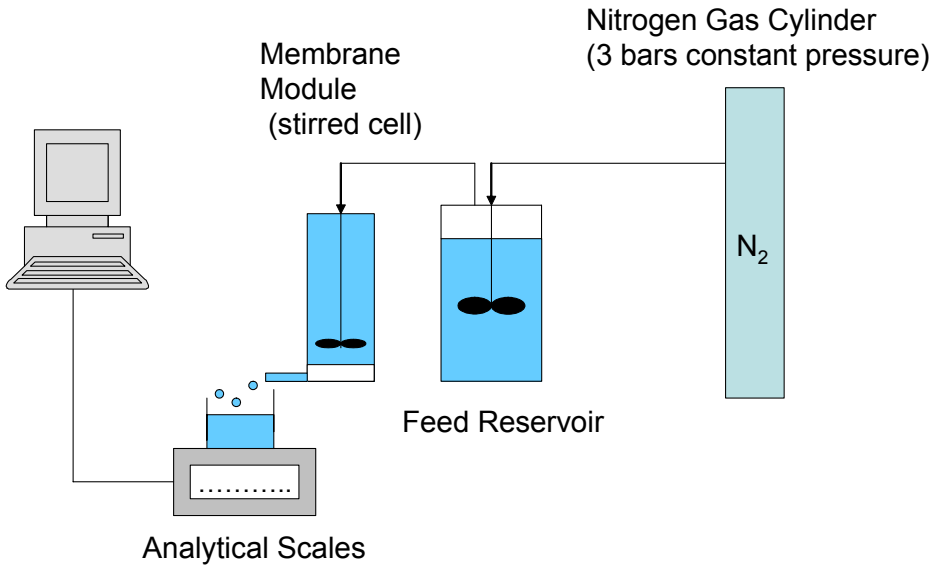

Fig. 14 Schematic diagram of the membrane test unit

Particle size analysis

As specified in section III.2.1.

ζ potential

As specified in section III.2.1.

Cake characterization

Membranes exhibiting cake formation were dried (at room temperature) and photographed using scanning electronic microscopy (*SEM, Joel-JSM-5600*).

Aluminum measurements

Residual aluminum in the permeate was measured using ICP (*Inductively Coupled Plasma, Cole-Parmer).*

Experimental procedure

1 liter of the kaolin suspension underwent electroflocculation for 7 minutes, in a rapid mix regime (using magnetic stirrer at 120 rpm), and then was transferred to a jar test apparatus (*Phipps and Bird, USA*) for an additional 20 minutes slow mixing (30 rpm). Samples were taken from the flocculated suspension for particle characterization (particle size distribution and ζ potential), before filtering through the membrane unit. The flux was measured through the membrane, at room temperature (~20^{o}C) at constant pressure (3 bars) over a 25 minute time span.

III. 3 Results and Discussion

III.3.1 Characteristics of an electroflocculated kaolin suspension

III.3.1.1 Changes in ζ potential and pH

The current applied in the EF process has a double effect, by both generating the coagulant species and by causing hydrolysis in which excess hydroxyl ions are formed at the cathode, resulting in an increase in pH. In these dynamic conditions, coagulation mechanisms shift, depending on the current applied. The shift in pH and consequent shifting speciation of aluminum mononuclear complexes causes the ζ potential of the electroflocculated suspensions to change. Figure 15 shows the change in ζ potential and pH as a function of applied current for a 15mg/l kaolin suspension at two different initial pH values: 5 and 6.5. The ζ potentials of the kaolin suspensions, without applying any current, were: -17.9mV and -21.7mV for pH 5 and 6.5 respectively.

The ζ potential depends on the potential at the surface of the particle and the composition of the Stern layer. It is an indirect measurement of the charge on particles, and its value determines the extent of the electrostatic forces of repulsion between charged particles. For coagulants such as hydrolyzed aluminum ions, as in this case, specific adsorption is dominant and generally caused by coagulant-colloid interactions. They bind to specific sites on the colloid surface and by doing so neutralize the electrostatic surface charge of the colloid.

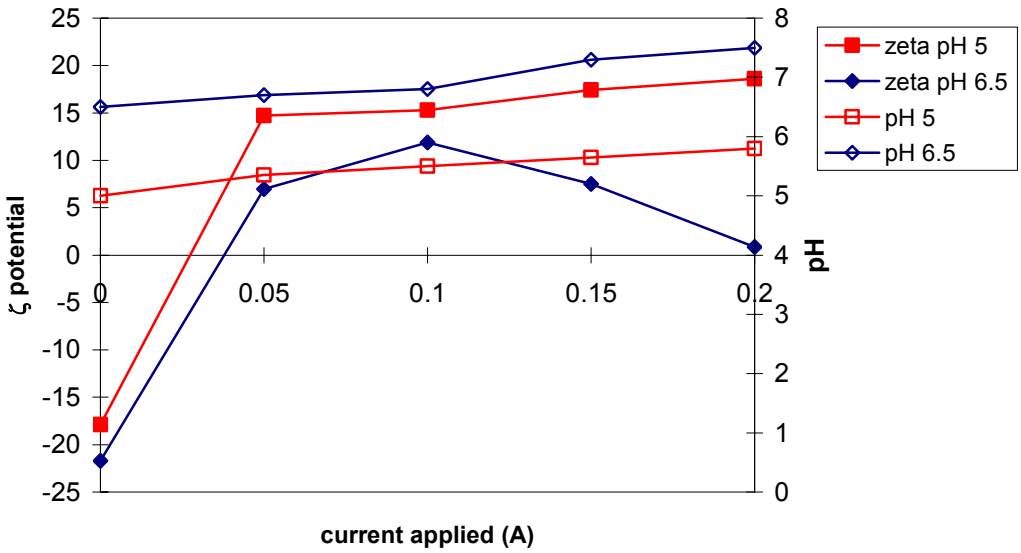

Fig. 15 Change in ζ potential vs. applied current for initial pH 5 and 6.5. C_{kaolin}=15mg/l, conductivity=1mS/cm, $t_{dosing+mixing}$=6min, G=30sec^{-1}

At pH 5 the governing aluminum mononuclear species in solution are Al^{+3} and $Al(OH)^{2+}$ (Duan and Gregory, 2003), and it is assumed that dominant coagulation mechanism is adsorption and charge neutralization. Therefore, the ζ potential of the suspension under these conditions becomes more positive as a function if the applied current, until stabilizing at +17mV, for an applied current of 0.1A and above (within the measured range). At 0.1A, the pH rises to 5.7 and conditions become favorable for aluminum hydroxide precipitation (transition *into* "sweep-floc"). Aluminum hydroxide is charged positively below its i.e.p (between pH 8-9), and therefore in the precipitation zone, the ζ potential stabilizes at a positive value. Increased aluminum hydroxide precipitation stabilizes the pH due to the removal of the excess hydroxyl ions from solution. This coagulation mechanism combines both destabilization and transport processes.

At pH 6.5 the governing coagulation mechanism is "sweep-floc", as at this pH formation of amorphous aluminum hydroxide is considered optimal. At this pH other positive mononuclear species, Al^{+3} and $Al(OH)^{2+}$, are also present, although in reduced amounts. These contribute to the charge neutralization and ultimately charge reversal, indicated by the change in ζ potential towards more positive values, reaching a maximum of +12mV, at 0.1A (fig. 15). At currents higher than 0.1A, a drop in the ζ potential occurs, and its value becomes less positive. At 0.2A, at a final pH of 7.5, the ζ potential reaches an iso-electric point (i.e.p), due to the presence of negative mononuclear species which counteract the effect of the positive species in solution. At 0.1A, the pH is 6.8. At currents above this the pH increases even more

and speciation shifts towards the aluminate ion, $Al(OH)_4^-$ - indicated by the less positive ζ potential.

III.3.1.2 Effect of mixing conditions in EF process

Adequate mixing conditions are required for optimal aggregation: to disperse the coagulant homogenously and to create collisions between particles. If the particles are submicron in size Brownian motion is appreciable, however as the particles grow into larger aggregates, other transport mechanisms become dominant. The applied velocity gradient (G) plays a major role in flocculation mechanisms, as it represents the shear rate in a mechanically agitated system. In the EF process the applied velocity gradient also affects the coagulation mechanisms, as it helps control the pH of the treated suspension and ultimately aluminum hydroxide precipitation. Experiments were conducted at pH 5, without applying a velocity gradient ($G=0sec^{-1}$) and these produced suspensions with a higher final pH, than those treated applying a velocity gradient (fig. 16).

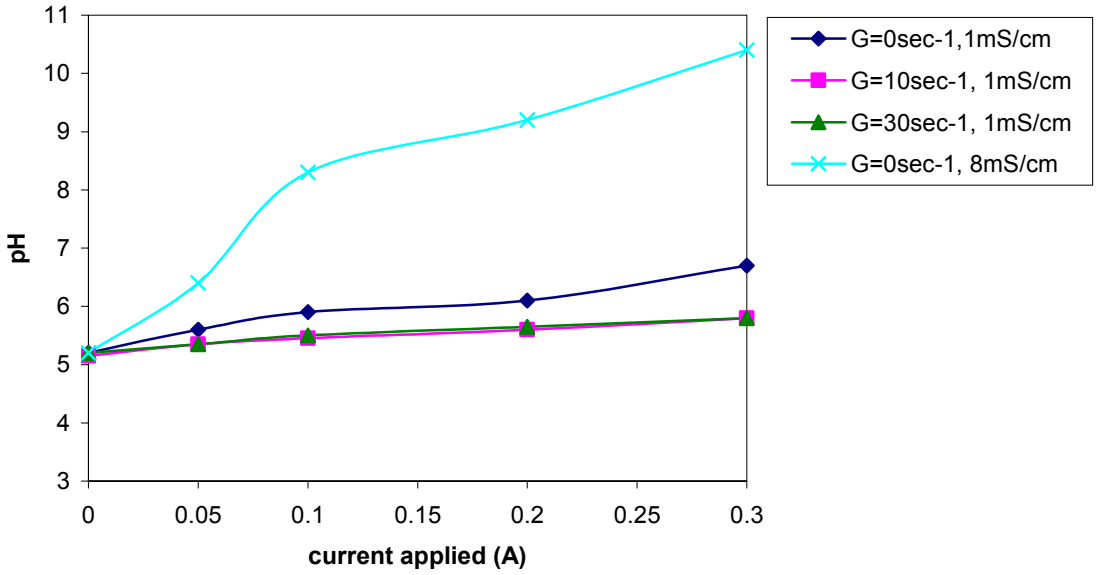

Fig. 16 Change in pH vs. applied current, for varying velocity gradients. C_{kaolin}=15mg/l, conductivity=1mS/cm, 8mS/cm, $t_{dosing+mixing}$=6min, initial pH 5.

For conductivity values of 1mS/cm, and velocity gradients of both $10sec^{-1}$ and $30sec^{-1}$ a similar result is obtained, the final pH not exceeding 6, for the maximum current used, 0.3A. However, the pH rises to 6.6, when a velocity gradient is not applied ($G=0sec^{-1}$). For experiments conducted with suspensions with high conductivity values (8mS/cm), the rise in

pH was even more substantial for G=0sec^{-1}, reaching 10.1 at 0.3A, for a suspension at initial pH 5. Applying a velocity gradient (G=10sec^{-1} and G=30sec^{-1}) did lower the pH to similar values shown in fig.16 for 1mS/cm suspensions. The significant increase in pH for high conductivity suspensions, when mixing conditions aren't imposed, is most likely due to a screening affect other charged particles produce when in high concentration in solution. The transport of ions, when mixing is not induced, is via diffusion. If other ions are present in large concentrations, the aluminum produced at the anode and the hydroxyl ions produced at the cathode won't be able to come in contact efficiently, because a dense barrier of other ions exists between them. Mixing "breaks" this barrier and enables efficient contact, thus resulting in aluminum hydroxide precipitation and a lower final pH.

The application of a velocity gradient does not only affect primary kaolin particle collisions, but also collisions between Al^{+3} and hydroxyl ions which result in aluminum hydroxide precipitation as colloidal matter - this is a key factor in maintaining a relatively stable pH throughout the EF process. Moreover, enhanced precipitation induces sweep floc coagulation which generally gives considerably improved particle removal as opposed to aggregation via charge neutralization alone. This can be explained by the greatly improved rate of aggregation, due to the increased solids concentration. The effect of mixing conditions on aluminum hydroxide precipitation has been studied in some detail by Clark et al. (1993) who showed that there is a competition between the formation of aluminum hydrolysis products and precipitated solid. With more intense mixing, the results indicated that precipitation would be favored.

III.3.1.3 Aggregates formed in EF

Morphological characterization of suspended aggregates is a microscopic technique which is complementary to macroscopic methods for characterizing flocculated suspensions. Image analysis was used to morphologically characterize the resulting aggregates (i.e. primary kaolin particles vs. aluminum hydroxide floc) and for quantifying their structure using a two-dimensional fractal dimension (D_2).

III.3.1.3.1 Morphology

Figure 17 shows types of aggregates and flocs obtained after EF (magnification x10).

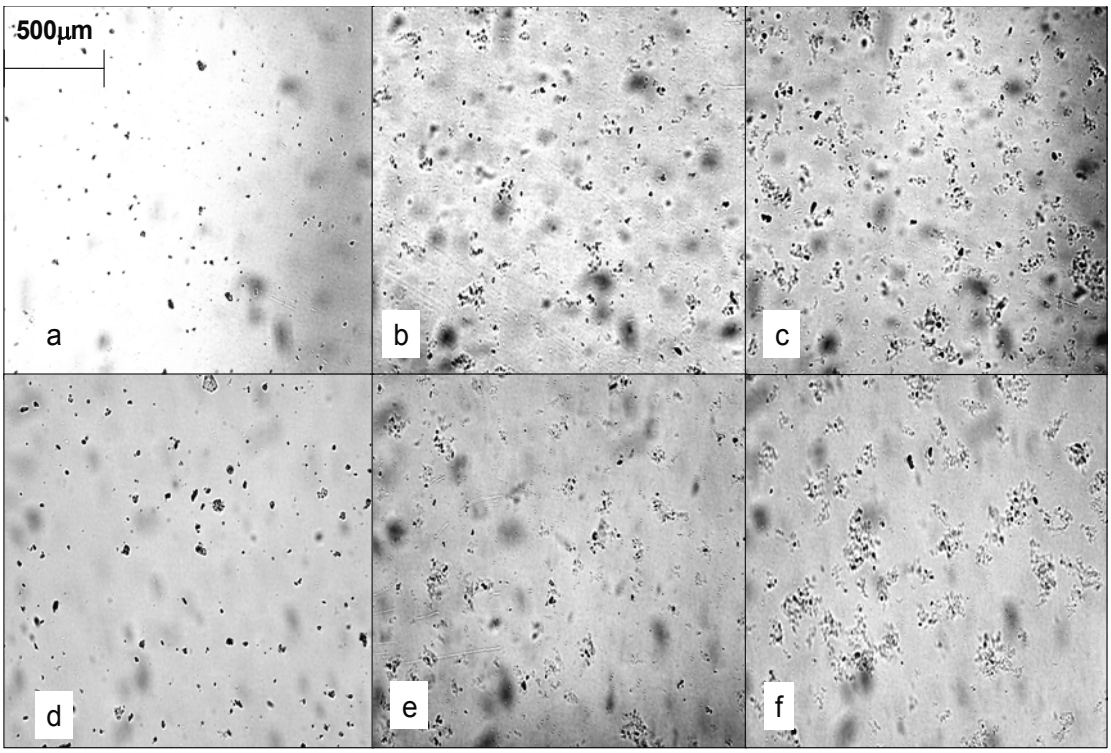

Fig. 17 C_{kaolin}=15mg/l, $t_{dosing+mixing}$=6min a. **pH 5, 1mS/cm, 0A, G=0sec^{-1}** b. **pH 5, 1mS/cm, 0.05A, G=30sec^{-1}** c. **pH 5, 1mS/cm, 0.1A, G=30sec^{-1}** d. **pH 5, 8mS/cm, 0.1A, G=0sec^{-1}** e. **pH 5, 8mS/cm, 0.1A, G=10sec^{-1}** f. **pH 5, 8mS/cm, 0.3A, G=10sec^{-1}**

The visible data shows distinct differences between aggregates, both in morphology and in size, obtained under different EF conditions. In general, a difference is evident between kaolin aggregates and aluminum hydroxide flocs. The former has a dense, compact structure, and the latter a more open, loose structure. Under control conditions, without applying current or velocity gradient (a.), the primary kaolin particles appear dispersed. Some minor aggregation of primary kaolin particles has occurred (indicated by larger black clusters). This can probably be explained by a degree of Brownian diffusion occurring, coupled with double layer compression (Verwey and Overbeek, 1948) promoted by the addition of electrolyte ($NaNO_3$) to achieve adequate conductivity values (minimum 1mS/cm) for operation of the EF cell. Applying a current and velocity gradient induces flocculation which results in precipitation of aluminum hydroxide and formation of flocs which enmesh the primary kaolin particles. These flocs increase in size as the current increases (b. and c.). At initial pH 5, raising the current shifts the coagulation mechanism from adsorption and charge neutralization more towards sweep-floc, because the pH shifts to values which favor precipitation. Under these conditions, a higher current will increase precipitation and consequently larger flocs will form. For higher conductivity values (8mS/cm), significant

kaolin aggregation occurs, and no aluminum hydroxide precipitation is observed, when a current is applied alone (d.), without applying a velocity gradient. The high level of electrolyte in solution, coupled with the aluminum dose has most likely lowered the repulsion barrier between primary particles, and enabled aggregation. Some aggregates observed are large in size (up to 50μm), and considering the time span of the experiments, it is unlikely Brownian diffusion is the primary transport mechanism. This raises questions regarding the effect of the electric field on particle transport in the EF process, which could explain the enhanced kaolin aggregation without applying a velocity gradient. For high conductivity values, when both current and velocity gradient are applied, similar results to those at lower conductivity values are obtained, and increased precipitation is observed (e. and f.). At pH 6.5, for all currents, with application of a velocity gradient, precipitation was observed. Moreover, floc size increased with current increase. At pH 6.5, the dominant coagulation mechanism is sweep-floc, for all currents applied. Although speciation shifts towards negative mononuclear species at the higher currents (0.2A, 0.3A produce a final pH of 7.3 and 7.5 respectively), increased precipitation occurs at the beginning of the process, due to the large amount of Al^{+3} introduced into solution. Despite the existence of negative mononuclear species at the end of the process, their effect on coagulation is negligible, because aluminum hydroxide flocs have already formed extensively.

III.3.1.3.2 Fractal dimension

The fractal dimension of aggregates/flocs in the experiments was based on imaging, and therefore is two-dimensional and is referred to as D_2.

The fractal dimension was used to quantify aggregate/floc structure, and subsequently served as a mathematical parameter for tracking differences between aggregates formed in different experiments, resulting from varying operational parameters, such as applied current (Al^{+3} dose), current density, pH, conductivity and G. Table 7 summarizes the results.

The values obtained without applying a velocity are similar for most experiments, and are between 1.60 ± 0.06 and 1.70 ± 0.08. These are representative of kaolin aggregation, in a dilute electrolyte, as in these conditions aluminum hydroxide precipitation is limited as no mixing is induced. However, at pH 6.5 and 0.3A, the D_2 calculated is low compared to these values – 1.50 ± 0.04. This can be explained by the fact that the high Al^{+3} dosage and pH have created some degree of precipitation, despite absent mixing conditions. This is probably via diffusion, as large amounts of Al^{+3} and OH^- ions are created in these conditions. The more open and loose structure which characterize aluminum hydroxide flocs, as opposed to kaolin aggregates, is the reason for the lower average D_2. In general, a trend is observed in which D_2

decreases as the current increases, when a velocity gradient is applied, although differences obtained from 0.05A and above are not significant.

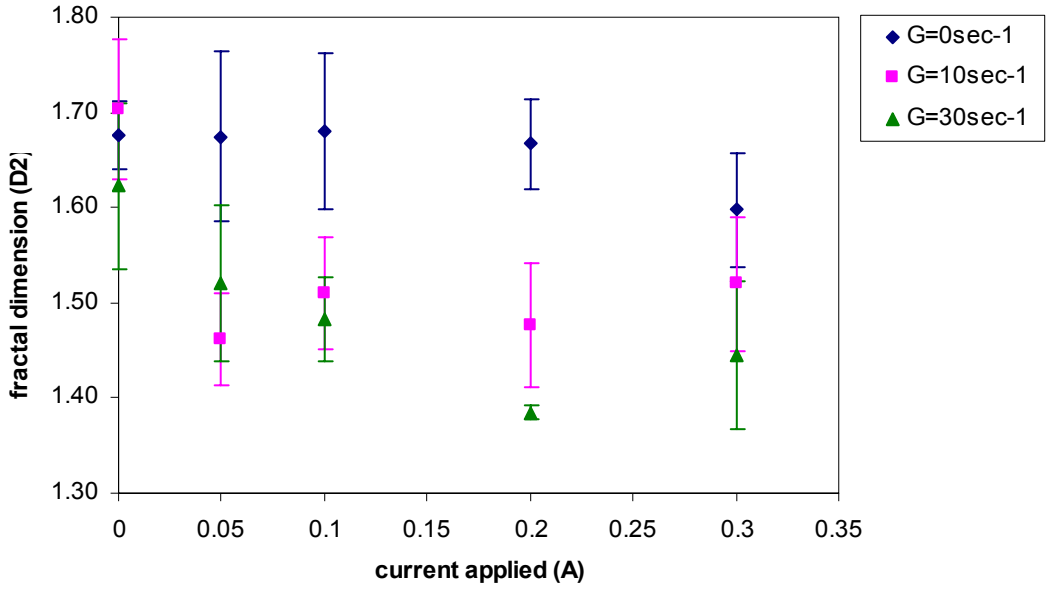

Fig. 18 Fractal dimension, D_2, vs. current intensity, for different G values, C_{kaolin}=15mg/l, $t_{dosing+mixing}$=6min, pH 5, conductivity=1mS/cm. Error bars represent one standard deviation.

Moreover, t-tests comparing D_2 values obtained for different currents between sets (i.e. different currents at same G), both at pH 5 and 6.5, indicated that these differences are indeed not appreciable (P>0.05). Figure 18 shows the differences in D_2 obtained at pH 5, as a function of applied current and velocity gradient.

D_2 for all currents applied, in the absence of mixing conditions, does not significantly change, and is between 1.60±0.06 and 1.68±0.09. Application of a velocity gradient does lower the resulting average D_2, because mixing induces aluminum hydroxide precipitation and floc formation. There is not an appreciable difference (based on t-tests) between D_2 values, when applying a velocity gradient, for all currents. Therefore, the resulting D_2 values for G=10sec^{-1} or G=30sec^{-1} are considered similar. For a doubled dosing period (2 min), there appears to be a more distinct difference between D_2 values obtained for different currents. For currents of 0.025A and 0.15A, and G=10sec^{-1}, the resulting D_2 values were 1.51±0.04 and 1.43±0.06, respectively. Therefore, for an increased dosing period (2 min), lower currents produced higher D_2 values, than for higher currents. When comparing current densities, for 1min and 2 min dosing, no significant differences are observed. For different current densities and identical doses, a trend is observed, at higher dosage levels: lower current densities produced lower D_2 values. To achieve equivalent doses using half current densities, a doubled dosing

period was required. In these conditions, despite the lowered dissolution rate of Al^{+3} ions (mg/sec), the ions first dissolved have a longer effective time to react in solution. This could lead to better growth and consequently larger flocs exhibiting lower D_2 values.

Table 7 Average two-dimensional (D_2) fractal dimensions obtained for different operational parameters.

Current (A)	Al^{+3} Dose (mg/l)	Current Density (mA/cm^2)	G (sec^{-1})	Conduct. (mS/cm)	T_{dose} (min)	pH	Ave. Fractal Dimension (D_2)	Standard Deviation
0	0	0	0	1	1	5	1.68	0.04
			10				1.70	0.07
			30				1.62	0.09
0.05	4	1.6	0	1	1	5	1.68	0.09
			10				1.46	0.05
			30				1.52	0.08
0.1	8	3.2	0	1	1	5	1.68	0.08
			10				1.51	0.06
			30				1.48	0.04
0.2	16	6.4	0	1	1	5	1.67	0.05
			10				1.48	0.07
			30				1.39	0.01
0.3	24	9.6	0	1	1	5	1.60	0.06
			10				1.52	0.07
			30				1.45	0.08
0	0	0	0	1	1	6.5	1.64	0.07
			10				1.64	0.05
			30				1.63	0.07
0.05	4	1.6	0	1	1	6.5	1.65	0.11
			10				1.57	0.09
			30				1.48	0.03
0.1	8	3.2	0	1	1	6.5	1.67	0.07
			10				1.49	0.04
			30				1.48	0.05
0.2	16	6.4	0	1	1	6.5	1.68	0.04
			10				1.51	0.05
			30				1.45	0.04
0.3	24	9.6	0	1	1	6.5	1.50	0.04
			10				1.48	0.06
			30				1.51	0.04
0.025	4	0.8	10	1	2	5	1.51	0.04
			30				1.50	0.06
0.05	8	1.6	10	1	2	5	1.48	0.07
			30				1.46	0.05
0.1	16	3.2	10	1	2	5	1.47	0.05
			30				1.44	0.04
0.15	24	4.8	10	1	2	5	1.43	0.06
			30				1.41	0.05
0	0	0	0	8	1	5	1.66	0.09
			10				1.59	0.07
			30				1.67	0.05
0.05	4	1.6	0	8	1	5	1.70	0.08
			10				1.50	0.06
			30				1.51	0.05
0.1	8	3.2	0	8	1	5	1.65	0.04
			10				1.47	0.07
			30				1.46	0.05
0.2	16	6.4	0	8	1	5	1.61	0.08
			10				1.46	0.04
			30				1.43	0.07
0.3	24	9.6	0	8	1	5	1.65	0.06
			10				1.48	0.03
			30				1.42	0.1

When comparing D_2 values obtained from suspensions with different conductivities (1mS/cm vs. 8mS/cm), some differences are observed for 0.1A and 0.2A, when a velocity gradient was not applied ($G=0sec^{-1}$). Figure 19 shows the shows the differences in D_2 obtained at pH 5, for different conductivities, as a function of applied current, with and without applying a velocity gradient.

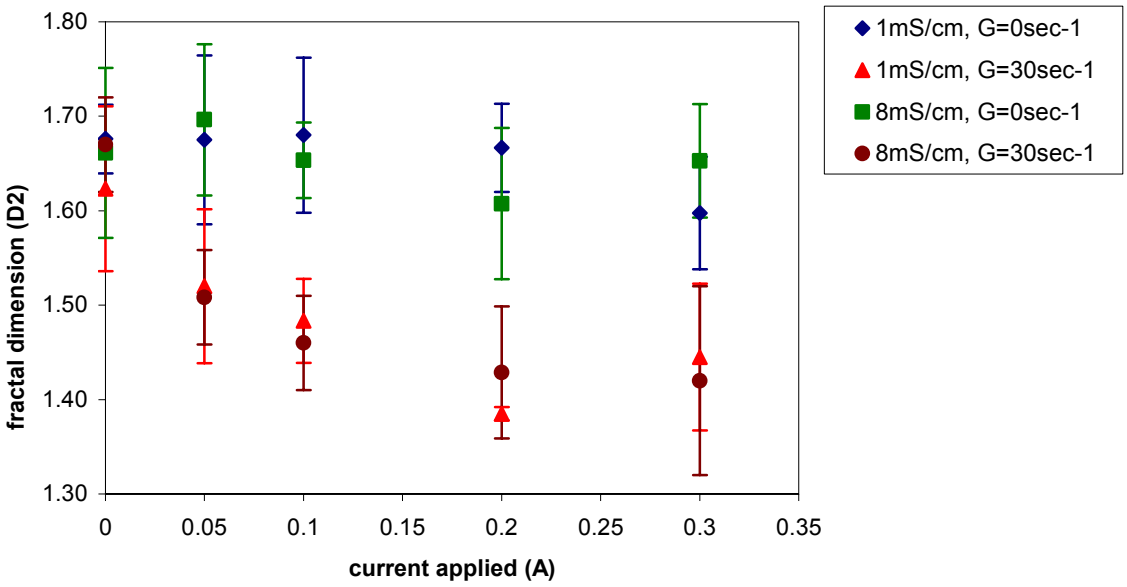

Fig. 19 Fractal dimension, D_2, vs. current intensity, for $G=0sec^{-1}$ and

$30sec^{-1}$, C_{kaolin}=15mg/l, $t_{dosing+mixing}$=6min, pH 5, 1mS/cm and 8mS/cm. Error bars represent one standard deviation.

The differences in D_2, between 1mS/cm and 8mS/cm, obtained for $G=0sec^{-1}$ and currents of 0.1A and 0.2A are directly related to the morphology of the kaolin aggregates, which do form even though a velocity gradient was not applied. The average D_2 obtained under these conditions is lower for 8mS/cm than for 1mS/cm. T-tests, comparing D_2 values obtained for same currents between sets (i.e. comparing 0.1A at 1mS/cm and 8mS/cm, at constant G), yielded probability values which indicated that differences could not be significant. However, one cannot ignore the images obtained under these conditions which show distinct differences in kaolin aggregation, as a function of conductivity. This underlines the advantage of using image analysis techniques as a complementary technique to other macro techniques, for verifying the true nature of aggregates and flocs formed. Figure 20 shows the differences between images obtained after EF of suspensions with different conductivities (magnification ×10).

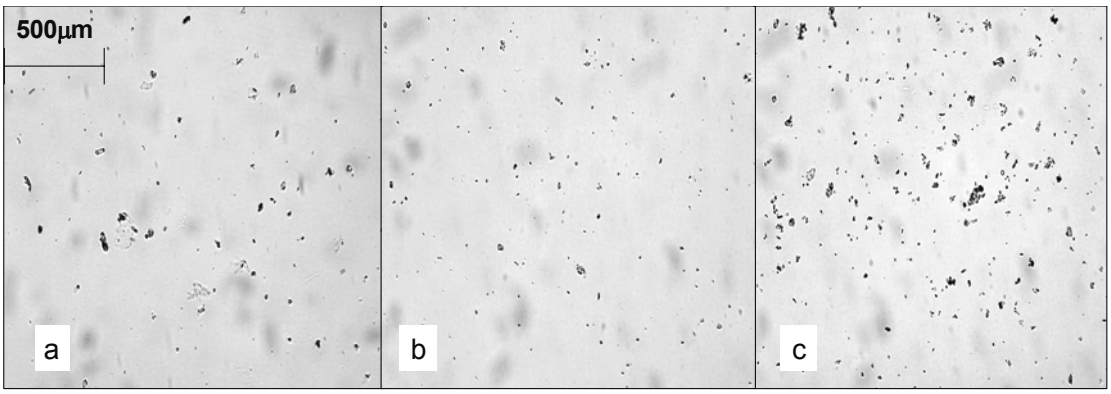

Fig. 20 C_{kaolin}=15mg/l, $t_{dosing+mixing}$=6min a. **pH 5, 1mS/cm, 0.1A, G=0sec^{-1}** b. **pH 5, 8mS/cm, 0.05A, G=0sec^{-1}** c. **pH 5, 8mS/cm, 0.1A, G=0sec^{-1}**

The images indicate that for higher conductivity values (8mS/cm), significant kaolin aggregation occurs, when a current is applied alone, without inducing mixing conditions. Minor aluminum hydroxide precipitation is observed, but evidently not sufficient to promote growth of flocs. The high level of electrolyte in solution, at 8mS/cm, coupled with an adequate aluminum dose (0.1A) has promoted flocculation via double layer compression and/or adsorption and charge neutralization. However, the size of the resulting aggregates (some up to 50μm) and the relatively short time span of the experiments (6 minutes total), pose questions regarding the primary transport mechanism which has enabled aggregation in these conditions – without inducing mixing conditions. Brownian diffusion exists, but it is unlikely it serves as the sole transport mechanism, enabling aggregation into large aggregates, within a short period of time. In EF, an electric field is induced, while the current passes through the cell. This could enhance particle transport, although in addition bubble formation could also serve as a supplementary mixing mechanism which would explain the enhanced kaolin aggregation occurring without application of a velocity gradient. For 8mS/cm, when both current and velocity gradient are applied, transport via diffusion becomes negligible and similar D_2 results to those at lower conductivity values are obtained as increased precipitation is observed.

Little literature exists on D_2 values of resulting aggregates/flocs in flocculation processes using alum; none exists on aggregates/flocs formed in EF. Gorczyca and Ganczarczyk (1996) reported D_2 values for alum flocs formed in inorganic clay and mineral suspensions to be between 1.71 and 1.97 ($\pm$0.05). Li and Ganczarczyk (1989) calculated fractal dimensions of alum flocs to be between 1.59 and 1.97, from measurements conducted by Tambo and Watanabe (1979). Chakraborti et al. (2003) found the D_2 values of flocs formed by flocculation of latex particles with alum to be between 1.94$\pm$0.18 and 1.48$\pm$0.08, depending

on alum dose, shear rate, and observation times. Although some D_2 values of aggregates/flocs formed in the EF process fall within the ranges reported by authors, in general the values obtained after EF are within the lower range. The unique physical-chemical conditions in EF, which differ from those created in conventional flocculation, affect coagulation/flocculation mechanisms and consequently the morphology of the resulting aggregates/flocs.

III.3.1.3.3 Particle size distribution

Particle size distribution analysis was carried out as a complementary procedure to image analysis, to maximize data on aggregate/floc formation in the EF process, and examine a connection between the fractal dimensions calculated and floc/aggregate size. From particle distribution measurements, a correlation can be observed between the D_2 and size. Figure 21 shows the undersize frequency % of sizes obtained at different currents (and densities) and dosing times.

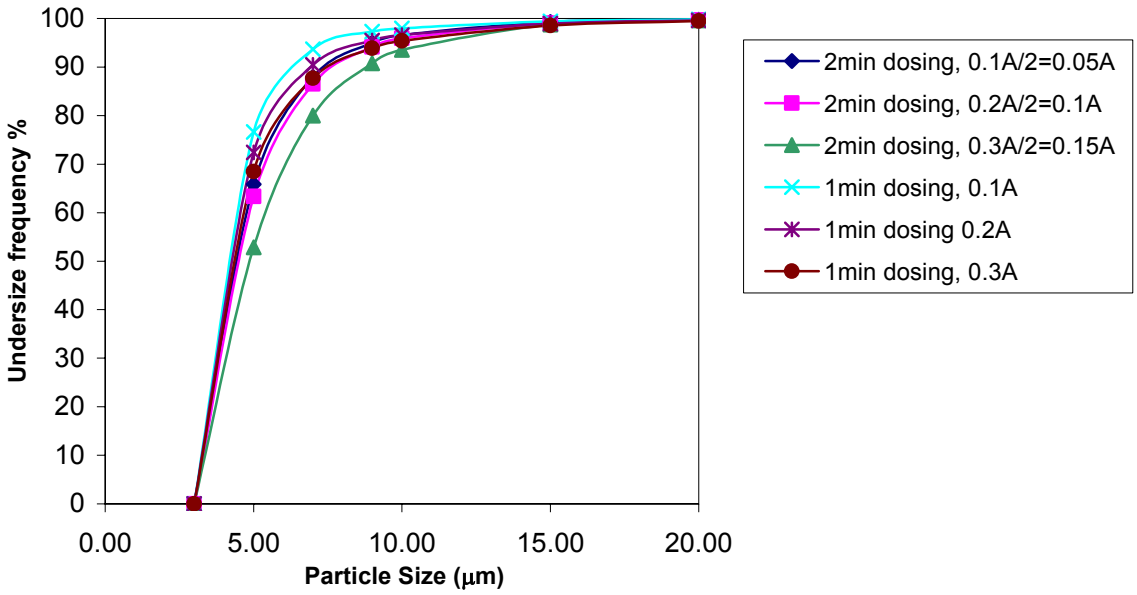

Fig. 21 Undersize frequency %, C_{kaolin}=15mg/l, pH 5, 1mS/cm, G=30sec^{-1}, varying currents (densities) and dosing times.

For 0.05A and 0.15A, a dosing period of 2 minutes, and G=30sec^{-1}, D_2 values were 1.46±0.05 and 1.41±0.05, respectively, although these differences are not considered significant. Particle size distributions show that for 0.15A, larger particles are obtained than for 0.05A. Thus, a trend can be detected in which lower D_2 values correspond to larger particle sizes. When comparing current densities, for equal total doses, a similar trend is observed. For a current density of 1.6mA/cm^2, 2 minutes dosing, the resulting D_2 value is 1.46±0.05. For 3.2mA/cm^2, 1 minute dosing, the average D_2 is 1.48±0.04. Particle counts show that higher current

densities (shorter dosing periods) produce smaller sizes, which correspond to higher D_2 values.

When observing particles counts conducted on suspensions with different conductivities, without the application of a velocity gradient, the same trend is observed: larger particles produce smaller D_2 values. Figure 22 shows the undersize frequency % of sizes obtained at different currents for suspensions with different conductivities.

For 0.2A, larger particles are observed at 8mS/cm than at 1mS/cm. In these conditions, the corresponding D_2 values were 1.61 ± 0.08 and 1.67 ± 0.05, respectively. Although the differences in average D_2 obtained for different conductivities are not considered significant, a correlation is observed, which also corresponds to image analysis results.

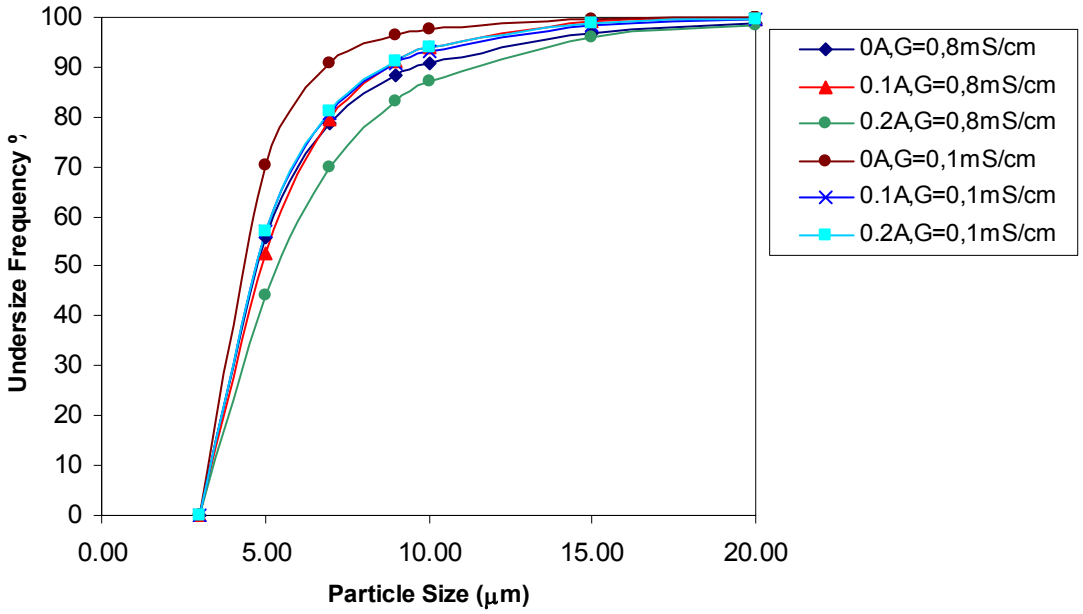

Fig. 22 Undersize frequency %, C_{kaolin}=15mg/l, $t_{dosing+mixing}$=6min, pH 5, conductivity=1mS/cm and 8mS/cm, G=0sec^{-1}

The connection between floc size and fractal dimension is typical of forming aggregates (Spicer and Pratsinis 1996; Kusters et al., 1997; Chakraborti 2003). Aggregation models, which have been used to calculate theoretical fractal dimensions of aggregates are based on the assumption that primary particles are solid and have a fractal dimension of Euclidean value (i.e. D_2=2). In this case, as clusters begin to form, and aggregates grow, the fractal dimension will decrease as size increases, until a point where the aggregates are sufficiently large in comparison to the primary particles that comprise it (Meakin, 1988). At this point, any other addition of particles will not have an affect on structure, and the fractal dimension

will not change. However, in real water systems, primary particles are not necessarily solid and in orthokinetic flocculation shear forces must be acknowledged as a limiting growth factor which can also affect the final structure, due to fragmentation and restructuring (Clark and Flora, 1991; Selmoulya, 2003).

III.3.2 Size and structure evolution of kaolin-$Al(OH)_3$ flocs in EF

III.3.2.1 Size distributions and solution changes over time

The initial stages of floc growth in the EF process were examined. Unlike conventional flocculation, in EF the aluminum dosing is additive over time (until the current is stopped) while simultaneously generating hydroxyl ions. Aluminum super-saturation leading to aluminum hydroxide precipitation depends primarily on aluminum dose and pH (Sposito, 1996) and therefore in the initial stages of EF, mass is continuously being added to the system, as dosing continues and the pH rises. The employed initial pH values were chosen to cover the pH range in which aluminum hydroxide precipitation would occur and floc evolution could be measurable. At pH 8 no significant floc formation was observed, hence results refer to pH 5 and 6.5. Figure 23 shows the evolution of size distributions over time for currents of 0.042A and 0.22A (maximum anode area), at initial pH 5 and 6.5. The size distribution graphs show the evolution of size over time, with modal diameters at the end of the process reaching above 200μm, with the spread reaching the upper detection limit of the instrument. For 0.042A, the growth appears similar for the initial 3 minutes of the process, for both pH values, while after 6 minutes, at pH 6.5 it is accelerated, resulting in a wider distribution spread. This behavior is also evident for 0.22A - the initial 3 minutes show similar size distributions after which at pH 6.5 an accelerated growth rate is observed. The initial 3 minutes appear to be an induction period, in which the aluminum hydroxide precursor particles are developing into sizes which will lead to enhanced aggregation as the process progresses. This period is considerably shorter for 0.22A and pH 6.5, as after only 3 minutes sizes as large as 100μm are already observed. The size distributions indicate that while growth into larger floc is occurring, smaller particles are simultaneously being formed, and thus a wider distribution spread. For 0.042A and pH 5 the size distribution narrows after 15 minutes, whereas at pH 6.5 after 10 minutes. For 0.22A, this occurs at pH 5 and 6.5, after 10 and 6 minutes respectively. Although colloidal particles of aluminum hydroxide are continuously being formed until the current is stopped, at 10 minutes, their presence in solution, as colloidal matter, depends on contact opportunities. A higher number of particles would increase the number of collisions, leading to formation of larger particles and providing additional contact opportunities for the submicron particles (Chowdhury et al., 1991). At pH

6.5 precipitation of aluminum hydroxide is considered optimal, therefore larger amounts of precursor particles are formed and for both currents, at this pH a more rapid growth rate is observed. For higher currents (0.22A) a significantly shorter induction period is observed. The higher growth rate observed for 0.22A, is due to increased dosage of aluminum, which will increase at this pH the precipitation of aluminum hydroxide, resulting in larger amounts of aluminum hydroxide precursor particles.

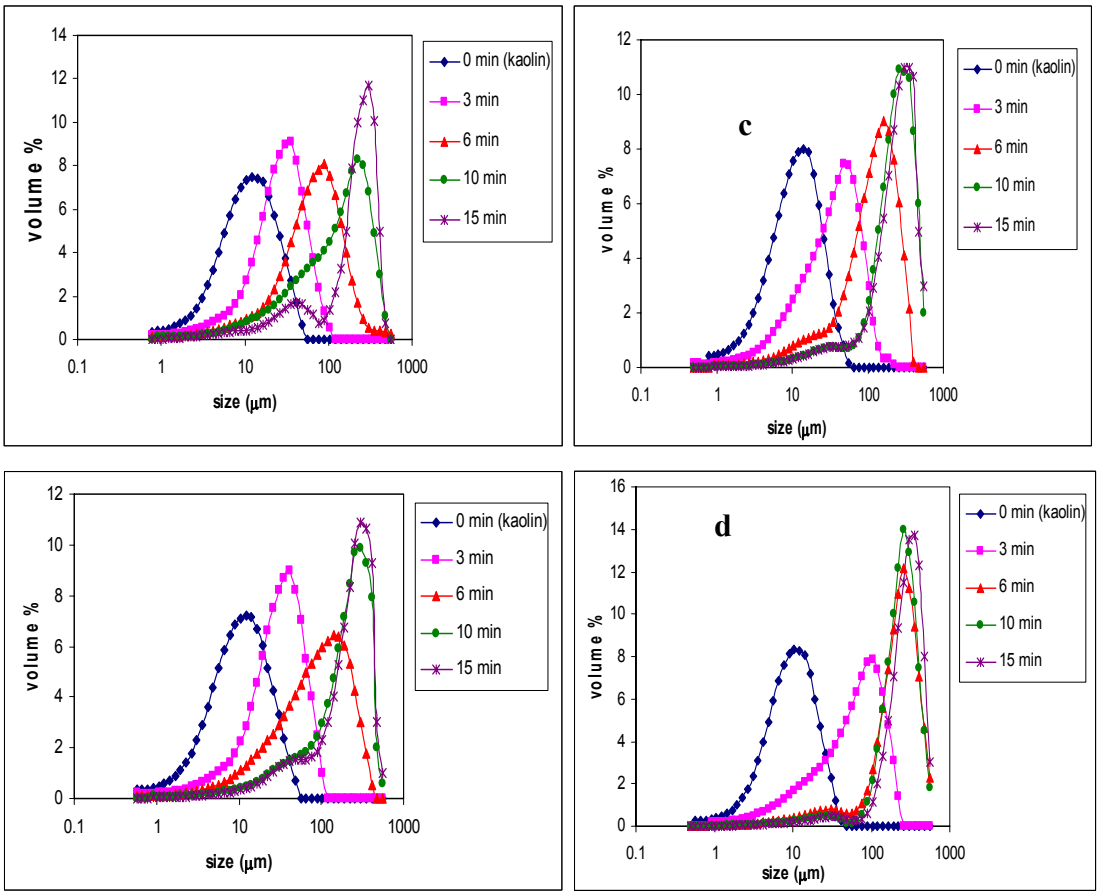

Fig. 23 C_{kaolin}=60mg/l a. **0.042A, pH 5** b. **0.042A, pH 6.5** c. **0.22A, pH 5** d. **0.22A, pH 6.5.**

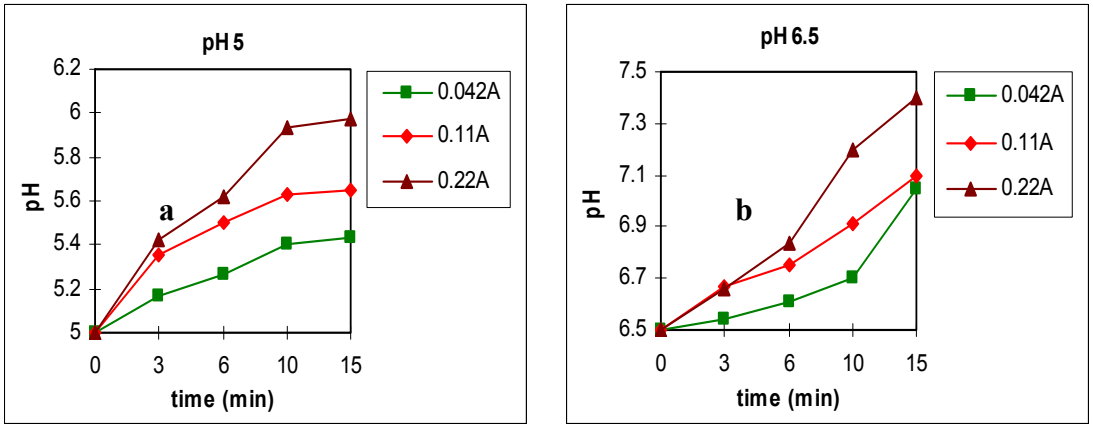

Fig. 24 Change in pH for each time interval. a. **initial pH 5** b. **initial pH 6.5.**

Although pH 5 is not considered an optimal sweep floc regime (Amirtharajah and O'Melia, 1990), the addition of hydroxyl ions into the solution coupled with the continuous aluminum dosing pushes the equilibrium towards enhanced aluminum hydroxide precipitation and substantial growth is observed – even so, at a reduced rate compared to pH 6.5. At pH 5 the positive soluble aluminum mononuclear species govern the solution (Duan and Gregory, 2003), although as the process progresses, the pH rises and conditions become favorable for aluminum hydroxide precipitation (transition *into* sweep-floc regime), which stabilizes the pH after 10 minutes (fig.24) due to the removal of the excess hydroxyl ions from solution. However, at pH 6.5, the pH increases rapidly at end of process compared to the beginning, due to the move *out* of sweep floc regime as speciation shifts towards soluble negative mononuclear species. Under these conditions removal of the excess hydroxyl ions is limited, as aluminum hydroxide precipitation is no longer favorable, hence the sharper rise in pH. Despite the increase in pH and shift away from optimal precipitation conditions at the end of the process, the growth at pH 6.5 is more rapid than at pH 5.

Growth of particles into larger flocs is not only dependent on particle precursor numbers, but also on their ability to form stable bonds. Surface charge also plays a role in determining floc evolution (Nowostawska et al., 2005) which is measured here in the form of ζ potential - indicating electrostatic repulsive forces in the suspension (fig. 25). The initial values of the kaolin suspension are -30 and -34 mV, which are the ζ potentials of the kaolin suspension at initial pH 5 and 6.5 respectively.

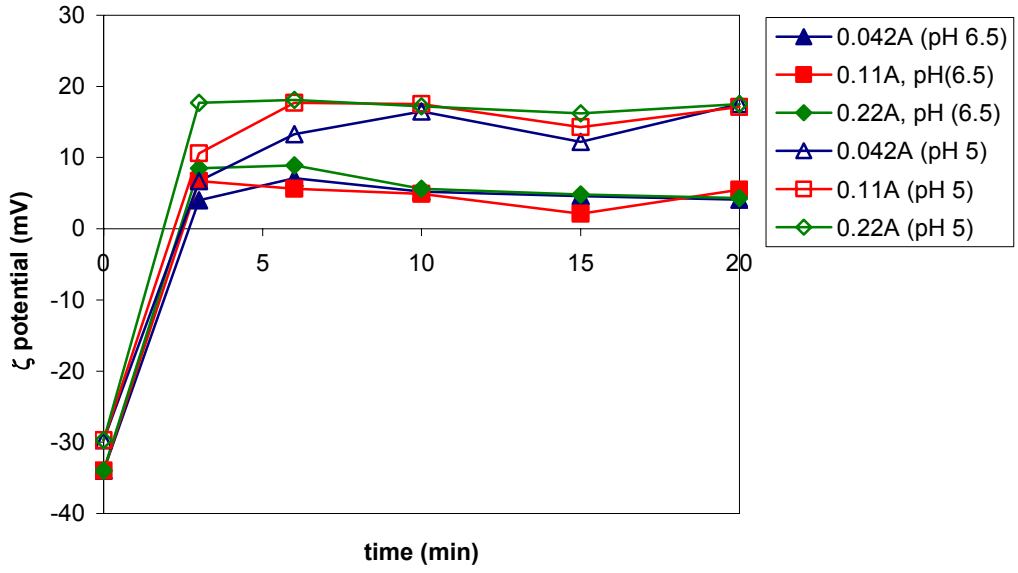

Fig. 25 ζ potential changes over time for C_{kaolin}=60mg/l, pH 5 and 6.5, 0.042A, 0.11A, 0.22A

Within 3 minutes of EF, for both pH values, the ζ potential "jumps" to positive values which is indicative of the positive aluminum ions generated in solution, and the hydrolyzed species subsequently formed. In the initial stages, at pH 5, positive soluble aluminum mononuclear species in solution are dominant, and the ζ potential of the suspension in these conditions becomes more positive compared to pH 6.5. Stabilization occurs at 3, 6 and 10 minutes for 0.22A, 0.11A and 0.042A respectively - as conditions become favorable for aluminum hydroxide precipitation. For the pH values reached from initial pH 5, for each current, the aluminum hydroxide will be charged positively, as its iso-electric point (i.e.p) is between pH 8-9 (Sposito, 1996). At initial pH 6.5 the process commences from optimal sweep floc conditions while shifting the speciation towards negative soluble aluminum mononuclear species as it progresses. The ζ potential in these conditions is less positive than at pH 5, as less positive mononuclear species are present throughout the (initial) stages. The aluminum hydroxide surface charge is still positive, but nearer its i.e.p. A slight drop in the ζ potential, towards less positive values, is measured for all currents after 6 minutes, where speciation towards the negative mononuclear species begins to impact (also indicated by a sharper rise in pH, as less hydroxyl ion is removed from solution in the form of aluminum hydroxide precipitate).

III.3.2.2 Floc growth stages

Several stages of floc growth occur during flocculation. Initially, precursor particle growth is dominant, after which particles combine and their size increases rapidly. As flocculation continues, the flocs form large, porous and open structures that are more susceptible to fragmentation by fluid shear (Tambo, 1991). As a result, the final floc size distribution is a balance between particle growth and breakage (Spicer and Pratsinis, 1996). Figure 26 shows the evolution of the volume mean diameter with time, for 0.042A and 0.22A with different current densities and pH values.

The graphs show that the current density does not affect the growth pattern of the flocs, within the ranges used in this experiment. Hence, all results now will refer to experimental data obtained using full anode area. Within the experimental conditions, the total dose of aluminum dictates the growth pattern, and factors such as current density and voltage (which is dependant on current density) do not impact floc development. All graphs exhibit sigmoidal behaviour and three development stages. The first stage is the induction of aluminum hydroxide precursor particles, and limited growth due to primary collisions between those

particles. Stage two exhibits enhanced growth of an exponential type, and in stage three the flocculation rate diminishes because of aggregate break up. These stages have been observed elsewhere (Kusters et al., 1997; Flesch et al., 1999). For both currents stage two commences at similar times (after 3 minutes), after which enhanced growth rates are observed for 0.22A,

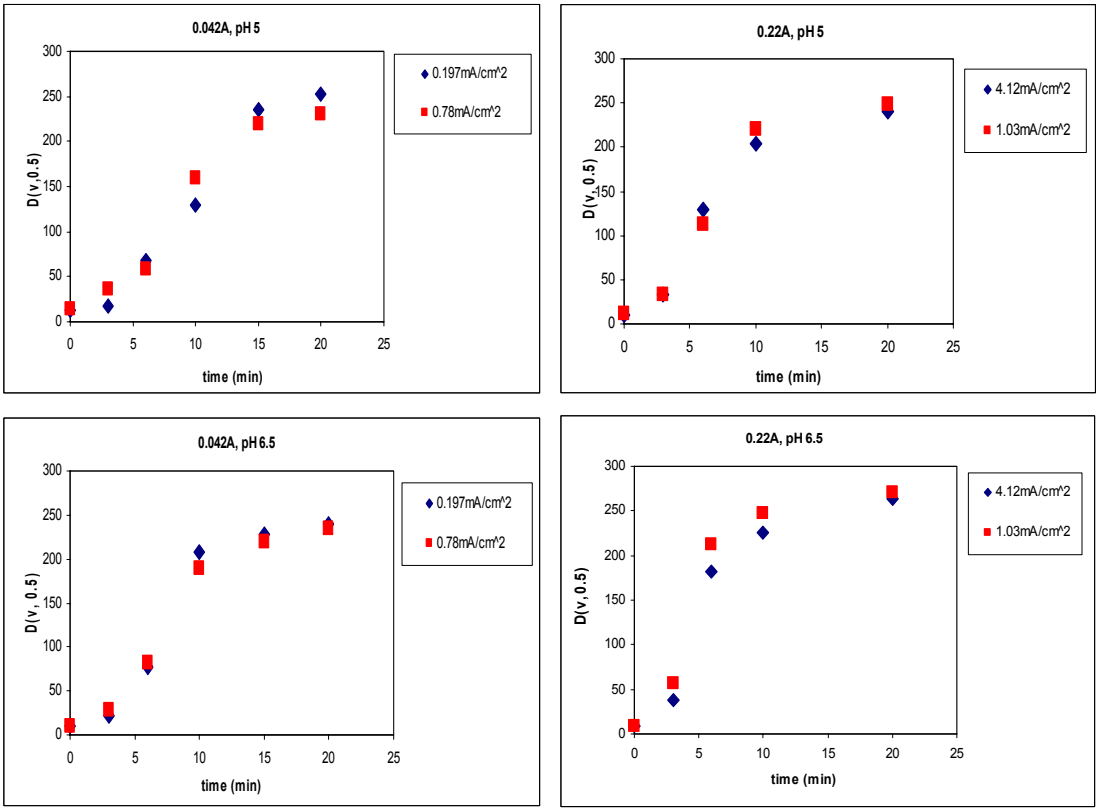

Fig. 26 Evolution of the volume mean diameter for various current densities and pH values, C_{kaolin}=60mg/

more so at pH 6.5. The transition to steady state (stage three) occurs when the flocs have reached a volume mean diameter of approximately 200μm, a size where disruption is caused by hydrodynamic stresses and fragmentation begins to dominate. The time of transition depends on the growth rate. For 0.042A and pH 5, this transition occurs at 15 minutes, while at pH 6.5 at an earlier time of 10 minutes. For 0.22A, pH 5 and 6.5 these times are 10 and 6 minutes respectively. In addition, for 0.22A and pH 6.5, the floc size obtained at steady state is larger than for all other conditions (above 250 μm). The increased aluminum dosing with this current, at an initial pH where aluminum hydroxide precipitation is optimal, increases the floc growth rate and apparently the strength of linkage between the particles comprising the floc, making it more resistant to breakage. This is in agreement with other studies (Francois, 1988), which found an increase both in floc growth rate and the collision efficiency with increased alum concentration during kaolin flocculation. Although at initial pH 5, the

aluminum equilibrium shifts into sweep floc regime as the process progresses, this has less impact on the growth rates, than when starting out in optimal sweep floc regime, where initial nucleation and growth are maximized.

In the growth stages (induction and exponential), before transition to a steady state due to fragmentation, the relationship between the volume mean diameter and time can be written as:

$$D(V,0.5) = Ke^{bt} \qquad (III.3.2.2\text{-}1)$$

where K is a fitting parameter and b is the growth factor, dependent on the unique flocculation conditions.

By fitting the initial growth curves with a simple exponential regression, b can be calculated. Table 8 summarizes the various growth factors obtained for various currents and pH values.

Table 8 Growth factors calculated from initial growth curves.

Initial pH	b (0.042 A)	R^2	b (0.11 A)	R^2	b (0.22 A)	R^2
5.0	0.236	0.98	0.303	0.92	0.381	0.99
6.5	0.297	0.98	0.329	0.94	0.528	0.99

Figure 27 shows the connection between growth factor and current, for each initial pH. A good degree of linearity is observed between the growth factor and applied current, within the current range used, higher currents producing higher growth factors. pH 6.5 yields not only higher growth factors, but also a higher growth dependency on current - which is larger by approximately 1.7 than that obtained at pH 5. These differences are most likely related to the generation of mass into the system in the primary stages of the process, where at initial pH 6.5 aluminum hydroxide early precipitation is increased more with increase in current, relatively to initial pH 5. However, the primary mass generated is not necessarily the sole reason for the differences observed, as surface forces also play a role in particle coagulation enabling growth into larger floc. Floc structure has also been found to affect the growth profile as a larger collision profile (a more open structure), enhances the collision frequency (Kusters et al., 1997; Flesch et al., 1999). Different alum doses have been shown to generate different floc structures (Tambo and Watanabe, 1979), thus the current applied in EF should also have a similar effect. However, in EF, the current does not only control the coagulant dosage, but it also creates a dynamic physical/chemical environment in which speciation shifts as the pH

rises, while micro-bubbles are being simultaneously formed as gaseous hydrolysis products are generated at the electrodes. All these are likely to have a profound effect on the evolving floc as floc structure is a crucial factor in understanding size evolution.

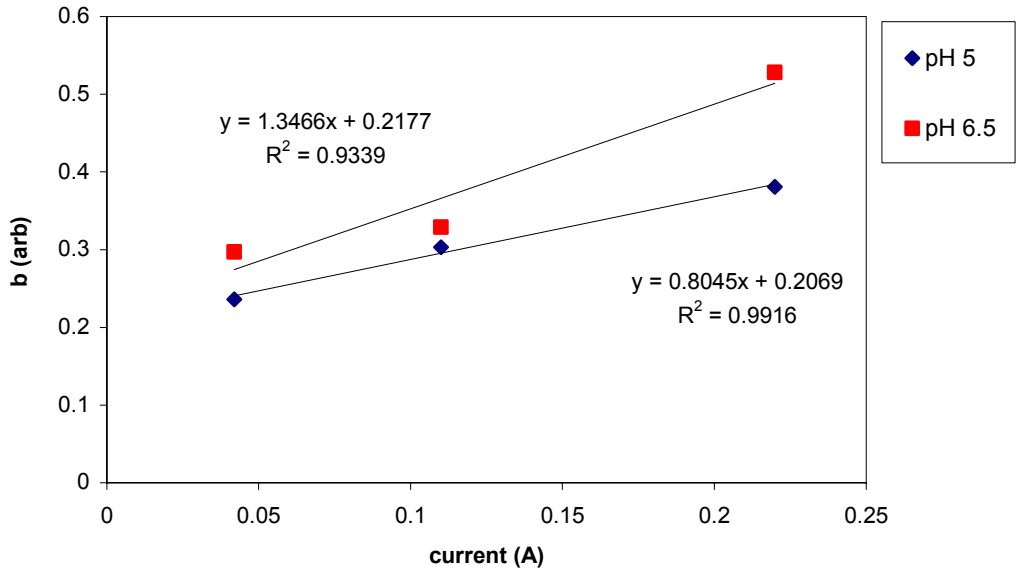

Fig. 27 Dependency of growth factor on current at different pH values

III.3.2.3 Structural evolution

Flocs undergo a series of processes including aggregation, fragmentation and, in some cases, structural rearrangement. The evolution of floc structure throughout the flocculation process depends on various factors such as floc size, formation and break-up rates, bonding forces and hydrodynamic forces (Selomulya et al., 2003). The change in floc structure can be quantified by monitoring the variation in the fractal dimension, or the scattering exponent (SE). As mentioned in the introduction, the SE will be used in this research to define the structural properties of the flocs.

To interpret scattering plots to obtain structural data on the flocs, the question whether the primary particles maintain independent scattering must be raised beforehand, that is if the RGD approximation is valid (eq. III.1.3.1.1.2-4a and III.1.3.1.1.2-4b). Precipitation of aluminum hydroxide precursor particles and their growth has been studied (Li et al., 2005). It has been shown that detectable precursors/nuclei appear in the range of 100nm. Due to the uncertainty of the aluminum hydroxide precursor particles nucleating, a refractive index of 1.59 can be used as an approximation, based on the refractive index range of other aluminum hydroxide crystals (Li et al., 2005). In this case, the limitations for assuming RGD

approximation for structural interpretation of scattering plots of aluminum hydroxide flocs are fulfilled:

$m = n_{Al(OH)3}/n_{water} = 1.59/1.33 = 1.195.$ $|m-1| = 0.195$ and

$(4\pi n_{water}/\lambda_{laser})L\,|m-1| = (4\pi 1.33/633)*100*0.195 = 0.5$

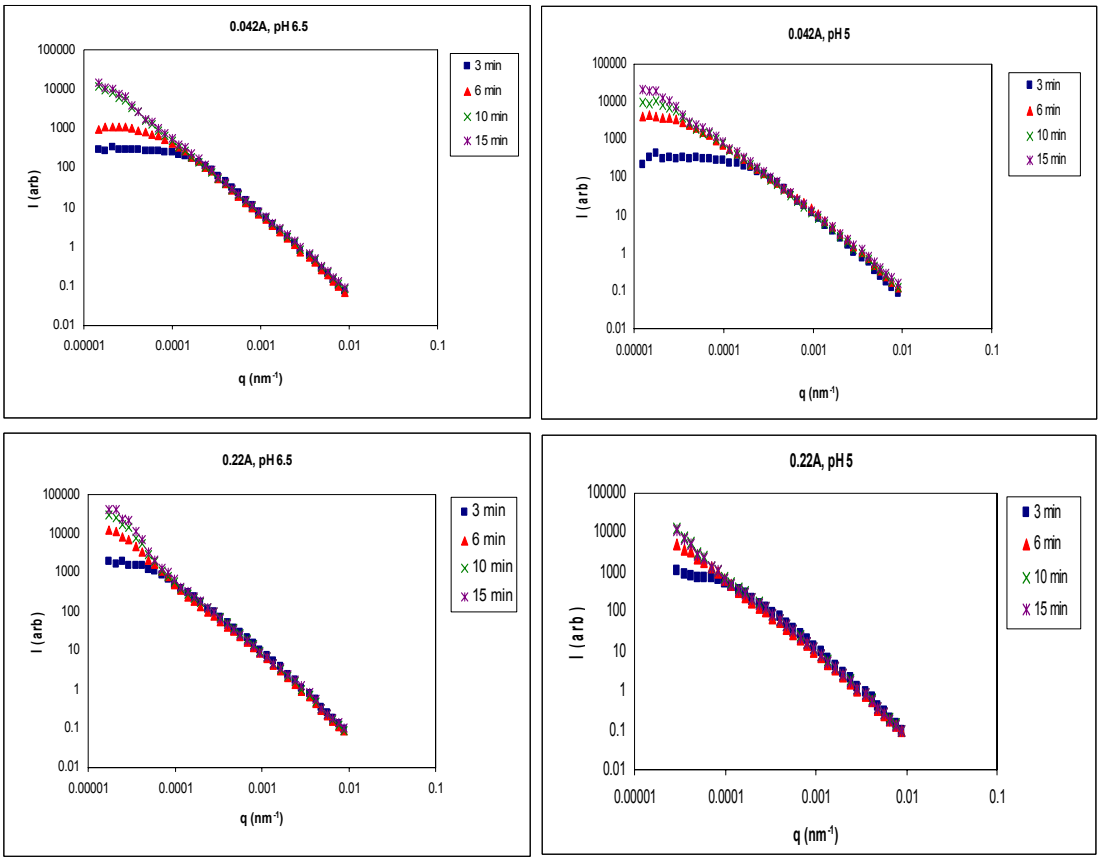

Fig. 28 Conventional static light scattering plots (log(I) vs. log(q)) for flocs forming as a function of time.

Fig.28 shows typical scattering graphs of flocs at different time intervals. The graphs obtained for 0.22A, at both pH values, show that transition into an angle independent scattering region at low q is hardly apparent. A mild transition does occur at the beginning of the process, at 3 minutes, after which the graphs exhibit a dependency on q, even in the low range. This is presumably a result of the large size of the flocs obtained for 0.22, after 6 minutes and above, for both pH values. For 0.042A, the transition is more apparent, and occurs for most time intervals, at both pH values, except at pH 6.5 after 10 and 15 minutes, again due to the size of the flocs. For all graphs, one decade of linearity is observed for: $1.4*10^{-4}<q<1.6*10^{-3}$. This region will be used to calculate the SE, from the slope of the scattering plots.

Table 9 Scattering exponents obtained for various currents and pH values.

Time (min)	**SE**, pH 6.5			**SE**, pH 5		
	0.042A	0.11A	0.22A	0.042A	0.11A	0.22A
3	1.83±0.04	1.78±0.02	1.77±0.02	1.75±0.06	1.86±0.02	1.78±0.03
6	1.93±0.01	1.95±0.01	1.78±0.01	1.78±0.02	1.81±0.02	1.84±0.02
10	1.89±0.01	1.88±0.02	1.81±0.02	1.88±0.01	1.90±0.01	1.87±0.02
15	1.93±0.01	1.93±0.01	1.86±0.01	1.87±0.01	1.87±0.01	1.87±0.02

The results show that for all currents and pH values compaction occurs during the process, resulting in a final SE, at 15 minutes, which is higher than that obtained during the initial 3 minutes. In some conditions, fluctuations in the structural evolution are observed. This indicates the extreme fragile nature of the flocs.

For 0.042A, the flocs formed at pH 6.5 are more compact than those at pH 5. However, for 0.22A, the differences between the two pH values are not as distinct. From comparing 0.22A to 0.042A, at pH 6.5 it is evident that the higher current (aluminum dose) produced less compact flocs, throughout all stages of the process. This also impacts the growth rate which has been observed to be higher at 0.22A, as the collision profile of the flocs forming is larger. Although for 0.22A, fragmentation starts at an earlier stage than for 0.042A (fig. 3.2.2-1) the flocs still maintain a more open structure, and reach a larger size by 15 minutes, thus indicating stronger linkage between particles comprising the floc.

This could be a result of the extent of transition out of favorable precipitation conditions. For 0.22A, compared to 0.042A, this transition is sharper, with the final pH reaching 7.4 as opposed to 7.0 for 0.042A. This affects the surface charge of the particles, as a higher pH will reduce the surface charge of the aluminum hydroxide precipitate shifting it towards its iso-electric point. A lower surface charge would decrease electrostatic repulsive forces, resulting in higher collision efficiency and a stronger floc (stronger bonds). Moreover, at 0.22A, the generation of hydrogen gas is increased and therefore more micro-bubbles are present. These can be incorporated in the floc, thus creating a more porous structure. Figure 29 illustrates these differences visually.

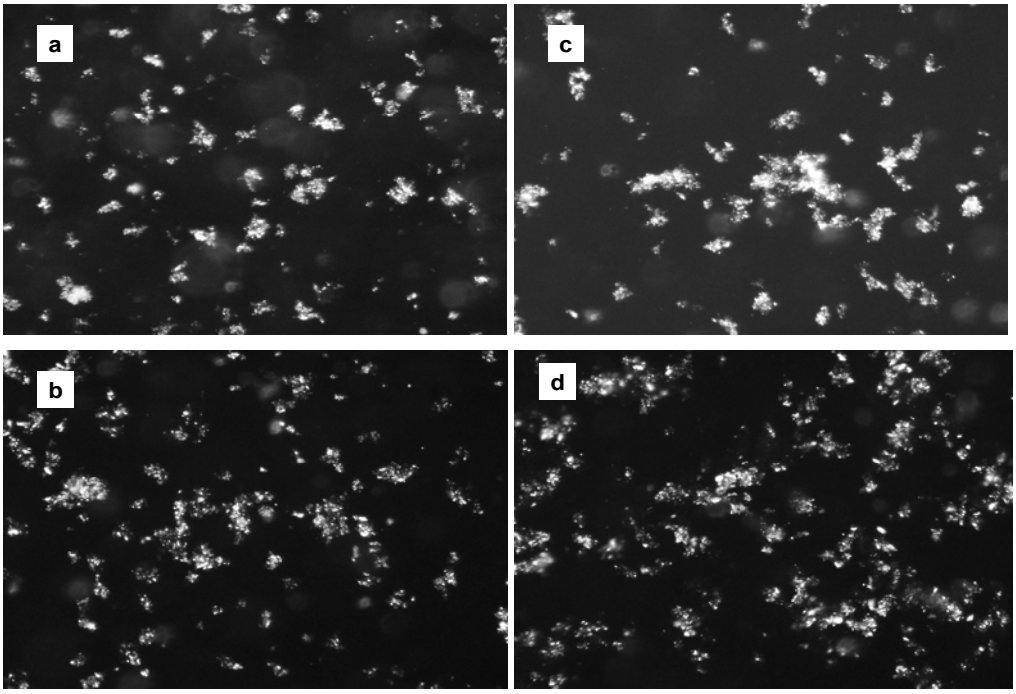

Fig. 29 Floc structures obtained at pH 6.5 for a. **0.042A, t=6min** b. **0.22A, t=6min** c. **0.042A, t=10min** d. **0.22A, t=10min**

For 0.042A and pH 6.5, the flocs are well defined, and compact in structure, whereas 0.22A yields structures which are extremely tenuous displaying a porosity which seems even transparent in some regions. For pH 5, differences in the SE for flocs obtained at different currents are not appreciable, which indicate a rather open structure, as shown in figure 30. At this pH, the transition into more favorable aluminum hydroxide precipitation conditions occurs at the later stages of the process (as the pH and aluminum dose rise), thus the mass introduced into the system is less than at pH 6.5. In this case, incorporation of the micro-bubbles into flocs containing less mass would probably result in a more open structure. The flocs also exhibit less strength, and despite their large collision profile do not reach the size obtained at pH 6.5 for 0.22A. At pH 5, the surface charge of the aluminum hydroxide precipitating is more positive (further from the i.e.p) than at pH 6.5, indicating that repulsive electrostatic forces are stronger.

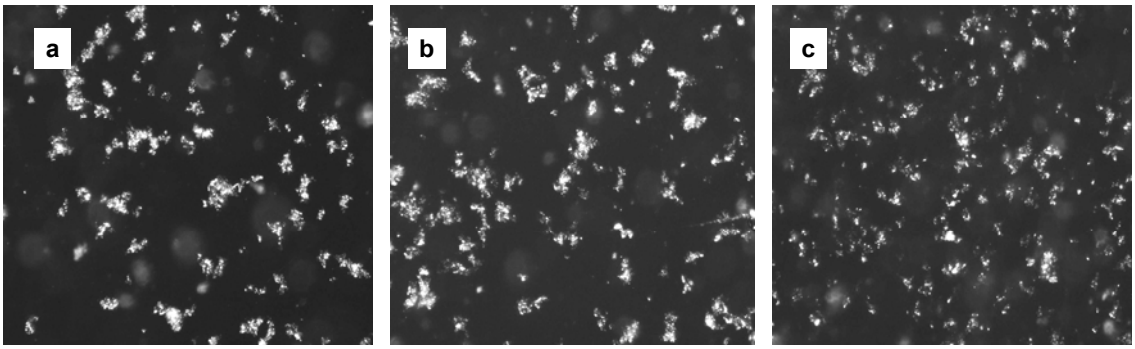

Fig. 30 Floc structures obtained at pH 5, and 10 min for a. **0.042A** b. **0.11A** c. **0.22A**

The above data shows that size and structure evolution of flocs in EF of a colloidal suspension stems from a delicate balance between mass introduced (particle numbers) at the initial stages of the process and the amount of gaseous products (in the form of microbubbles) in solution – both are current dependent. The initial particle numbers are also a function of pH, which creates, in conjunction with the current, conditions favorable for aluminum hydroxide supersaturation and precipitation. However, these also affect the surface charge of the flocs forming, which in turn affects the strength of the bonds between the precursor particles and ultimately the collision frequency and size of the floc. All these parameters, which are intertwined, are summarized in a conceptual model (fig. 31) which predicts floc structure and size, with reference to the specific conditions studied here (EF of a model kaolin suspension).

At pH 5 less mass is generated as floc sweep regime is not optimal, and the repulsive surface forces at this pH are stronger for all currents, therefore the collision efficiency (α) is lower. The floc structure depends on the ratio of microbubbles/mass, as more open structures evolve, as the ratio increases. For lower currents this ratio is maintained (a low current results both in low mass and less microbubbles), but the reduced mass will result in flocs exhibiting a smaller collision frequency (β) that evolve slowly – but still portray a porous structure. For higher currents, the collision frequency is larger as more mass is generated along with hydrolysis products, resulting in a more rapidly evolving porous structure.

At pH 6.5 more mass is generated as the conditions are optimal for aluminum hydroxide precipitation. The repulsive surface forces are weaker, indicated by a ζ potential which is nearer to the i.e.p of aluminum hydroxide – hence, the collision efficiency is higher. For lower currents, the microbubble/mass ratio is smaller, and coupled with the reduced mass will result in a more compact floc which evolves slowly. For higher currents, microbubble generation is increased, resulting in a more open structure, but exhibiting strength. These flocs have both a large collision frequency and large collision efficiency – hence, the increased growth dependency on current and increased growth rate.

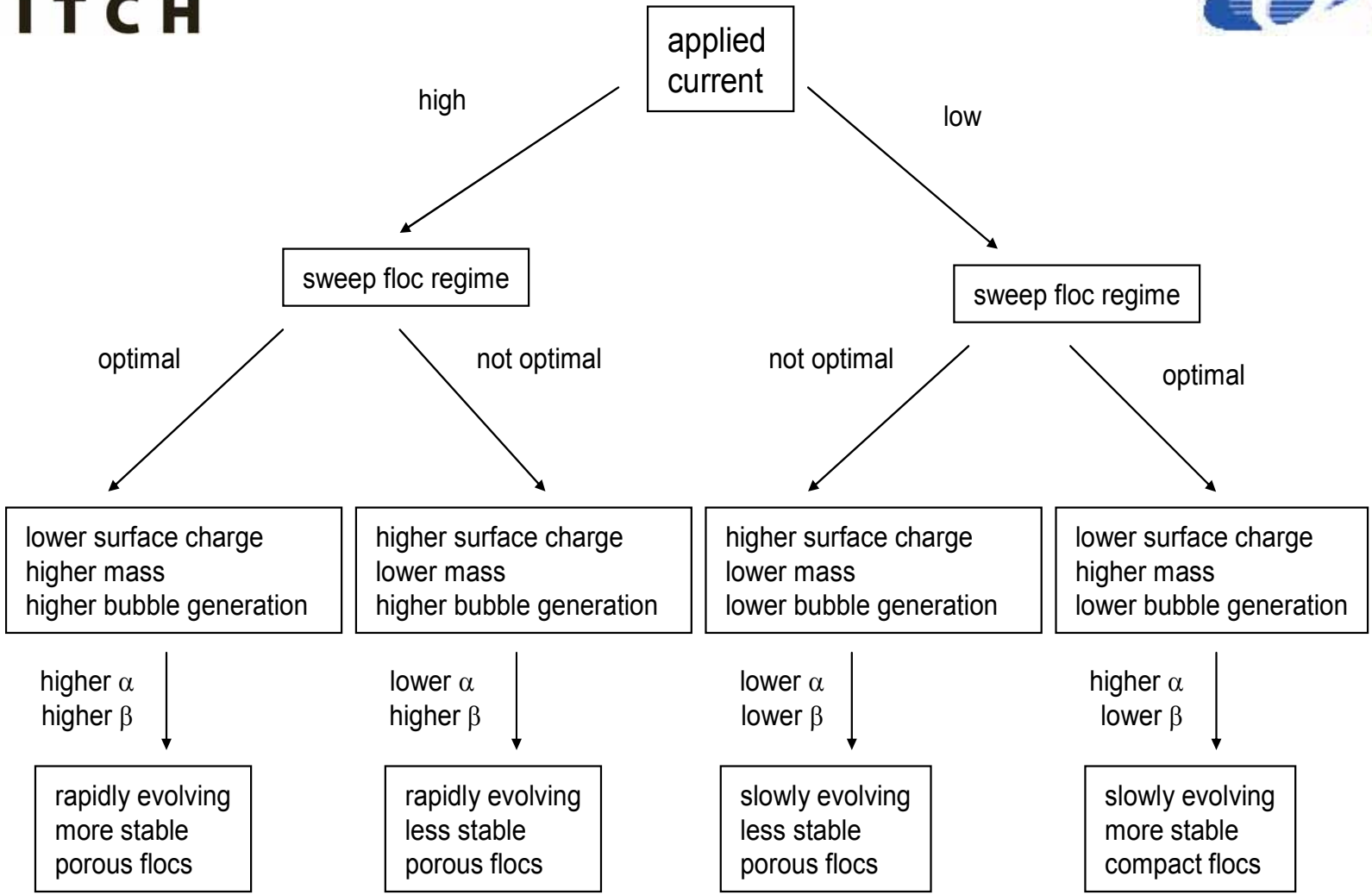

Fig. 31 Conceptual model predicting floc evolution – rate and structure.

III.3.3 Evaluating EF as an alternative to CF

A comparative study between EF and CF was carried out, using aluminum as EF coagulant and alum as CF coagulant. A direct comparison between EF and CF is problematic, as both systems do not operate on an equivalent basis. In EF the coagulant addition is a function of current and time, whereas in CF it is a discrete (shot-fed) process. However, fundamental differences between these two processes do exist, and are manifested in the resulting solution and aggregate/floc characteristics. These differences should not be overlooked, as it is necessary to evaluate EF as a viable alternative process to CF. To create conditions, on which a theoretical comparison could be based, alum dosing was performed additively over time, and final dosing was set at 10 minutes for both processes.

III.3.3.1 pH 5 and 8

For pH 5 and 8 minimal floc formation was observed, except for pH 8 and 160mg/l alum, where sufficient growth occurs. Figure 32 summarizes size distributions over time for various alum doses and initial pH values.

The graphs show that floc evolution is limited for pH 5, as opposed to EF, where at this pH sufficient floc growth was observed for all currents applied. At pH 8, floc evolution is observed for 160mg/l whereas in EF, at this pH no formation was evident, for all currents applied. The growth at pH 8 and 160mg/l alum is limited compared to EF, with modal diameters not reaching above 200μm. However, the induction period, appears to be short, and within 3 minutes modal diameters have reached above 100μm. This was observed for high currents at optimal precipitation conditions in EF. Most likely the high alum dose and alkaline conditions have accelerated aluminum hydroxide precursor formation and thus the faster growth pattern. Despite fast initial growth stages the flocs do not reach the sizes obtained in EF, which could be a function of repulsive electrostatic forces. Figure 33 shows the changes in ζ potential over time for initial pH values of 5 and 8, and alum dosing.

The graph shows that for 160mg/l at pH 8, the ζ potential becomes less negative over time, as more alum is introduced into the system. Although at 6 minutes dosing the pH has dropped within optimal precipitation conditions (figure 34), the ζ potential is still quite negative (-10mV), indicating that indeed repulsive forces are a limiting growth factor. At pH 5 the pH values drop over time, thus the ζ potential is more positive, as positive soluble aluminum mononuclear species govern the solution. Electrostatic repulsive forces are decreased but generation of precursor particles which relies on aluminum hydroxide precipitation is the limiting factor - and therefore limited growth is observed.

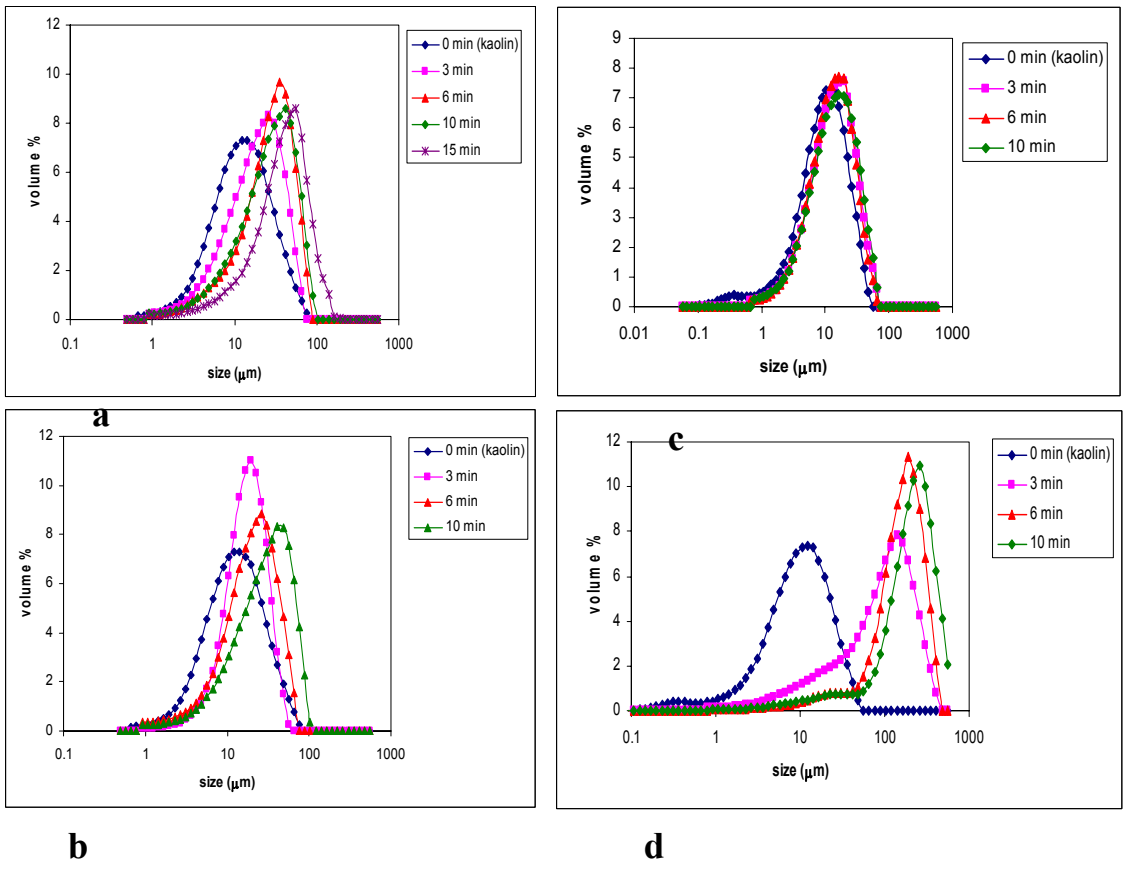

Fig. 32 C_{kaolin}=60mg/l a. **30mg/l alum, pH 5** b. **160mg/l alum, pH 5** c. **30mg/l alum, pH 8** d. **160mg/l alum, pH 8.**

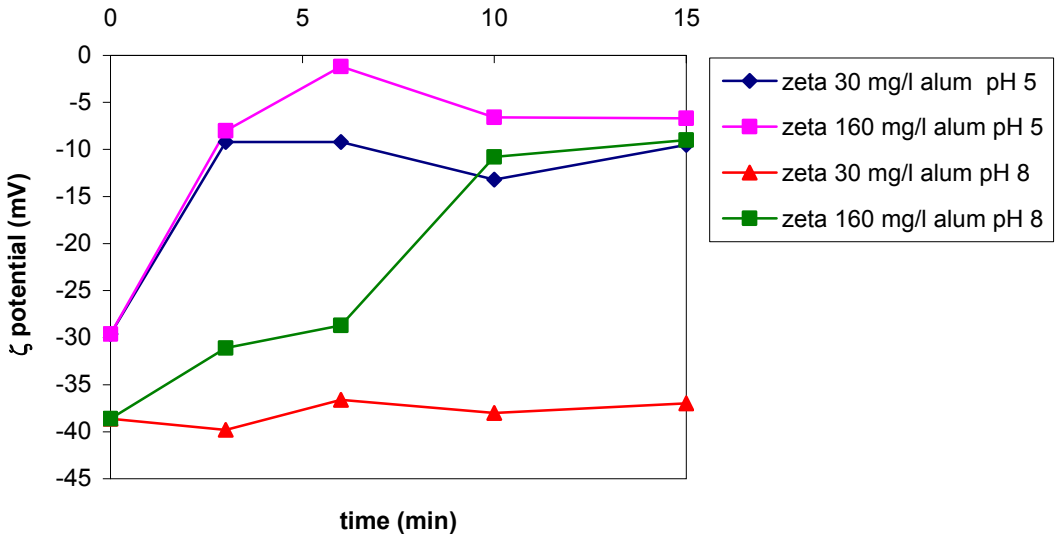

Fig. 33 ζ potential as function of time for alum dosing, C_{kaolin}=60mg/l, initial pH 5 and 8.

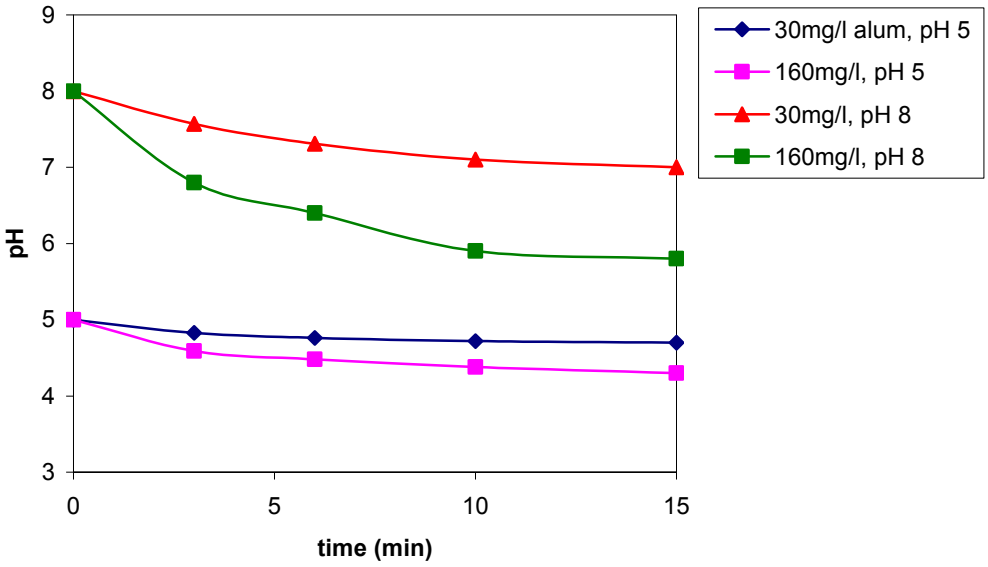

Fig. 34 Change in pH for alum doses, C_{kaolin}=60mg/l, pH 5 and 8.

III.3.3.2 pH 6.5

At pH 6.5, optimal aluminum hydroxide precipitation conditions, growth is observed for all alum doses. Figure 35 shows evolution of size distributions over time for alum dosing at pH 6.5. Increased growth is observed for 30mg/l alum and 80mg/l alum with modal diameters at the end of the process reaching above 200µm and above 150mm, respectively, with the spread reaching the upper detection limit of the instrument. For 160mg/l the growth is less pronounced as final modal diameters are smaller than those achieved with the lower alum concentrations. As in EF, an induction period is observed, in which precursor particles are formed, over the initial 3 minutes, although for 30mg/l this is significantly shorter, as within this period sizes as large as 100µm are already observed.

All the size distribution exhibit wide spreads, as like EF, the dosing is additive, resulting in simultaneous aluminum hydroxide precursor particle formation and flocculation into larger floc. However, higher growth rates are observed for EF. The unique conditions EF creates lowers the mass generation limitation due to continuous hydroxyl ion formation with pushes the equilibrium, according to Le Chatelier's principle, towards enhanced aluminum hydroxide precipitation for all currents applied. The changes in pH are distinctly different between the two processes with pH increase observed in EF, as opposed to pH decrease in CF (fig. 36).

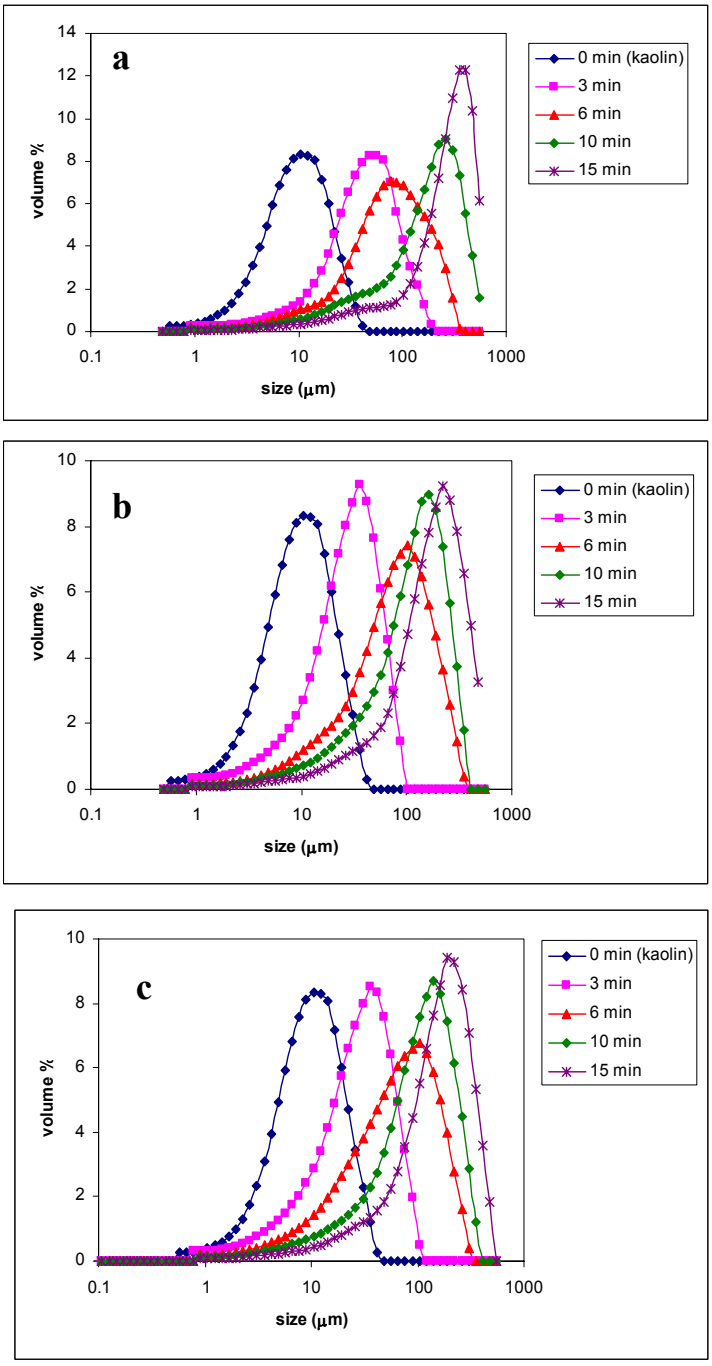

Fig. 35 C_{kaolin}=60mg/l a. **30mg/l alum, pH 6.5** b. **80mg/l alum, pH 6.5** c. **160mg/l, pH 6.5**

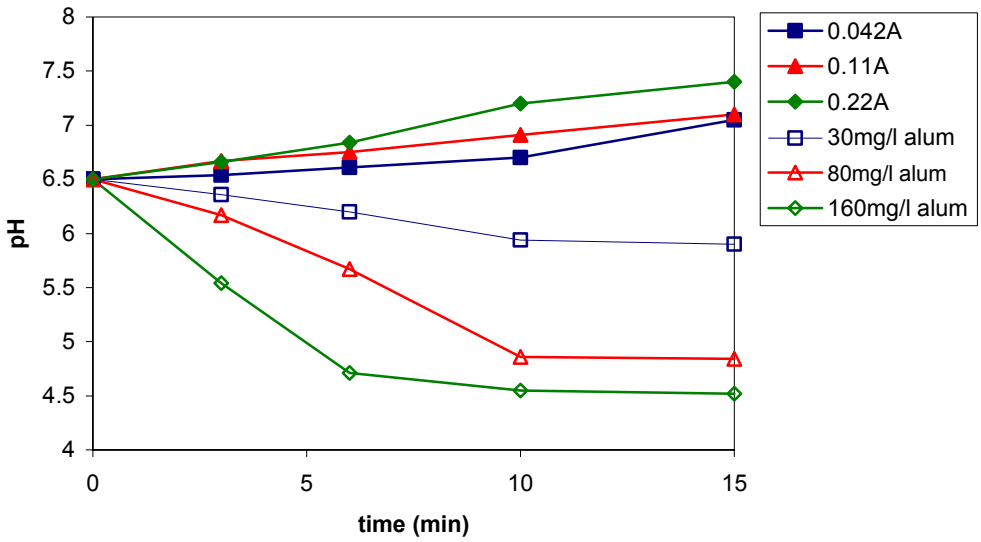

Fig. 36 Changes in pH over time in EF and CF, C_{kaolin}=60mg/l, for various alum or aluminum doses.

The pH for 80mg/l and 160mg/l alum rapidly decreases at 6 minutes dosing, reaching pH values below 5, by the end of the process. Dosing with 30mg/l alum, however, decreases the pH marginally, which stabilizes at 6 during the final stages of the process. 30mg/l alum generates a larger number of precursor particles, as all stages of the process are within sweep floc regime, hence the increased growth rate and larger final sizes. For the other doses, transition out of sweep floc regime towards positive mononuclear speciation is pronounced, which limits the amount of mass generated throughout the process which in turn limits floc growth. The growth exhibited with these doses stems from the initial stages, where aluminum hydroxide precipitation is optimal.

As specified previously, the growth of particles into larger flocs is not only dependent on particle precursor numbers, but also on their ability to form stable bonds. As such, surface charge impacts floc evolution. Figure 37 shows the differences in ζ potential between EF and CF at pH 6.5.

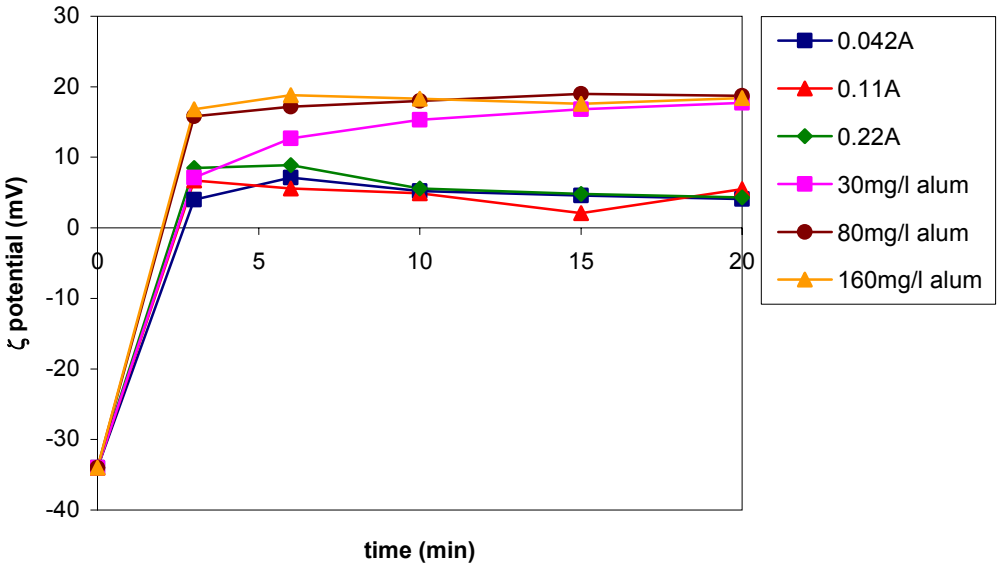

Fig. 37 Figure 3.3.2-3 ζ potentials of suspensions over time, C_{kaolin}=60mg/l, for EF and CF, initial pH 6.5

The graph shows that for EF the ζ potential is less positive, therefore electrostatic repulsive forces are decreased - hence the enhanced growth rates compared to alum dosing. Although both processes commence from identical pH value, within optimal precipitation conditions, the ζ potentials are different, due to the differences in solution chemistry, primarily the pH.

EF generates hydroxyl ions thus reducing the positive ζ potential of the precursor particles towards an i.e.p, and reducing electrostatic repulsive forces between precursor particles. CF, on the other hand, removes hydroxyl ions from solution, thus maintaining stronger repulsive forces between precursor particles manifested in a more positive ζ potential in solution. Unlike CF, EF creates conditions in which both mass generation limitations and surface charge limitations are reduced, which can explain enhanced growth profiles compared to the conventional process. Figure 38 shows the growth stages of flocs for initial pH 6.5, for EF and CF.

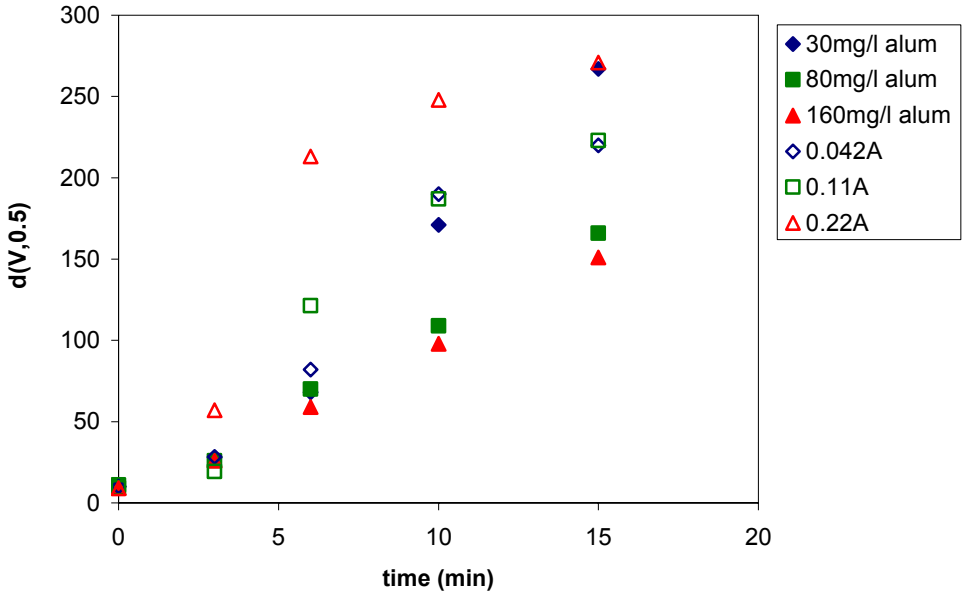

Fig. 38 Evolution of volume mean diameter for various currents and alum doses, initial pH 6.5.

The graph shows that the growth rate of flocs formed in EF, for all applied currents, is faster than that using CF. For 30mg/l alum the final sizes are similar to those attained for 0.22A, but the path is different. While for 0.22A fragmentation is observed at 6 minutes, for 30mg/l this begins at 15 minutes, indicating a lower flocculation frequency and smaller growth profile. For 80mg/l and 160mg/l alum the growth patterns are devoid of sigmoidal behavior, as the sizes attained are not large enough to undergo fragmentation. As opposed to EF, there is no correlation between dose and growth factor in CF, as floc evolution depends on a delicate balance between optimal precipitation conditions and surface properties (i.e. electrostatic repulsion forces). Because the former limitation is reduced in EF, floc formation is observed over a wider range of pH values and aluminum doses compared to CF in which floc formation is restricted to a far narrower pH/dosing range.

III.3.3.2.1 Structural properties

Growth kinetics can impact structural properties. In EF fast growth profiles have shown to produce flocs prone to fragmentation as larger sizes are attained more quickly, and these are more susceptible to shear forces and can undergo compaction and restructuring. In CF, the growth profiles of flocs formed with higher alum doses do not exhibit a diminished flocculation rate indicating a dominant fragmentation stage. However, for 30mg/l alum, this stage is observed after 15 minutes. At this lower dosage the flocs do exhibit final sizes equivalent to those measured for 0.22A, although the growth path indicates a slower growth rate. Slower growth rates, and reduced exposure to hydrodynamic forces should affect the structural properties of the flocs.

Scattering plots were used to obtain the structural data. Figure 39 shows typical scattering plots of flocs formed with alum dosing at different time intervals.

The graph obtained for 30mg/l alum shows that transition into an angle independent scattering region at low q is hardly apparent for flocculation times above 3 minutes. A mild transition occurs within 3 minutes after which the graph exhibits a dependency on q, even in the low range. This is due to the large size of the flocs obtained for 30mg/l. The other graphs, for 80mg/l and 160mg/l alum, show a stronger transition into a q independent range for most times, although for 15 minutes flocculation this is less apparent due to the larger sizes obtained at this time. For all the graphs, one decade of linearity is observed for: $1.4*10^{-4}<q<1.6*10^{-3}$. This region will be used to calculate the SE, from the slope of the scattering plots.

The results show that the flocs are less prone to compaction. The SE for the higher doses changes marginally throughout the process, maintaining generally a stable value. For these doses floc growth has been shown to be limited, and no substantial difference between values is observed over time. For 30mg/l alum, the SE decreases with time, indicating growth into a more porous structure. In this case, both precipitation conditions and surface forces enabled growth into larger floc exhibiting a stability which was not observed for equivalent sized flocs obtained in EF. Images of types of flocs formed by alum dosing are shown in figure 40. The lower dose formed flocs which appear well defined with clear structures evolving, whereas the flocs obtained at higher doses appear "fluffy", exhibiting a transparency which is not observed at the lower dose. As discussed previously, in EF the flocs undergo compaction and restructuring which is indicative of their fragile nature. Moreover, their enhanced growth rates render them susceptible to hydrodynamic shear forces for longer periods of time, as larger sizes are attained more rapidly. A comparison of SE values obtained in CF to the values obtained in EF (Table 10) demonstrates that structural evolution of the flocs obtained in CF is different. For adequate flocculation conditions (i.e. sufficient growth) in CF, flocs evolve from a more compact structure into a more porous structure, whereas in EF evolution is generally from a less compact structure into a more compact one, although fluctuations have also been observed. This behavior sheds some light on the flocculation mechanisms occurring in EF as opposed to CF. In EF electrostatic repulsive forces are weaker, resulting in a higher flocculation efficiency and more successful collisions. The gaseous products formed in the process could also play a role in the adhesion of precursor particles together, acting as additional "glue". The combination of these would enable a diffusion limited type of reaction, resulting in a fragile floc, exhibiting porosity in early stages of growth, but more easily disrupted by shear forces, thus undergoing restructuring and compaction. In CF electrostatic repulsive forces are stronger, resulting in a reaction limited type of reaction which exhibits slower growth rates (lower flocculation efficiency) and produces flocs which are more compact in the early stages of growth. These are able to develop into more porous structures, because they are less affected by shear forces, due to their relatively tighter structure compared to the very loose structure obtained in EF. However, the final structure will be limited to shear forces within the system.

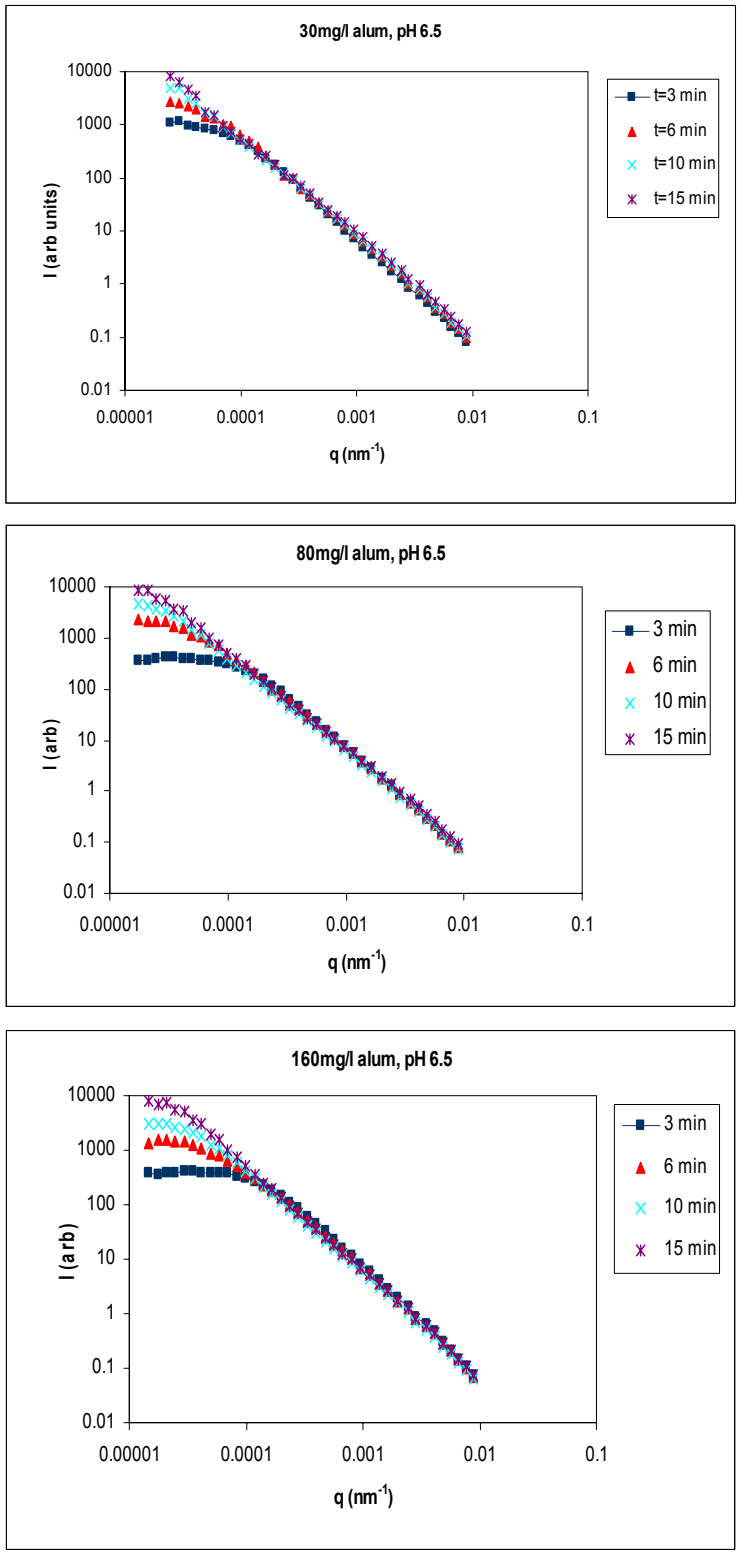

Fig. 39 Conventional static light scattering plots (log(I) vs. log (q)) for flocs forming as a function of time for alum dosing.

Table 10 Scattering exponents obtained for various alum doses at pH 6.5

Time (min)	SE		
	30mg/l alum	80 mg/l alum	160 mg/l alum
3	1.99±0.03	1.87±0.02	1.81±0.03
6	1.91±0.02	1.89±0.01	1.84±0.01
10	1.83±0.01	1.82±0.01	1.84±0.01
15	1.78±0.02	1.84±0.01	1.86±0.01

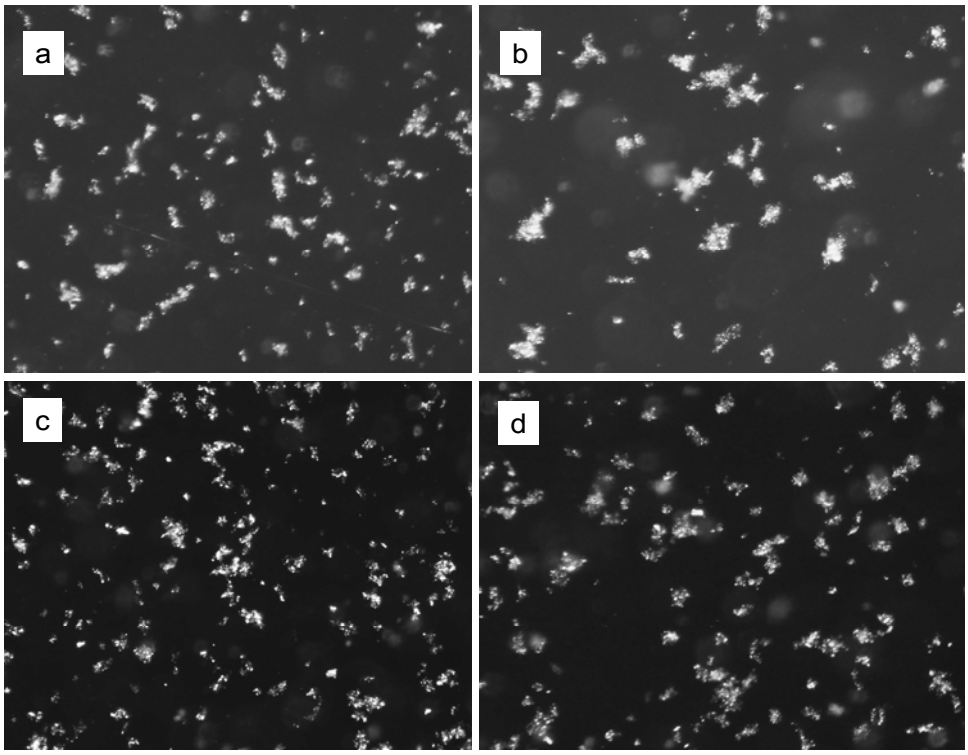

Fig. 40 Floc structures obtained at pH 6.5 for a. 30mg/l alum, t=6min, b. 30mg/l alum, t=10 min c. 80mg/l alum, t=6min d. 80mg/l alum, t=10min.

III.3.4 EF as pretreatment to colloidal ultrafiltration

III.3.4.1 Characteristics of the kaolin suspension undergoing ultrafiltration

As discussed previously, the current applied in the EF process has a double effect, by both generating the coagulant species and by causing hydrolysis in which excess hydroxyl ions are formed at the cathode, resulting in an increase in pH. This impacts the ζ potential which serves as an indicator for coagulation efficiency. Figure 41 shows the change in pH and ζ potential as a function of applied current for a 15mg/l kaolin suspension at different initial pH values. The ζ potential of the kaolin suspensions, without applying any current: -17.9mV, -21.7mV and -23.7mV for pH 5, 6.5 and 8 respectively.

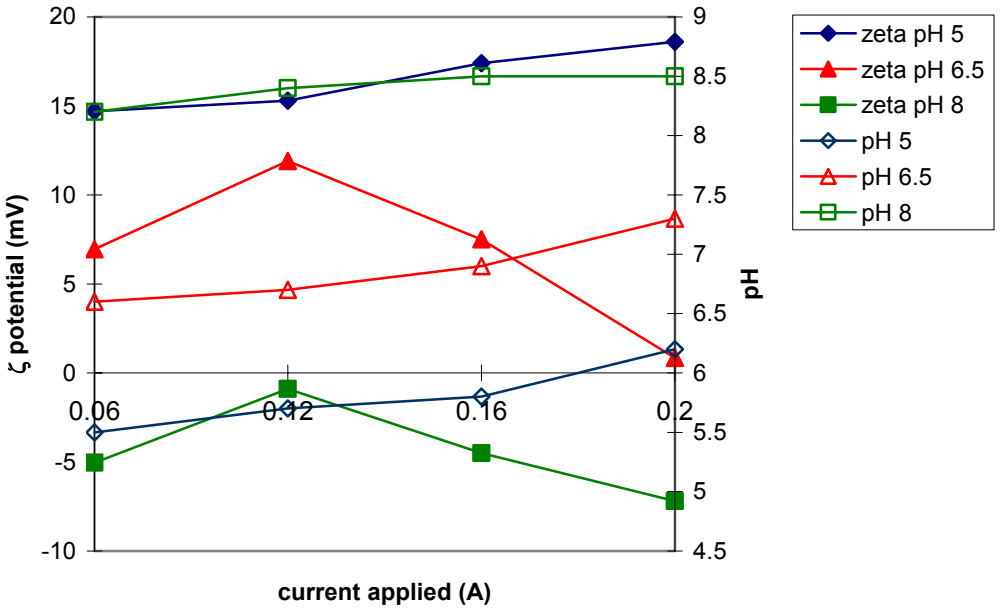

Fig. 41 Change in pH and ζ potential vs. applied current for pH 5, 6.5 and 8. C_{kaolin}=15mg/l, t=7min.

III.3.4.2 Membrane ultrafiltration

The permeate flux was measured for suspensions, that had undergone electroflocculation using aluminum as the anode material. The aluminum doses were controlled by the applied current, which was kept constant during each run. The results show that pre-EF enhances the permeate flux at pH 5 and 6.5, but only marginal enhancement is observed at pH 8. When treating relatively dilute suspensions, the concentration layer, if formed, contributes negligible resistance to the actual cake resistance (Waite, 1999), thus the assumption is that the primary fouling factor is cake formation. However, all flux curves show a degree of pore blocking for all pH values. The residual aluminum in permeate was also measured. These are shown in figure 42.

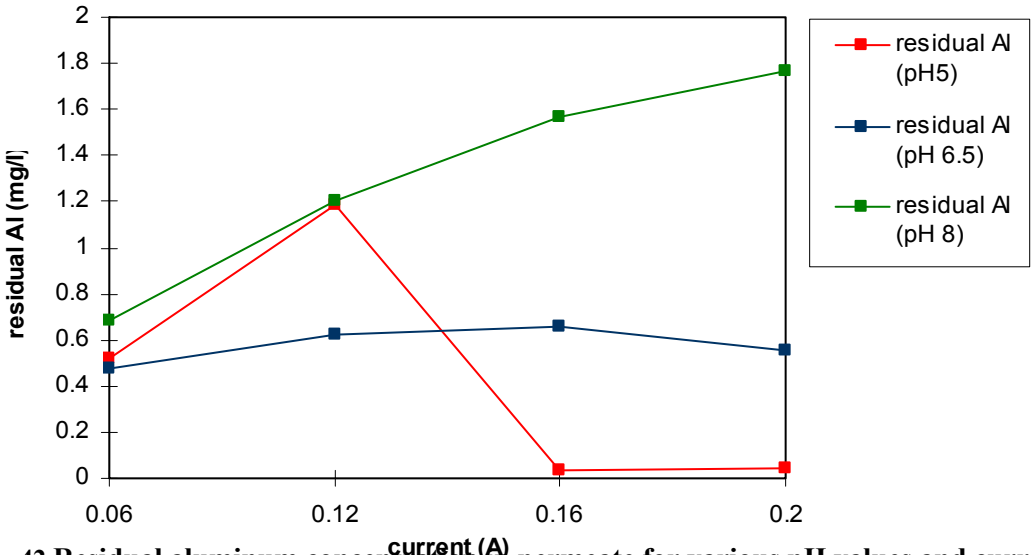

Fig. 42 Residual aluminum concentration in permeate for various pH values and currents.

III.3.4.2.1 pH 5

At initial pH 5 filtration of kaolin causes significant flux decline, and by the end of the run it has reached 40% of the initial flux (fig. 43). Pre-EF of the suspension improves the filtration, and at all currents flux enhancement is observed. At 0.06A the maximum flux enhancement occurs, by which the flux has improved by 15%, reaching a critical flux at 55% of the initial flux. At 0.12A, 0.16A and 0.2A similar behavior is observed, by which the permeate flux reaches critical flux at 60% of the initial flux. The difference in membrane behavior obtained after EF at 0.06A relatively to the other applied currents can be explained by the transition to a different coagulation mechanism, which occurs at higher doses of aluminum.

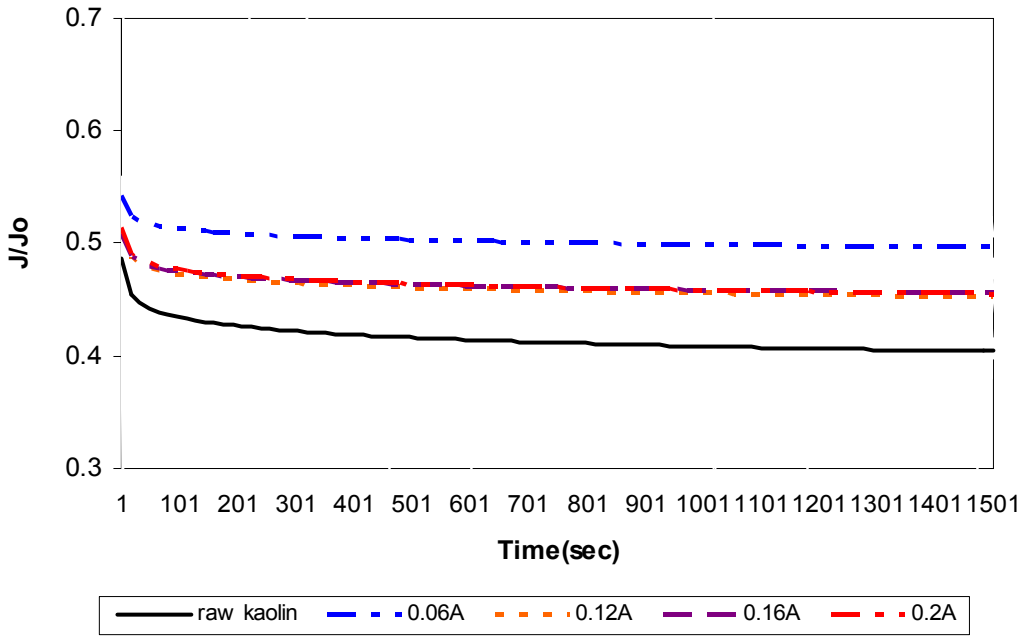

Fig. 43 Permeate flux (J) as a fraction of initial flux (Jo) over the course of ultrafiltration of an electroflocculated kaolin suspension, C_{kaolin}=15mg/l, initial pH 5, at various applied currents.

At pH 5 the governing aluminum species in solution are Al^{+3} and $Al(OH)^{2+}$, and therefore it can be assumed that at this initial pH the dominant coagulation mechanism is adsorption and charge neutralization, although some aluminum hydroxide does precipitate in these conditions. In this case it appears that at the minimum applied current, 0.06A, adsorption and charge neutralization is the dominant coagulation mechanism, thus producing aggregates that form a more stable cake on the membrane surface, which has a higher porosity than the dense, compact cake formed by filtration of kaolin (fig. 44a). At the higher currents, 0.12A, 0.16A and 0.2A we observe improved membrane behavior due to increased formation of aluminum hydroxide in solution, which catches the smaller particles (by "sweep floc" mechanism) thereby enhancing the permeate flux. However, the decline in flux relative to the flux obtained at 0.06A, is due to increased cake formation of gelatinous aluminum hydroxide on the membrane surface. From SEM analysis, aluminum hydroxide

seems to form a "blanket" on the membrane surface, and exhibits different characteristics than the cake formed from filtration of raw kaolin, which appears to be very dense and tightly packed (fig. 46). In addition, aluminum hydroxide flocs, unlike kaolin particles (which have an average size of 1μm), are large enough to be sheared from the membrane surface (Weisner et al., 1989). Particle size distribution measurements of the electroflocculated suspension show an increase in particle counts for particles between 5μm-10μm for the higher applied currents. Since permeability of the filter cake and back transport by hydrodynamic forces both increases with increasing particle size (Fu and Dempsey, 1998), this can also explain the flux enhancement. This, however, may not be the sole factor that causes this difference between the two types of suspensions – density and morphology may also play an important role here. Previous results have shown that at pH 5, for all currents EF produces flocs with a similar porosity (exhibited by lower scattering exponent or fractal dimension), although very fragile and undergo compaction. In light of this, increase in membrane performance can be connected not only to floc size, but also to floc stability and structure, which impacts the porosity of the cake formed on the membrane surface.

The residual aluminum measured in the permeate at the higher currents was 0.030mg/l and 0.039mg/l (for 0.16A and 0.2A respectively) (fig. 42), indicating optimal coagulation-flocculation, in which nearly all the aluminum (~98%) was removed from solution, caught on the membrane surface as an aluminum hydroxide mesh. At 0.06A the coagulation mechanisms are in transition due to the formation of a variety of aluminum hydrolysis species. The final pH was 5.5 (fig. 3.4.1-1) and the residual aluminum measured was 0.5 mg/l (fig. 42), which indicates that a large fraction (~21%) of the aluminum was not precipitated as aluminum hydroxide, but was present as soluble species (Al^{+3} and $Al(OH)^{+2}$). Moreover the positive ζ potential of the suspension indicates a transition through charge neutralization for all the currents, so we can assume the major factor causing the differences between the lower current and higher currents is a balance between the quantity of aluminum hydroxide present, the presence of colloidal aluminum hydroxide which has not sufficiently flocculated and could cause a degree of pore blocking, and the structural stability of the flocs.

III.3.4.2.2 pH 6.5

At initial pH 6.5 filtration of kaolin causes significant flux decline, and by the end of the run it has reached 40% of the initial flux (fig.43). Pre-EF of the suspension improves the flux, and for applied currents of 0.12A, 0.16A and 0.2A identical flux behavior is observed, by which the permeate flux reaches critical flux at above 60% of the initial flux. For an applied current of 0.06A there is a 5% drop in the flux compared to the other currents, and the permeate flux reaches critical flux at 55% of the initial flux. At pH 6.5 the dominant coagulation mechanism is sweep floc, due to increased formation of amorphous aluminum hydroxide, although at the higher currents the pH increases significantly (fig.44) and speciation shifts towards $Al(OH)_4^-$ which decreases coagulation efficiency - indicated by the less positive ζ potential. This does not seem to affect the membrane behavior within the dosages used at this pH, because a wide range of currents produced the same results. Therefore, the improved membrane behavior observed here was due to

the formation of aluminum hydroxide flocs in solution, which catch smaller particles and form a more permeable cake on the membrane surface. Moreover, aluminum hydroxide flocs are large enough to be sheared from the membrane surface and therefore the cake thickness is stable, resulting in a stable flux. Particle size counts performed between 5µm-20µm indicate that at 0.06A sizes obtained are on average smaller than those formed at other currents, therefore the cake is less porous and a minor difference in membrane behavior is observed. Particle size distribution measurements show that for 0.12A, 0.16A, and 0.2A the counts between 5µm-20µm are nearly identical, which can explain the similar flux obtained at these currents. Moreover, floc structure analysis at higher currents at pH 6.5 has shown that more porous flocs are obtained than at lower currents, which would result in a more porous cake and lower fouling degree.

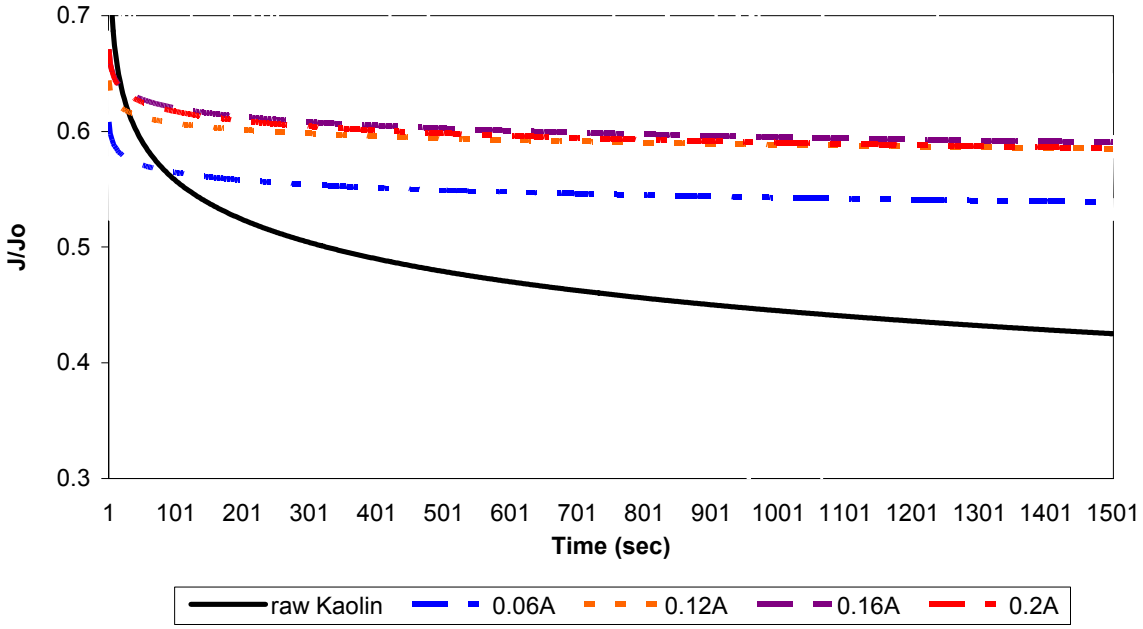

Fig. 44 Permeate flux (J) as a fraction of initial flux (Jo) over the course of ultrafiltration of an electroflocculated kaolin suspension, C_{kaolin}=15mg/l, initial pH 6.5, at various applied currents.

III.3.4.2.3 pH 8

At initial pH 8 filtration of kaolin causes significant flux decline, and by the end of the run it has reached 50% of the initial flux (fig. 45).

Pre-EF does not improve the flux significantly, and for all currents similar flux behavior is observed, by which the permeate flux reaches steady state at 55% of the initial flux (only a 5% improvement relative to the flux obtained when filtering the raw kaolin). At pH 8 the ζ potential of kaolin is more negative, compared to that at pH 5 and 6.5, therefore the particles are more readily rejected from the membrane

(which is hydrophilic and charged negatively), which can explain a slight increase in the initial flux relative to the flux at pH 5 and 6.5. At pH 8 the dominant species is $Al(OH)_4^-$, and therefore no real improvement is observed because coagulation conditions are not optimal. Some aluminum hydroxide precipitates, which is visible, and forms a cake on the membrane surface, but still primary kaolin particles are present in large quantities in solution, because no efficient coagulation occurs. Colloidal aluminum hydroxide could also be present as flocculation conditions are not sufficient. These particles can enter the cake pores and thus reduce the flux, by pore blocking mechanism. The minor improvement in membrane behavior observed here was due to some formation of

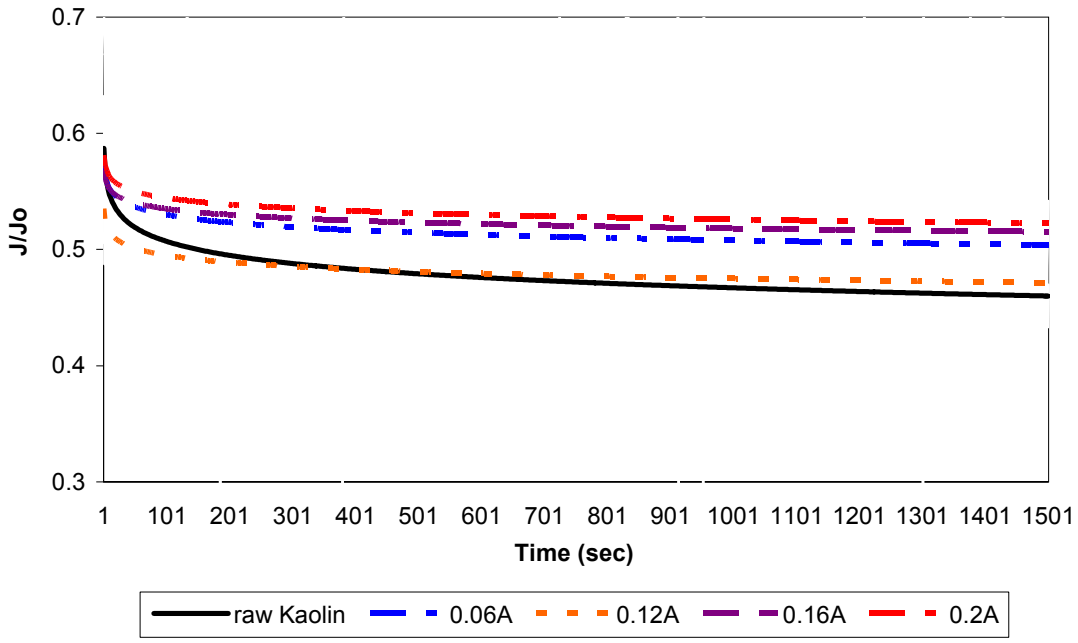

Fig. 45 Permeate flux (J) as a fraction of initial flux (Jo) over the course of ultrafiltration of an electroflocculated kaolin suspension, C_{kaolin}=15mg/l, initial pH 8, at various applied currents.

aluminum hydroxide flocs in solution, which catch a fraction of the smaller particles. The permeate aluminum measurements indicate a large quantity of soluble aluminum which increases with applied current (0.68 mg/l (~28%) and 1.76 mg/l (~22%) for 0.06A and 0.2A respectively), thus corroborating the shift in speciation towards soluble aluminum mononuclear species ($Al(OH)_4^-$ at pH 8).

Particle size distribution measurements show nearly identical counts for all currents, between 5μm-20μm, which can explain the similar flux obtained at these currents. However, particle distribution measurements show much lower counts than those at pH 5 and 6.5, which indicates that less colloidal particles are present. At pH 5 and 6.5 more aluminum hydroxide precipitates as colloidal matter, contributing to the particle counts. At pH 8 the aluminum solubility equilibrium has shifted towards the negative soluble species ($Al(OH)_4^-$), less aluminum hydroxide precipitates resulting in lower particle counts.

III.3.4.2.4 Cake characteristics

Figure 46 shows the visible differences in cakes formed on the membrane surface from filtration of a kaolin suspension and a pre-electroflocculated kaolin suspension.

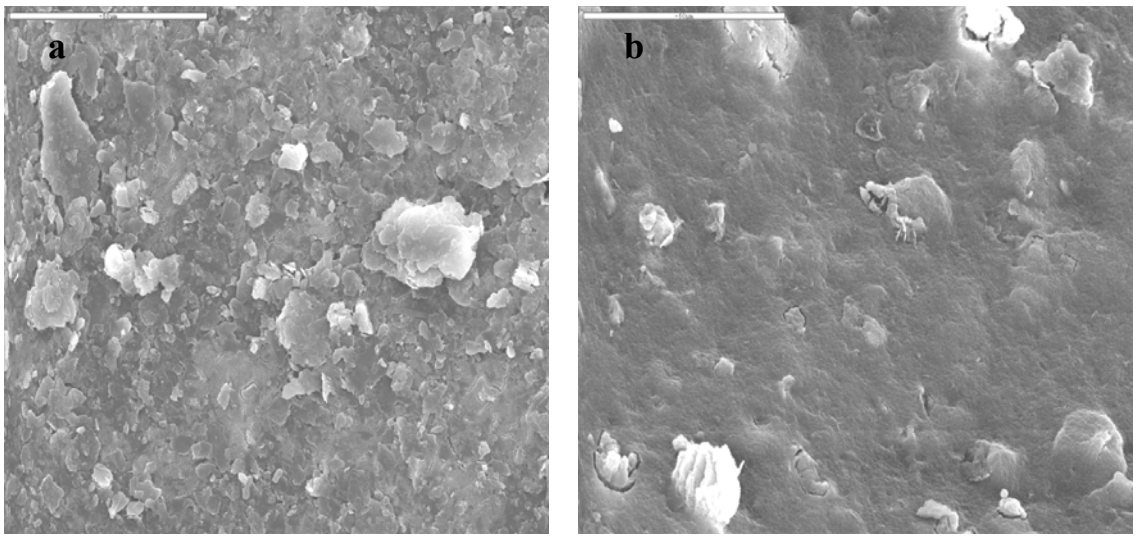

Fig. 46 Cake on membrane after filtration a. **after raw kaolin suspension** b. **after pre-electroflocculated kaolin suspension.**

Filtration of the raw kaolin suspension produced a cake which exhibits a dense and compact form with the kaolin plates tightly packed together. The cake image obtained after filtration of a pretreated kaolin suspension shows a "loose" type of cake, lightly rested on the membrane surface.

III. 4 General Discussion

This study has identified key mechanisms dictating the coagulation/flocculation behavior in EF, and related these to operational parameters such as applied current and reaction time. These parameters dictate first and foremost the amount of coagulant generated within the system, in this case the aluminum ion Al^{+3}. However, the applied current has an additional effect as it also causes the pH to rise, due to hydroxyl ion at the cathode, a product of the hydrolysis which occurs simultaneously. As such, unlike conventional coagulation, the final pH will always be higher than the initial pH. The continuous rise in pH, as more hydroxyl is produced, results in the shifting of coagulation mechanisms throughout the process, until the current is stopped, allowing the pH to stabilize and the species to reach equilibrium. This is evident by the changes in ζ potential as a function of current, which is directly linked to the surface charge of the particles and is indicative of the coagulant species in solution. The degree of pH change, however, can be controlled by adequate mixing conditions. Hence, the application of velocity gradient in EF is not only important to ensure aluminum hydroxide precipitation and floc formation, but also to control the pH increase which, without application of a sufficient mixing regime, can rise to values, depending on type of water being

treated, which are detrimental to the process. Velocity gradients used in lab and full scale flocculation systems (10-30sec^{-1}) were found to be sufficient to stabilize the pH.

An additional mixing mechanism has been identified, which is induced by the passage of current through the system. When lowering the diffusion barrier between primary particles, without applying mixing conditions, aggregation of primary particle was observed when currents were applied. The extent of aggregation in these conditions is indicative of another transport mechanism other than Brownian diffusion. This transport could be induced by the electrical field formed by application of a current, and/or by bubble formation within the system.

When considering EF as an alternative to CF, the differences between the processes should be understood. These differences, small as they may be, are manifested in the chemical and physical characteristics of the treated suspension and resulting aggregates or flocs. Moreover, the kinetics of floc growth and the floc formation range are of utmost importance, as particle removal in water treatment relies primarily on precipitation of metal hydroxide and formation of a stable sweep floc regime. In EF the sweep floc regime is wider than in CF, due to the hydroxyl formation which pushes the equilibrium, according to Le Chatelier's principle, towards enhanced aluminum hydroxide precipitation. Based on the results, figures 47 and 48 demonstrate the differences of the sweep floc ranges in CF and EF, respectively.

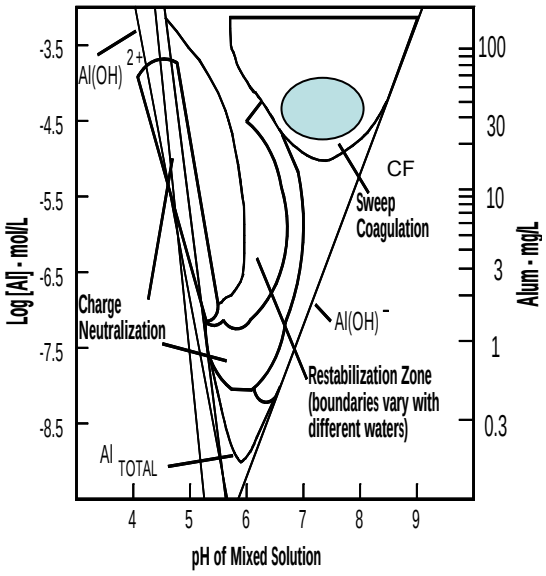

Fig. 47 Sweep floc zone in CF

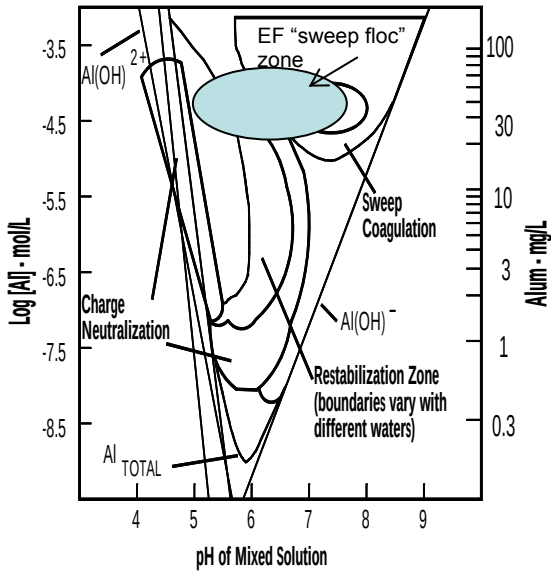

Fig. 48 Sweep floc zone in EF

EF can be considered advantageous over CF as it is able to produce flocs over a wider range of doses and pH values. Thus overdosing effects in EF are less pronounced than in CF. This versatility produces a range of floc "types", depending on conditions of operation and has clear implications to many processes of importance in water and wastewater treatment as flocs can be "tailored" for specific processes, depending on

EF can be considered advantageous over CF as it is able to produce flocs over a wider range of doses and pH values. Thus overdosing effects in EF are less pronounced than in CF. This versatility produces a range of floc "types", depending on conditions of operation and has clear implications to many processes of importance in water and wastewater treatment as flocs can be "tailored" for specific processes, depending on requirements. The structural properties of these flocs and growth rates are dependent on specific operating parameters, primarily the initial pH and current applied.

Growth patterns of flocs formed in EF exhibited for *all* currents applied, for initial pH values of 5 and 6.5, sigmoidal growth behavior, including three typical stages: induction, exponential growth and fragmentation, as found in CF only within optimal dose limits. For adequate precipitation conditions, EF forms generally larger floc sizes than CF, for equivalent doses of aluminum. This, however, would depend on operating conditions, as low alum dosing in these conditions was found to produce equivalent floc size, although at a decreased growth rate. Floc growth in EF has been found to be quicker than in CF and shows a dependency of growth rate on current (dose), with higher growth rates obtained at higher currents. This dependency depends on the initial pH, and a higher dependency exists for enhanced precipitation zones (pH 6.5). This is derived from the stronger linkage between particles within this zone, coupled with increased mass and microbubble generation for higher currents – resulting in larger collision frequencies and collision efficiencies which in turn result in an enhanced growth rate.

Differences in structural evolution patterns between the two processes have also been identified – for adequate flocculation conditions (i.e sufficient growth) in CF, flocs evolve from a more compact structure into a more porous one. In EF, however, the evolution is generally from a less compact structure into a more compact one, although fluctuations have also been observed. EF produces more fragile flocs, which are more susceptible to shear forces, and undergo compaction and in some cases structural fluctuations. It seems that the flocculation mechanism in EF is of a diffusion limited type, with flocs forming at higher growth rates, compared to CF, exhibiting a higher collision frequency and collision efficiency. This behavior is especially evident at pH 6.5, where electrostatic repulsive forces are weaker. CF, on the other hand, exhibits a flocculation mechanism of a reaction limited nature, resulting in flocs which are more compact in the early stages of growth but are able to develop into more porous structures because they are less affected by shear forces.

EF produces flocs which *initially* are more porous than those formed in CF. By comparing the fractal dimension of resulting flocs, over a limited mixing period, to reported values in the literature regarding flocs formed in CF using alum, we find that flocs formed in EF generally fall within the low range of values, indicating a more porous structure. *Without* taking into account restructuring effects, which occur at fragmentation stages when floc size is large enough to be affected by shear forces, a correlation was found

between fractal dimension and aggregate size – lower fractal dimensions were obtained for larger aggregate sizes. This is consistent with flocculation models which have been developed based on conventional coagulation (Diffusion Limited Model and its variants). However, in real water systems, primary particles are not necessarily solid exhibiting fractal dimensions of Euclidean values (i.e.D_2=2) and in orthokinetic flocculation shear forces must be acknowledged, as these can cause fragmentation and restructuring. Thus, the final structures will depend on the shear forces within the system, and on the fragility of the flocs.

Although in EF current density can affect the aluminum dissolution rate, in this study floc growth was found to be independent of current density, and dependent on absolute current intensity.

Current application time was found to affect growth, and for longer dosing periods, larger flocs were obtained. As coagulant efficiency is dependent on the time of reaction in solution, this can be explained by conventional coagulation theory.

With regard to EF as a potential pretreatment to ultrafiltration – this study has proven the efficiency of the process on a practical level. EF can serve as an efficient pretreatment, with enhanced flux observed at pH 6.5 for higher currents, where sweep floc dominates and more porous floc structures are obtained. Although the major fouling factor is cake formation, the flux curves show indication of a degree of pore blocking for all pH values. This can be due to aluminum hydroxide colloidal particles which have not efficiently undergone flocculation, and/or kaolin primary particles still "free" in solution. The differences in critical flux can be attributed to cake properties, such as thickness and porosity, which are a function of the quantity of precipitate in solution and floc structure, respectively. At pH 5 and 8, the flux obtained from pre-electroflocculated suspensions was lower than that obtained at pH 6.5. At pH 5 and 8, less aluminum hydroxide precipitates and more primary kaolin particles are still present in suspension (not captured in the flocs forming), but also colloidal aluminum hydroxide which has not sufficiently flocculated. These can enter the cake pores and cause "self contamination", resulting in increased flux decline. Moreover, for pH 6.5, particle counts indicate that larger flocs are present which can be readily sheared from the membrane surface resulting in a "thinner" cake, which can also explain flux enhancement, compared to other pH values.

These results demonstrate the potential of EF in general as an alternative to conventional flocculation and more specifically as a pretreatment to membrane ultrafiltration. This thesis provides the conceptual development and experimental justification which shed light on the mechanisms of the process. Thus, EF is a reliable and versatile technology that has considerable potential for water treatment and reuse.

III.4.1 Conclusions

EF, although an acknowledged technology, has never been researched at a level aimed at unraveling its underlying mechanisms. Research has focused on efficiency and performance, rather than on the

fundamental basics which is the core of understanding the mechanisms and ultimately will lead to better system design and process control. This thesis has begun the process of elucidating the mechanisms of EF and evolving the technology from an empirical one to a firmly rooted scientific one, which has a promising future in water and wastewater treatment. The major conclusions of this research are summarized below:

- EF cannot be considered an "equivalent" process to CF. The hydrolysis which occurs simultaneously in EF has a major impact on the coagulation mechanisms which are in continuous transition while a current is applied and on resulting flocculation mechanisms as these are a function of aluminum hydroxide precipitation and surface repulsion forces.

- The final pH in EF will always be higher than the initial pH, thus differing from CF in which a decrease in pH occurs. The magnitude of pH rise can be controlled with sufficient mixing conditions.

- The applied current in EF affects particle transport, by the electrical field induced and/or by bubble formation within the system.

- EF is a versatile process exhibiting a wider sweep floc regime than CF, and is able to produce a wider range of floc "types" depending on conditions of operation.

- The flocculation rate in EF is generally higher than in CF. Growth rate is dependent on absolute current rather than current density, with higher growth rates obtained for higher currents. This dependency is increased in optimal aluminum hydroxide precipitation conditions.

- The floc structures formed in EF are initially more porous and fragile than those formed in CF. They are more susceptible to shear stress, and therefore more prone to compaction and restructuring.

- For optimal sweep floc conditions, the flocculation mechanism in EF is of a diffusion limited type while in CF it is more of a reaction limited nature.

- EF can serve as en efficient pretreatment to membrane ultrafiltration of colloidal particles. Differences in critical flux can be attributed to cake properties, such as thickness and porosity, but also to amount of colloidal aluminum hydroxide present that can cause a degree of pore blocking. Aluminum hydroxide precipitation conditions and surface charge of the evolving flocs dictate floc growth and structure – which vary according to initial pH and current applied. Best performance was observed for pH 6.5 for higher currents, where the balance between aluminum hydroxide precipitation and particle surface charge is optimal. These enable a diffusion limited type of reaction and growth into more porous structure (lower SE) resulting in a less compact cake.

Chapter IV-1. D3.3.6 EF–SF–CW and EF–UF–CW configurations study reports.

Integrating system of CW (Constructed Wetland) an EF (ElectroFlocculation process)–GF/MF/UF (Granulated/Micro/Ultra Filtration) study

Date of deliverable M24-M28

ACKNOWLEDGEMENTS

The following researchers from other institutions have had a meaningful contribution to this research:

Avital Gasith, Prof., Tel-Aviv University (Constructed Wetland)
Hadas Maman, Lecturer, Tel-Aviv University (Particles, Biofouling)
Gil Markovich, Prof., Tel-Aviv University (Nanoparticles)
Dana Milstein, PhD student, Tel-Aviv University (Constructed Wetland)

They are all co-authors in published papers. Yet, we would like to extend our appreciation and cordial thanks to all of them and their students.

Avner Adin

and the whole HUJI team

IV-1. 3rd year report

Summary

The to-date research focused on laboratory experiments on electroflocculation and field and laboratory experiments evaluating the efficiency of removal of selected nutrients by CW and its combination with other techniques (GF, EF). According to the hypothesis, the electro-physical system will have a major advantage over the CW itself, mainly by the increased efficiency and seasonal stability of the phosphorus removal process.

This hypothesis has been positively validated by the research conducted in the first part of the project. The general results show, that the combination of three methods (CW, GF, EF) has much higher efficiency of removal of selected nutrients then any single method or the combination of the two of them. The achieved efficiency of the total phosphorus removal by the hybrid method at the level of 97% (resulting in P concentrations of <0.4 mg/L) is by far an excellent result, incomparably higher in relation to other techniques. Good results were achieved for total suspended solids (TSS) removal, which increases from 25% (EF–GF) to 42% (CW) up to 60% (EF–GF–CW). In addition to the phosphorus removal the system is capable of meaningfully reducing some of the total organic carbon (TOC) (53%) and may also have additional abilities of reduction of associated pathogens, heavy metals, and, possibly – endocrine disruptors.

The order of the applied technologies had a great importance to the result. In general, the removal was higher if the system started with the CW, and was followed by the other two techniques. Location of the CW at the end of the technological line resulted often with the increase of some parameters. The great advantage of the hybrid method is also the overall costs of operation – reducing electrical energy use and elimination of chemical discharges to freshwater. Future work will further evaluate the electroflocculation mechanisms, and focus on further evaluation of EF–GF–CW configuration on nutrients removal, and examine EF–GF effect on water quality. It will also concentrate on improving the colloid removal and modeling EF hybrid processes, e.g., EF–UF.

Bench-scale study was firstly performed in the laboratory with artificially constituted water. It could be concluded, that EF can serve as an efficient pretreatment to membrane ultrafiltration of colloidal particles. Differences in critical flux can be attributed to cake properties, such as thickness and porosity, but also to amount of colloidal aluminum hydroxide present that can cause a degree of pore blocking. The effects of EF on the energy costs and fouling mechanisms of the membrane as a polishing treatment step and the optimal operation conditions (pH value, electric current intensity) of the process were further investigated. It was demonstrated that pretreatment by EF is highly efficient in reducing fouling in microfiltration. At optimal condition (pH 6-6.5, 1 μg/liter of Al^{3+}) the energy that can be saved when using EF can be 10 times fold as compared to filtration without adding EF.

Dealing with wastewater effluent treatment, membrane biofouling identification and ways to combat it have had to receive some special attention, due to its major potential economical impact. Alginate and Pseudomonas Aeruginosa bacteria have been identified as a dominant organic particle fouling component and as a dominant biofouling component. However, the use of hydraulic models to characterize a complex system including both has not been examined yet. In this work, different mixtures of those two components are filtered through a dead end laboratory UF membrane system and flux data is analyzed by means of hydraulic models. Short term preliminary experiments (60 min), in which components were examined alone and together, showed an excellent fit (R^2>0.99) to the linearized form of the 'Cake Filtration' model. This excellent fit allowed model extrapolations in which a partial 20 min database enabled forecasting the total 60 min flux verses time curve with good accuracy (max flux deviation <10%). Calculated Alginate specific cake resistance ($1.05–1.45\times10^{16}$ m/Kg) was found to fit with earlier work ($1.11\pm0.08\times10^{16}$ m/Kg). Long term preliminary experiments (Stage 1: 20 min filtration, Stage 2: 72 hr pressure relaxation, Stage 3: 40 min filtration), in which components were examined alone and together, showed an excellent fit (R^2>0.99) to the linearized form of the 'Cake Filtration' model for both Stage 1 and Stage 3. Long term preliminary experiments have also showed significant flux recovery (>40%). This was probably caused by the domination of pressure relaxation effect over biofouling formation effect, and will be further investigated as the work continues.

Alginate has been used as a model polysaccharide in the studies of biofouling and activated sludge bioflocculation. Yet, little has been known for its potential existence in the sludge biomass so far. In order to characterize alginate in the biomass, alginate-like polymers were extracted from different kinds of biomass, e.g. activated sludge, anoxic denitrifying granules, pilot scale aerobic granules and biofilms. Various advanced techniques as UV-visible spectroscopy, secondary derivative FT-IR, ^{1}H and ^{13}C NMR, MALDI-TOF MS, electrophoresis and biochemical assays have been employed to analyze the extracted polymers. Results demonstrate that bacterial alginates do exist in the biomass. Besides their similarities in UV-visible spectra and MALDI-TOF MS spectra with the commercial seaweed alginate, they have their specific characteristics as high degrees of acetylation and being the hydrolysates of alginate lyases. Alginates fine monomer sequences contribute to some different properties of the biomass.

Metal in the form of nanoparticles (NPs) may improve its bactericidal performance in a water/wastewater suspension, which may help to minimize biofouling. The impact was evaluated by calculating log reduction. TEM microscopy was used to characterize the nanoparticles. The activity of the nanoparticles was found associated with concentration as well as with the numerical ratio between NPs and bacteria and NPs mean size. Electrostatic attraction or repulsion between the NPs and the negative charge components in the E.coli membrane were not found as a crucial mechanism for inactivation performance.

To achieve a better understanding of the treatment processes, the particles in secondary effluents (Shifdan WWTP) were characterized, using automated image analysis. The capability to analyze and characterize

particle shape and size by such advanced methodology can significantly assist in improving many process units, particle separation systems in particular. It was shown that filter removal efficiency can be determined by various size and shape parameters, where different information is obtained for each analysis.

During the field work, a necessity had arisen to further investigate the iron behavior. The oxidation processes of iron in electroflocculation cell were investigated for a pH range of 5-9 and a voltage of 3-25 V (corresponding to 0.05-0.4 Amperes). It was demonstrated and proven that, for all practical purposes, in all the pH and electric currents investigated, the form of iron that dissolved from the anode is Fe^{+2} (Ferrous). The gap between the amount of theoretical dissolution as calculate by Faraday's Law and the amount of dissolved iron ions that were observed can indicate two phenomena in electrochemical cells:

With a lower pH, dissolution of the anode is possible even without the operation of an electric current. This leads to higher dissolution rates than the theoretical dissolution rates when the electric current is operated.

The lower amounts of iron that were dissolved at a higher pH indicate that some of the electrons of the electric current participate in other reactions apart from the reaction of anode dissolution. Our results demonstrated that there is a probability that this second reaction is not the reaction of oxygen evolution; while a number of researchers have claimed that this reaction is the second major reaction near the anode.

The oxidation rates of the dissolved Fe^{2+} (ferrous) ions to Fe^{3+} (ferric) ions are almost similar to the known oxidation rates of iron in non electrochemical cells.

Dissolved oxygen plays an important role in the EF process and has far-reaching influence on the following filtration. A dissolved oxygen exhaustion point (DOEP) can be determined. 1.3 mg/L DO concentration in this study could be regarded as the deflection point of ferrous accumulation in this study.

Aeration-enhanced EF system could keep the DO level higher than DOEP, thus enabling the predominance of ferric hydroxide, rather than ferrous hydroxide, in the bulk water, which could provide better removal efficiency.

EF combined with microfiltration could provide excellent results in residual iron and turbidity. It was not necessary to use ultrafiltration for their removal.

Aeration-enhanced EF process hybrid with microfiltration exhibited the potential to provide better removal results of iron. The effluent could meet the stringent standard of unrestricted irrigation and directly river discharging.

The abovementioned studies are based on M.Sc. research study entitled "Coupling physicochemical (electroflocculation) with natural (constructed wetlands) processes for tertiary effluent treatment", and Ph.D. research "Electroflocculation of a model colloidal suspension: coagulation/flocculation mechanisms and their impact on flux in membrane ultrafiltration" were completed. Two M.Sc. studies "Electroflocculatuion-

granular filtration pretreatment for constructed wetlands" and "Particle characterization in wastewater effluents" were completed and the thesises were submitted to review.

Two Ph.D. studies, one on modeling electroflocculation-membrane filtration fouling, and one on nanoparticles membrane filtration; as well as one M.Sc. research on electroflocculation–membrane filtration pretreatment for constructed wetlands are continuing.

During the third year two papers have been published (Water Research and Separation Science and Technology). Two papers on oxidation processes of iron in electro-flocculation (coagulation) cell have been accepted to publication by Desalination and J.Hazardous Materials.

One paper on silver nanoparticles - E.coli colloidal interaction in water has been submitted for publication

Two conference presentations and two posters have been presented.

IV-1.1 INTRODUCTION

IV-1.1.1 Oxidation Processes in Iron Electro-Flocculation (Coagulation)

The expected water source crisis anticipated for the world according to UN reports (UN Environment Program, 2006) is a challenge for innovative water treatment technology and for more intensive examinations of the "old" methods in order to understand the processes and determine their optimal operating methods.

One of the modern processes that is currently drawing attention both scientifically and practically is electroflocculation (electro coagulation) (Chen et al., 2002, Ofir et al., 2000, Harif and Adin, 2007). This method is an alternative to "conventional" coagulation in view of several advantages: Easy operation, less sludge quantities, avoidance of chemical usage and, most importantly, no anions such as chloride and sulfate have been added to the solution (Mollah et al., 2001). Unlike "conventional" coagulation where the coagulants are added to the water as salts, in the electroflocculation process, the aluminum or iron ions, used as the coagulants, are added to the water by dissolving the anode in an electrochemical cell. These coagulant ions ultimately lead to the aggregation of the original particles in the water, which removes in a later sedimentation or filtration process. In the case of iron being used as the coagulant, there are a large number of researches (Den et al., 2006, Matteson et al., 1995, Abuzaid et al., 2002) which have demonstrated that electro flocculation is a very efficient for removing particles from water. The motivation for this research into iron oxidation processes in the electrochemical cell is that some basic mechanisms in the processes of iron oxidation in the electrochemical cell remain unclear and several questions arise from the theoretical description of the electroflocculation process in modern literature.

Modern electroflocculation literature commonly describes the following reactions near the anode and cathode:

Near the anode:

Reaction 1: $M_{(s)} \rightarrow M^{+n}{}_{(aq)} + ne^-$

Some authors (Mollah et al., 2004, Den et al., 2006, Matteson et al., 1995) also claim the presence of an oxygen evolution reaction:

Reaction 2: $2H_2O \rightarrow O_{2(g)} + 4H^+{}_{(aq)} + 4e^-$

Near the cathode:

Reaction 3: $2H_2O + 2e^- \rightarrow H_{2(g)} + 2OH^-{}_{(aq)}$

These reactions explain the appearance of bubbles near the cathodes and the anodes during the process and can also explain the pH increase during the process (dependent on the solution alkalinity and electrochemical process intensity (the intensity of electric current and operation time).

The connection between the intensity of the process (the intensity of electric current and operation time) and the amount of coagulants dissolved into the solution from the anode, is describe by Faraday's Law (1832):

$$w = \frac{ItM_w}{nF}$$

where: I - the current intensity (Ampere), t – operation time (sec), M_w - molecular weight of the metal ($\frac{g}{mol}$), F – Faraday's constant ($96485\frac{C}{mol}$), n - the number of electrons involved in the reaction, w - the quantity of metal that was dissolved (g).

Faraday's Law, as written without any correction factor, is valid only when all the electrons that flow in the system and are measured in the ampermeter, participate in the anode metal dissolution reaction (reaction 1). This law indicates one of the electric charge transfer mechanisms between the solution and the anode Faraday's Law, without the correction factor, it claims that this is the only mechanism occurring near the anode. Therefore, when using Faraday's Law without correction factor, there should not be any other reactions near the anode such as the oxygen evolution reaction (reaction 2).

While older literature from the beginning of the 20th Century (Glasstone, 1942) discusses the need to correct Faraday's Law when there are more reactions near the anode then just the anode dissolution reaction, modern literature generally describes the process by writing the Faraday's Law without any correction factor and also writing the two reactions (1+2), which is, in fact, a contradiction in terms.

While, over recent years, for a number of reasons, there has been a tendency to use iron instead of aluminum as the coagulant ions, the scientific understanding of iron dissolution in electrochemical cells is much more complex, because of the two forms of iron ions that can exist in the solution: Fe^{2+} (ferrous) and Fe^{+3} (ferric). While most authors assume that the form of iron ions that dissolve from the anode is Fe^{2+}, this assumption

still lacks direct evidence (Heidmann and Calmano, 2008) and some researchers claim that the dissolved iron is Fe^{3+} (Mollah et al., 2004, Ofir et al., 2007). When attempting to understand the electroflocculation process, it is very important to clearly understand what form of iron is dissolved. Lacking any answer, the number of electrons that participate in each metal atom dissolution reaction from the anode remains unknown and consequently there is a 33% uncertainty regarding the theoretical value of iron dissolution rate. Furthermore, Fe^{2+} and Fe^{3+} have different coagulation processes and there could be Fe^{2+} oxidation to Fe^{3+} reaction in the process which should be taken into mind.

When the form of dissolved iron ions is Fe^{2+}, the following oxidation reaction of Fe^{2+} to Fe^{3+} could occur:

Reaction 4: $4Fe^{2+} + O_2 + 2H_2O \rightarrow 4Fe^{3+} + 4OH^-$

Morgan and Lahav (2007) demonstrated the strong dependence of Fe^{2+} oxidation to Fe^{3+} reaction rates on the pH and oxygen saturation conditions in non - electrochemical processes. Under alkaline conditions, the Fe^{2+} will immediately oxidize to Fe^{3+} (pH 14-7.6). At a lower pH the rates would be much lower until, at pH 4, the oxidation process becomes negligible.

While reaction 4 is not connected directly to the electrochemical process, it is affected by the amount of oxygen in the water and, thus, by the importance of the oxygen evolution reaction (reaction 2) and also by the redox state of the solution. According to some authors, both of them (the oxygen state and the redox state) can be changed as a result of the electroflocculation process.

At 25 °C, the solubility product of $Fe(OH)_2$ and $Fe(OH)_3$ is 8×10^{-16} (mol/L) and 4×10^{-38} (mol/L), respectively. So the predominance of ferric hydroxide can produce more dense flocs which are beneficial for adhesion, coagulation and later sedimentation. The oxidation of Fe^{2+} to Fe^{3+} can also compensate for the consumption of hydroxyl in the bulk water as shown in reaction 4.

IV-1.1.2 Electroflocculation – constructed wetland hybrid for improved phosphate removal in effluent reuse

Discharge of effluent into streams and rivers is a common practice worldwide. In arid lands competition for the freshwater for human use diminishes stream flow and effluents often make much of the base flow. In such situations stream health and rehabilitation highly depend on effluent quality. Strict standards for effluent disposal call for economic and efficient treatment alternatives. Various sources of wastewater contain growing concentrations of phosphorous and nitrogen cause eutrophication of natural water bodies (Feng et al., 2003). One of the consequences of eutrophication is decreasing of dissolved oxygen which adversely affects fish and other aquatic life, diminishing biodiversity.

Constructed wetland (CW) is an environmental friendly technology for treating wastewater or polishing effluent that is becoming increasingly popular in many parts of the world (Haberl, 2003). It is designed and constructed based on natural marshes (Kadlec and Wallace, 2008). CWs are often classified by the pattern of

effluent flow in the system (e.g., Brix, 2003). In free-flow (surface flow) systems wastewater flows above the ground through emerged, submerged and floating aquatic vegetation. In subsurface flow systems wastewater moves through a porous medium such as gravel or aggregates, in which rooted hydrophytes grow (USEPA, 2000).Subsurface systems are further classified into horizontal flow (HF), in which anaerobic conditions prevail, or vertical flow (VF) which maintains aerobic conditions. Low flow velocities coupled with the presence of roots and solid substrate, promote settling and filtration of particulate material. Biofilm of diverse microrganisms that develops on the porous medium is responsible for most of the biotransformation and mineralization of pollutants. (e.g, Vymazal, 2003; Kadlec and Wallace, 2008). CWs usually remove organic matter and nitrogen (N) compounds efficiently but are less efficient in removing phosphorous (P) compounds (Kadlec and Wallace, 2008).Retention of P in CWs includes peat/soil accretion (mostly in natural and free flow systems), soil adsorption, precipitation and plant uptake (Vymazal, 2003). In subsurface systems removal by plants is limited and requires plant harvesting annually. The adsorption and chemical precipitation of phosphorus is much more vigorous at the initial operation stage because the process has finite capacity (EPA, 2000). As a result, CW capacity for phosphorous removal is quite limited. For the latter reason we considered coupling CW with physicochemical process that is expected to complement the naturally occurring processes by removing phosphorous efficiently.

Chemical precipitation is widely used for phosphate removal. The common precipitants used are aluminum sulphate and ferric chloride. Chemical treatment involves the addition of high amounts of chemicals resulting in undesirable ions residues and extra salinity being discharged in the treated wastewater (Feng et al., 2003). Electroflocculation (EF) is an electrochemical method that utilizes an electric current to separate and clear solid and dissolved pollutants from wastewater.

This method enables water treatment free of additional chemicals, thus offers an alternative to the use of metal salts. EF has been increasingly used in North America for pretreatment of a variety of industrial wastes (Mollah et al., 2001). EF can be considered an alternative process to conventional flocculation, although they are somewhat different. The difference between these processes is manifested in the chemical and physical characteristics of the treated suspension and resulting aggregates (Harif and Adin, 2007). The flocs formed by EF are relatively large and contain less bound water. They are also more stable and therefore amenable to filtration (Abuzaid et al., 2002). The optimum pH for turbidity and phosphate removal is around 5–9 in electroflocculation-electrofloatation by using aluminum and titanium electrodes. In that range the hydrolysis and polymerization of Al^{+3} give rise to the formation of such species as $Al(OH)^{+2}$, $Al_2(OH)_2^{+4}$, $Al(OH)_3$ and charged hydroxo-cationic complexes such as $Al_{13}(OH)_{32}^{+7}$, which are efficient coagulants (Ge et al., 2004). Current density is a major factor in determining the removal rate of phosphate by EF, low initial concentrations of 10–50 mg/l existing in effluents may achieve 90% phosphate removal under low current density values of $5mA/cm^2$, duration 7 minutes (Bektas et al., 2004). The overall goal of the investigation was to assess the utility of a tertiary treatment that couples a physicochemical process, i.e.,

electroflocculation, with natural processes taking place in constructed wetland, to facilitate compliance with stringent standards for river rehabilitation as well as for other uses of treated effluents. Here we examine phosphorous removal applying iron electrodes and vertical flow CW treatment.

IV-1.1.3 Characterization of bacterial alginate extracted from biofilm matrix

Biofilms are dense bacterial communities characterized by close association of bacterial cells generally attached to a solid surface and surrounded by a saccharide matrix. Extra cellular polysaccharides (EPSs) are the major components of bacterial biofilm matrix. They play an essential role in biofilm structure (S. Leone et al, 2006).

To disclose biofilm matrix formation mechanism in water purification system, a few investigations employed alginate as a model EPS (Ye et al, 2005, 2006). Alginate can be produced both by seaweeds and bacteria (algae alginate and bacterial alginate). It is a family of linear EPS consisting of 1, 4-1inked uronic acid residues: β-D-mannuronic acid (M) and α-L-guluronic acid (G) residues with random sequences in the molecule.

Reasons for taking alginate as a model EPS are as follows: 1) Bacteria genera *Pseudomonas* and *Acetobacter* are known to secret bacterial alginate (Remminghorst et al, 2006). Their ubiquitous in nature make bacterial alginate as a popular EPS. 2) As one of the ionic polysaccharides, alginate is capable of forming complexes of unique structure with divalent cations (Ca^{2+}, etc.) easily, resulting in a highly compacted gel network (Remminghorst et al, 2006). 3) During this gel formation process, alginate has the ability to entrap macromolecules (proteins, DNA etc.) and bacteria (Khotimchenko et al, 2001), leading to its possibility to be one of the skeleton part of biofilm matrix.

The importance of alginate on biofilm formation has been confirmed by several investigations (Lee and Elimelech, 2006; Katsoufidou et al, 2005; Maleriat et al, 2000). Yet, it is worth noticing that most of current studies utilized algae alginate in their experiments, very few focused on direct alginate extraction from biofilm matrix and characterization. Due to the fact that differences still exist between alginates secreted by algae and bacteria, such as acetylation degree, ratio of mannuronic acid residue to guluronic acid residue (M/G ratio), and etc., more information would be collected if direct alginate characterization could be performed. To achieve this purpose, bacterial alginate was extracted from a lab-scale biofilm reactor, identified and characterized in the current research. Interaction between Ca^{2+} and the extracted alginate was investigated as well.

IV-1.1.4 Silver nanoparticles - *E.coli* colloidal interaction in water and their effect on *E.coli* survival

Silver in its ionic form (Ag^{+}) is an environmentally friendly anti-microbial commonly used against many species of bacteria including *Escherichia coli* (Feng et al, 2000; Silvestry-Rodriguez et al, 2007; Gentry, Cope, 2005; Poon, Burd, 2004; Zhao and Stevens, 1998). Recent investigations of silver in the form of nano-particles (Ag-NPs) have demonstrated a similar effect, yet in a smaller concentration than the ionic.

Effective concentration of Ag-NPs and Ag^+ were reported at the nano-molar and the micro-molar levels, respectively (Lok et al, 2006; Pal et al, 2007). NPs generally exhibit inherent unique characteristics such as large specific surface area, modified structure, controlled surface composition and reactivity that provide them with remarkable physical, chemical and biological properties (Lok et al, 2006; Pal et al, 2007; Morones et al, 2005;. Parashar et al, 2008). Development of new preparation methods that yield high concentrations and stable dispersions of Ag-NPs, leads to a widening range of antibacterial applications (Panacek et al, 2005; Fernandez et al, 2008; Sondi et al, 2003; Kassaee et al, 2008; Doty, 2005).

Although Ag-NPs have been demonstrated to effectively inactivate bacteria and inhibit microbial growth (Morones et al, 2008; Sondi et al, 2003; Baker et al, 2005;. Shrivastava et al, 2007; Kim et al, 2007; Sondi and Salopek-Sondi, 2004; Lok et al, 2007; Yoon et al, 2007; Li et al, 2005), the mechanism is yet to be fully understood. The bactericidal property of Ag-NPs is partially similar to that of silver ions (Pal et al, 2007). Ag-NPs, like silver ions, attach to phosphate and sulfur groups that are part of the phospholipid cell membrane or to membranal proteins (Morones et al, 2005; Hatchett White, 1996) and cause a severe damage to the cell and its important functions such as permeability, regulation of enzymatic signaling activity and cellular oxidation and respiratory processes (Pal et al, 2007; Shrivastava et al, 2007; I. Sondi and Salopek-Sondi, 2004; Holt, Bard, 2005). Ag-NPs that penetrate bacterial cell, accumulate inside the cells and led to toxicity level that may cause death of the organism (Li et al, 2005) Additionally, Ag-NPs can bind to the DNA inside bacterial cells, preventing its replication (Feng et al, 2000; Pal et al, 2007), or interact with bacterial ribosome (Yamanaka, Hara, 2005). Both Ag+ and free radicals derived from the Ag-NPs are mentioned as responsible for the antimicrobial activity (Pal et al, 2007; Fernandez et al, 2008; J Kim et al, 2007).

Recent studies have focused on some of the physicochemical properties of Ag-NPs, to identify exactly which of the physical or chemical properties of these particles are responsible for the impact on microorganisms. Ag-NPs mode of inactivation on *E.coli* was found to be associated with NPs concentration, bacteria type, NPs shape, presence of Ag(I) and NPs size (Pal et al, 2007; Panacek et al, 2005; Baker et al, 2005; Sondi et al, 2004). Moreover, bacterial growth at a given concentration of silver was found to be dependent on the initial number of cells (Pal et al, 2007; Sondi et al, 2004). In the present study an integrated approach is proposed to elucidate the combined impact of Ag-NPs particle size, dose and initial number of bacterial cells on inactivation of planktonic cells suspended in water. Most of the applications involving bactericidal activity of Ag-NPs so far considered for such particle immobilized on a solid support. However, the focus of this study is on pretreatment technique based on the application of Ag-NPs in suspension. Such a pretreatment can be effective in controlling the formation of biofouling in water systems like distribution pipelines or membrane filtration processes. The bactericidal activity of the NPs is hypothesized to be associated with the ratio between the number of NPs to the number of bacterial cells. Thus, a higher ratio

will increase the frequency of particle-bacterium collisions and attachment and increase bacterial inactivation.

Furthermore, previous studies suggested electrostatic repulsion or attraction as a mechanism to explain the bactericidal properties of Ag-NPs (Yamanaka, Hara, 2005; Stoimenov et al, 2002). It is known that the surface of bacteria is negatively charged due carboxylic and phosphonates groups in the other membrane (Yamanaka, Hara, 2005). Yet, both Ag-NPs with negative zeta potential and charge (Pal et al, 2007; Kim et al, 2007; Sondi and Salopek-Sondi, 2004) and metal oxide NPs with positive zeta-potential and charge (Yamanaka, Hara, 2005), as well as positively charged silver ions (Dibrov et al, 2002) have shown bactericidal activity. Although electrostatic forces between particles are expected, still, electrostatic attraction as a significant mechanism for NPs attachment to bacteria was not previously studied.

In the present study, molecularly capped silver NPs (Ag-MCNPs) were prepared either negatively or positively charged. These particles were prepared accordingly to elucidate the influence of capping agent charge on the ability of the NPs to inactivate planktonic *E.coli* suspended in water, to inhibit bacterial growth and to further support the hypothesized numerical particulate ratio approach. The experiments were carried out in aqueous suspensions containing varying amounts of NPs and *E.coli* cells.

IV-1.1.5 Characterizing shape of effluent particles by image analysis

Filtration is an advanced tertiary wastewater treatment used to reduce the particulate content of effluents. It is especially important to remove particles from effluents as particles can clog drip irrigation systems and enhance membrane fouling (Adin and Sacks 1991). Particles in the effluent are generally evaluated through analysis of turbidity. Turbidity is the most common parameter used for monitoring particles however it is insensitive to particles in the size of a few microns (Gregory, 1998), and does not provide information on the size, and concentration of the individual particles in the water. Moreover, turbidity may not be the best true measure of particle removal processes. Adin (1999) concluded that optimum removal of submicron particles upon alum coagulation was represented by turbidity measurement while removal of particles larger than 1 μm was measurable best through particle size analyzers. Thus, to obtain more sensitive data on particles it is necessary to employ particle counting methods that provide information on particle size distribution.

The size of irregular particles may be simplified to one parameter by defining particles as spheres and isolating the "equivalent spherical diameter" (ECD). Natural particles actually acquire a variety of complex shapes as spheres, ellipsoids, rods, plates or combination of these. Therefore the assumption of particles as spheres is not satisfactory with particles from water and wastewater effluents as they are not spherical in nature and are frequently in aggregates.

There are a variety of methods to measure particle size such as microscopy methods including imaging techniques, light interaction methods, electrical property methods, sedimentation methods, sorting and classification methods. Comparison of particle sizing obtained by different methods is difficult. In most

applications of particle distribution analysis usually the size of the particle is defined and not the shape. Microscopy and image analysis are common methods to characterize shape of particles. However analysis of particles by microscopy is limited to a small number of images thus data is not statistically representative, data analysis is laborious and results can be subjective. The use of dynamic digital image analysis of particles is increasingly being recognized as a sensitive and rapid technique to characterize particle size, shape, count and transparency which can provide insights to particle density and composition (Douglas, et al, 2004; Thomas and Moore, 2004). This technology generates data by capturing direct images of each particle in flowing liquids through automated sample introduction, image acquisition and analysis.

The shape of particles may be correlated to the process wastewater effluents undergo. For example, activated sludge treatment normally yields particles of a well defined, typically oval shape, while wastewater reservoir effluents contain a variety of particles typically characterized by gelatinous particle shape (Adin, 1999). The specific objectives of this study are to characterize particles through particle size and shape parameters (such as circularity, feret max diameter, equivalent spherical diameter and transparency) for various water samples such as effluents from an in-line filtration process with or without use of a coagulant and effluents from secondary treatment after UV and chlorine exposure. Over the last decades, depth filtration has been studied extensively with respect to particle removal (Amirtharajah, 1988), however removal was usually based on size and not on other parameters such as shape. Knowledge of the number, size and shape distribution of the particles present in water, before and after filtration, can provide designers and operators means for improving filtration efficiency. Although the shape has been stated as significant for various processes, the relationship between particle shape and size on process removal efficiency has not been widely investigated in wastewater treatment plants (WWTP) and this type of analysis may provide a new look into particles.

IV-1.1.6 Research objectives and coverage of this report

The overall goal of the research project is to develop and demonstrate an innovative model of integrated system of CW (Constructed Wetland) and EF for upgrading secondary effluent to the level that will permit their use for stream rehabilitation, park irrigation and other municipal uses that require high quality reclaimed wastewater. The work includes evaluation and comparison of the efficiencies of a constructed wetland and the electrochemical technology, in parallel and in series; Optimisation of the design and operation of those technologies, including granular filtration (GF) or membrane filtration (UF/MF) particle separation steps, under site-specific conditions; Assessment of the ecological suitability of the polished effluent as a source of water for stream rehabilitation and downstream reuse; Cost and social impact evaluation of a full scale CW-EF operation, training and education.

This report covers the further development, evaluation and comparison of the efficiencies of a constructed wetland and the electrochemical technology, in parallel and in series; optimisation of the design and operation of those technologies, including granular filtration (GF) or membrane filtration (UF/MF) particle

separation steps, under site-specific conditions; and, more basic studies targeted at better understanding of electroflocculation and membrane fouling mechanisms.

IV-1.2 MATERIALS AND METHODS.

IV-1.2.1 Electroflocculation – constructed wetland hybrid

Standard (chemical) jar tests with extended settling time of 2 hrs were conducted with secondary effluent, aluminum sulfate (alum) or ferric chloride that served as coagulants. In "modified jar tests" a sample was withdrawn from the jars, immediately after flocculation period, and filtered through a filter paper (Whatman 545). An EF cell was built where various electric current intensities were applied during different time cycles (represents coagulant dose) while rapid mixing 800 ml of secondary effluent, followed by 10 minutes of slow mixing and filtration through a filter paper. 12-cm^2 aluminum or iron strip served as anode.

The continuous flow bench-scale experiments were conducted using 1-liter cell equipped with two perforated iron electrodes with an area of 114.22 cm^2, preceding a filter of 39 cm bed depth and 1 mm grain size. Artificial wastewater was prepared as described elsewhere (Egozy, 1996) with additional phosphate stock solution containing 2.865 g/l KH_2PO_4. Wastewater flow rate was 130 ml/min, implying contaminant injection flow rate of 0.65 ml/minute for a dilution ratio of 1:200. A bench-scale, horizontal-flow CW consisting of two units (basalt and dolomite beds) with a total area of 0.216m^2 followed. Filter backwash was activated when a pre-set time/turbidity/ΔP was reached. pH was adjusted, turbidity, particle count, TOC, DOC, phosphate, aluminum and iron were analyzed (specific on analytical equipment may be obtained from the authors).

A pilot EF–CW system (Fig. 49) was built at the Shafdan municipal, activated sludge wastewater treatment plant, comprising of the following components: (a) pre-strainer, (b) up-flow EF generator (EFector, TreaTec21 Industries Ltd.), 1.4 m^3 in volume, 1.25 m in diameter, containing 12 pairs of perforated iron electrodes, (c) granular filter, 1m bed depth and 0.6mm effective grain size, (d) 4 m^3 filtered water tank, used also for system backwash and flushing, and (e) a complex of CW ponds were constructed in the Shafdan WWTP (Tel-Aviv – Dan metropolitan area; Constructor Ofra Aqua Plants, modified by Moran consulting, design, & construction of aquatic ecosystem) (Fig.50). The system included several series of three successive wetland ponds (ca. 35m^2 each), vertical or horizontal subsurface flow and one free flow. The results reported here relate to a treatment by a single VF pond. The VF ponds were packed from top to bottom with an 8cm layer of basalt (20-30mm); 9 cm of basalt (2-3mm); 8 cm basalt (5-10mm); 8 cm dolomite (8mm); 15 cm basalt (3-6 mm) and 20 cm of dolomite (50-60mm) at the bottom. *Cyperus papyrus*, *Canna sp.*, *Iris pseudoacorus*, *Phragmites australis* and *Juncus ensifolius* were planted, but by the third year *Cyperus papyrus* dominated the system. 'Shafdan' secondary effluents characteristics (annual average): turbidity–6.4 NTU, phosphate–2.7 mg/l as P, BOD–12 mg/l, COD–51 mg/l, nitrogen–9.2 mg/l as N, pH 7.35, Fe<0.1 mg/l.

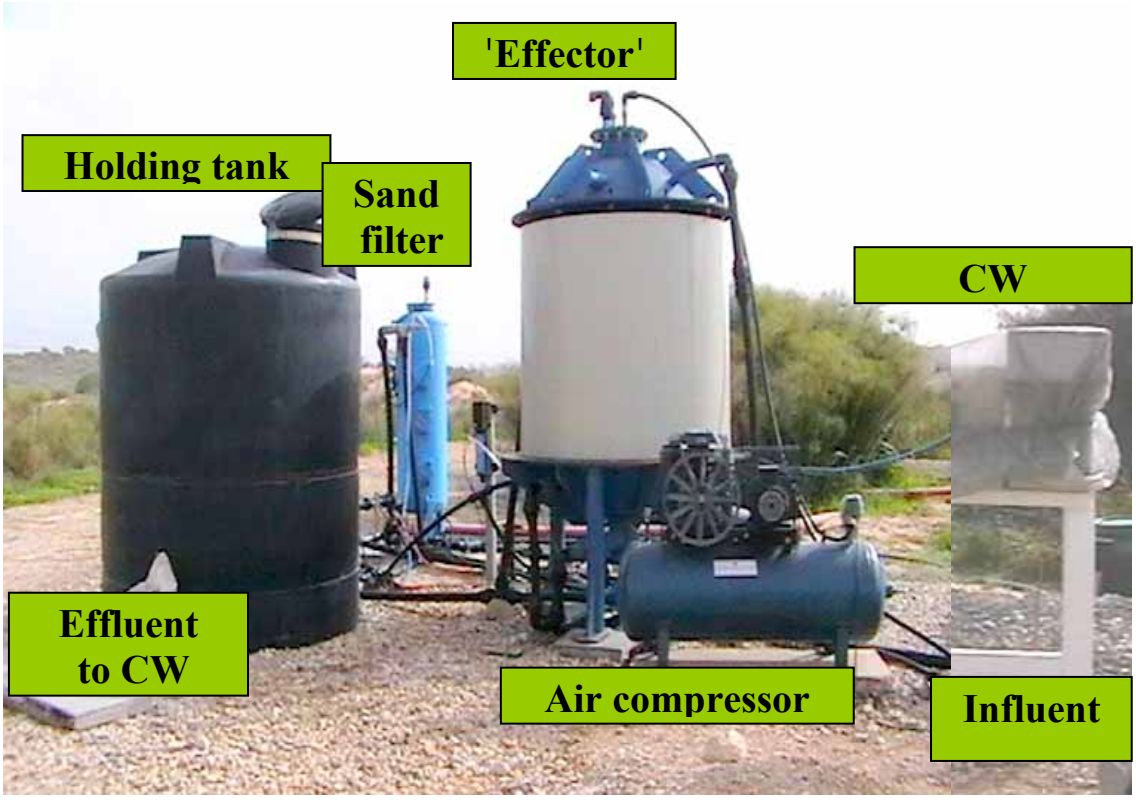

Fig. 49 The EF–CW pilot system

Fig. 50 Shafdan Waste Water Treatment Plant. (Wetland area is shown by the arrow)

IV-1.2.1 Iron oxidation processes.

Tap water

Solution: The examined solution was designed to represent tap water conditions with a conductivity of approx. 1 mS. This was achieved by adding different quantities of NaCl in order to arrive at the desired conductivity. In addition, in order to stabilize the pH, an organic buffer was added (8.32 g/l of Mops (Roth company) for pH 5.67 and 1.5 g/l of Glycin (Roth company) for pH 8.9). Organic buffers were used instead of the commonly used orthophosphate or carbonate buffers because of the possible formation of precipitates which could have influenced the iron dissolution rates.

Three different experiments sets were designed:

Experiments set 1: The aim of this set of experiments was to find out what type and quantity of iron are dissolved under defined conditions (pH 5, 6, 7, 8, 9, and electric current 0.05, 0.1, 0.2, 0.4 A). According to Faraday's Law, the theoretical value of dissolved Fe^{2+} in each case was 3.5 mg/l. Hence the operation time duration was converse to the electric current (for current 0.05, 0.1, 0.2, 0.4 ampere the time was 4, 2, 1, 0.5 min, respectively). Each test was performed at least 3 times for each condition (pH and electric current) and the results averaged to determine the amount of iron that dissolved in each condition.

Since there was an indication of very rapid Fe^{2+}/Fe^{3+}oxidation rates at several pH values, it was necessary to "freeze" the oxidation state of the iron immediately after its dissolution. This was done by adding 1,10-phenanthroline (100 mg/l) into the solution before starting the electrochemical process. The 1,10-phenanthroline forms a red colored complex with Fe^{2+} ions but not with Fe^{3+}. So if the Fe^{2+} ion is the type that dissolves, the 1,10-phenanthroline will compound it and prevent further oxidation. The absorption of light (wavelength 510 nm) is linear for a concentration of Fe^{2+} between 0.5-4 mg/l. Thus, by adding the 1,10-phenanthroline to the solution, it was also possible to determine the Fe^{2+} ions concentration. The total iron concentration was determined by AAS. In addition, at the beginning and end of each test, the oxygen and redox potential were measured.

Experiments set 2: This experiments set was designed to observe whether there is dissolution of the iron unconnected to the electric current and, if so, at which pH values it occurs, respectively. The results of this experiments set should help to explain the iron dissolution rates, which were investigated in experiments set 1. The same procedure performed as in the experiments set 1, the only difference being that, in this experiments set, no electrochemical reaction occurred as the electric current was zero. Each test was performed at least 3 times for each pH and the results averaged to determine the amount of iron that dissolved in each condition.

Experiments set 3: This experiments set's goal was to understand the oxidation rates of Fe^{2+} to Fe^{3+} and the pH dependence of the rates. The solution in this experiment sets was the same as in the two previous

experiments sets but without 1,10-phenanthroline, because its reaction with the Fe^{2+} ions delays or prevents the oxidation process. An electric current of 0.2 A was applied for 1 min at different pH values (5, 6, 7, 8, 9) and then the Fe^{2+} ions concentration was measured using the phenanthroline method at fixed time intervals. The redox potential and oxygen values were also determined.

Electrochemical cell: A glass made from an electrochemical cell was build in order to hold the electrodes at a fixed distance of 5 mm from each other. This cell was immersed in a 2 liter glass beaker and a glass mechanical stirrer (without a magnetic field which could have affected the experiment results) was placed in the middle of the cell. The velocity of the mechanical stirrer in all the experiments was 250 rpm, which resulted in very fast mixing in the cell. The electric current was supplied by a DC power supply (Startron, maximum 30 V and 6.4 A).

Electrode: The anode electrode was made of iron (mild steel ST 37-2) and the cathode of stainless steel (in order to prevent the possibility of additional dissolution from the cathode (Mollah et al., 2004, Picard et al., 1999)). The size of each electrode was 78 mm high×99 mm wide×2 mm thick in deep. Each electrode had 28 holes in order to enable a flow of water in the cell and good mixing. Before each test, the iron anode was immersed in an HCl solution for at least 30 min to remove the oxide layer. Thereafter, in order to clean the surface of iron particles, the electrode was rinsed, then immersed in distilled water for 10 min and re-rinsed with distilled water.

Measurements: The following parameters were measured during the experiments:

pH (Knick pH meter 765 calimatic), conductivity (WTW, cond 315), redox potential (WTW, pH meter pH 191, redox electrode (KCl 3M, Schott, blue line 31 Rx), oxygen (WTW, Oxi 323). The concentration of total iron was measured by flame AAS (Perkin-Elmer 1100B). Before the sampling of the total iron each sample was acidified with a 1.4 M HNO_3 solution. The concentration of ferrous was measured using the 1,10-phenanthroline method (Clesceri et al., 1989).

Synthetic wastewater.

The schematic diagram of electroflocculation hybrid with mechanical, micro- and ultra- filtration in this study is shown in Fig.51. All the experiments were performed at a constant room temperature of 25°C.

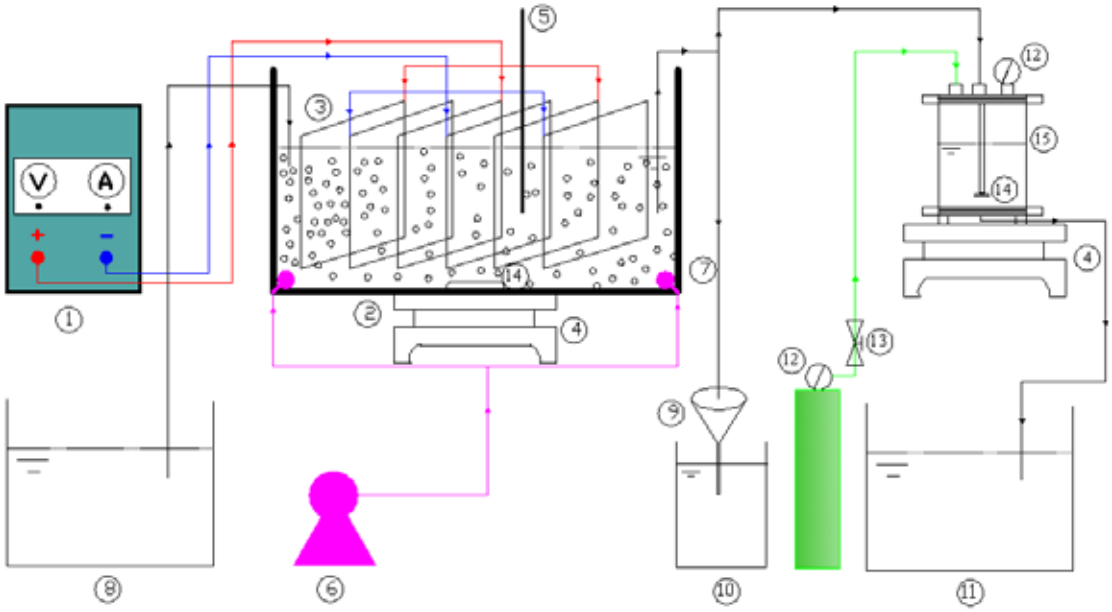

Fig. 51 Schematic diagram of electroflocculation-filtration hybridization (1 DC power supply; 2 Electroflocculation vessel; 3 Iron electrodes; 4 Magnetic stirrer; 5 Oxygen meter; 6 Air Pump; 7 Diffusers; 8 Influent tank; 9 Funnel with paper filter ; 10 Effluent bottle; 11 Effluent tank; 12 Pressure Gauge;13 Pressure regulator; 14 Magnetic stirrer bar; 15 Membrane module)

Electroflocculation. The 14L EF vessel (200 mm width, 400 mm length and 250 mm height) includes six 270 mm × 80 mm × 3 mm iron electrodes with an effective area of 400 cm^2. Plastic stay bearings were put at the bottom of the vessel to support the electrodes 25 mm above the bottom. The net spacing between the iron electrodes is 26 mm. Three pairs of anodes and cathodes are connected in parallel to a DC external power supply. During the EF process, the current was kept at 4.2 A and the voltage found its value accordingly. The EF operation time was fixed at 30 min to keep unification for all the experiments. Before each experiment, all the electrodes were mechanically scrubbed using paper sanding sheet (Klingspor, KL361, J-FLEX, P280, Germany) to remove rust and any precipitates. Occasionally, each of the electrodes was submerged into10% HCl solution for half an hour for intensive cleaning.

Two air diffusers were set at each side of the EF vessel. Compressed air was generated by aquarium air pump (Atec, AR-8500, China). Adequate mixing conditions were created due to aeration and the hydrogen bubbles generated at the cathodes. Without aeration, Magnetic stirrer was used to homogenize the bulk water. With aeration, the compressed air could break all the floating flocs and enabled all the aggregates to suspend in the bulk water. After the electroflocculation operation, all flocs could coagulate and settle down to the bottom due to the high density of ferric flocs produced in this process. Without aeration, the fine hydrogen bubbles could float up part of the flocs and the aggregates in the EF vessel were either in floatation or sedimentation patterns.

Mechanical filtration. During this process, samples were taken from the EF vessel after the operation of electroflocculation, and filtered through filter paper (Whatman, 11 μm, England). The filtered samples were collected in the effluent bottle waiting for further tests.

Membrane filtration. Following the EF process, microfiltration (Microdyn-Nadir, PH-PES 1μm, Germany) and ultrafiltration (Microdyn-Nadir, PH-PES 150kDa, Germany) experiments were carried out sequentially. Siphon was used to transfer the bulk water immediately from the middle of the vessel into the membrane unit. In order to stir the solution thoroughly in the membrane filtration module to mitigate membrane blocking, a draft-tube with a magnetic stirrer bar and a magnetic stirrer (Heidolph, MR3000D, Germany) were employed.

The membrane filtration module was constructed of plastics with dead-end filtration mode having a working volume of 1.5 liters. This module was connected with compressed nitrogen gas bottle ranging 0–12 bars. The replaceable membrane plates were cut in a circle of 15 cm^2 area. During filtration, the trans-membrane pressure was fixed at 0.5 bars and 1 bar for microfiltration and ultrafiltration through the pressure regulator that connected to the compressed nitrogen gas bottle.

Synthetic wastewater. The synthetic wastewater used in this study was comprised of the following reagents: $NiSO_4 \cdot 6H_2O$, 99.3%, J.T. Baker, N.J., NaOH (99%, BDH Laboratory Supplies, England), HCl (37%, Biolab, Israel) and NaCl (99.9%, BDH Laboratory Supplies, England). Ni (II) initial concentration was fixed at 20 mg/L by mixing proper amount of nickelous sulfate with distilled water. Sodium chloride was added to the solution to increase the conductivity to 1.5 mS/cm and reduce electrodes passivation. The synthetic wastewater solution pH was adjusted by using 1:10 (volume) hydrochloric acid and 0.1 M NaOH to 7.8. The synthetic wastewater was prepared in large amount for all the experiments. The dissolved oxygen (DO) concentration in the bulk water was 85% saturation.

Chemical analysis. pH meter (Metrohm, PHM83, Copenhagen), conductivity meter (SML, CDM210, Canada), oxygen meter (MRC, L539070, Israel) and turbidimeter (HACH, 2100N, USA) were employed in this study. The concentrations of the metal ions (Ni and Fe) were analyzed by an Inductively Coupled Plasma Spectrometer (ICP, Perkin Elmer, Optima 3000XL, USA) according to the Standard Methods,2005). The concentration limitation was in the range of 0–1mg/L. All samples were diluted appropriately before testing. The ferrous concentration (Fe^{2+}) in the bulk water was determined according to phenantroline method (Standard Methods, 2005. DO was tested on line after one minute of initiation.

IV-1.2.3 Characteritization of bacterial alginate extracted from biofilm matrix

Reactor setup. A lab-scale submerged biofilm reactor with a working volume of 10 L, an internal diameter of 30cm and a filling height of 30cm was used for conducting the experiment. The reactor was filled with PVC carriers within its working volume, and continuously fed with a synthetic wastewater containing sodium acetate as the sole carbon source (COD loading rate of 6.0 kg m^{-3} d^{-1}) at 25ºC. More details are

specified in (FAO, 1997). 0.5L returned activated sludge from Tuandao municipal WWTP, Qingdao, China was seeded when the reactor was startup. The air flow rate in the reactor was 2L min^{-1}.

Measurement and analysis

Alginate extraction. The biomass on carriers was collected. The alginate was extracted from the biomass according to (Mchugh, 2003) with modifications. The biomass was washed twice with deionized water and dried at 105°C. 1g dried biomass was extracted by 100ml 0.2mol L^{-1} sodium carbonate at 80°C for two hours. After filtration, the supernatant pH was adjusted to 2 by adding 0.1 mol L^{-1} H_2SO_4. The precipitation produced was collected by centrifugation (5000 rpm), and dissolved in 0.1 mol L^{-1} NaOH. Sodium alginate in the supernatant was precipitated by 50%(v/v) ethanol, washed twice in 80%(v/v), once in 96%(v/v) ethanol and lyophilized.

Freeze-dried crude sodium alginate was redissolved in phosphate-buffered saline (PBS) supplemented with 5 mM $MgCl_2$ and 1mM $CaCl_2$, incubated with DNAse I and RNAse A (each at 100ug/ml) at 37°C overnight. Proteinase K was added afterwards (100 ug/ml) for 4h with incubation at 56°C. Enzymes were inactivated by heating for 30 min at 80°C. The ethanol precipitation procedure was repeated once.

The purified alginate was chemically identified by FAO methods (FAO, 1997).

Characterization of the extracted alginate

FT-Raman spectroscopy. The extracted alginate was characterized by recording its FT-Raman spectra on the Raman spectrometer (Labram Infinity, France; He:Ne laser with excitation wavelength of 632.8 nm).

Mass spectrometry. MALDI-TOF MS of the extracted alginate was performed according to [1] with a Bruker Biflex III mass spectrometer (Bruker Daltonics, USA).

Interaction between Ca^{2+} and the extracted alginate. To examine the influence of Ca^{2+} concentrations on the interaction between Ca^{2+} and the extracted alginate, 500 mg L^{-1} extracted sodium alginate solution was extruded through 20ml syringes into $CaCl_2$ solution with Ca^{2+} concentrations of 20 mg L^{-1}, 40 mg L^{-1}, 100 mg L^{-1}, 500 mg L^{-1}, 1000 mg L^{-1} and 2000 mg L^{-1} respectively.

Samples at 20 mg L^{-1} were also deposited onto a newly cleaved mica sheet, air dried (1 h) in a dust-free enclosure, imaged by an atomic force microscope (AFM) (SPM-9500J3, SHIMADZU, Japan).

Triplicates were conducted for each experiment above.

IV-1.2.4 Silver nanoparticles - E.coli colloidal interaction in water

Materials. *E.coli* ATCC 35218 was purchased from Hy-labs (Rehovot, Israel). The Luria-Bertani (LB) medium used in growing and maintaining the bacterial culture was supplied by Difco Laboratories. The formula for 1 L is Tryptone-10g, yeast extract-5g and Sodium chloride-5g. 3-Mercaptopropionic acid (MPA) 99% was obtained from Aldrich. Silver nitrate was obtained from Carlo Erba reagents. Sodium borohidride

99% and Polylysine 26300MW were obtained from Sigma-Aldrich. Hydrogen tetrachloroaurate(III) trihydrate was obtained from Sigma-Aldrich, G4022-1G.

Preparation of Ag-MCNPs and Au-MCNPs. The synthesis of the NPs is based on reducing metal ions in solution in the presence of several types of stabilizing agents. Aqueous silver nitrate ($AgNO_3$) 0.04M as the source of silver ions was mixed with mercaptopropionic acid (MPA) 0.03M as an anionic stabilizing agent or Polylysine 4.8 mM as a cationic stabilizing agent. The anionic capping agent, mercaptopropionic acid, is a small, widely available, inexpensive anionic surfactant from the family of thiol containing molecules. Thiol groups are know form strong bonds to gold and silver surfaces and thus are the best anchor group to the silver surface and the carboxyl group provides the negative charge around neutral pH conditions. Analogous amine containing thiols that should be able to provide the positively charged counterpart under neutral pH are not able to stabilize the silver nanoparticle colloidal dispersion. A possible reason for this asymmetry is the high affinity of the amine group to the silver and gold surfaces. In this case the bi-functional thiol-amine molecules act as efficient cross-linkers between the nanoparticles and induce aggregation and precipitation of the nanoparticles. Thus, for cationic silver nanoparticles, low molecular weight polylysine was found as a very good surfactant, allowing to obtain stable isolated single or few particle dispersions with a high zeta potential value, indicating high positive charge density at the polylysine coated particle surfaces with minimal inter-particle cross-linking, probably due to both the strong electrostatic and steric repulsions.

The solution was stirred and the pH was adjusted to 7 using sodium hydroxide (NaOH). Sodium borohydride ($NaBH_4$) was added slowly to the solution in order to reduce the Ag ions. A dark brown color appeared while adding the sodium borohydride until the solution appearance stabilized. Finally, stable MCNPs of 4-20 nm sizes with negative or positive charge were obtained. A dispersion of relatively narrow size distribution of about 7 nm mean size was obtained after removing larger particles and aggregates by centrifugation at 13,500 rpm for 10 min for Ag-Polylysine particles (Ag-PL) and centrifugation at 13,500 rpm for 30 min for Ag-MPA particles (Ag-MPA). The Synthesis of gold nanoparticles (Au-MCNPs) was followed by a similar protocol as Ag-NPs, with aqueous gold chloride tri-hydrate 0.04M used as the source of gold ions.

Methodology for studying the effect of MCNPs on inactivation of E.coli. To examine the effect of MCNPs on *E. coli* inactivation, *E.coli* ATCC 35218 was grown in 80 mL of a liquid LB medium to a mid-log phase culture (optical density of about 0.4 at 570 nm). *E.coli* in the range of 10^5–10^8 colony forming units (CFU) were suspended in 1 mL of distilled water supplemented with negatively or positively surface charged MCNPs. The particles concentration in the suspensions varied from 1 to 60 μg mL^{-1}. A suspension with the same conditions but without NPs was used as a control. A suspension of Au-MCNPs with the same surfactants and average size was used as another control for NPs of similar size but of a presumably inert metal. Pure surfactant solutions (poly-lysine, MPA) were used as vehicle control. The suspensions of

bacteria and NPs were well mixed by Vortex and aliquots of 50 µl were cultured on LB agar plates. The plates were incubated in 37°C for 24 hours. Colonies were enumerated and log reduction ($\log_{10}N_0/N$) for each treatment was calculated relative to the colony number of the untreated bacteria (N_0). N is the number of bacteria that survived the treatment (CFU). All experiments were performed under sterile condition and in triplicates.

The interaction between *E.coli* and NPs was examined by transmission electron microscopy (TEM). As a first step of specimen preparation, a sample containing distilled water, 10^7 CFU mL^{-1} *E.coli* and 45 µg mL^{-1} of Ag-MCNPs or Au-MCNPs were prepared. A drop of 10 µL was deposited on a TEM copper grid with a lacy carbon film. In order to fix the bacteria, the grids were exposed to a 2.5% glutaraldehyde in PBS solution for 30 min. Grids were washed three times in phosphate buffer saline (PBS) and three times in distilled water, to clean the grids from salt and buffer deposits. The bacteria-NP specimens were imaged in a TEM (FEI Tecnai F20).

Methodology for studying the effect of Ag-MCNPs on growth rate. To study the effect of MCNPs on bacterial growth, a fresh colony of mid-log phase *E.coli* (10^8 CFU mL^{-1}) grown in LB medium was well mixed with 50 µg mL^{-1} Ag-PL (sample PL50) and 33 µg mL^{-1} Ag-PL (sample PL33) in water. Two mL aliquots of each suspension (treated or non-treated bacteria) were inoculated into 100 mL of fresh LB medium (without NPs). The suspensions were agitated on a shaker bath. Growth trends were monitored by measuring optical density at 570 nm at predetermined intervals. The reference of the spectrophotometer was the same LB medium without bacteria.

Characterization. The optical density of the bacteria cultures in liquid LB were evaluated using a UV200RS spectrophotometer. Particles size distribution (PSD), average particle size; morphology and colloidal stability of the Ag-MCNPs were characterized by TEM. The size characterization of the samples was carried out on TEM images using the software "Digital Micrograph" by Gatan. The data was statistically analyzed using the software OriginPro 6.1. Zeta potential measurements were conducted in an electrophoretic light scattering apparatus (Zeta Sizer-Nano series Malvern Instruments) to examine the colloidal stability and charge of the NPs.

IV-1.2.5 Characterizing shape of effluent particles by image analysis

Pilot Plant

A filtration pilot plant was constructed at a WWTP designed to produce effluents that follow guidelines for Israeli unrestricted irrigation (Halperin, 1999). The pilot plant is a unit located near the actual wastewater reuse facility (Shafdan, Tel Aviv, Israel). The secondary effluent from activated sludge basin flows into the tertiary pilot plant which is based on in-line filtration process that integrates the coagulants during the processes to reduce effluent particulate load.

The pilot plant units are high-rate deep bed filters with filtration velocities of 10-15 m/sec and a flow of 5 m^3/hr each one. The filters are 1.4 m high and are composed of two layers with 70 cm anthracite and 70 cm sand with porosity of 0.27 and 0.43 mm respectively. The coagulant Poly Aluminum Chloride (PAC) at concentration of 2.3 mg/L was added directly on the filter media to improve filtration in a process termed in-line filtration while the other filter is identical but without addition of coagulant. Samples for analysis include secondary effluent prior to filtration, samples after filtration and backwash samples. Samples after filtration will be termed "PAC" or "NPAC" for filtration with or without PAC respectively. The goal is to determine removal efficiency through particle size and shape parameters. A control system is responsible for measurement of the pressure before and after the filter that controls the backwash automatically at a backwash flow of 11 m^3/hr and velocity of 35 m/hr. The filtration process run is 6 to 8 hours or 300 cm of head loss.

Additional samples after secondary treatment in another WWTP (Ramat HaSharon, Israel) after UV or chlorine disinfection are held in a reservoir and examined after two weeks to study the correlation between size and shape parameters. These samples will be termed "Chlorine" or "UV". Another inorganic sample taken from soil and separated to the silt fraction was analyzed and termed "Silt". Soil samples were collected from the North Negev region, Israel which is characterized by high silt content. The separation method for the silt fraction was based on the piped method (Day, 1965).

Image Analysis

Particles suspended in liquid are analyzed by the "Micro Flow Imaging" (MFI) technology (DPA 4100, Brightwell Technologies Inc, Ottawa Ontario, Canada). This apparatus employs a digital camera with an illumination and magnification system to capture in-situ images of suspended particles in a flowing sample. Basically a sample fluid is drawn through a flow cell and a sections of the fluid are illuminated with LED light source at λ= 475 nm, magnified and imaged onto a digital camera. These captures images are automatically analyzed to determine various size and shape parameters that represent the two dimensional projection of the particles.

Analysis was conducted with low magnification set point with particle analysis between 2.25–400 μm. The pixel density is 1.3 Mega pixels, and the size of each pixel is 6.7 × 6.7 μm, with a field of view of 1760 × 1400 μm with a resolution of 0.25 μm. The threshold value which separates background from particles is predefined however there is a possibility for manual threshold and background is subtracted by optimizing illumination. During the run images of particles in binary and grey scale files are obtained, with predefined number of images captured for each run. System calibration is conducted with polymer microspheres with mean diameters of 5 μm ± 0.05 μm and 10 μm ± 0.1 μm with narrow size distributions and certified by manufacturer (Duke scientific, USA).

The geometric characteristics of samples were expressed in the following parameters:

1. ECD (µm) is the equivalent circular diameter.

2. Circularity is a dimensionless number between 0–1, where circularity =1 for a spherical particle and circularity =0 non spherical particle. It is defined as (circumference of an equivalent area circle) / (perimeter of the particle).

3. Average Intensity is defined as (sum of all pixel intensities in object)/(Number of pixels). A pixel with intensity greater than the predefined threshold will be considered by the system to be carrier fluid, while intensity levels below the threshold will be considered to be particles. High intensity means transparent particles.

4. Max Feret's (or Ferret's) Diameter is defined as the max diameter between two points on the perimeter between which a line can be drawn within the perimeter.

5. Area is defined as the total numbers of pixels covering the object.

6. Perimeter is defined as the total number of perimeter pixels.

IV-1.3 RESULTS AND DISCUSSION

IV-1.3.1 Electroflocculation – constructed wetland hybrid

Field pilot stage

CW performance**.** Wetland performance was evaluated after three years of operation (mature system). The following average removal efficiencies (n= 6, Table 11) were recorded after treatment in the first VF pond. Relative to inflow concentrations BOD and TSS removal was high (>60%) resulting in concentration suitable for stream rehabilitation. Excellent ammonia removal (>90%) was achieved following efficient nitrification in the first VF pond. As a result the effluent of the first VF pond was enriched with nitrate. Nitrate removal was attained in the last, free-flow pond (final concentration 0.8±0.8 mg/l nitrate-N) and overall total nitrogen removal was >50% (final concentration 2.1±1.1 mg/l). No removal of phosphate occurred in the wetland mature system.

Table 11 Average removal efficiency and effluent concentration of selected water quality variables after treatment of Shafdan secondary effluent in vertical subsurface flow constructed wetland

Parameter	Removal (%)	Final concentration (mg/l)
BOD	63±16	2.3±1
TSS	67±20	1.5±0.9
NH4-N	93.2±5.5	0.15±0.12
NO3-N	-211.2±237.9	1.9±1.45
PO4-P	-11.3±49.3	1.3±0.6

Phosphorous removal by EF-CW systems (Fig.52)**.** Total phosphorous (TP) removal by different treatment configurations is depicted in Fig. 4. CW alone removed up to 20% of TP, while EF alone removed 10–-40% of TP regardless of Fe concentration. Filtration improved TP removal to an average of 90% when Fe concentration exceeds 5 mg/l, with optimum 97% TP removal reaching TP concentration <0.3 mg/l. For Fe<5 mg/l TP removal by EF–GF–CW ranged 75–89% resulting in TP concentration <0.7 mg/l at all times. Laboratory experiments presented earlier had shown similar results. When EF-GF preceded CW treatment, TP removal depleted to a maximum of 83% removal for Fe>5 mg/l, with TP concentration of 0.3-0.7mg/l. Comparing the later with the above mentioned results indicate that CW consistently contributed additional phosphorous to the effluent; that could be explained by formation of a phosphorous 'reservoir' supplied by (a) Shafdan's secondary effluent between EF treatments, and (2) plants decay, and released by water of lesser concentration.

CW–EF–GF configuration showed similar results to the EF–GF treatment, reaching an average of 90% TP removal, re-convincing that CW did not affect the TP level after granular filtration. Those results indicate that the latter is the best configuration for TP removal from wastewater.

Still, it is possible that a long term flow of low phosphorous wastewater through the CW would have eliminated the phosphorous reserve and so would improve on the EF–GF–CW results. This long term operation could not have been carried out under current conditions for technical limitations. When observing residual Fe concentration after EF–GF, results show that only for initial Fe concentration >12 mg/l there is a 95% Fe removal by granular filtration and only for initial Fe concentration >15 mg/l there's less then 0.5 mg/l Fe in the filtrate. This indicates that raising coagulant does effect both phosphorous removal and residual coagulant concentration. Raising coagulant dosage, with the enhanced conveying streams, induced by the increased current intensity, creates more opportunities for successful particle collisions and flocs formations, which can be further removed by the sand filter.

Turbidity, TSS and TOC removal by EF-CW systems. Table 12 summarizes the field pilot results of the different system configurations experimented in this work. Extra turbidity is formed within the system by the ferrous/ferric addition. It is possible that the extra turbidity is a result of a delayed oxidation of bivalent to trivalent iron. That mechanism has to be further investigated. Turbidity removal is optimized only with enhanced sand filtration. The wetland constantly reduced residual Fe concentration by at least one order of magnitude but not less then levels of 0.2–0.5 mg/l Fe. Some amount of Fe passes through the sand filter and the CW bed causing lowest residual turbidity of 0.88 NTU. Results for carbon load removal showed a similar picture with EF–GF capability of reducing about 20–30% of the TOC in the system, depending on coagulant dose, as shown in the bench scale study. Again, adding the CW improved organic matter removal and when CW preceded the electroflocculation unit, TOC removal was 53% at best.

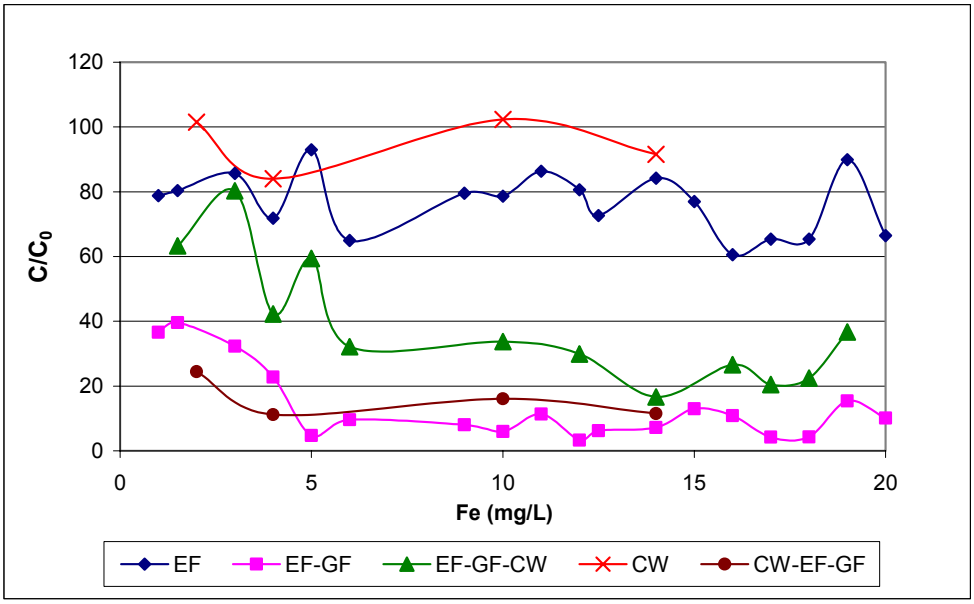

Fig. 52 Residual phosphorus in 'Shafdan' secondary effluent for different treatments. C_0=1-3 mg/l TP. Flow rate 1.5 m^3/hr.

Table 12 Field pilot results of different configurations.

	Influent	Outlet EF-GF	Outlet CW	Outlet EF-GF-CW	Outlet CW-EF-GF	No. of exp.
TP, mg/l	1.40±0.54	0.22±0.18	1.10±0.15	0.53±0.33	0.17±0.04	35
Turbidity,NTU	3.3±0.8	3.2±1.7	09±0.3	2.4±0.9	12±0.38	30
TOC, mg/l	12.2±2.3	10.8±1.4	8.0±0.8	9.4±1.4	6.4±0.6	20
TSS, mg/l	4.9±2.6	4.8±2.1	1.4±1.0	2.5±1.3	0.6±0.2	25

Particles removal by EF-CW system

Particle count and particle size distribution were analyzed at the range 2–350 μm (HIAC Royco Liquid Particle Counting System 9703). The influent water was treated at five concentration of iron added by EF. Particles count and distribution were measured in influent, after EF, EF-GF and EF-GF-CW treatments. The typical cumulative particle size distribution and a normalized differential particle concentration of such experiments is shown in Fig.53 and Fig.54, respectively.

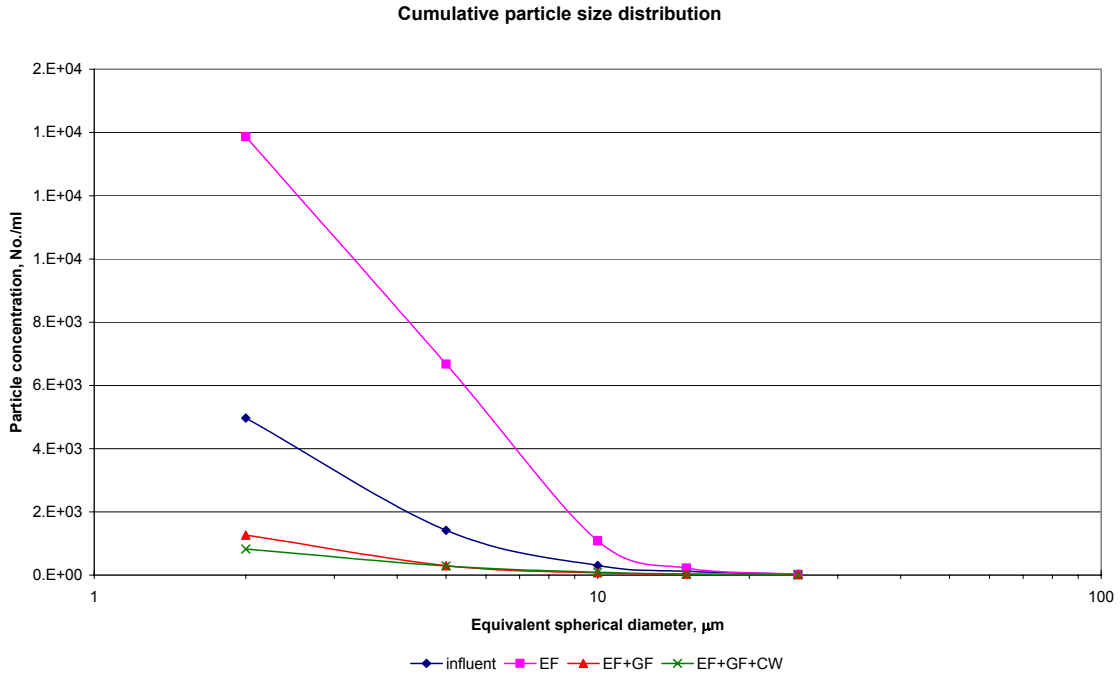

Fig. 53 . Particle size distribution. Shafdan EF-CW pilot plant.

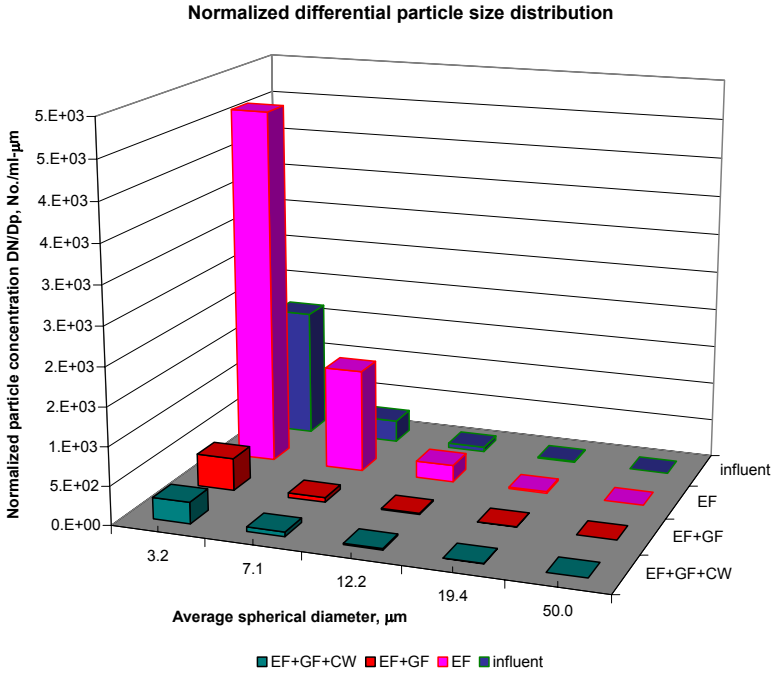

Fig. 54 Normalized differential particle size distribution. Shafdan EF-CW pilot plant.

Fig. 55 summarizes the particle removal efficiency at different stages of treatment at different iron concentration. It can be seen, that the particle concentration grows after electroflocculation and reduced up to 80–90% after complete treatment.

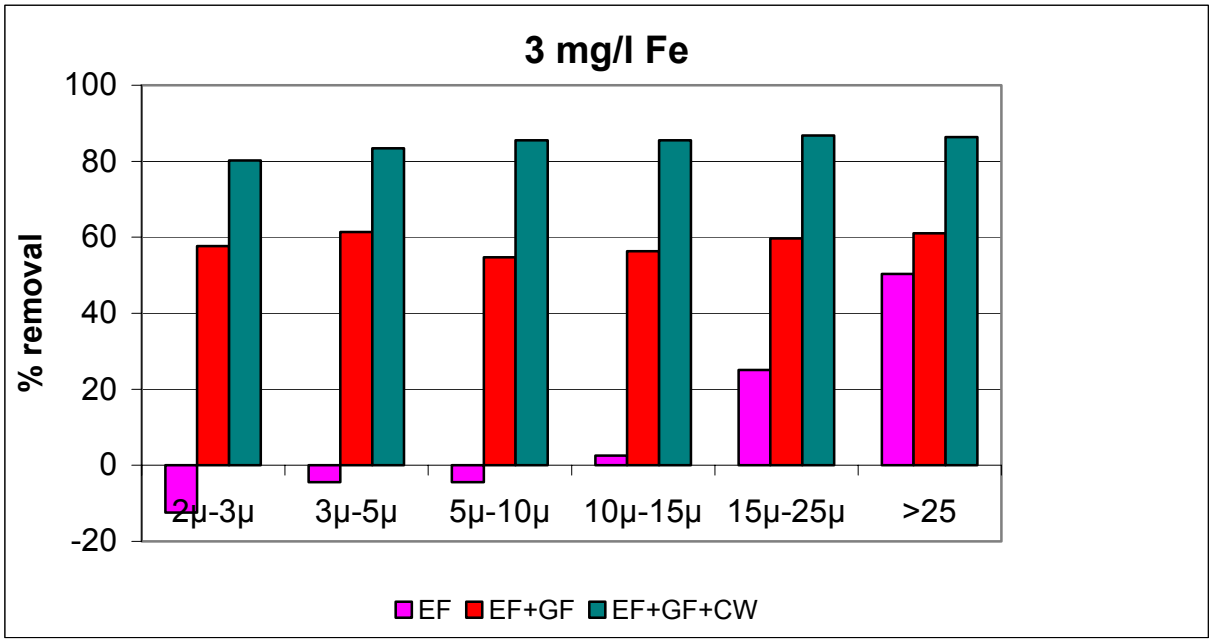
3 mg/l Fe
% removal
100
80
60
40
20
0
-20
2µ-3µ
3µ-5µ
5µ-10µ
10µ-15µ
15µ-25µ
>25
EF
EF+GF
EF+GF+CW

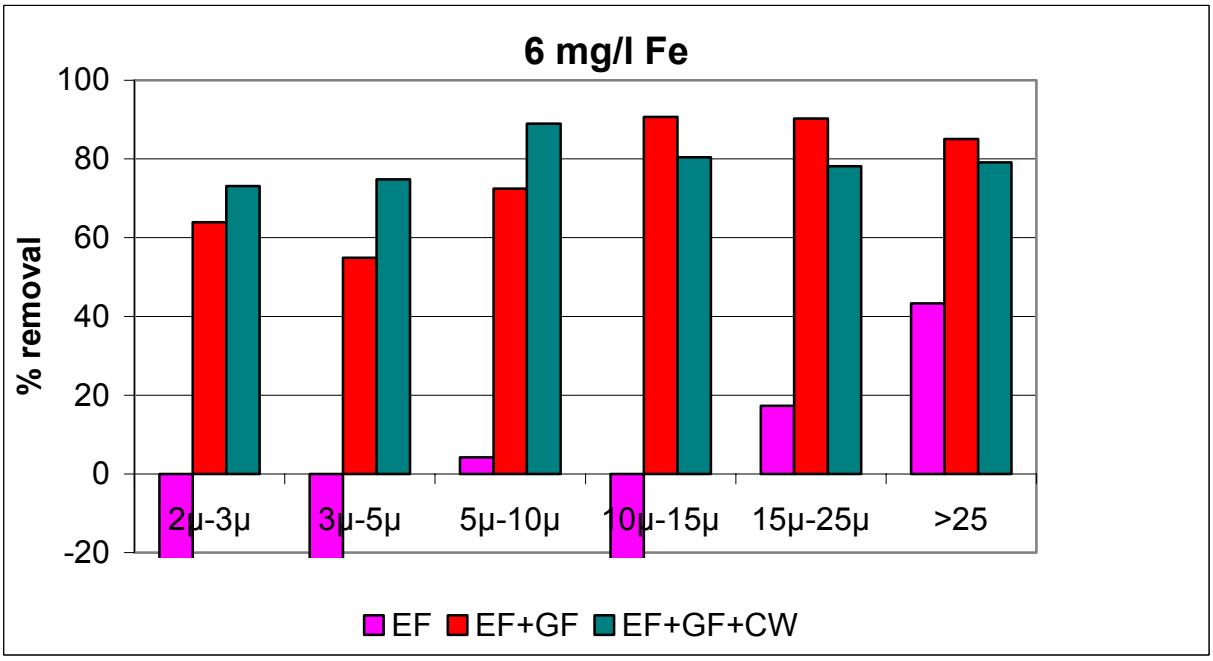
6 mg/l Fe
% removal
100
80
60
40
20
0
-20
2µ-3µ
3µ-5µ
5µ-10µ
10µ-15µ
15µ-25µ
>25
EF
EF+GF
EF+GF+CW

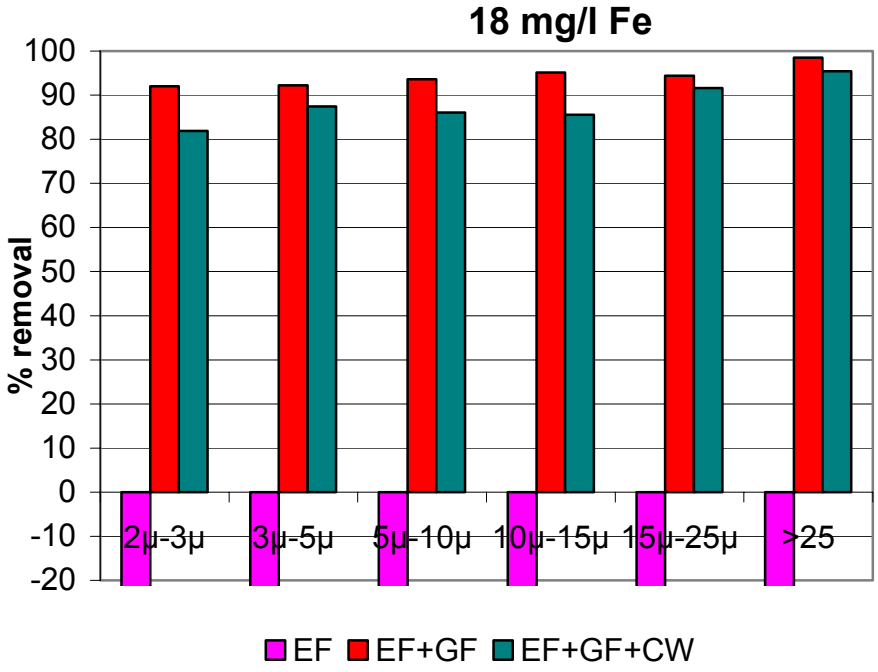
18 mg/l Fe
% removal
100
90
80
70
60
50
40
30
20
10
0
-10
-20
2µ-3µ
3µ-5µ
5µ-10µ
10µ-15µ
15µ-25µ
>25
EF
EF+GF
EF+GF+CW

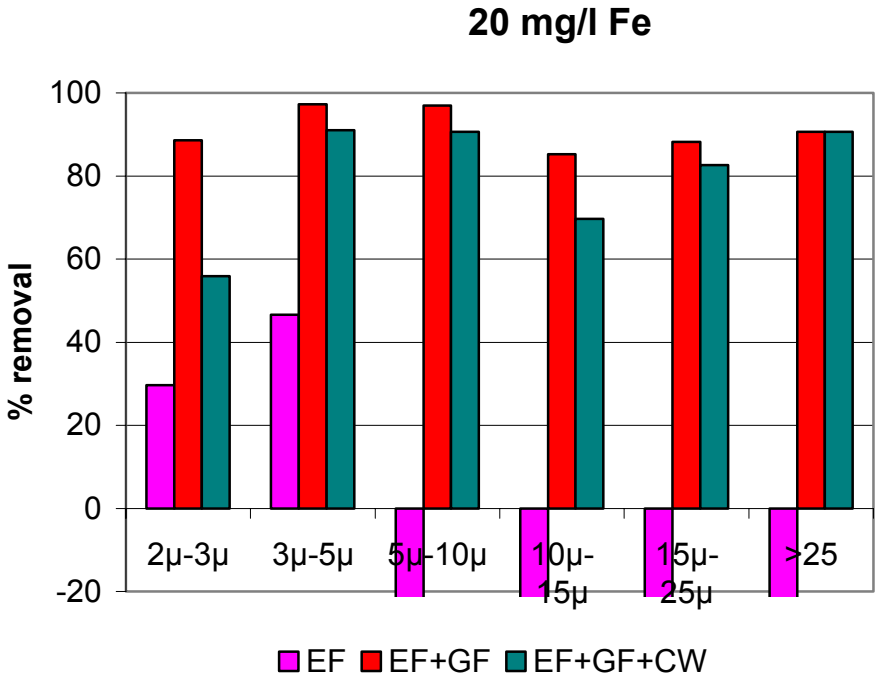
20 mg/l Fe
% removal
100
80
60
40
20
0
-20
2µ-3µ
3µ-5µ
5µ-10µ
10µ-15µ
15µ-25µ
>25
EF
EF+GF
EF+GF+CW

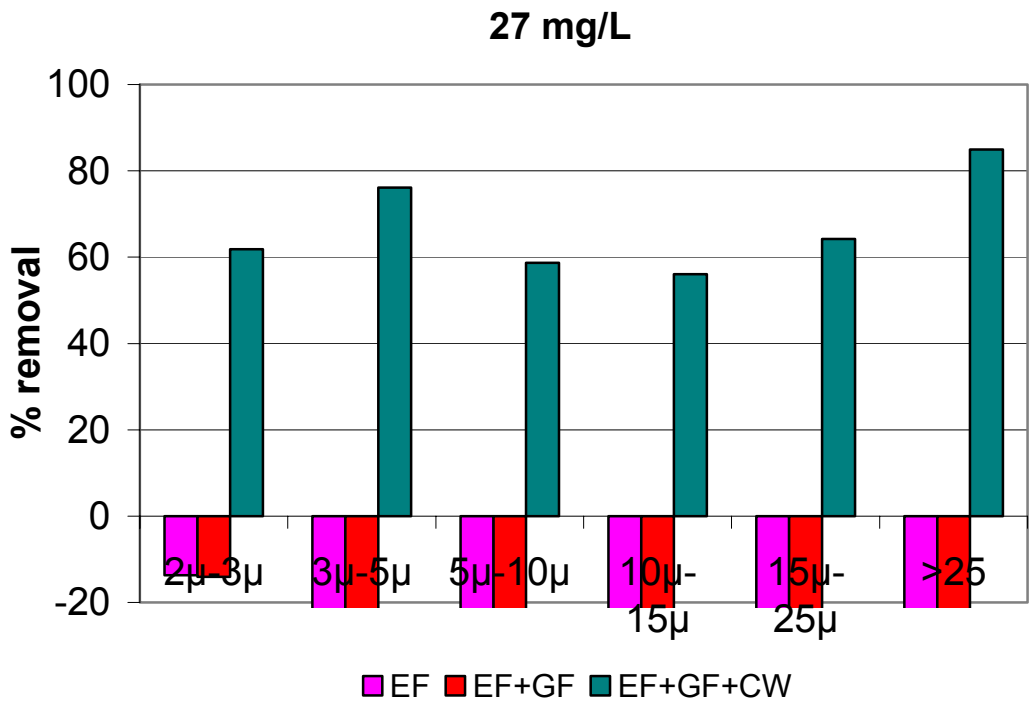

Fig. 55 Particles removal efficiency as a rate of different iron concentration. Shafdan EF-CW pilot plant

IV-1.32.2 Iron oxidation properties

Tap Water

Tables 13, 14 represent the average ratio between the measured Fe^{2+} and the total iron concentration for various pH and electric current values, according to the results of the first experiments set. At lower pH values (5, 6) the Fe^{2+} to Fe total ratio is more then 90% while at higher pH (7-9) the ratio is about 82%. In all the electric current intensity the Fe^{2+} to Fe total ratio is between 84-91%.

Table 13 Average Fe^{2+}/ Total Fe ratio as a function of measured pH.

pH	Number of experiments	Average Fe^{2+}:total Fe (%)	Standard deviation (%)
5	34	90	12.7
6	37	96	9.5
7	29	82	13.7
8	30	83	7.4
9	24	83	12.6

Table 14 Average Fe^{2+}/ Total Fe ratio as a function of measured electric current.

Electric current	Number of experiments	Average Fe^{2+}:total Fe (%)	Standard deviation (%)
0.05	46	87	15
0.1	42	88	12
0.2	35	91	10
0.4	30	84	12

Iron dissolution results for set experiments 1 are shown in Fig 8-10. While for all the experiments the theoretical concentration of dissolved iron was 3.5 mg/l, the actual results showed concentrations of more then twice that value (>8 mg/l) at lower pH values (5,6) and almost half that value (1.7 mg/l) at a higher pH (9) value (Fig. 56). Since at pH values of 5, 6, 7 the buffer was Mops and at pH values of 8, 9, the buffer was the same quantity of Glycin (1.5 g/l), it was preferable to show the results in two separate illustrations (Figs. 57, 58).

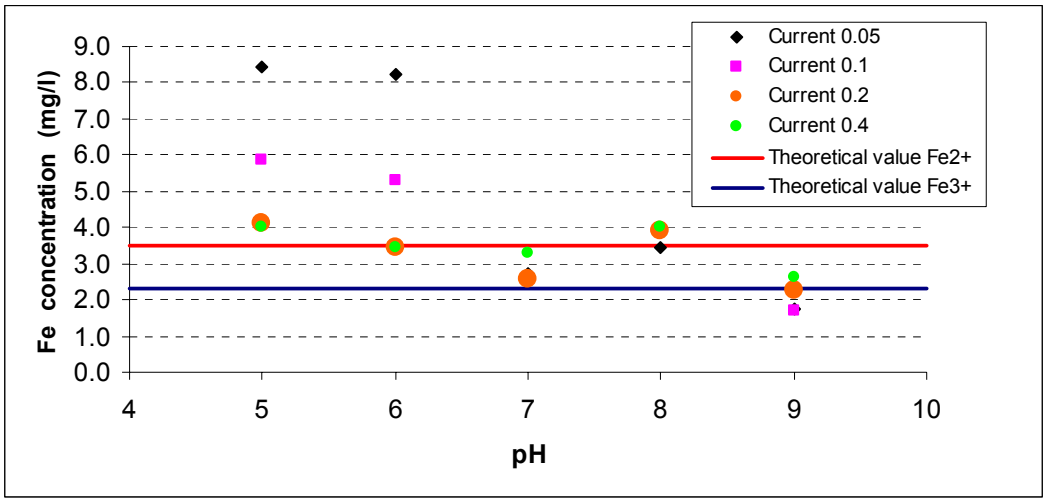

Fig. 56 The concentration of dissolved iron for each pH and electric current. Each point represents the average of 3 measurements.

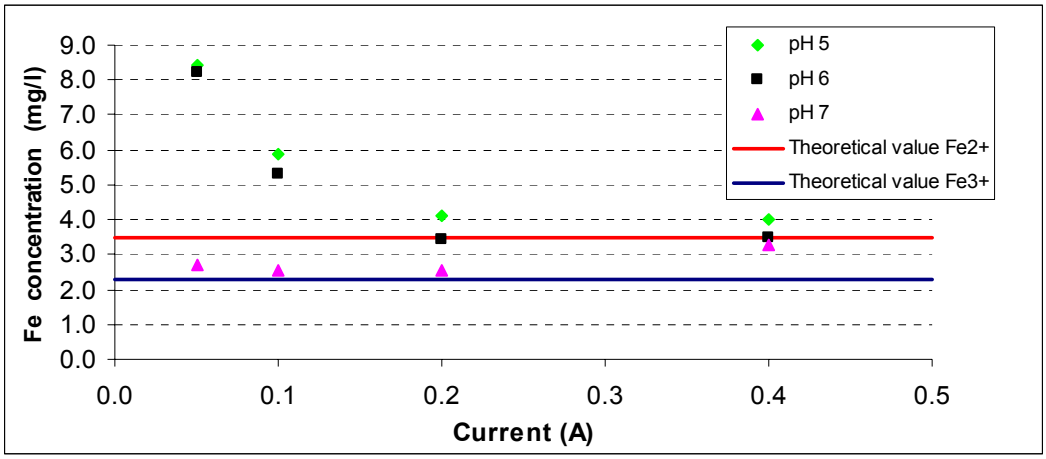

Fig. 57 The concentration of dissolved iron for each electric current in pH 5,6,7. Each point represents the average of 3 measurements

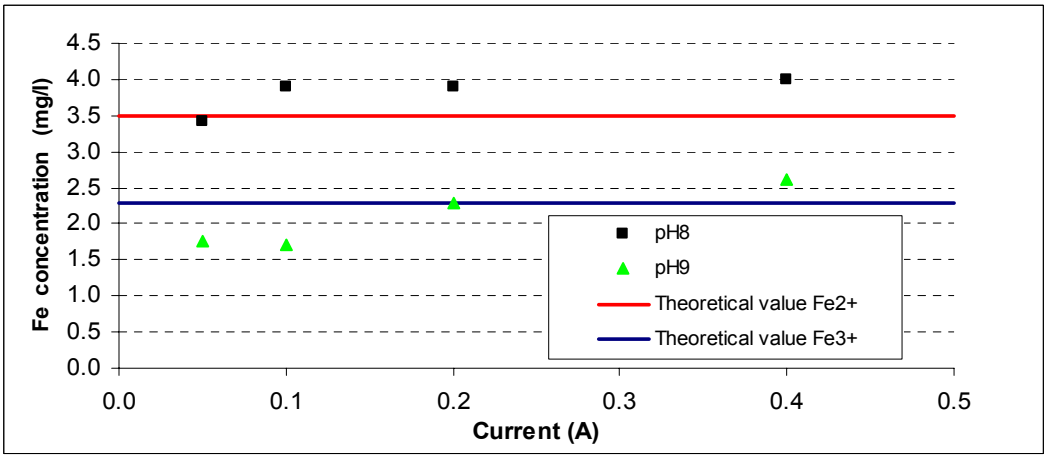

Fig. 58 The concentration of dissolved iron for each electric current in pH 8,9. Each point represents the average of 3 measurements

In all the experiments the oxygen saturation level (OSL) kept its level or decreased but never increased as can be seen in Fig.59 for pH 9.

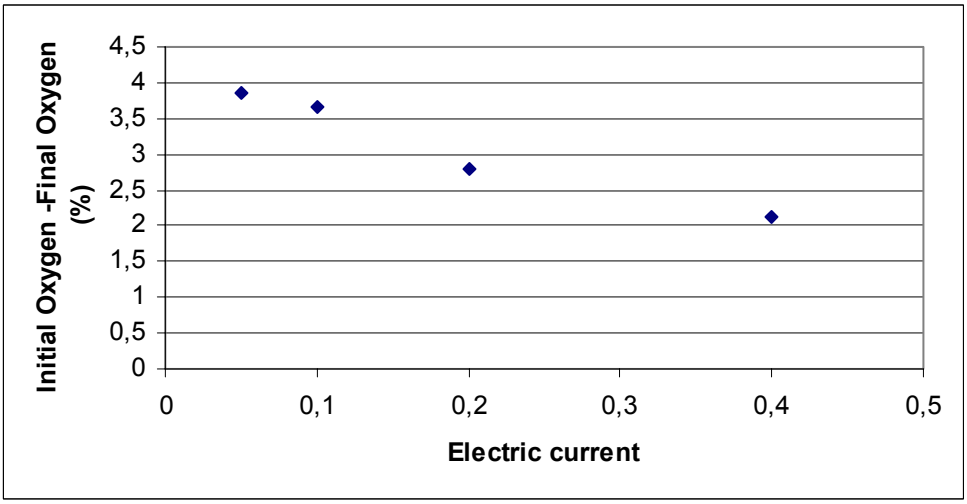

Fig. 59 The change in the oxygen saturation level (OSL) before and after electroflocculation at pH 9 for different currents.

The high iron dissolution rates observed at pH values of 5 and 6 during the electroflocculation process raised the possibility that iron may be dissolved considerably even without activating an electric current at those pH values. Consequently, the second experiments set explored the dissolution rates of iron at different pH values without activating an electric current, the results are presented in Fig.60. The figure shows, that iron dissolution after 4.5 minutes time at pH 5, 6, 7 was significantly greater than for pH 8, while at pH 9 it was totally negligible. A comparison between Fe^{2+} ions concentration and total iron (not shown here), revealed that the iron that was dissolved without current application constituted entirely of Fe^{2+} ions at all pH values.

Studying the reaction rates of Fe^{2+} oxidation to Fe^{3+} for different pH values showed no oxidation at pH 5, moderate oxidation at pH 6 and highly rapid oxidation at 7-9 pH values (third experiments set, Fig.61).

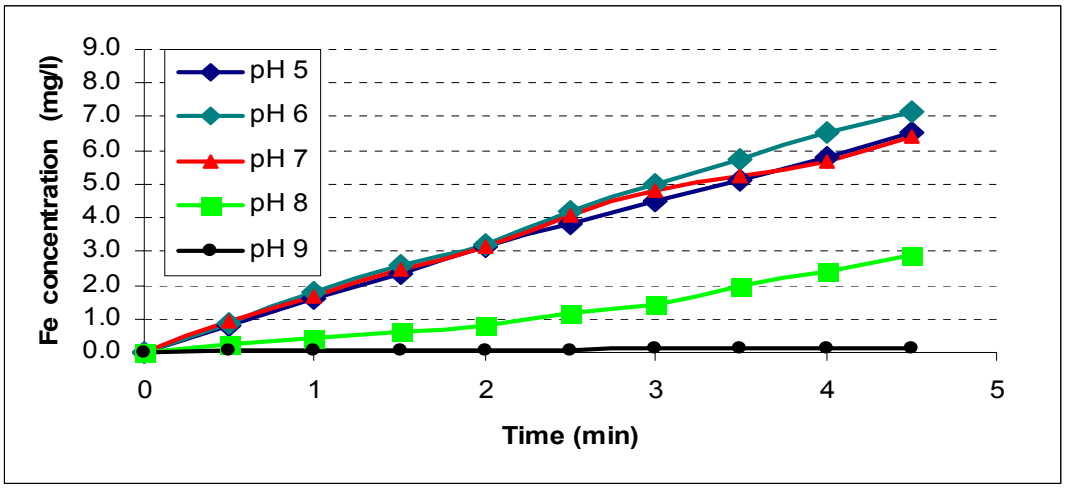

Fig. 60 Ion dissolution without electric current application. Each point represents the average of 3 measurements.

With no electric current activation, at lower pH (pH 5-7) the high iron dissolution rates is in accordance with high rate of oxygen consumption while in higher pH (pH 8,9) the low iron dissolution is in accordance with lower rates of oxygen consumption (Fig.62).

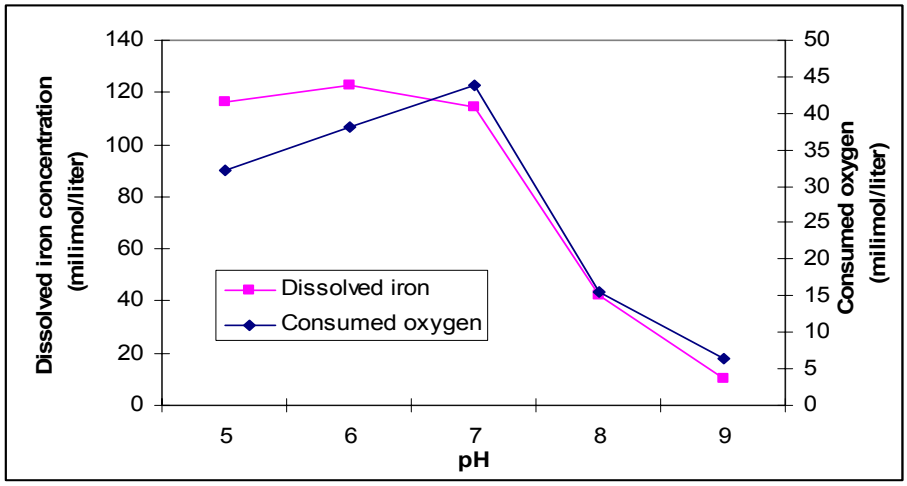

Fig. 61 The concentration of iron after 4.5 minutes of dissolution without activating the electric current and the number of mol of oxygen that were consumed for different pH.

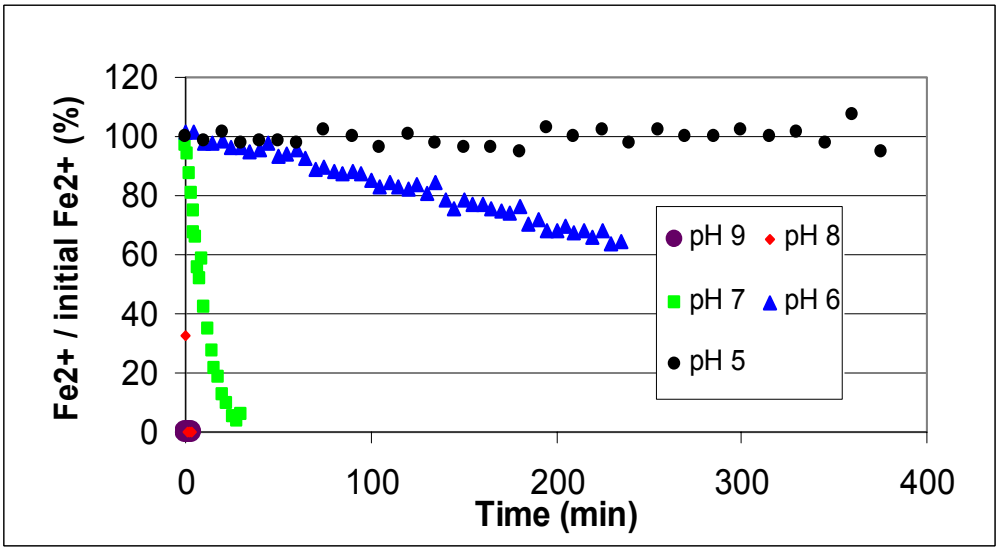

Fig. 62 Oxidation rates of Fe^{2+} to Fe^{3+} ions for pH values of 5-9.

The oxidation rate of Fe^{2+} to Fe^{3+} at pH 7 and the corresponding measured oxygen molarity were measured. Fig. 63 depicts the ratio between the Fe^{2+} moles which where oxidized to Fe^{3+} and the number of moles of dissolved oxygen consumed with time. The ratio was nearly constant at 3.5.

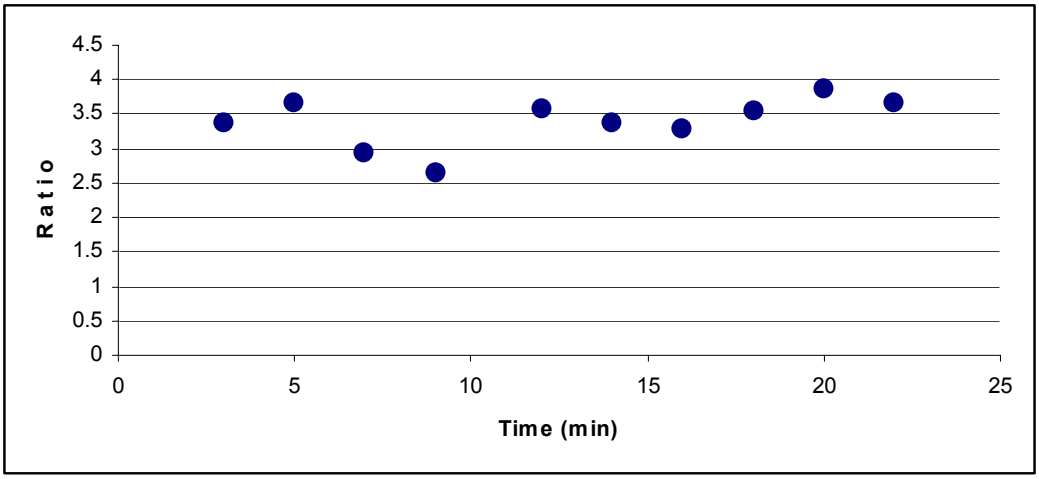

Fig. 63 The ratio between the Fe^{2+} moles which where oxidized to Fe^{3+} and the number of moles of dissolved oxygen consumed with time.

Synthetic wastewater

Effect of dissolved oxygen on EF process

Electroflocculation process was undergoing Mode One, without aeration and Mode Two, with aeration.

EF process without aeration

According to Faradays' law, with the assumption that: 1. Iron emits from the electrodes is ferrous ion and, 2. DO concentration in the bulk water is zero, the calculated ferrous concentration is shown in Fig.64, basing on the formula as follows:

$C = (I \cdot t\, MW) \times 1000 / (V \cdot N \cdot F)$

where C, ferrous concentration (mg/L), V, bulk water volume (L), I, current intensity (A), t, time (s), MW, molecular weight of iron (55.85 g/mol), N, number of electrons involved (Ferrous: 2), and F, Faraday's constant (96,485 coloumbs/mol).

In Mode One, during the first seven minutes, when the dissolved oxygen concentration exhausted rapidly from 6.6 to 1.3 mg/L, the increase rate of ferrous concentration K_1 was 1.3205. From 7 minutes to 30 minutes, the dissolved oxygen concentration dropped to almost zero. During that period, the increase rate of ferrous concentration K_2 was 4.3326, which was more than three times higher than the first period value

when the dissolved oxygen was abundant. In Fig.65, total iron increases linearly with time. The initial proportion of ferrous concentration to total iron was greater than 80%, probably due to the inadequate contact between ferrous and dissolved oxygen in the bulk water. After complete mixing, the calculated ratio dropped during the initial 7 minutes from 80% to 40%, further on it increased steadily with time to 90% and in parallel to the total iron curve. After the EF process in Mode One, bulk water pH varied from 7.8 to 6.7±0.2. There was a deflection point in the ferrous concentration curve related to the almost complete DO exhaustion (DOEP). This point coincided with the minimum point in the Fe^{2+} to total iron ratio curve. During the initial 7 min ferrous concentration increased linearly in much more moderate rate till DOEP. DOEP could be regarded as an indicator to the mode of ferrous ions accumulation. The slight drop of pH might due to the over consumption of hydroxyl by ferric and ferrous ions in the bulk water. It was enlightened from the results in Mode One that aeration mode in EF should be experimented later.

Aeration-Enhanced EF process

In Mode Two, when compressed air was introduced into the EF system, the dissolved oxygen concentration dropped initially and stabilized at 3.5 mg/L (Fig.66). During this process, the ferrous concentration was kept at a very low level, and ferric hydroxide rather than ferrous hydroxide was predominant. The pH value stabilized at 6.9±0.2.

Comparing with total iron concentration in Fig.67, there was not significant influence of total iron generation with or without aeration. The initial drop of DO concentration was probably due to the oxygen diffusion rate from the external air was slower than the oxygen utilization rate by ferrous ions. The DO concentration in EF vessel with aeration mode can be controlled by optimizing the diffusers type to generate more tiny bubbles and increasing the oxygen proportion in the external air.

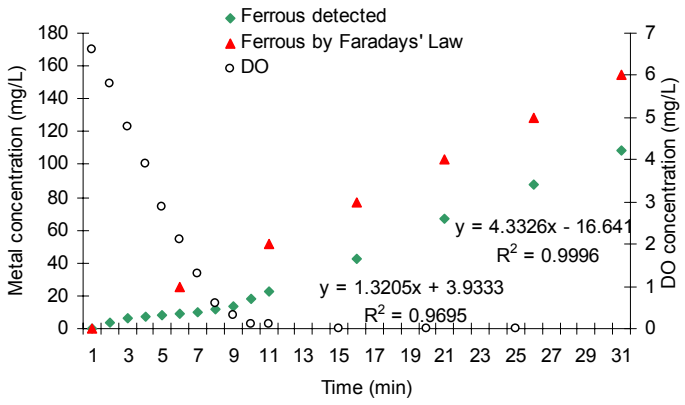

Fig. 64 Influence of DO on ferrous concentration in EF process

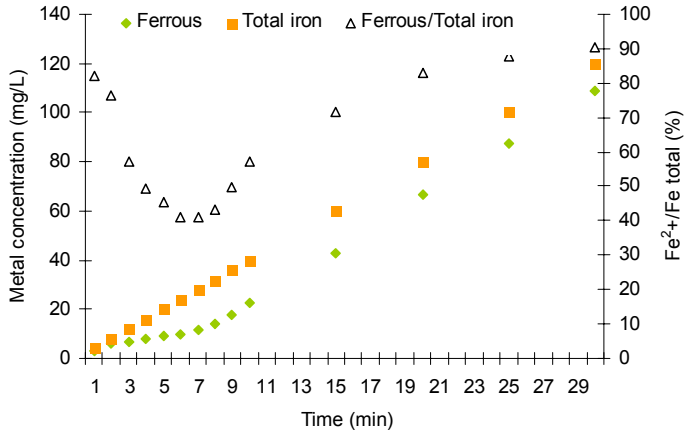

Fig. 65 Ferrous to total iron ratio development during EF without aeration

EF hybrid with different filters

The residual iron concentration is shown in Fig.68. Hybridization of aeration-enhanced EF with all types of filtration exhibited better removal efficiency and less residual metal concentration.

As illustrated in Fig.68, effluent turbidity after EF with direct filter paper could reach 80 NTU or larger no matter with or without aeration. And the effluent took on an unpleasant color because of the existence of iron hydroxide. After 30 min settling and paper filtration, turbidity value could be reduced sharply. Effluent turbidity could be eliminated after membrane filtration.

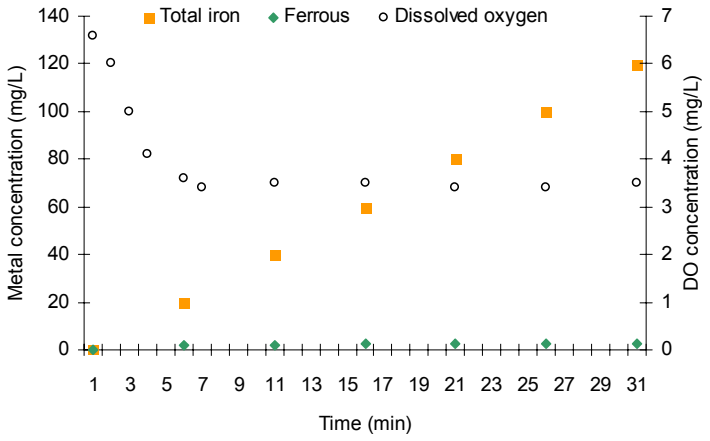

Fig. 66 Variation of ferrous and total iron during aeration-enhanced EF

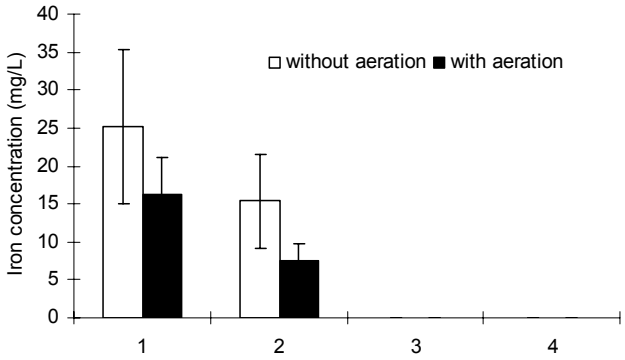

Fig. 67 Residual iron concentration after EF-filtration hybridization (1 EF followed by mechanical filtration; 2 EF followed by 30 min settling and mechanical filtration; 3 EF followed by microfiltration; 4 EF followed by ultrafiltration)

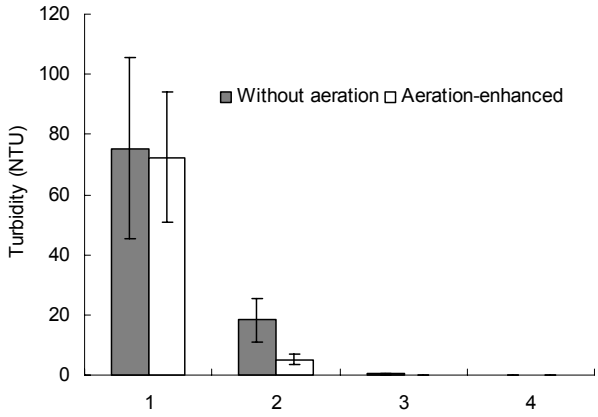

Fig. 68 . Turbidity after EF-filtration hybridization (1 EF followed by mechanical filtration; 2 EF followed by 30 min settling and mechanical filtration; 3 EF followed by microfiltration; 4 EF followed by ultrafiltration)

IV-1.3.3 Characterization of bacterial alginate extracted from biofilm matrix

Alginate extraction

Biofilm covered on carriers after 15 days (Fig.69b). During alginate extraction, soft gel precipitates appeared in the supernatant when its pH reduced to 2. These precipitates were soluble in NaOH, demonstrating reversible sol-gel transition as the pH altered between alkali and acidic condition, which is attributed to the typical characteristics of alginic acid.

After enzymatic purification, the alginate recovered from biofilm matrix amounted to (164±21) $mg \cdot gVSS^{-1}$ (organic content). It displayed positive results to all the FAO alginate identification tests, which confirms that large amount of bacterial alginate existed in the biomass.

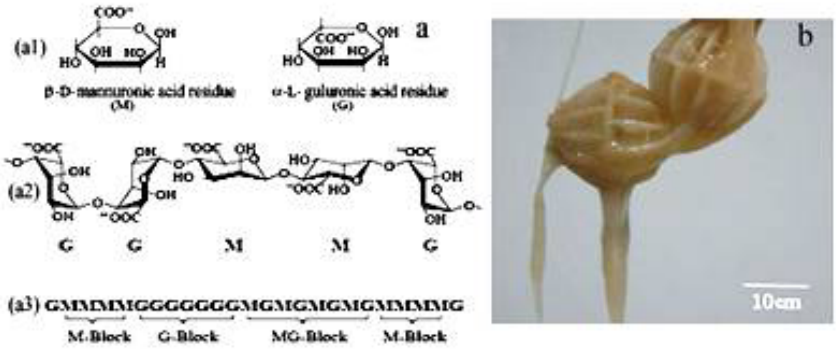

Fig. 69 Alginate structure (after [13]) and the biomass from lab-scale submerged biofilm reactor. (a1) uronic acid residues in alginate molecule (M vs.G); (a2) the alginate polymer; (a3) blocks of the alginate polymer; (b) biomass of lab-scale submerged biofilm reactor.

Raman spectrum

Raman spectrum demonstrated those typical peaks of bacterial alginate (Fig. 70a). The peak at 3274 cm^{-1} was attributed to the OH stretching vibration in intramolecular bonding. The strong peak at 2934 cm^{-1} was assigned to $-COCH_3$ group. Peaks at 1629 cm^{-1} and 1466 cm^{-1} were assigned to antisymmetric and symmetric vibrations of ionic COO^- group respectively. The pattern of absorptions in the 1100-1000cm^{-1} region was attributed to the COC and CCC bonds of the uronic acid skeleton. In addition, the peak at 3080 cm^{-1} was due to the appearance of C=C, which might be caused by the effect of alginate lyases.

Alginate refers to a family of polysaccharides containing β-D-mannuronic acid (M) and α-L-guluronic acid (G) residues. The proportion of these two residues (M/G ratio) determines the diversity of alginate's physicochemical properties and reactivity (. Maleriat et al, 2000). This M/G ratio was able to be obtained by Raman spectroscopy (Salomonsen et al, 2008; Pereira et al, 2003): M and G residues manifested their characteristic Raman peaks at 1100 cm^{-1} and 1025 cm^{-1} respectively. The intensity ratio of these two peaks provided information of M/G ratio. Based on this method, the M/G ratio of the extracted alginate was calculated as 1.19 (Fig. 71a), which indicated that the quantity of M residues existed in this alginate was more than G residues.

MALDI-TOF Mass spectrum

The extract's molecular weight distribution was determined by MALDI-TOF MS. It was found that the extracted alginate was oligosaccharides blend with low molecular weight and short molecular chain. The most abundant component at m/z 728 (Da) only contained four residues; the highest molecular weight one at m/z 2353 (Da) had 13 residues. Some of these oligosaccharides had acetyl groups, which is one of the characteristics of bacterial alginate.

Considering the appearance of C=C in Raman spectrum, it could be predicted that those alginate oligosaccharides within the biofilm matrix were the product of alginate lyases. Alginate lyases can be secreted by a number of bacteria species, they usually cut alginate molecules by β-elimination, produce C=C

between C4 and C5 of mannuronic acid residues (.Wong, et al, 2000). Similar result was also reported by (S. Leone et al, 2006) that the biofilm matrix of Pseudomonas sp. OX1 grown on phenol was mainly constituted by alginate oligosaccharides. So far, EPS with higher molecular weight (>10,000 Da) has been considered as the model substance for biofilm formation. However, the current research indicated that, oligosaccharides with molecular weight less than 2500 Da may also play a part in biofilm formation.

Alginate -Ca^{2+} interaction

During the investigation on alginate-Ca^{2+} interaction, it was observed that as the soluble sodium alginate drops (500 mg L^{-1}, 0.5mm in diameter) contacted with $CaCl_2$ solutions, they spread on the surface and form white gel-like film quickly. These alginate–Ca film inclined to be stronger and extended to a larger area as Ca^{2+} concentration rose from 20 to 2000mg L^{-1} (Fig.71a-71f). The mean size of those films at Ca^{2+} 20 mg L^{-1} was 10 µm in length, 2µm in width and 0.2µm in thickness by AFM observation (Fig.71a). In comparison, the films' length and width enlarged to more than 30 mm and 20 mm respectively with the same drops of sodium alginate at Ca^{2+} 2000 mg L^{-1} (Fig 71f).

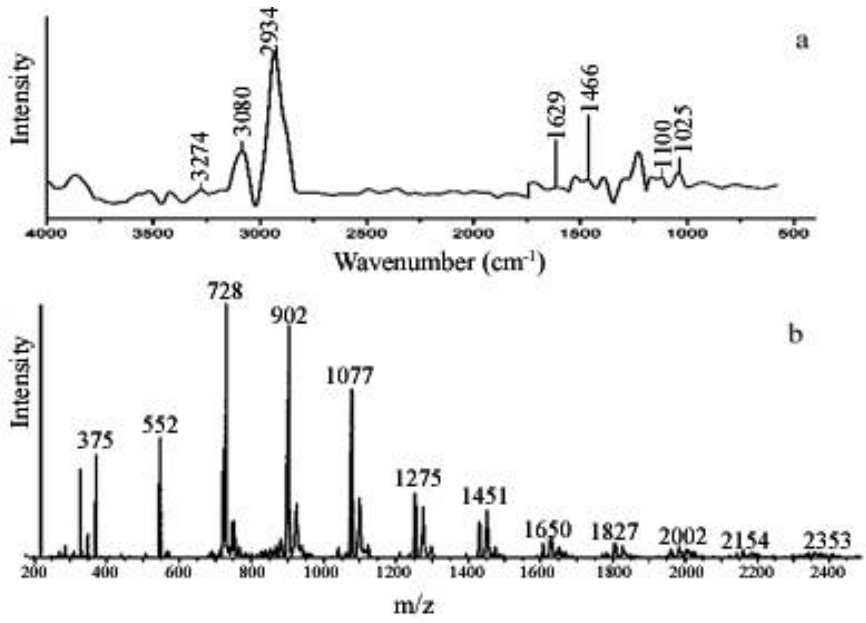

Fig. 70 Raman and MALDI-TOF MS spectra of the extracted alginate. (a) Raman spectrum; (b) MALDI-TOF MS spectrum.

Alginate concentration was also an important factor that determined gel-like film formation. Under sufficient Ca^{2+} (2000 mg L^{-1}), as alginate concentration increased from 250 mg L^{-1} to 1000 mg L^{-1}, gel-like film with tremendously improved strength could be seen (Fig.71h-71i).

Alginate consists of M and G residues. Due to their particular shapes and modes of linkage respectively, three types of blocks as G block, M block and MG block, which are substantially different, can be formed.

They distribute randomly in alginate chains (Fig.71a3). Specifically, the G-block is buckled (Fig.71a2). If two G-blocks are aligned side by side, diamond shaped holes result. Their dimensions are ideal for the cooperative binding of divalent cations, typically Ca^{2+}. This is the so-called "egg-box" model (Wong, et al, 2000).

Under fixed concentration of alginate, the more the Ca^{2+} ions are, the more alginate chains they will crosslink, and the stronger and larger the alginate-Ca^{2+} film will be (Fig.72). Vice versa, if the concentration of Ca^{2+} is fixed, the higher the concentration of alginate is, the more the alginate chains exist, and the easier the Ca^{2+}-G block complex can be formed. Therefore, although the alginate within biofilm matrix is oligosaccharides blend with low molecular weights, it is still able to build gel-like film with Ca^{2+}. This gel-like film could be an important part of biofilm skeleton.

In addition, the extracted alginate has more M residues than G residues according to the result of Raman spectroscopy, which indicated that there were large quantities of M-blocks. As the M-block has flat ribbon-like shape T.A. Davis et al, 2003), it may contribute to the stretching out of the alginate-Ca film on the surface.

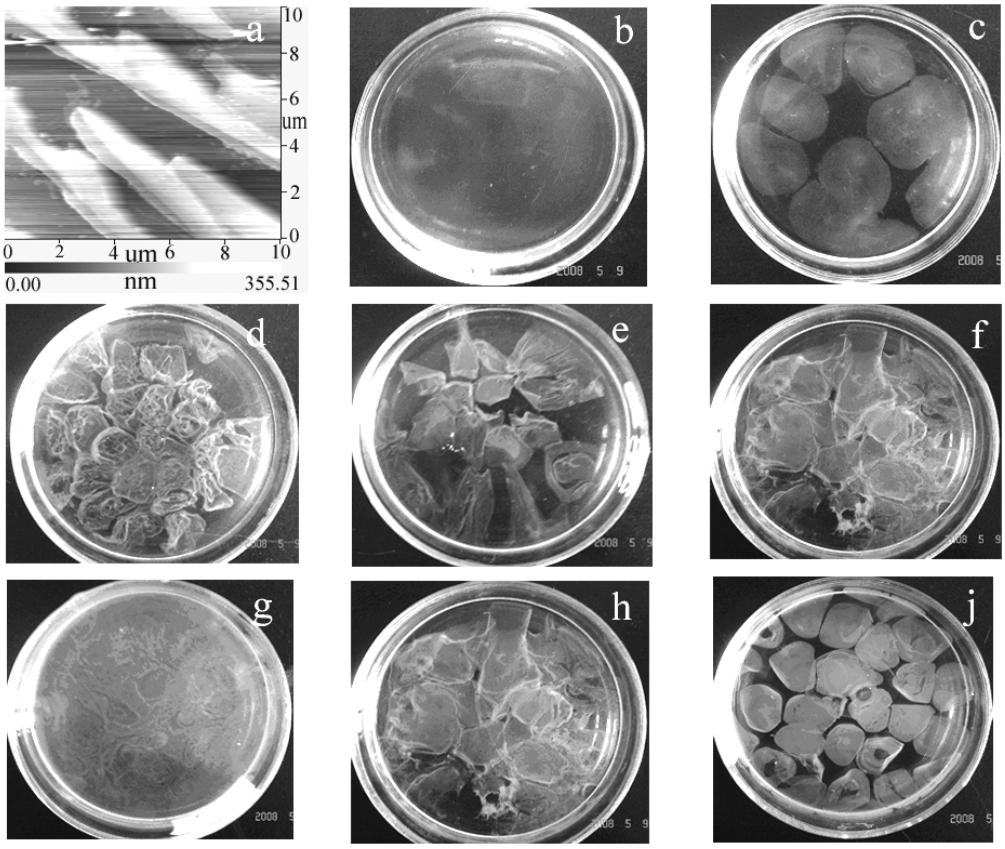

Fig. 71 Interaction between Ca^{2+} and the extracted alginate. a-f: alginate concentration 500 mg L^{-1}, Ca^{2+} concentration 20 mg L^{-1} to 2000 mg L^{-1} respectively; g-h: Ca^{2+} concentration 2000 mg L^{-1},alginate concentration 250 mg L^{-1} to 1000 mg L^{-1}.

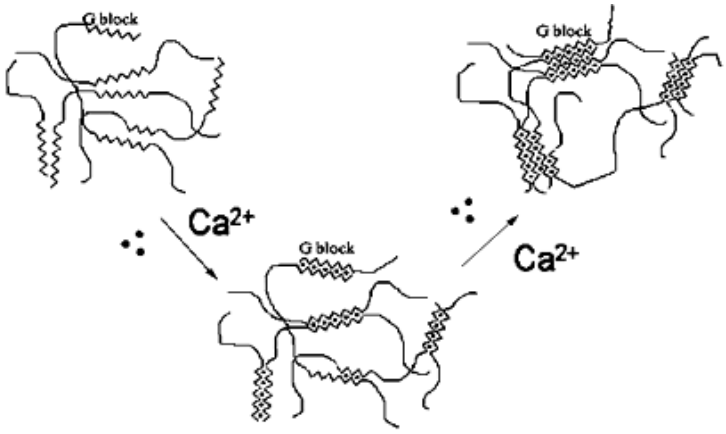

Fig. 72 "Egg-box" model of alginate-Ca^{2+} interaction (after Donali and Paoletti, 2009).

IV-1.3.4 Silver nanoparticles - *E.coli* colloidal interaction in water

Under the preparation conditions described in the methods section, the Ag-MCNPs had roughly spherical shapes with relatively narrow size distributions, formed stable dispersions, and were positively or negatively charged. Zeta potential values obtained were 40.2 mV and 46.1 mV for the positive Ag-PL and negative Ag-MPA particles, respectively. These values are characteristic of stable colloids. Table 15 displays the details of the various NP samples (A-D), indicating surfactant type and charge, centrifugation conditions and the resulting mean size. Two substantially different mean sizes of each of the MPA and PL coated MCNPs were obtained. Figure 73 shows size distribution histograms of particle types A and B that were evaluated by analyzing the TEM micrographs.

Figure 74 presents a representative TEM micrograph of NPs type A which appear well dispersed when stabilized with Poly-Lysine.

Table 15 Characteristics of Ag-MCNPs.

Type	Surfactant and Charge	Centrifugation Condition (rpm/min)	Mean size (nm)	Standard Deviation (nm)
A	PL - Positive	13500/10	7.2	2.8
B	MPA -Negative	13500/30	6.7	2.9
C	PL - Positive	-	12.5	3.5
D	MPA -Negative	-	15	5

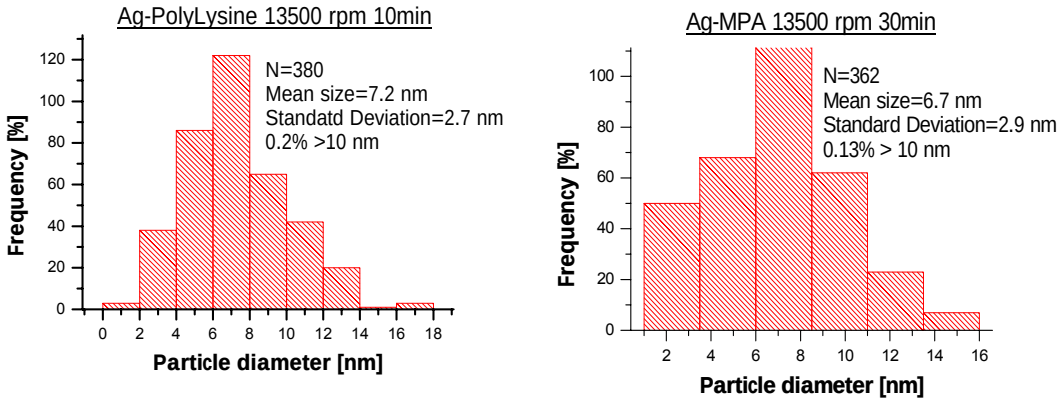

Fig. 73 Particle-size distribution histogram of MCNPs.

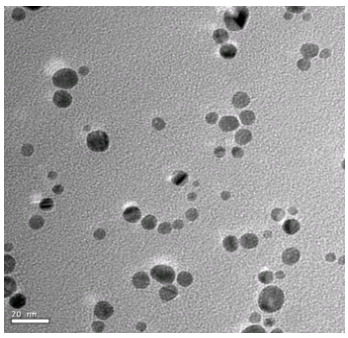

Fig. 74 TEM micrograph of stable NPs type A (the scale bar is 20 nm).

In this study, the impact of MCNPs on survival of planktonic *E.coli* cells suspended in aqueous suspensions was assumed to be associated with the interaction between the Ag NPs and the suspended microorganism (termed also bio-colloid), thus the experimental setup included varying amounts of the two types of particles (i.e. NPs and bio-colloids). The MCNPs were stable when diluted in water with the *E. coli* as no precipitation was observed.

The role of the MCNPs' charge in determining the interactions between NPs and bacteria is not yet completely understood. Some studies postulated that electrostatic attraction between negatively charged membrane components and positive NPs surface charge is crucial for the interaction between bacteria and NPs. On the other hand, Stoimenov (20002) and Hamouda (2000) assumed that particles with the same charge as the bacteria would induce electrostatic repulsion and prevent the interaction between the particles. Figure 75 presents the impact of MCNPs surface charge and concentration on log inactivation of planktonic *E.coli* in water. Increase in NP concentration, either with positive or negative charged particles, resulted in similar increase in log inactivation. The increase in bactericidal activity of Ag-NPs in the solid-state also showed an increase in inactivation with NP concentration (Morones et al, 2005; Sond et al, 2003; Baker et al, 2005; Shrivastava et al, 2007; Kim et al, 2007; Sondi and Salopek-Sondi, 2004; Kim et al, 2007). One of the main directions in similar studies is the development of anti-bacterial surfaces with biocidal activity for a

variety of applications. The present work is aimed towards a different goal; the suspended NPs in water can be used as a disinfectant in water systems prior to membrane filtration processes. In the current study, complete inhibition of *E.coli* was observed at lower silver concentrations compared to surface supported particles (Sond et al, 2003), which indicates that mixing the MCNPs with the bio-colloids provided improved inactivation probably due to the higher collision probability between the NPs and bio-colloids in suspension. Moreover, Ag-PL and Ag-MPA at 8μg/mL showed approximately 5 $\log_{10}$ reduction with similar standard deviations. These results imply that under these test conditions, the influence of electrostatic attraction or repulsion between the MCNPs and the negative charge components in the *E.coli* membrane are probably insignificant for bacterial inactivation.

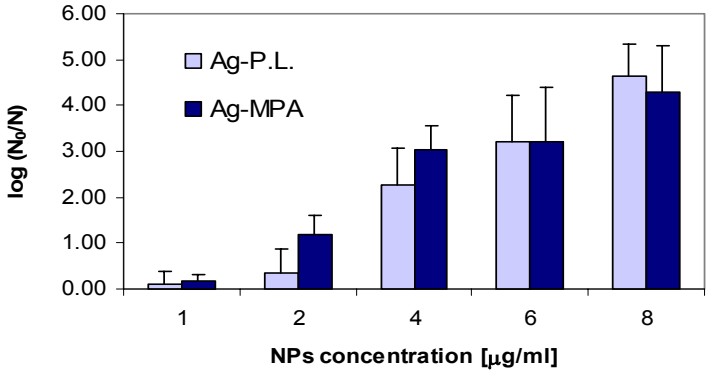

Fig. 75 Impact of surface charge and various concentrations of MCNPs on bacterial inactivation. $N_0 = 2.4*10^7$ CFU mL^{-1}

The effect of Ag NP size on bacterial activity was demonstrated previously, indicating that small particles were more active than larger particles per identical silver mass unit. The mean diameter of each NPs type (either PL or MPA Ag-NPs as presented in Table 15), its concentration and the silver density was used to estimate the number density of the particles. The ratio between the number of NPs and the number of bio-colloids (NPs/N_0) was calculated for each sample. Fig.76 illustrates the inactivation ability of MCNPs types A-D in relation to the ratio of NPs to bio-colloids. MCNPs type B at 6 μg mL^{-1} and MCNPs type D at 45 μg mL^{-1} showed similar NPs/N_0 ratio and similar $\log_{10}$ reduction. The activity of Au-MCNPs is presented in Fig. 78 and as expected, the treatment with gold NPs did not result in inactivation. Pure surfactant solutions, which were used as vehicle controls, showed nearly 100% survival of *E.coli.* These results are consistent with findings by Li et al., (2005) that reported an improved antimicrobial effect with increasing NP concentration P. While other researchers observed particle size dependence, the present work clearly demonstrates that within the size range of approximately 5-15 nm the important parameter is the NPs/N_0 ratio rather then NPs size itself.

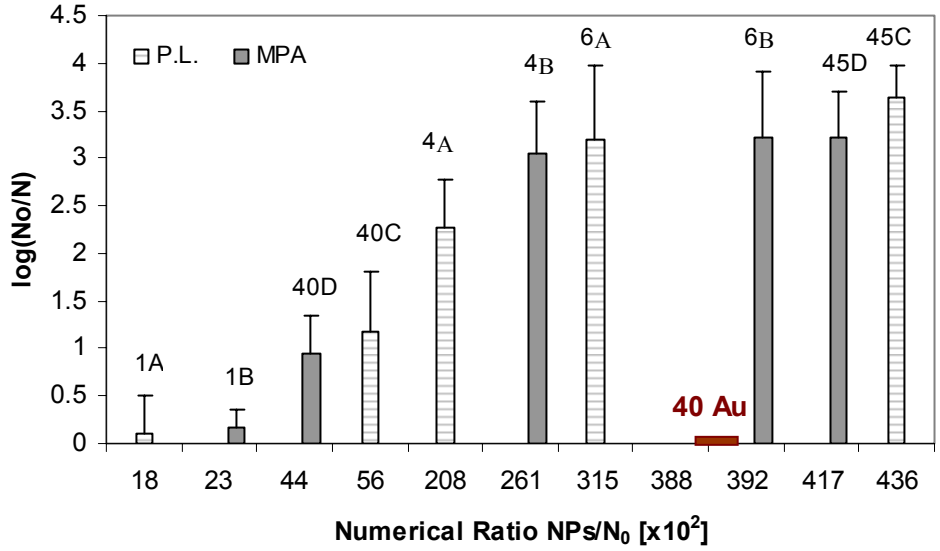

Fig. 76 Bacterial inactivation versus NPs/N_0. The number and letter above each column represent concentration in μg/mL and type of MCNPs, respectively.

The effect of the initial number of bacterial cells on the extent of inactivation with Ag-NPs was previously reported (Pal et al, 2007; Sondi et al, 2004). To elucidate this phenomenon within the framework of a particle-cell interaction approach, for a fixed MCNP concentration the concentration of the bacteria was varied. Fig.77 presents the logarithmic number of cells surviving treatment versus the ratio of NPs to bio-colloids. The experimental set-up was conducted using mid-log phase bacteria diluted by a factor of ten to obtain 10^5 to 10^8 CFU mL^{-1} of bio-colloids, which were mixed with MCNPs type A at a concentration of 2, 7 and 12 μg mL^{-1}. The logarithmic number of cells surviving treatment is expressed as log (N+1) following the approach used by Pal et al. (2007), which allows presenting logarithmically samples in which no colonies were detected in a treated volume (50 μl and complete inactivation N=0). Initially, for low NP to bacteria ratios a constant high survival was observed up to about 1000 NPs per bacterium. Above this a first order linear relationship is observed between the bacteria logarithmic surviving cells and ratio of NPs to bio-colloids. With increasing ratios of NPs to bio-colloids, complete inactivation was observed around a ratio of 2×10^6. Regression analysis was performed on all the data fields used to fit the linear sections of the log inactivation curve with regression coefficient (R^2) of 0.98. The linear curve was described by the following equation:

$$\text{Log}(N+1) = A - B\ NPs/N_0$$

where: A, B are empirical coefficients.

Under these test conditions A and B were found to be 13.2 and 1.6 respectively. This equation can be used to evaluate the inactivation potential of NPs at given silver nanoparticles and bacterial concentrations.

In Figure 76 the concentration of bacteria was fixed while the concentrations of MCNPs varied, while in Fig. 77 for each MCNPs (Ag-PL) concentration (2, 7, 12 μg mL^{-1}) the concentration of bacteria varied. Thus, in both cases the log inactivation of planktonic *E. coli* depends on the NPs/No ratio.

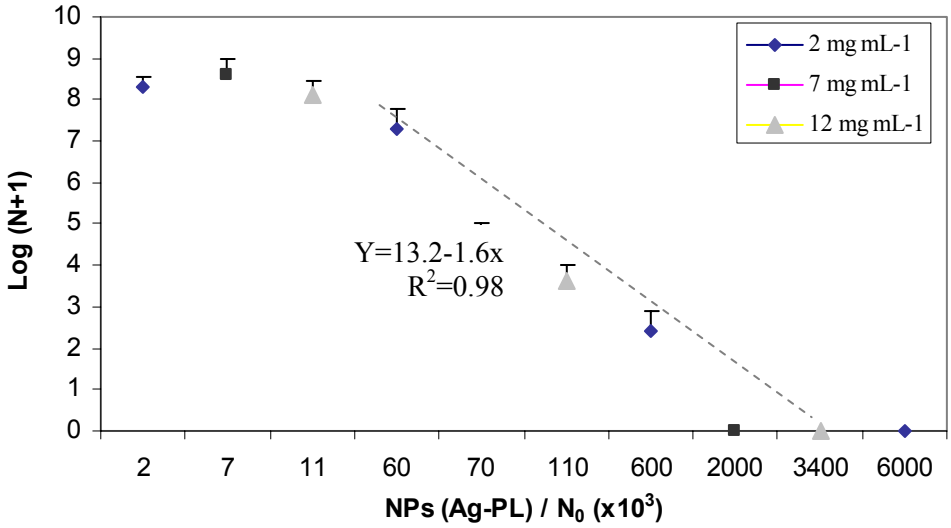

Fig. 77 Inactivation presented as log (N+1) versus the NPs//N_0 ratio.

It is suggested that the inactivation effect of MCNPs on bacteria is associated with collision and attachment efficiencies (so-called successful collision) between two particles of different sizes – NPs which are in the nanometer size range and bio-colloids (bacteria cells) which are in the micrometer size range. While the collision frequency relies mainly on particle transport mechanisms, such as hydraulic shear or diffusion, it may be expected that the attachment probability would be a function of the physicochemical properties of the MCNPs such as charge, size or interface structure. In the present work it was found that the impact of MCNPs on tested bacteria is independent of charge. Further study is needed to examine the dependence of interface structure as a crucial factor. The suspensions in this work were sheared by mixing, implying that the dominant transport factor is a velocity gradient rather then Brownian motion. The frequency of collisions in that case, according to the classical Smoluchowski approach (Gregory, 2006), is a function of the sum of the two particles' diameters to the 3rd power, the velocity gradient and the particles concentration (number of NPs and bio-colloids) as presented in equation 1.

$$J_{ij}=\frac{1}{6}N_iN_jG(d_i+d_j)^3$$

Where: J is the frequency of collisions per unit volume between particle types i and j, N_i and N_j are their number densities and d_i and d_j are the respective diameters.

Generally, the MCNPs and the bacteria have diameters that differ by two orders of magnitude. Hence, the impact of the NPs size on the collision rate is negligible. The mixing time was kept constant in all samples, few seconds by Vortex following 10 minutes of shaking.

This particulate approach assumes that inactivation effect increases with increasing number of NPs that can be attached to a bacterium. The results that were presented in Figs. 28-29 support this assumption and also explain previously reported dose and size dependences.

Previous reports found Ag-NPs attached to bacteria cell membranes and also found NPs inside the cells. Morones (2005) indicated that only NPs with a diameter of less than 10 nm showed direct interaction with few bacteria strains including *E.coli* and *Pseudomonas aeruginosa*. Xu et al, (2004) on the other hand, showed that Ag-NPs with sizes up to 80 nm were accumulated inside *P. aeruginosa* living cells, demonstrating that these Ag-NPs were transported through the inner and outer membrane of the cells (Xu et al, 2004) Figures 78-79 show TEM micrographs of Ag-MCNPs and Au-MCNPs attached to *E.coli*. Although visually the TEM micrographs of both Ag-MCNPs and Au-MCNPs appear to be similar, the inactivation activities of both particles are different. As opposed to Ag-MCNPs, Au-MCNPs did not show any inactivation ability. *E.coli* as gram-negative bacteria has a layer of peptidoglcan and a layer of lipopolysaccaride that are lacking strength and rigidity (Brock et al, 1991). This structure endows the NPs with accessibility to anchoring sites on the cell wall (Shrivastava et al, 2007). It is assumed that the inactivation ability of MCNPs is associated with the amount of successful attachments of NPs to anchoring sites.

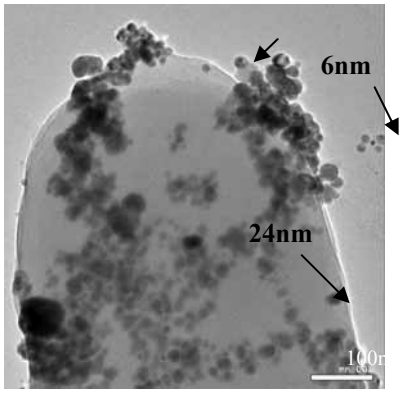

Fig. 78 TEM micrograph of *E.coli* after treatment with Ag-MCNPs. bar=100nm

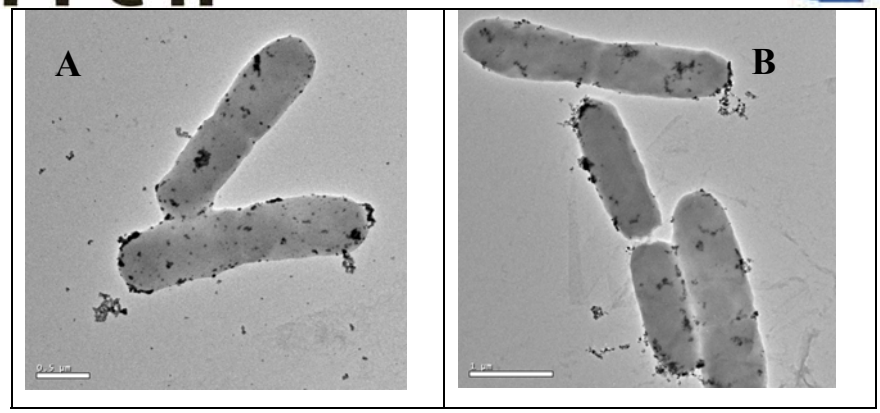

Fig. 79 TEM micrograph of *E.coli* treated with MCNPs. A=Au-MCNPs. B=Ag-MCNPs

Observing results in Fig.81 is that the kinetics of the growth process in all three curves follows typical growth curves of bacterial population.

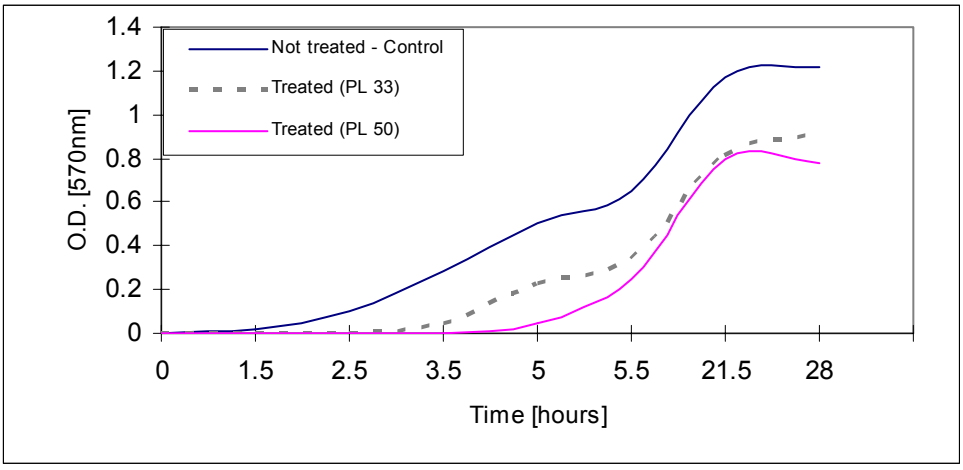

Fig. 80 Growth curves for treated and control *E.coli* in a LB medium, measured through the optical density of the solution.

IV-1.3.5 Characterizing shape of effluent particles by image analysis

Particle Size Distribution

Figure 81 illustrates the particle size distribution (PSD) as a function of ECD along the filtration run for PAC and NPAC samples. The retention time for the specific filter velocity and media porosity studied was approximately 2.5 minutes; therefore 2.5 minutes were subtracted from the actual time effluent samples were taken to obtain a corrected time. PAC filter reached 300 cm of head loss after 240 minutes and therefore filtration run was terminated at that time for PAC and NPAC filters and backwash followed. Results indicated that a large number of particles or flocs (approximately 60%) of the filter influent are compacted in the lower size range between 2.5-3 μm. Usually the PSD in wastewater effluents is not normally distributed

(Aguilar et al, 2003)) as observed in this study. According to the PSD and the integrated total count, a higher concentration of particles in the effluent was observed for NPAC filter compared to PAC filter.

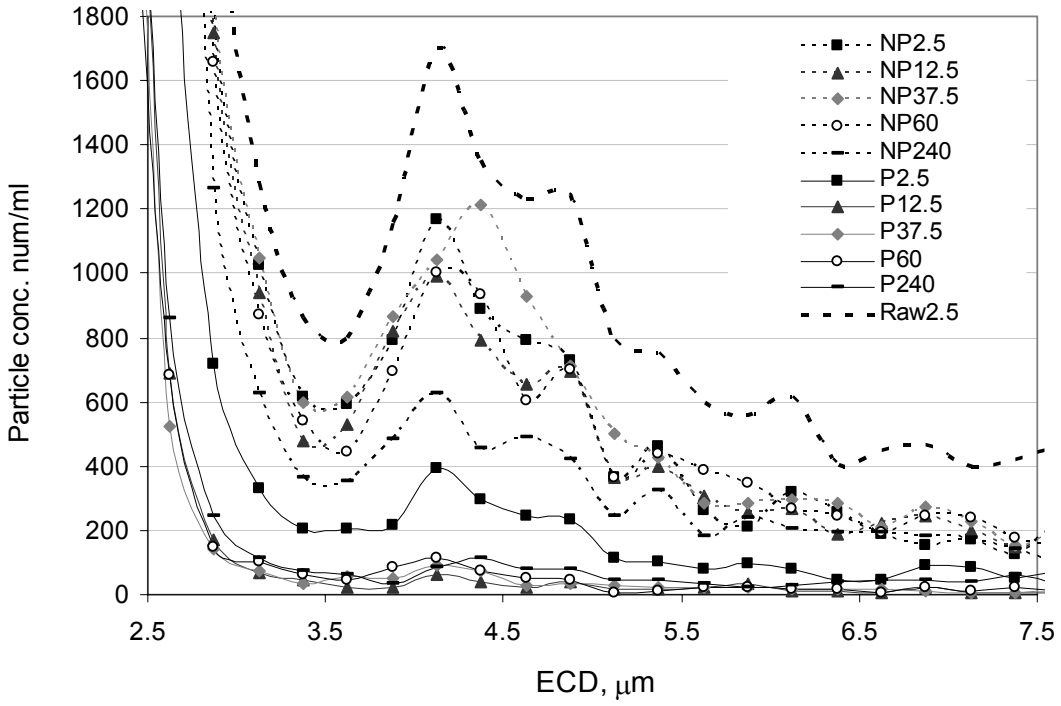

Fig. 81 Particle size distribution (PSD) as a function of ECD filtered effluent with and without PAC.
- **NP represents effluent of NPAC filter (dotted lines) while P represents effluent of PAC filter (full lines). Numbers in legend represent corrected time sample collected from filter effluent.**

Average turbidity values of the filter influent is 3.15±0.25 NTU. From 2.5 min till the end of the filtration run (240 min), the average effluent turbidity reduced to a value of 0.6±0.04 NTU for PAC filter. After 2.5 min of filtration, the average effluent turbidity value remained constant with a value of 1.8±0.17 NTU, for NPAC filter. In general, filter ripening takes place when a significant reduction in the filtrate turbidity occurs and beyond that value filtrate turbidity remains at steady filtration values. This shows that with PAC on turbidity basis it takes approximately 12.5 minutes to reach ripening while with NPAC samples effluent quality based on turbidity does not improve over time, thus filter ripening is not attained.

Similarly, total particle count from 2–100 μm shows that with PAC after 12.5 minutes total count reduced from approximately 46,000 particles/ml to 5,000 particles/ml. For NPAC sample the total count after 2.5 minutes up to 60 min remains constant with an average of 37,000 particle/ml and after that count decreases to about 30,000 particle per ml and remains constant at that value. Thus, based on PSD, with PAC sample it took 12.5 minutes for the filter to mature, while for the NPAC filter, the filter did not mature. However, turbidity values were not sensitive as particle count to the change after 120 min in total count of the NPAC samples.

Particles transport to the filter media grain by different mechanisms which depend on the particle size. Small particles (<1 μm) are transported by diffusion while larger particles are transported by gravity, interception and straining. PSD analysis can allow obtaining more accurate filtration models and improve our understanding of filtration (Kaminski et al, 1997). The larger particles in the inflow raw suspension are probably aggregates of biomass that were not removed in the secondary sedimentation prior to filtration. Yao et al., (1971) showed that filter effluent particles in the size range of 1–2 μm in size are minimally removed by the filter. In this study, particles less than 2.5 μm are not measured and probably represent dispersed particles or microorganisms. The high concentration of particles in size range of 3.5–5.0 μm for NPAC samples may imply minimum transport for particles with a dimension close to minimum transport efficiency such as *Cryptosporidium* particles Amirtharajah, 1988) or it may demonstrate the impact of filter influent PSD shape on effluent PSD shape. Effluent samples after filtration for NPAC show the same distribution shape as raw sample but with lower counts while with PAC particles larger than 3.5 μm are totally removed. The influent PSD samples at different times showed similar pattern and concentration numbers except for influent at 120 min that had approximately 50% lower particle count, with similar distribution pattern (data not shown).

Filter Removal Efficiency

Percent Relative Removal Efficiency (RRE) is calculated by

$$\% \, RRE = (\frac{C_i - C_e}{Ci}) \cdot 100$$

where C_i is influent concentration of raw sample and C_e is concentration at the effluent with PAC (PAC) or without PAC (NPAC).

Influent particles from secondary treatment may show variability in their concentration and size distribution therefore Ci was sampled simultaneously with Ce to determine removal. Percent RRE of particles as a function of ECD is illustrated in Fig.82. During depth filtration the suspended particles are removed by attachment to the filter media or to particles that were previously retained and serve as additional collector sites that result in improved removal efficiency (Darby et al, 1992). Removal efficiency (RRE) is higher along samples with PAC as compared to samples that pass the filtration without inserting PAC. Application of flocculants highly improved removal efficiency and the difference is noticed even at the beginning of the filtration run. Without PAC, removal efficiency of filtration process based on size is low for the small particles and higher for the larger particles, while with PAC removal efficiency is constant at all particle size range.

Adin and Elimelech, (1989) found that removal efficiency of secondary effluent filtered through a sand bed showed linear removal up to 10 μm followed by constant 80% removal for larger particles. Specifically, after 60 min without PAC (NPAC), removal was low (removal 40–60%) for the smaller particles below 10

μm and higher for the larger particles (removal 60–80%). With NPAC filter after 240 min, removal was higher than at 60 min filtration time especially for the smaller particles below 10 μm (removal 70–80%) and similar to 60 min filtration for the larger particles. Improved removal of the small particles was not correlated to the effluent NPAC turbidity measurements. At 60 and 240 min for the PAC filter, removal efficiency is constant at all particle size range from 2.5–30 μm with values between 85–100%. This means that PAC captures also small particles thus results in an effluent with a narrower distribution.

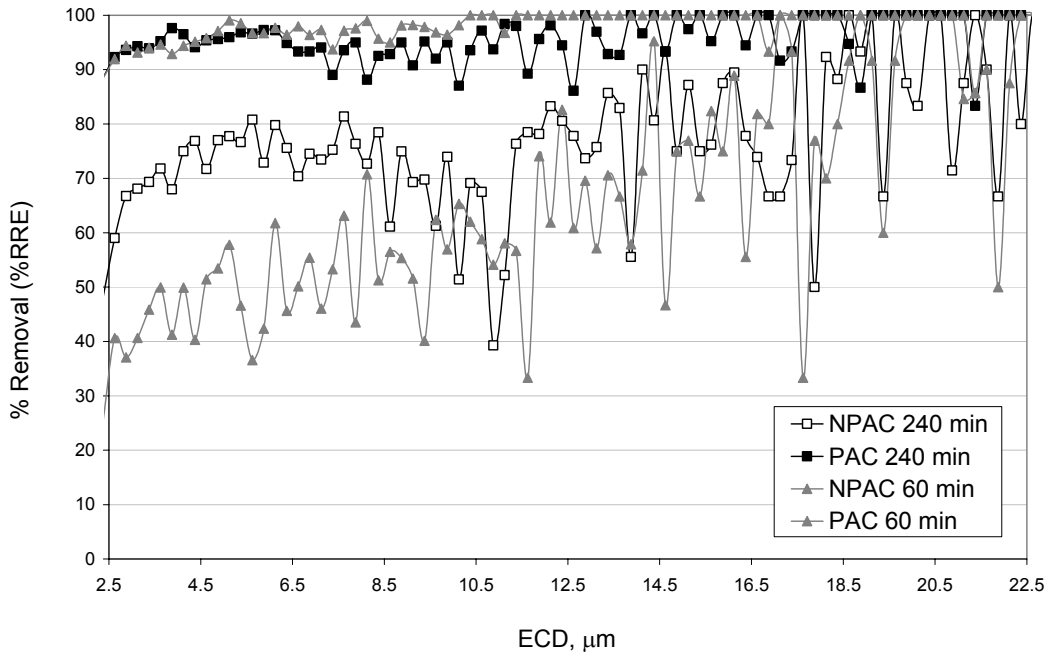

Fig. 82 Percent removal of particles as function of ECD for PAC and NPAC samples after 60 and 240 min of filtration.

Removal of particles by granular filtration is a simultaneous process of particle attachment to the collector, detachment and reattachment of those detached particles in deeper layers of the filter or detachment towards the effluent as observed herein as spikes in Fig.83. The spikes in the graph that relate to sudden lower removal efficiencies in particle removal imply that larger particles may be leaving the filter compared to particles that entered the filter, suggesting particle detachment. This occurs since the structure of accumulated deposits on the filter are not equally strong, and under the hydrodynamic forces caused by the flow this structure may be partially destroyed and may disintegrate previously fixed flocs (Mintz, 1966). The spikes in the graph are more obvious after 60 min for NPAC sample. After 240 min for NPAC filter, there is less detachment and a higher efficiency removal for the smaller particles, since particles that were previously removed may act as an additional collectors (Amirtharajah, 1988). Detachment or floc break off of the captured particles might occur and impact particle effluent morphology over time. Hydrodynamic mechanism for particle transport to the filter is a result of particle rotation across streamlines and is related to particle shape (Ives, 1982). Thus, particle shape can influence net removal and will be further investigated.

Shape determination of particles based on perimeter is mostly useful when particles analyzed are for particles with a narrow size range to reduce the influence of shape changing with size (Ives, 1982). Tysmans et al., (2007) showed that since the perimeter of the particle projection is resolution dependent, it may result in different circularity values for circular particles depending on the particle size. They concluded that larger particles and finer resolution result in more accurate measurements. For example, a 100 μm particle had a circularity of 0.99, particles in the size range between 15–90 μm had a circularity of 0.98 but for a 6 μm particle the circularity was 0.88. Since removal of particles in filter effluent as a function of circularity may depend on the size, data was analyzed in size bins. Narrowing down the particle range may strengthen the conclusion that particles with a lower circularity are more easily captured by the filter compared to particles with higher circularity, especially evident for the smaller particles with different circularities.

Generally the shape of particles in wastewater is very complex as natural particles are not spherical when observing the 3 dimensional (3D) images of particles. Particle shape can be described by the circularity which is the ratio of the perimeter of a circle with the same area as the particle divided by the perimeter of the actual particle image. Circularity has values in the range 0–1, with a perfect circle a circularity of 1 while an irregular object has circularity closer to zero. Fig. 83 illustrates percent removal of particles as function of circularity for PAC and NPAC samples at various filtration times. Removal based on circularity shows that with PAC high removal efficiency occurs at all particles with all circularity values. With NPAC samples it is evident that removal improves over time (120 min compared to 240 min) and improved removal occurs with less circular particles. However the improved removal is not entirely correct, as particles with a variety of circularity values even for the small particles are minimally removed, while large particles whether circular or not are highly removed. Therefore it would be more accurate to study removal based on circularity by dividing particles to size bands and observing removal as a function of circularity for narrow size bands as suggested previously by Hentschel and Page (2003).

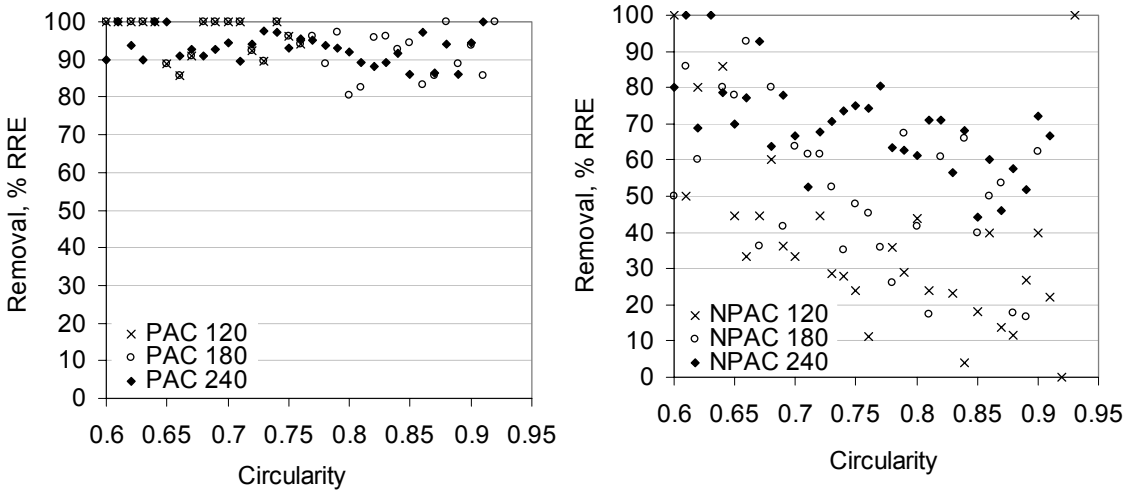

Fig. 83 Percent removal of particles as function of circularity for PAC (left image) and NPAC (right image) samples after 120, 180 and 240 min of filtration.

Fig. 84 illustrates removal based on circularity after 120 min of filtration for particles between 2.5–5 μm, 5–10 μm and above 10 μm. Particles with lower circularity are removed more efficiently compared to the highly circular particles. These results also suggest that the spikes in the size based removal may be due to the more circular particles for similar size range that are removed less efficiently and not necessary due to detachment of previously retained particles as suggested by other researchers. For particle with circularity below 0.6 at all size range removal was near 100%. Between circularity of 0.6 to 0.9, there is a trend in decrease in removal efficiency with an increase in circularity for particles up to 10 μm. In a few cases negative removal based on circularity was observed, which repeated it self in all samples for the higher circularity values. Negative values can be obtained in the case of having more particles in the effluent than the influent for a specific circularity, which suggest that larger flocs may breakdown and form smaller more circular particles or that particles in the effluent are more circular than influent particles. Removal of NPAC filter at 120 min based on feret diameter shows that longer more elongated particles are retained by the filter almost completely (above 95%) for particles with feret max above 12 μm. Removal on ECD basis for NPAC sample is gradual and there is not a cut off value of ECD that results in complete removal as with feret max number. For Pac samples at 120 min, above feret number of 6 μm removal is complete along the filter run time. This point may be very important in evaluation of the minimum feret max value that results in complete particle removal. To conclude, using statistical test for coupling size and shape "coupled distribution" for each individual sample has an advantage when comparing samples (Tysmans et al, 2007), and is suggested as future work.

Correlation between Shape Parameters: Circularity and ECD

The goal of this experiment was to test the impact of ECD on circularity with irregular shaped particles. The increase in particle ECD was obtained by intentionally increasing sample concentration of latex beads at a size of 90.7±17.7 μm overtime to induce particles to contact closely other particles and form various particle dimensions. Fig.85 illustrates circularity versus ECD for latex bead particles, while the insert represent the PSD of the latex beads. It is obvious that there is a decrease in circularity with increase in ECD. This experiment shows the difficulty in interpreting particle shape parameters for irregular shaped effluent particles that are secondary particle s composed of primary particles with a variety of shapes.

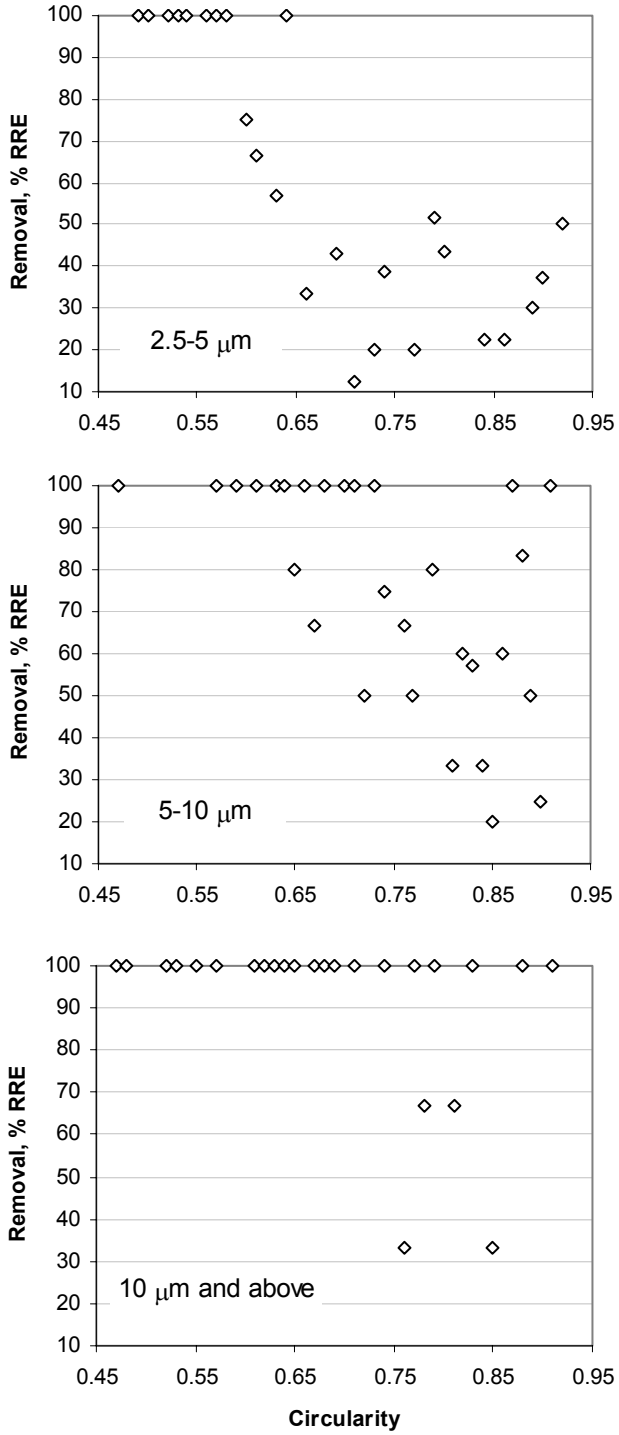

Fig. 84 Removal based on circularity after 120 min of filtration for NPAC samples between 2.5-5 μm, 5-10 μm and above 10 μm

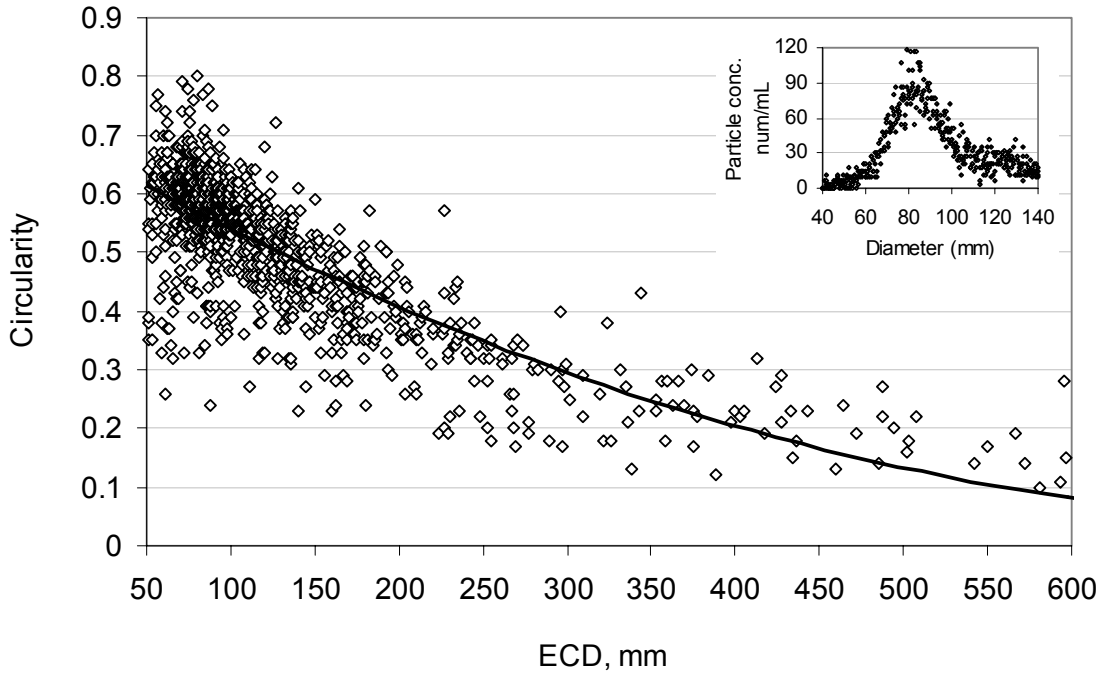

Fig. 85 Circularity versus ECD for latex bead particles. The insert represent the PSD of the latex beads

Correlation between Shape Parameters: Feret diameter, ECD and count

Many floc morphological characteristics are important when modeling floc behavior, such as the longest dimension, width, and shape factors (Skafel and Krishnappan, 1995). To understand the floc characteristics, samples that are uniform and spherical were first analyzed. Two types of polysterene microspheres were analyzed in this study, where an ECD of 5 µm correlated to an average Feret diameter of 5.55 µm and an average ECD of 10 µm correlated to and average feret diameter of 10.4 µm. Thus, with disperse spherical particles, the ECD and feret diameters match. Latex bead used in this study formed various shapes such as doublets, triplets and a variety of irregular forms, when their concentration in the sample was intentionally increased. Table 16 shows selected images of latex beads taken from the image analyzer, with its corresponding ECD and feret max diameter. A linear relationship is noticeable between feret diameter and the number of particles that join each other in a row. For example, a feret of 88 µm is obtained for one latex bead particle, 162 µm for two particles in a row, 254 µm for three particles in a row and 355 µm for four particles in a row. When particles join each other in other more compact configurations (not in a line), the feret max is less than that obtained if the same number of particles will be theoretically stretched in a continuous row. It is difficult to understand results obtained even for particles that are originally relatively spherical with narrow PSD in their disperse state. However, working with mean diameters (RCD) can lose information while feret number is not a mean

Table 16 Selected images of latex beads, with its corresponding ECD and feret max diameter.

Latex bead image	ECD (µm)	Feret Diameter Max (µm)
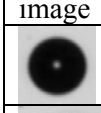	83.13	88.13
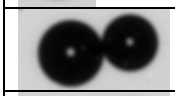	118.63	162.13
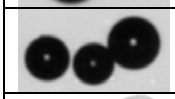	151.88	253.38
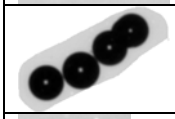	198.63	354.63
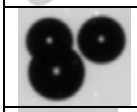	193.88	152.88
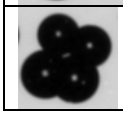	185.88	214.13

Samples after secondary treatment in a WWTP (Ramat HaSharon, Israel), were disinfected either with UV or chlorine (termed “UV” or “chlorine”), held in a reservoir and examined after two weeks for particle analysis. Fig.86 illustrates the PSD of the chlorine sample. A bimodal distribution was obtained where most of the particles are near the 4-5 µm and other mode occurs between 14–19 µm. Representation by image analysis can provide indication of the type of particle being analyzed, as the modes can be correlated with the image of the particles.

Fig.87 illustrates a 3D plot of ECD as a function of feret number for chlorine sample above. For a particle with a certain ECD, the feret diameter spans over a wide range from circular particles that feret equals to ECD, to elongated particles where feret max is larger than ECD. This data shows that for most particles feret is equal or larger then ECD, thus most of the natural particles in this effluent are elongated even for the small particles. Most of the particles are in the size range up to 3.5 µm, while the small particles are more circular as the feret span in the small particles is narrower compared to larger particles (on ECD basis).

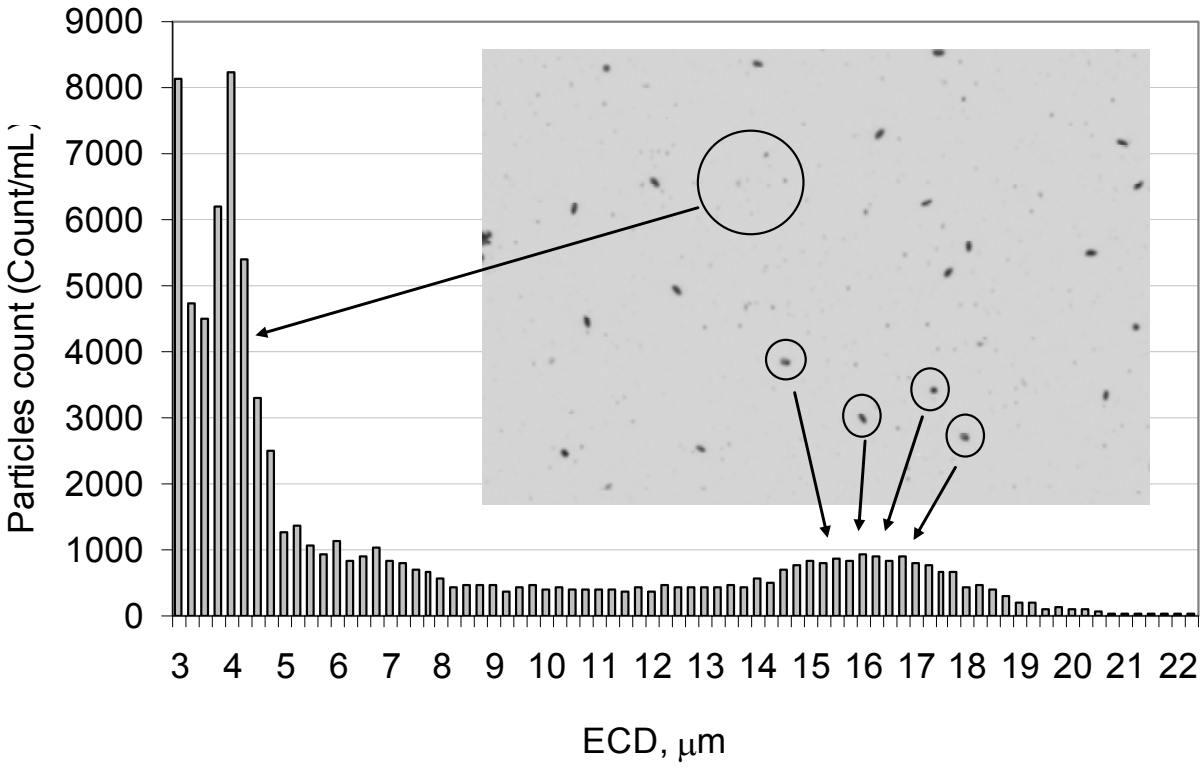

Fig. 86 PSD of chlorine samples (the insert represents and image taken by the image analyzer).

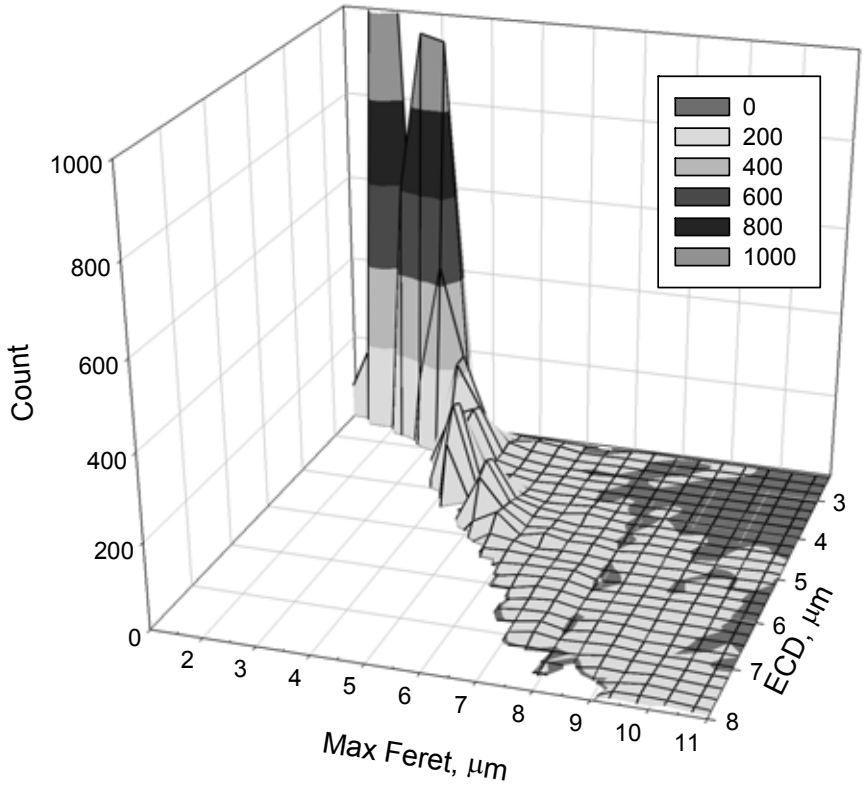

Fig. 87 3D plot of ECD as a function of feret max diameter for chlorine samples.

Correlation between Shape Parameters: Intensity and ECD

Intensity is defined as the sum of all pixel intensities in object divided to the total number of pixels. Particles with higher intensity are more transparent and intensity may provide information about particle makeup. Fig.90 shows the intensity of samples as a function of ECD. An inorganic sample taken from soil was separated to the silt fraction was analyzed and termed "Silt", the other particles are as previously determined. Data for the natural particles in the effluent of chlorine, UV and raw filter effluent up to approximately 10 μm fall on top of each other, while the silt particles and the larger mode in the chlorine sample fall on other areas in the graph. Since algae particles can develop in the reservoir of secondary effluents (8), and chlorophyll was detected in both UV and chlorine samples, it is possible that algae particles are dominant in the chlorine samples PSD mode (Fig.88). Backwash of PAC particles contains mostly a mixture of mostly organic biological and detritus particles. Various intensity levels were detected with decrease in intensity as ECD increase (data not shown). For example, 2–5 μm particles had intensity of 190–200, 5–10 μm particles with intensity of 170–200 and 10–50 μm particles with intensity range of 160–190 μm. Since flocs are mixed particles it may be difficult to relate transparency to chemical characteristics of specific particles.

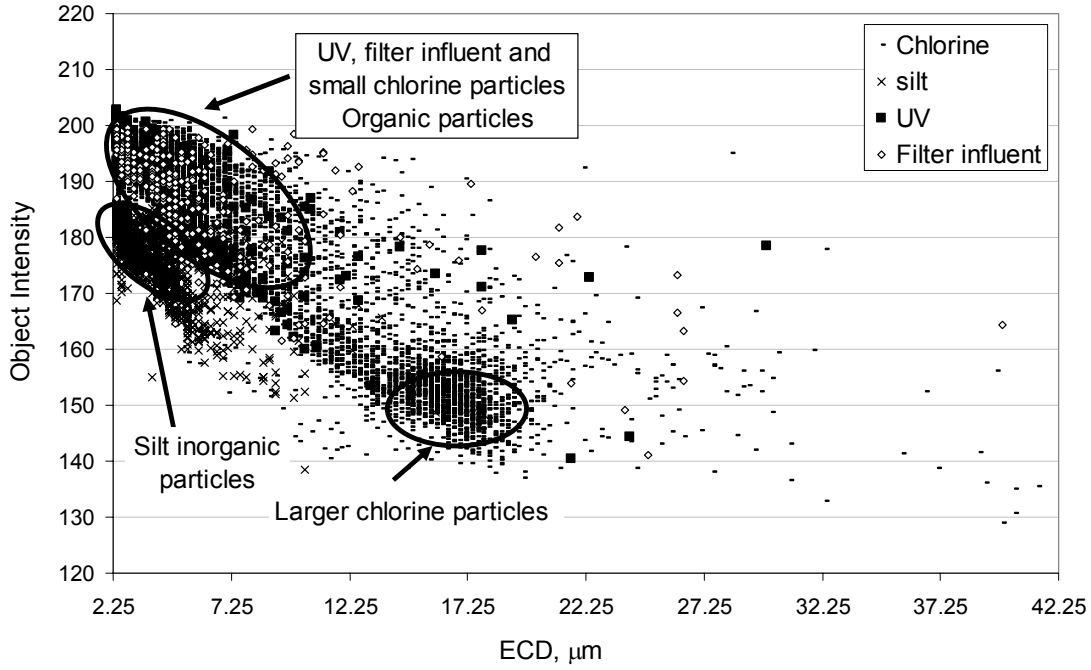

Fig. 88 Intensity as a function of ECD for Chlorine, silt and UV samples

The optical absorption of inorganic particles such as silt and clay has very high to very low absorbance depending on the elements; organic detritus has generally high absorbance and biological organisms have usually low absorbance (Rabanski and King, 2002). The organic detritus particles range from submicron to 100s of microns, while the inorganic particles range up to a few microns. Assuming absorbance is related inversely to particle transparency, may result in higher transparency for biological organisms and lower transparency for organic non-biological matter in effluents.

Automated image analysis provides also shape and transparency parameters bedsides particle size and can possibly be used to target specific microorganisms or to discriminate between different size populations. Coupling intensity measurements with other size and shape parameters and the actual images may further be used as a foot print to identify particle makeup however with natural particles this may be complicated as they are a blend of various particle types. Chavez et al., (2004) has suggested that particle size distribution as measured by the electrical sensing technology (Coulter counter), can be used as a tool to monitor the microbial quality of wastewater. Clancy et al., (2005) showed that dynamic image analysis technology can be used to identify and enumerate biological particles in raw and treated waters such as *Cryptosporidium oocysts* and algae, and complement manual microscopy.

Issues to consider

Fig.89 illustrates images of effluent samples. The right image represents the image itself, while the left image represents the perimeter of the particle as analyzed for shape parameters. It is clear that there are two different particles in the floc imaged; one of biological organic origin and the other is a floc of organic origin. In the image it is apparent that a microorganism is associated with an organic effluent particle that may be protected from disinfection either by diffusion of chlorine or penetration of photons with UV.

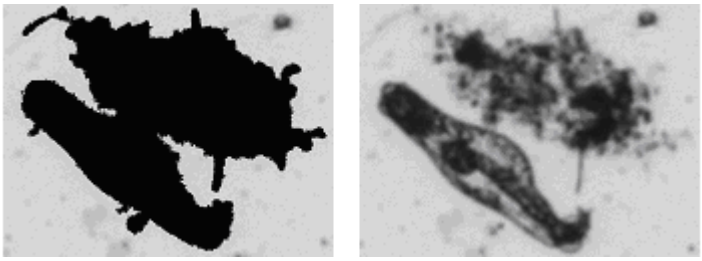

Fig. 89 Images of an effluent floc as captured by image analysis.

IV-1.4 FURTHER DISCUSSION IN RELATION WITH PROCESSES INTEGRATION

Practically thinking, the EF unit (EFector) – constructed wetland hybrid system implies shorter residence time and better water quality, thus reduces land, construction and maintenance costs of the constructed wetlands as well as water loss. Overall, the different configuration has different advantages in contaminates removal from the wastewater. The combination of the two treatments (electroflocculation and constructed wetland) contributed to the removal of contaminates in every inspected aspect. Contaminants removal was at best when the constructed wetland preceded the electroflocculation unit, but a good sand filtration is needed in order to remove turbidity. A full scale system may be in use both for river and lake rehabilitation and tertiary wastewater purposes. It can be modular, with relative small footprint and automatically controlled according to pre-set currents and backwash sequence.

In case of heavy metal residues in the effluents, EF without aeration hybrid with micro- or ultra- filtration or EF with aeration followed by 30 min settling and paper filtration could meet the effluent standard of nickel from metal finishing industrial wastewater in Israel. After aeration-enhanced EF hybrid with membrane filtration, the residual nickel and iron concentration could meet the standard of unrestricted irrigation and even directly discharge into rivers in Israel.

In the field, paper filter used in this study can be replaced by other non-membrane filtration method, like sand filter. Settling can be achieved in the EF vessel, and electroflocculation process could work in sequencing-batch mode or by construction an extra settling tank after the EF process. Those two options are at the cost of increasing the footprint of the total treatment unit. The alternative depends on the financial feasibility study in the field. With the introduction of air in the EF process, the flocs generated displayed better coagulation and flocculation ability in electroflocculation and settling stages. DOEP possesses practical value as an indicator to start aeration.

As pointed out earlier, biofouling, resulting from microbial EPS, is a highly troublesome issue regarding membrane filtration of wastewater effluents. Bacteria that grew in a liquid medium supplemented with Ag-NPs showed growth inhibition (Pal et al, 2007; Shrivastava, et al, 2007; Sondi and. Salopek-Sondi, et al, (2004). In the present study, the bacteria were treated with Ag-PL before inoculation to the LB medium without NPs. In Figure 8 two bacterial growth curves are shown. One curve refers to non treated bacteria as control, while the two other curves refer to bacteria that were treated with 33 and 50 μg mL^{-1} Ag-PL. Aliquots of 2 mL were inoculated into 200 mL LB medium for the control and PL33 and into 100 mL LB medium for the PL50. The reduction of PL50 was 5.6 orders of magnitude. The first observation in Fig.32 is that the kinetics of the growth process in all three curves follows typical growth curves of bacterial population (lag phase in which bacteria are adapted to fresh medium, exponential growth phase and stationary phase with no net increase or decrease in the population). Moreover, under the test conditions, the lag phase of the treated bacteria was found to be more prolonged compared to non treated bacteria, and the final population in the stationary phase was similar for the two treatment types but lower than the control. These results suggest that Ag-NPs can inhibit bacterial growth. Further studies are needed to obtain the dependence of growth rate on the MCNPs/N_0 ratio.

Touching the issue of disinfection, and re-examining Figure 41, it is apparent that a microorganism is associated with an organic effluent particle that may be protected from disinfection either by diffusion of chlorine or penetration of photons with UV. This image shows the importance of observing the images beyond obtaining particle size distribution for the large particles (flocs) prior to disinfection. This technology may be possibly useful to detect particles that are by size smaller than the pore size of membranes, however due to their elongated shape (feret and circularity) they may be retained on the membrane.

IV-1.5 CONCLUSIONS

1. Complementing CW treatment with a physicochemical process of electroflocculation can provide a tertiary treatment that effectively polishes secondary municipal effluents. While EF effectively reduces phosphate in both soluble and particulate forms CW treatment provides a transport-attachment trap to turbidity that escapes the electro-physico-chemical process and removes organic matter and N compounds.

2. Previous laboratory tests showed that electroflocculation coupled with sand filtration effectively removed phosphate and suspended particles in contrary to the wetland gravel performance. The wetland gravel removed effectively organic matter, possibly by microbial degradation, as opposed to the EF-GF configuration.

3. Field pilot results show that the EFector is capable of removing up to 97% of the total phosphorus, getting final concentrations smaller than 0.4 mg/l. Former electro-jar tests followed by continuous-flow, bench-scale results showed similar capabilities of up to 96% removal. The system is optimized for phosphorous removal by controlling current intensity, which represents coagulant dose and by controlling flow rate, which controls reactor residence time and turbulence.

4. The hybrid process also enhances suspended solids (87%) and organics removal (53%) in addition to phosphorus removal. A well designed sand filtration following the EFector is highly recommended.

5. For iron oxidation processes in an electro-flocculation system for treating water the following conclusions can be drawn:

- For practical calculation purposes, the type of iron that dissolved from the anode is Fe^{2+} for pH 5–9 and voltage of 3–25 V.
- There is a possibility of a high Fe^{2+} dissolution rate of the iron anode (mg/l/min) at lower pH values without activating an electric current. This phenomenon can decrease the life expectancy of the anode and also lead to time during an electroflocculation process which is different than what can be attributed to common current intensity-time multiplication as represented by Faraday's Law.
- The electro-chemical dissolution of iron is different at different pH values. At a higher pH values, the iron dissolution can be dramatically lower than the value calculate according to Faraday's Law without a correction factor and, therefore, there are also other reactions (apart from the iron dissolution) which occur simultaneously near the anode.
- Dissolved oxygen plays an important role in the EF process and has far-reaching influence on the following filtration. With the introduction of oxygen into bulk water, iron emission from the electrodes did not increase.

- A dissolved oxygen exhaustion point (DOEP) can be determined. 1.3 mg/L DO concentration in this study could be regarded as the deflection point of ferrous accumulation in this study.

- Aeration-enhanced EF system could keep the DO level higher than DOEP, thus enabling the predominance of ferric hydroxide, rather than ferrous hydroxide, in the bulk water, which could provide better nickel removal efficiency.

- EF combined with microfiltration could provide excellent results in residual iron and turbidity. It was not necessary to use ultrafiltration for their removal.

- Aeration-enhanced EF process hybrid with microfiltration exhibited the potential to provide better removal results of iron. The effluent could meet the stringent standard of unrestricted irrigation and directly river discharging.

6. Bacterial alginate exopolysaccharide was successfully extracted from lab cultured biofilm matrix. Alginate yield after enzymatic purification amounted to (164±21) mg·gVSS^{-1}(as organic content). It is partially O-acetylated oligosaccharides blend with mannuronic acid residue to guluronic acid residue ratio of 1.19. By cross linkage with Ca^{2+}, this extracted alginate is capable of forming gel-like film, which demonstrates that low molecular weight alginate oligosaccharides also greatly contributes to the formation of biofilm matrix. Direct alginates extraction and characterization supplies important information for the role of bacterial exopolysaccharides in building up biofilm matrix.

7. The effect of Ag-MCNPs on *E.coli* can be described by a colloidal particles interaction model. Ag-MCNPs effect on *E.coli* inactivation was particle number dependent and log inactivation of *E.coli* showed linear fit with the ratio between the number of NPs and the bio-colloidal particles measured as initial bacteria cell count. It could be explained by the increase of NP-bacterium collision frequency.

8. Au-MCNPs that were used as a control of similar size but presumably inert metal did not show any inactivation ability. Electrostatic attraction or repulsion mechanisms in Ag-MCNPs and *E.coli* cells interactions were not contributing to the inactivation process.

9. Filter removal efficiency can be determined by various size and shape parameters, where different information is obtained for each analysis.

10. Results suggest that the particle size distribution is not the sole important characteristics in evaluating water effluents as particles are highly heterogeneous with respect to their size and shape.

11. Image analysis has a potential in evaluating efficiency of particle separation processes however more robust statistical analysis need to be used to allow coupling all the size and shape parameters into a meaningful tool to evaluate for example the optimum coagulant dose in contact filtration processes.

IV-2. 4th year report

ABSTRACT

The overall goal of the research in this phase of the project was to examine the potential of coupling physicochemical processes, such as electrocoagulation and membrane filtration, with natural processes, such as constructed wetland, for upgrading secondary effluent quality to the level that would comply with stringent standards for river rehabilitation. The specific objectives of the investigation of this reported stage were as follows: (a)To study the effect of electrocoagulation on effluent quality as a polishing process following constructed wetland and pretreatment of membrane filtration units (CW–EF–MF/UF), (b)To evaluate the efficiency of a constructed wetland (CW)–electrocoagulation (EF)– membrane filtration (MF/UF) treatment in nutrients and suspended solids removal, and (c) To study the effect of electrocoagulation on fouling mitigation of membrane filtration units while developing new parameters and tools to better understand it and cope with it.

Experiments where electroflocculation (EF) followed by granular filtration (GF) act as a post treatment to constructed wetland (CW) has been completed and results are presented. The results strengthen previous indications that there is a slight improvement of the overall process of CW-EF-GF configuration over EF-GF-CW configuration reported last year.. The comprehensive reporting on this innovative topic including process optimization, which is in the framework of MS thesis, is in advanced stages and expected to be ready by the end of the current academic year.

Based on literature, one of the major advantages of coagulation-flocculation in general over the natural system in contaminant removal is expresses in phosphorous removal. It was therefore expected that the EF unit would remove both soluble and particulate phosphorus. The laboratory tests showed that EF–UF/MF not only effectively removed phosphate and suspended particles, but greatly increased phosphate and turbidity removal rate. Constructed wetland and polishing pond not only improved water quality but also changed particle property. The addition of EF as the pretreatment of membrane filtration significantly improved the filtration curve and reduced the filtration energy requirement.

Therefore, it seems that the combination of both units would multiply their treating abilities. The system can be optimized for phosphorous removal primarily by controlling EF working time, which actually represents coagulant dose. Constructed wetland–electroflocculation–membrane filtration system implies shorter residence time and better water quality, thus reduces land, construction and maintenance costs as well as water loss.

Membranes in water and wastewater treatment are frequently susceptible to fouling. Although membrane fouling has been much investigated in the last two decades, solutions are far from being complete. Therefore the effects of pretreatment with iron or aluminum electrodes have been investigated. The effects of aluminum-based electroflocculation pretreatment on filtration energy consumption and fouling mechanisms

in dead-end microfiltration were investigated in this phase of the research. Silica-CMP suspensions were pretreated by electroflocculation at various operation times (0 to 4 min, constant electric current of 0.4 A) followed by different slow mixing times (0 to 30 min) and filtration without any sedimentation step. A new method for filtration-energy appraisal was proposed to define the optimum conditions for operation. Fouling mitigation by electroflocculation was found to be dependent on fouling intensity, dominant fouling mechanism, suspension, pH and electroflocculation operation time. Filtration energy was minimized by 90% in a pH range of 6 to 6.5. Scanning electron micrographs of the fouled membrane surface showed the important role played by the sweep-coagulation mechanism in mitigating fouling. When internal fouling was the dominant mechanism, the amorphous aluminum-hydroxide solids formed a layer that filtered out the primary particles, protecting the membrane pores from plugging. Aluminum-hydroxide particles also reduced the hydraulic resistance of the cake when the external fouling mechanism dominated. Significant energy reduction was observed, even without the slow mixing step, as a result of the local flocculation conditions near the membrane surface. Additional energy savings were obtained due to the significantly higher initial flux restoration rates (>90%) imposed by treating the suspension with electroflocculation.

Control of biofouling and its negative effects on process performance of the membranes is a serious operational challenge. Molecularly capped silver nanoparticles (Ag-MCNPs) were used as a pretreatment strategy for controlling biofilm development in aqueous suspensions using the model organism *Pseudomonas aeruginosa*. Biofilm control was tested in a two-step procedure: planktonic *P. aeruginosa* was exposed to the Ag-MCNPs and then the adherent biofilm formed by the surviving cells was monitored by applying a model biofilm formation assay. Under specific conditions, Ag-MCNPs retarded biofilm formation, even when high percentage of planktonic *P. aeruginosa* cells survived the treatment. For example, Ag-MCNPs (10 $\mu g \cdot ml^{-1}$) retarded biofilm formation (>60%), when 50 percent of the planktonic *P. aeruginosa* cells survived the treatment. Moreover, stable low value of relative biomass has been formed in the presence of fixed Ag-MCNPs concentrations at various biofilm incubation times. Our results showed that Ag-MCNPs pretreated cells were able to produce EPS although they succeeded to form relatively low adherent biofilm. These pretreated cells appear well preserved and undamaged under TEM HPH/freeze micrographs, yet the intra cellular material seems to be pushed towards the peripheral parts of the cell, possibly indicating a survival strategy to the presence of Ag-MCNPs. The lower value of relative biomass formed in the presence of Ag-MCNPs could be associated with molecular mechanisms related to biofilm formation or continuous release of silver ions in the sample. However, further research is required to examine these factors.

The role of exopolysaccharides in biofilm provides information on biofouling control. To understand exopolysaccharides structure-function relationship, alginate-like exopolysaccharide was specifically extracted from aerobic granular sludge (a special case of biofilm) cultivated in a pilot plant treating municipal sewage containing a large fraction of slaughterhouse wastewater. The exopolysaccharide was

identified by the FAO/WHO alginate identification tests, characterized by biochemical assays, gelation with Ca^{2+}, blocks fractionation, spectroscopic analysis as UV-visible, FT-IR and MALDI-TOF MS, and electrophoresis. The yield of extractable alginate-like exopolysaccharide reached (147±6) mg/g SS. It resembled seaweed alginate in UV-visible and MALDI-TOF MS spectra, and distinguished from it in the reactions with acid ferric sulfate, phenol-sulfuric acid and Coomassie brilliant blue G250. Characterized by its high percentage of poly guluronic acid blocks, it was capable to form rigid, non-deformable gels in $CaCl_2$. Widely distributing, this exopolysaccharide is one of the main exopolysaccharides in aerobic granular sludge. It plays a significant role in providing aerobic granular sludge a highly hydrophobic, compact, strong and elastic structure.

IV-2.1 INTRODUCTION AND SCIENTIFIC BACKGROUND

Water and energy have been identified by Smalley as the two top challenges for the 21st century (Smalley, 2004).Water quality and available quantity are being challenged by increased pollution from point and non-point sources such as industry and agriculture, respectively, and the ever-increasing population. Third-world countries generally have neither the infrastructure nor capital to adequately address the water problem. Although the wastewater treatment process is a well-established engineering science, the need for process incorporation, decentralized treatment and simplified processes have opened new challenges and new opportunities particularly in developing countries (Lindell, 2004). Innovative, cheap and effective methods of purifying water for human consumption as well as to clean the wastewater from industrial effluents before discharging into any other water systems are needed. In this study the combination of three secondary effluents treatment processes, i.e., constructed wetland (CW), electroflocculation (EF) and granular (GF) and membrane (UF or MF) filtration has been investigated.

Constructed wetland. Constructed wetland (CW) is an environmental friendly technology for treating wastewater or polishing effluent that is becoming increasingly popular in many parts of the world (Haberl, 2003). It is designed and constructed based on natural marshes (Kadlec and Wallace, 2008). CWs are often classified by the pattern of effluent flow in the system (e.g., Brix, 2003). In free-flow (surface flow) systems wastewater flows above the ground through emerged, submerged and floating aquatic vegetation. In subsurface flow systems wastewater moves through a porous medium such as gravel or aggregates, in which rooted hydrophytes grow (USEPA, 2000).Subsurface systems are further classified into horizontal flow (HF), in which anaerobic conditions prevail, or vertical flow (VF) which maintains aerobic conditions. Low flow velocities coupled with the presence of roots and solid substrate, promote settling and filtration of particulate material. Biofilm of diverse pre-treatment that develops on the porous medium is responsible for most of the biotransformation and mineralization of pollutants. (e.g, Vymazal, 2003; Kadlec and Wallace, 2008). CWs usually remove organic matter and nitrogen (N) compounds efficiently but are less efficient in removing phosphorous (P) compounds (Kadlec and Wallace, 2008).Retention of P in CWs includes peat/soil accretion (mostly in natural and free flow systems), soil adsorption, precipitation and plant uptake (Vymazal, 2003). In subsurface systems removal by plants is limited and requires plant harvesting annually. The adsorption and chemical precipitation of phosphorus is much more vigorous at the initial operation stage because the process has finite capacity (EPA, 2000). As a result, CW capacity for phosphorous removal is quite limited. For the latter reason we considered coupling CW with physicochemical process that is expected to complement the naturally occurring processes by removing phosphorous efficiently.

Electroflocculation (EF) Electroflocculation (electrocoagulation) presents an alternative method to conventional (chemical) flocculation with several advantages: easy operation, lower quantities of produced sludge, avoidance of chemical usage and, most importantly, no anions such as chloride or sulfate need to be added to the solution (Mollah et al., 2001). Unlike conventional flocculation in which the coagulants are added to the water as salts, in the EF process, the coagulants (iron or aluminum) are added to the solution by dissolving the anode in an electrochemical cell. These coagulant ions ultimately lead to aggregation of the original particles in the water, which are removed in a later sedimentation or filtration process.

When the anode is made of iron, during the electrochemical process the following main reactions occur near the electrodes:

Near the anode:

Reaction 1: $$Fe_{(s)} \rightarrow Fe^{+2}{}_{(aq)} + 2e^{-}$$

Reaction 2: $$2H_2O \rightarrow O_{2(g)} + 4H^{+}{}_{(aq)} + 4e^{-}$$

Near the cathode:

Reaction 3: $$2H_2O + 2e^{-} \rightarrow H_{2(g)} + 2OH^{-}{}_{(aq)}$$

Reactions 2 and 3 explain the appearance of bubbles near the cathode and anode during the process. It can also explain the concomitant rise in pH, dependent on solution alkalinity, electrical current intensity and operation time.

The theoretical relationships between the electric current, I (A), operation time t (sec) and mass of the dissolved metal W (g) are traditionally described by Faraday's law:

$$W = \frac{M_w It}{nF}$$

Where M_w -Molecular weight (g mol^{-1}), n - oxidation number, F - Faraday's constant (A sec mol^{-1}).

Ben-Sasson et al. (2009) showed the appearance of chemical anodic dissolution of iron, independent of the electric current (reaction 4) in acidic pH, which leads to higher dissolution rates then the theoretical calculations.

Reaction 4: $$Fe_{(s)} \rightarrow Fe^{+2}{}_{(aq)} + 2e^{-}$$

Lower dissolution rate than the rates calculated by Faraday's law means that part of the electrons of the electrochemical current participate in reactions different from anode dissolution (reaction 1) such as oxygen

evolution (reaction 2). Therefore, some authors added correction factors to Faraday's law such as current efficiency (Heidmann and Calmano, 2008, Jiang et al., 2002) or faradic yield (Carmona et al., 2006) to describe the gap between the theoretical and the experimental dissolution rates.

The Fe^{2+} ions that dissolved from the anode may farther oxidize to Fe^{3+} as describe in the following reaction:

Reaction 5: $$4Fe^{2+} + O_2 + 2H_2O \rightarrow 4Fe^{3+} + 4OH^-$$

Reaction 5 is pH and oxygen saturation level dependence. Ben-Sasson et al. (2009) showed that essentially, reaction 5 rates in electrochemical cells are not different from non electrochemical cells. Under alkaline conditions, the Fe^{2+} ions will immediately oxidize to Fe^{3+} (pH 14-8). At lower pH, the rates will be much lower and below pH 5, the oxidation process becomes negligible. The oxidized ferric (Fe^{3+}) ions will proceed in the following general hydrolyzing reactions (Duan and Gregory, 2003):

Reaction 6: $$Fe^{3+} \Leftrightarrow Fe(OH)^{2+} \Leftrightarrow Fe(OH)_2^{+} \Leftrightarrow Fe(OH)_3 \Leftrightarrow Fe(OH)_4^{-}$$

The significance of each hydrolyzed form and the solubility of the dissolved iron depended on the pH values of the solution as present in Fig. 90.

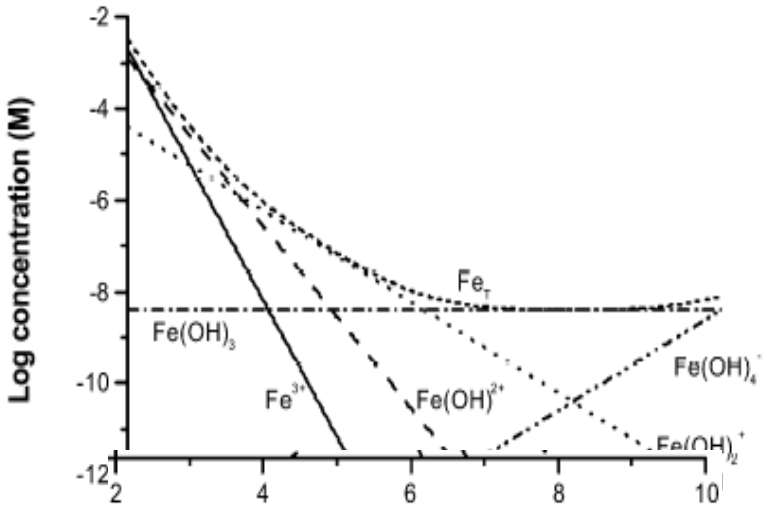

Fig. 90 Concentration of monomeric hydrolysis products of Fe(III) in equilibrium with amorphous hydroxides, at zero ionic strength and 25°C (After Duan and Gregory, 2003)

When the coagulant concentration is below the solubility value, the soluble iron forms act to destabilize the particle either by neutralization of the particle charge or by compressing the particle's electric double layer which lead to so-called destabilizing flocculation type. When the coagulant concentration is above the solubility value, the particles are adsorbing or get sweeping by the amorphous solids hydrolyzed iron that formed (such as $FeOH_{3\ (S)}$) which lead to sweep-flocculation type (Duan and Gregory, 2003).

Electroflocculation for phosphorus removal. As well known, eutrophication is one of the main problems nowadays encountered in the monitoring of the environmental water sources in the industrialized countries. This phenomenon, that is responsible for the dramatic growth of algae occurring in internal and coastal waters, is caused by the excess phosphorus concentration in the effluents from municipal or industrial plants discharged in the environment (Sommariva et al., 1996). The usual forms of phosphorus found in solutions include orthophosphate, polyphosphate and organic phosphate. The principal phosphorus compounds in wastewater are generally orthophosphate forms together with smaller amounts of organic phosphate. In the countryside, where agriculture and animal husbandry are the main industries, wastes from these activities will contribute to the accumulation of P in soil and water bodies. These phosphorus compounds, dissolved in surface or ground waters, are responsible for the eutrophication in closed water systems, especially in lakes and enclosed bays where the water is almost stagnant.

Phosphorus removal techniques are chemical treatments like adsorption, chemical precipitation, ion exchange, electrodialysis, hybrid systems containing fly-ash adsorption, membrane filtration and electroflocculation. Adsorption and chemical precipitation among the above methods have been widely used for phosphate removal (Ugurlu and Salman, 1998). The removal of phosphate from aqueous streams consists of the conversion of soluble phosphate to an insoluble solid phase. This solid phase can be separated from water by means of sedimentation or filtration. In wastewater applications, the most common and successful methods to precipitate phosphate involve the dissolved cations Al^{3+}, Ca^{2+}, Fe^{3+} and to a lesser extent of Fe^{2+}. It was found that when iron and aluminum are present in the water, $FePO_4$ and $AlPO_4$ forms in the low pH range (<6.5) and at higher pH range (>6.5) iron and aluminum increasingly convert to oxides and hydroxides. A higher pH is more suitable for precipitation of phosphate with calcium as apatites and hydroxyapatites.

Phosphate, pyrophosphate, triphosphate and higher polyphosphate anions are known to form complexes, chelates and insoluble salts with number of metal ions such as iron. Some of the complexes such as $FePO_4$ have low solubility that lead to solid formation which have easier removal procedure. Phosphate anions are also sorption onto iron-hydroxide amorphous solids that formed when the sweep flocculation mechanism is operating. Both the iron-phosphate complex reactions, the solubility of the those complexes and the sorption rate of phosphate anions to the iron-hydroxides is highly dependent on the pH value, iron and phosphate concentration and the appearance of other metals such as Ca^{2+} (Stumm and Morgan, 1970).

While phosphate removal by iron conventional flocculation or by aluminum based EF are found wildly in the literature, only few works were dedicated to the more complex subject of phosphate removal by iron based EF. Irdemez et al. (2006) showed high removal of phosphate (more then 80%) by iron based EF treatment in synthetic solution. They observed the following trends: (1) the higher the electric current density the higher phosphate removal rates, (2) higher phosphate concentration will lead to lower removal rates. Irdenez et al. (2006) found that when the solution pH was controlled in synthetic solution, the optimal pH value for phosphate removal was 6-7. High phosphate removal rates (almost 90%) by iron based EF was found also by Vesudevan et al., (2009) for water at pH 8. Their type of water was unclear.

Ultrafiltration (UF) and microfiltration (MF) can highly polish secondary effluents, but they still have low capacity for phosphate removal from secondary effluent. In addition, their colloidal fouling i.e. the accumulation of the retained particles on the surface or inside the pores of the membrane, leads to hundreds percents increase of the consumed energy and to higher operational costs of the filtration process. While the high rate of population growth in developing countries is expected to cause a severe fresh-water shortage in the forthcoming years with potential devastating consequences, a major obstacle in the establishment of water-purification systems in such areas is the operational cost due to high energy demands. Also, the more energy that is consumed, the higher air pollution intensity is. Consequently, global efforts are being made to develop low-energy operation conditions for the existing water purification methods.

The most prevalent contaminants found in sweet water are small particles, colloids, which are in the size range of 1-1000 nanometers. These colloids include viruses, bacteria, dissolved organic matter, industry waste products, pesticides and more. Currently, the most reliable technologies for treating colloidal contamination are membrane-based processes called: microfiltration (MF) and ultrafiltration (UF). Still, their large-scale application is limited as results of their main operational problem: the colloidal fouling. Colloidal fouling is the accumulation and plugging of particles on the membrane surface or inside the membrane pores which may leads to hundreds percents increase of the consumed operational energy. In the literature there is description of several colloidal fouling mechanisms (Hermia, 1982) that can be divided into two main groups:

- Internal fouling – a set of mechanisms which are responsible for decrease of membrane permeability as a result of decrease in pores area free to flow or decrease the number of open pores.

- External fouling – fouling mechanism that results from colloids accumulation on the membrane surface that leads to construction of additional layer (cake) with additional hydraulic resistance.

The cake layer which leads to external fouling may also reduce it by stopping the smaller particles from entering the membrane pores, this concept of cake filtration is referred to as secondary membrane effect (Arora and Davis, 1994).

Kuberkar and Davis (2000) propose a model that describes the relationship between flux and medium resistance as a result of internal fouling, external fouling and the secondary membrane effect for constant viscosity:

$$J_t = \frac{\Delta P}{\frac{R_0}{1 - K_m \int_0^t (J_t \ell^{\frac{-\int_0^t J dt}{D}}) dt} . + K_c \int_0^t J_t dt}$$

Where J_t - flux ($\frac{m}{s}$), ΔP - pressure (Pa), R_0 - initial membrane resistance ($\frac{Kg}{m^2 s}$), K_m - internal fouling coefficient, K_c - external fouling (cake) coefficient, D - secondary membrane effect coefficient.

<u>*UF/MF pretreatment by EF*</u>. Ben-Sasson and Adin[1] (2009) observed high improvement in the filtration energy i.e. fouling mitigation, when colloidal silica synthetic solution was pretreated by iron based EF for dead-end MF. The desired flocculation mechanism was found to be sweep-flocculation. The EF effects were different for the internal and external fouling mechanisms. In the internal fouling, the iron-hydroxide layer that formed on the membrane surface filtered out the small particle and prevented them to penetrate the pores of the membrane. In the external fouling the EF changed the composition of the cake and reduced its hydraulic resistance. Different results were achieved by Bagga et al. (2008) and Al-Malack et al. (2004), who showed only marginal or negligible effect by iron based EF on fouling mitigation of both cross-flow and dead-end MF. Higher removal of virus and selenium were observed by Zhu et al. (2005) and Mavrov et al. (2006) when the solution was pretreated by iron based EF before dead-end MF.

Pretreated by aluminum based EF for MF yield a dramatic fouling mitigation both in crossflow (Pouet and Grasmick, 1994) and dead-end (Ben-Sasson and Adin[2], 2009) operation mode. Harif et al. (2006) demonstrated that the addition of aluminum based EF before dead-end UF of kaoline solution may lead to 20% higher fluxes at pH 5 and 6.5.

Electroflocculation (EF) presents an alternative method to conventional (chemical) flocculation with several advantages. Pretreatment by iron based EF showed significant colloidal fouling mitigation in MF of synthetic solution ([2]Ben Sasson and Adin, 2009). Therefore, the addition of EF before UF/MF may give two benefits besides the secondary effluent polishing; (1) it may mitigate the colloidal fouling (2) it may lead to higher phosphate removal rates. Here we explore the capacity and optimization of the hybrid processes EF+MF or EF+UF in polishing secondary effluent, particularly phosphate removal and fouling mitigation.

The severe energy losses resulting by the colloidal fouling has generated a number of inventions and research methodologies aimed at reducing this loss. One of the methods that were offered in order to

challenge the colloidal fouling is pretreatment by coagulation before the membrane filtration. It is believed that the increase of the particles size and the particles aggregation resulted by coagulation are leading to both prevention of the internal fouling and decrease of the external fouling.

While the effects of conventional coagulation as fouling mitigation method were widely discussed in the literature, only few works were dedicated to investigate the potential of EF as fouling mitigation method. Therefore, there was lack of information and some of the knowledge was unclear which obscured the understanding of the potential efficiency of the hybrid process (MF+EF). Only one article was found in the literature regarding the hybrid process of aluminum based EF and MF. It showed possible significant fouling reduction in cross-flow MF; still the operational conditions for achieving this result were not discussed. Also there was not found any information regarding the effects of aluminum based EF on dead-end MF mode. Regarding iron based EF, both in cross-flow and dead-end operation modes, former researchers claimed for only marginal or negligible effects on MF performances.

In addition, most of the former works involved fouling mitigation methods based their conclusions on flux comparison methods. Applying mitigation fouling methods such as EF may be costly in terms of both money and energy. It is therefore important to understand not only if a fouling-mitigation method can improve membrane filter performance (e.g., increase the flux), but also how much energy is actually saved and what the optimum operational conditions are as well.

The most challenging type of membrane fouling currently is biofouling. Biofouling is the generally accepted term for the unwanted accumulation of microorganisms on surfaces (Flemming, 2002) caused by adhesion and growth of microorganisms, under the significant help of the self produced extracellular polymeric substances (EPS). Membrane biofouling can cause a variety of negative effects on membrane performance, including loss of flux, contamination of permeate and more (Ridgway and Flemming, 1996). It becomes membrane technology's “Achilles heel” (Flemming, 2002). Worldwide biofouling results in an annual cost of billions of dollars, affecting membrane filtration technologies, water treatment and supply facilities. Membrane biofouling is commonly controlled by regular membrane replacement, costly periodic chemical cleaning procedures or by chemical formulation of the membrane materials controlling the characteristic of their surface. However, the effect of these approaches is limited, the risk of elevated levels of harmful disinfection by-products (DBPs), many of which are carcinogens (Krasner et al. 2006) or can damage the membrane, has given rise to consider alternatives for biofilm control.

Ionic silver and silver compounds are known as an environmentally friendly biocide agent used for years in many fields from disinfecting medical devices and home appliances to water treatment (Silvestry-Rodriguez et al. 2007, Bosetti et al. 2002). Silver in the form of nanoparticles (Ag-NPs) showed improved antimicrobial performance. Previous studies have reported of good bacterial inactivation and growth inhibition ability by the particles (Pal et al. 2007, Sondi and Salopek-Sondi 2004, Shrivastava e al. 2007). Unlike conventional chemical disinfectants, AgNPs are relatively inert in water and do not expected to

produce harmful DBPs. Moreover, membrane in which AgNPs were embedded showed positive results in antifouling investigations (Damm et al. 2007, Deng et al. 2008).

Based on the application of AgNPs in suspension, using of these particles to control development of biofilms by prevent the ability of microorganisms to grow and multiply on target surfaces, appears like a promising sustainable and environmental friendly technique.

Biofilm are surface-adherent communities of microorganisms embedded in their own microbial-originated matrix of protective and adhesive extracellular polymeric substances (EPSs), mainly polysaccharides, lipids and proteins (Bishop, 2007; Denkhaus et al., 2007). The EPS may also contain components from the surrounding environment as DNA (Steinberger et al., 2005). The biofilm habitat represents a primary mode of growth and living for most microorganisms on earth (Flemming, 2002); wherever there is water, a surface support and available nutrients, a biofilm will form (Bishop, 2007). In the water industry, biofilm formation is beneficial when it is the fundamental basis of treatment technologies such as biofiltration and biodegradation (Denkhaus et al., 2007; Flemming, 2002). Biofouling, however, is the undesired deposition of microorganisms and their EPSs on various surfaces (Flemming, 2002). Avoiding biofouling and its negative effects on process performance of water systems is a serious operational challenge in all of the water sectors, including pipes, water-distribution systems, filtration processes, cooling facilities and power plants.

Current approaches to preventing or removing biofouling use disinfectants as a pretreatment or apply frequent chemical cleaning (CIP) after biofilm has formed. However, microorganisms in biofilm develop a tolerance to the cleaning procedures, and a mature biofilm is persistent and difficult to completely eradicate (Kierek-Pearson and Karatan, 2005; Flemming, 2002). Moreover, periodic cleaning is costly and can damage process surfaces. Oxidative disinfectants may enhance the formation of biodegradable organic substances that can be utilized by microorganisms, thereby promoting biofilm formation. Furthermore, the use of oxidative disinfectants results in elevated levels of harmful disinfection by-products and can damage surfaces such as polyamide desalination membranes (Momba et al. 2000). Due to these limitations, alternatives are being sought to control biofouling in water systems such as distribution pipelines or membrane-filtration processes. In this study, a pretreatment technique for controlling potential biofouling based on the application of molecularly capped silver nanoparticles (Ag-MCNPs) suspended in water is presented.

The antimicrobial properties of silver compounds and silver in its ionic form (Ag^+) have been applied in a wide range of applications including water systems (Kim et al., 2004; Silvestry-Rodriguez et al., 2008). Exposure to silver is considered safe for humans; yet, a standard of 0.1mg/L of soluble silver is allowed in drinking water (WHO, 2004). Moreover, most strains of bacteria have not yet developed resistance to Ag^+ (Silver, 2003). Turner and colleagues (Harrison et al., 2004) found Ag^+ to be the most toxic of 17 different metals tested for the eradication of biofilm while screening various microorganisms, among them,

Pseudomonas aeruginosa. Recent studies have demonstrated superior performance of silver nanoparticles (Ag-NPs) over Ag^+ in controlling the growth and activity of various microorganisms (Lok et al., 2006), and Ag-NPs have been shown to inactivate planktonic *Escherichia coli* in aqueous suspensions (Dror-Ehre et al., 2009). Many researchers in the field refer to Ag-NPs as a new class of materials that can be used in a broad range of applications as an antibiotic (Choi et al., 2008; Fernandez et al., 2008; Morones et al., 2005; Nel et al., 2006), or even in consumer products such as food containers, films and face creams, or as important textile finishing biocides (Chopra, 2007; Kramer et al., 2006). Moreover, effective prevention of *P. aeruginosa* biofilm formation has been achieved in catheters coated with a matrix of Ag-NPs (Roe et al., 2008) or Ag-releasing rubber (de Prijck et al., 2007). With regard to membrane-filtration processes for water treatment, hybrid nanofiltration and ultrafiltration membranes with immobilized Ag-NPs have shown good anti-biofouling ability (Lee et al., 2007; Zodrow et al., 2009). These applications of Ag-NPs involve the creation of antibacterial surfaces by immobilized or surface-supported NPs. However, an aqueous suspension of NPs can also be used as a pretreatment in water systems prior to the main treatment units, such as membrane filtration.

The pre-treatment with Ag-MCNPs presented in this study was aimed at controlling or retarding biofilm formation on surfaces in water; it was not meant as a treatment for the eradication of existing or mature biofilm or as a disinfection process. The effect of □re-treatment with Ag-MCNPs on the development of biofilm in an aqueous suspension was determined using the model organism *P. aeruginosa* and a model biofilm formation assay.

Exopolysaccharides have been recognized as key elements that shape and provide structural support for biofilms (Sutherland, 2001). Likewise, they are also highly involved in aerobic granular sludge matrix structure. They could function as a buffer layer for the cells against the harsh external environment, serve as carbon and energy source during starvation and sustain long-term stability of the aerobic granules (Wang and Lin, 2007; Wang et al., 2006).

To date, exopolysaccharides content in the extracted extracellular polymeric substances (EPS) was employed as a parameter to evaluate their role in the formation of the matrix of aerobic granules and sustaining its stability (Adav and Lee, 2008). However, extracting EPS from aerobic granules was difficult due to their compact structure (Adav and Lee, 2008). Different extraction methods yielded different quantities of exopolysaccharides. Data reported in literature altered from (6.2±0.1) mg/gVSS by high speed centrifugation (10,000× g, 20min), to (109.3±15.3) mg/gVSS by ultrasound-formamide-NaOH (Adav and Lee, 2008). Such great divergence displays that the value of exopolysaccharides content obtained, is highly decided by the extraction method, more than reflecting the real quantity in the sludge granules. Misinformation may be brought if the role of exopolysaccharides is assessed simply by these measured values.

Furthermore, aerobic granules contain a mixture of microbial species, so various kinds of exopolysaccharides would be synthesized, while they do not contribute equally to the structure and properties of the granules. Some polysaccharides have shown to play a dominant role in maintaining the integrity of the structure, while others do not possess this function (Sadovskaya et al., 2005). Therefore, further investigation focusing on functional exopolysaccharides extraction and characterization are useful to increase the understanding of granule formation and morphology.

Aerobic granular sludge was characterized as hydrogel; the existence of gel-forming exopolysaccharides was believed in aiding granule formation (Annual report, 2008). Bacterial alginate, the exopolysaccharide with unique gel-forming properties was successfully extracted from aerobic granules cultivated in lab-scale reactors. Its presence connected with the integrity of the granules (Lin et al., 2008). Yet, information about its structure-function relationship is still lacking. To further understand the correlation between alginate property and formation of aerobic granules, alginate-like exopolysaccharide (ALE) was extracted from aerobic granular sludge cultivated in a pilot-scale reactor treating municipal sewage that also contained a relatively large fraction of slaughterhouse wastewater, and was identified and characterized by chemical, spectroscopic and electrophoresis analysis.

IV-2.2 MATERIALS AND METHODS

IV-2.2.1 A Hybrid System of Constructed Wetland, Electroflocculation, Granular Filtration and Membrane Filtration for Upgrading Secondary Effluent

The research work consisted of four successive steps, two at constructed wetland site and one in the laboratory:

(a) Field, constructed wetland treatment of the secondary effluent from Shafdan wastewater treatment plant

(b) Field, EF/GF treatment of the secondary effluent from Shafdan wastewater treatment plant

(c) Field, constructed wetland treatment of the secondary effluent from Shafdan wastewater treatment plant followed by EF-GF treatment.

(d) Batch experiments for EF treatment and membrane filtration

Field stage

Field stage constructed wetland and polishing pond are shown in Figs. 91 and 92, respectively.

Fig. 91 Constructed wetland

Fig. 92 Polishing pond

A complex of CW ponds was constructed in the Shafdan WWTP (Tel- Aviv – Dan metropolitan area; Constructor Ofra Aqua Plants, modified by Moran consulting, design, & construction of aquatic ecosystem). The system included several series of three successive wetland ponds (ca. 35m^2 each), vertical or horizontal subsurface flow and one free flow. The results reported here relate to a treatment by a single VF pond. The VF ponds were packed from top to bottom with an 8cm layer of basalt (20–30mm); 9 cm of basalt (2–3mm); 8 cm basalt (5–10mm); 8 cm dolomite (8mm); 15 cm basalt (3-6 mm) and 20 cm of dolomite (50-60mm) at the bottom. *Cyperus papyrus*, *Canna sp.*, *Iris pseudoacorus*, *Phragmites australis* and *Juncus ensifolius* were planted, but by the third year *Cyperus papyrus* dominated the system.

A pilot EF–CW system (Fig. 49) was built at the Shafdan municipal, activated sludge wastewater treatment plant, comprising of the following components: (a) pre-strainer, (b) up-flow EF generator (EFector, TreaTec21 Industries Ltd.), 1.4 m^3 in volume, 1.25 m in diameter, containing 12 pairs of perforated iron electrodes, (c) granular filter, 1m bed depth and 0.6mm effective grain size, (d) 4 m^3 filtered water tank, used also for system backwash and flushing

Laboratory stage (batch systems)

The electroflocculation devise consisted of an inner cylinder cathode made of stainless steel 2.5 cm in diameter and 27 cm in length and outer cylinder anode made of iron 10 cm in diameter and 27 cm in length.

A bench-scale membrane system (Fig. 93) consisting of N_2 pressure cylinder, pressure regulator (SYC IR2010), 2 liters supply chamber and 100 ml membrane cell was also used in this research. Three types of membrane, microfiltration membrane (0.01um pore size, Sterlitech) and ultrafiltration membranes (100KD

and 10KD cutoff, Trisep Co., USA) in 2.5 mm diameter rounded discs were examined. The fouling parameter was measured by relative flux with an electronic balance (Sartorius, BS3100S) connected to PC. The flux was recorded every 30 second and processed by BAL6 computer program.

1000ml samples of secondary effluent from Shafdan wastewater treatment plant, wetland outlet and polishing pond outlet respectively were pretreated by electroflocculation before went into the membrane filtration system. A constant electric current of 0.4 A was operated (DC power supply – Topward 6030D) with different EF operation time (0, 1, 2, 4 min respectively) under conditions of fast mixing (350 rpm). The continuing step was slow mixing at 40 rpm for 10 minutes. The filtration process was operated under constant pressure of 3 bars.

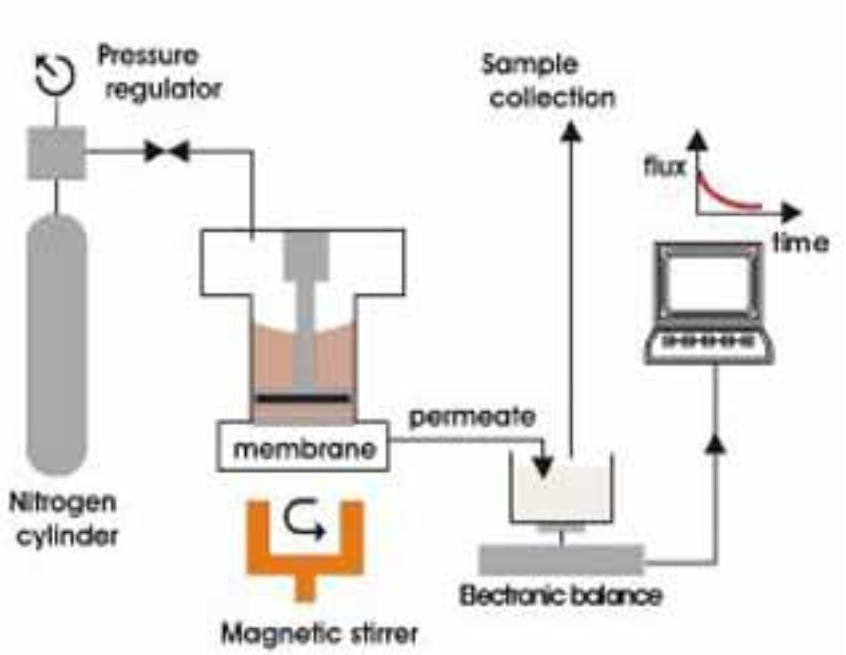

Fig. 93 Dead end cell for pretreatment tests

The pH was measured by digital pH meter model 201 Orion research. Turbidity measurements were conducted with 2100N Turbidimeter by HACH. The particle count was determined using Liquid Particle Counting System Model 9703 by HIAC/Royco. TOC was measured using a TOC-V CPN Shimadzu corporation. Phosphate and iron were analyzed with ICP (OPTIMA 3000XL, Perkin Elmer).

Morphology of the fouling layer on the membrane was examined by scanning electronic microscope (JSM 5410LV).

IV-2.2.2 The Effects of Electroflocculation Pretreatment on Fouling Mechanisms, Filtration Energy and Contaminants Removal Rates in Microfiltration

The effect of EF pretreatment on dead-end MF was studied in this research through answering the following research questions: (a) How much filtration energy can be saved by the addition of EF pretreatment? (b) How are the internal and external fouling mechanisms in MF affected by EF pretreatment? (c) What is the desired flocculation mechanism—sweep coagulation or particle destabilization—in the hybrid (EF + MF) process? (d) What are the optimal operating conditions in terms of pH and electric current intensity values? (e) What are the effects of EF pretreatment on the removal rate of contaminants?

In order to answer the first energetic question a new method for energy calculations was proposed to comprehend and realize the effect of EF pretreatment on energy minimization in MF. This method also enables optimizing the system's operational conditions.

The experimental sets were planed in order to achieve the research goals and to answer the above research questions.

First set - Silica colloids synthetic suspensions (pH 6-8) were pretreated by aluminum and iron based EF at various operation times (0 to 4 min, constant electric current of 0.4 A) followed by different slow mixing times (0 to 30 min) and MF without any sedimentation step. The purpose of this set was to investigate the effect of EF on each type of fouling mechanism (internal and external) and to explore the dependency of the hybrid process (EF+MF) performances on the pH and the dissolved coagulant dose.

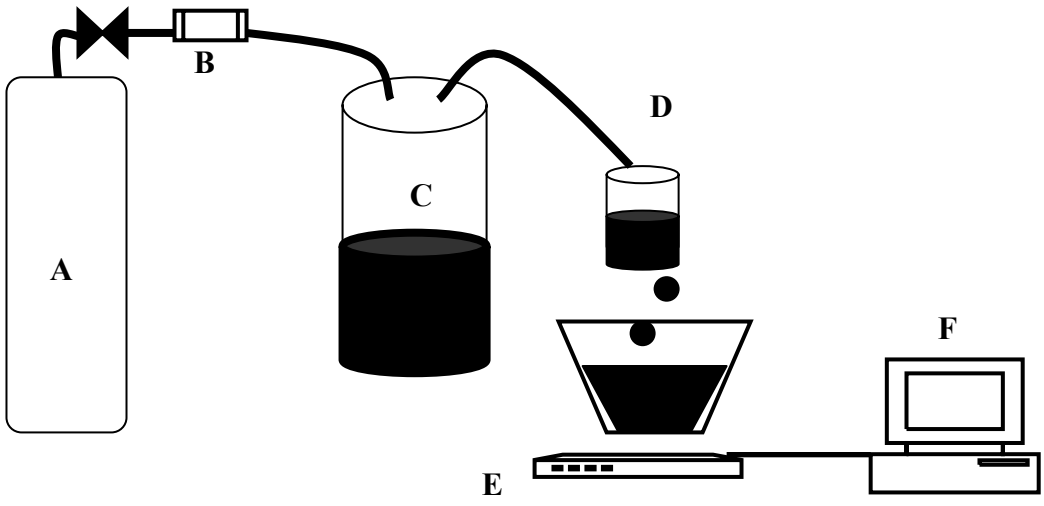

Fig. 94 The membrane system: A–nitrogen tank, B–pressure regulator, C–supply chamber, D–membrane cell, E–technical balance, F–computer

Second set – synthetic solutions of dissolved organic matter (pH 6-8) were pretreatment by different operation times of iron and aluminum based EF (0 to 12 min, constant electric current of 0.3 A) followed by MF. This set was designed to study the effects of EF on MF contaminates removal rates.

A membrane system based on the one previously described (Fig. 95) consisting of a N_2 tank, a pressure regulator (SYC, IR2010), a 2-liter supply chamber and a 100-ml membrane cell was used in this research. The flux was measured every 10 s by technical balance (Sartorius, BS3100S) and processed by the computer program

Track edging polycarbonate membrane discs (Sterlitech), 2.5-mm diameter with 0.1-µm pore size, were used in all experiments. These membranes were selected for their smooth surface, very simple pore shape (cylindrical) and uniform pore size, which helped to separate between the internal and external fouling mechanisms.

The basic solution was made up of highly pure water (Haifa Chemicals Industry) after RO and ionic-exchange treatment with the addition of 1 mg/l $NaHCO_3$ as a pH buffer. Further addition of 0.2 mg/L $NaNO_3$ provided an electric conductivity of 1 mS/cm, simulating the average electric conductivity of tap water. pH was adjusted with HNO_3 to achieve pH values of 6, 6.5, 7, 7.5 and 8.

LUDOX AM-30 colloidal silica (Sigma-Aldrich, 420875), (12 nm; 1.5 mg/l) was added to the basic solution for the internal fouling experiments and 25 mg/L silica powder (NanoAmor) was added to the basic solution for the external fouling experiments. The powder was subjected to 11 min of sonication (Sonics Vibracell, VCX 750 Watt) to yield steady particle aggregates, 0.5 µm in size.

The EF device consisted of an inner-cylinder cathode made of stainless steel, 2.5 cm in diameter and 27 cm in length, and an outer-cylinder anode made of aluminum, 10 cm in diameter and 27 cm in length.

After suspension preparation, a constant electric current of 0.4 A was maintained (DC power supply, Topward 6030D) for the examined EF operation time under conditions of fast mixing (350 rpm). The second step consisted of slow mixing at 40 rpm for 20 and 30 min for the external fouling and internal fouling experiments, respectively. The following filtration process was operated under a constant pressure of 2 bar. Suspension samples (10 ml) were taken for Inductively Coupled Plasma mass spectrometry (ICP) (Perkin Elmer, Optima 3000XL) prior to EF, after EF and after membrane filtration to determine silica and aluminum concentrations. After filtration, the fouled membrane which had been pretreated, or not, by EF was visually analyzed by scanning electron microscope (SEM) (JEOL, JSM 5410LV).

The common way of studying methods aimed at fouling mitigation, which is based on flux comparisons, has several disadvantages and, more importantly, does not answer the most important practical question regarding energy, i.e., how much energy can be saved by adding the method in question? Therefore, in this research we evaluated the filtration energy using a new energy-appraisal method.

In constant-pressure operational mode, the filtration energy is defined as the integration of filtration power over time (Blankert et al, 2006)

$$E = \int_0^t \Delta P J A dt = \Delta P V$$

where E is the energy (J), J is the flux (m/s), A is the membrane surface area (m^2) and ΔP is the pressure (Pa). However, non-fouled and fouled suspensions of fixed volume in constant-pressure mode consume the same filtration energy, while intuitively the non-fouled suspension is expected to consume less filtration energy. To solve this semi-paradox, the role of filtration time must be considered in the filtration-energy calculation. If the fouled suspension is to be given the same filtration time as the non-fouled suspension, the filtration pressure must be increased; in other words, its consumed filtration energy will be higher. A comparison of filtration energies under equal filtration times for the examined cases constituted the basic principal of the proposed method.

In the first step, the three fouling parameters (K_m, K_c, D) of Kuberkar and Davis's model (Kuberkar and Davis, 2000) were determined for a suspension that had not been treated by EF. This was done by fitting the model reconstruction to the filtration curve of the untreated suspension. This model was chosen because it describes filtration of mono/bi-dispersed particle suspensions, matching the conditions in our study. Moreover, this model separates, describes and simplifies the physical mechanisms of fouling during filtration while successfully reconstructing the raw data filtration curves.

In the second step, a novel computer program calculated the operation pressure (ΔP^*) required for the untreated suspension to have the same filtration time as the EF-treated suspension. This was achieved by reconstructing the filtration curve of the untreated suspension using Kuberkar and Davis's model and the fouling parameters found in step 1.

Finally, the filtration-energy ratio between untreated and EF-treated suspensions was calculated according to the following equation:

$$E_{ratio} = \frac{E_{withoutEF}}{E_{with\ EF}} = \frac{\Delta P^* V}{\Delta P_0 V} = \frac{\Delta P^*}{\Delta P_0}$$

where E_{withEF}, $E_{withoutEF}$ are the filtration energies for EF-treated and untreated suspensions, respectively, under the same filtration times, ΔP_0 is the operation pressure of the filtration experiments (2 bar), ΔP^* is the calculated pressure required for the untreated suspension to have the same filtration time as the treated one.

IV-2.2.3 Using Silver Nanoparticles as a Method to Minimize the Formation of Biofouling in Membrane Filtration Systems.

Difco™ LB broth (LB) (Difco Laboratories), used to grow and maintain the bacterial cultures, consisted of (in 1 l): 10 g tryptone, 5 g yeast extract and 5 g NaCl. Silver nitrate ($AgNO_3$) was obtained from Carlo Erba reagents. Sodium borohydride ($NaBH_4$; 99%), hydrogen tetrachloroaurate (III) trihydrate and Gentian Violet (GV) solution were obtained from Sigma-Aldrich.

NP synthesis is based on reducing metal ions in solution in the presence of stabilizing agents. As the source of Ag^+, 50 mL of 0.04 M aqueous $AgNO_3$ was mixed with 0.03 M trisodium citrate as an anionic stabilizing agent. Citrate is a small, widely available, inexpensive anionic surfactant, which binds weakly to metal surfaces. It forms stable dispersions of gold and silver nanoparticles with a high zeta potential value, but can be easily replaced by other surfactants, such as proteins, phospholipids, or other molecules that have a high affinity to silver. The solution was stirred and the pH adjusted to 7 using NaOH. $NaBH_4$ (50 ml of a 0.004 M solution) was added slowly to the Ag^+/citrate solution in order to reduce the silver ions. A dark brown color appears upon addition of $NaBH_4$, and addition was continued until the solution's appearance stabilized, yielding stable MCNPs. Molecularly capped gold NPs (Au-MCNPs) that were used as a size control for inactivation of planktonic cells and biofilm formation, were synthesized following the same protocol with 50 ml of 0.004 M aqueous hydrogen tetrachloroaurate (III) trihydrate as the source of the gold ions.

Particle size distribution, average particle size, morphology and colloidal stability of the MCNPs were characterized by Tecnai F20 TEM (FEI, Eindhoven, The Netherlands). Size characterization of the samples was carried out on TEM images using Digital Micrograph software (Gatan Pleasanton, CA, USA). The data were statistically analyzed using OriginPro 6.1 software.

Pseudomonas aeruginosa (ATCC 27853) was used as the model bacterium because the species is ubiquitous in water systems and frequently found in biofilm. Pure cultures were grown in LB medium and incubated overnight at 37^{o}C with shaking. One ml of overnight bacteria were grown in 10 ml of fresh liquid LB medium to reach a mid-log phase recognized by OD_{570} value of ~0.16 which is equivalent to a cell density of ~10^8 CFU ml^{-1}. In general, *P. aeruginosa* was suspended in water and enumeration was performed on LB agar plates incubated at 37^{o}C for 24 h.

The working suspension was prepared by diluting *P. aeruginosa* (at ~10^8 CFU ml^{-1}) 10-fold in filtered water supplemented with Ag- or Au-MCNPs to a cell count of ~10^7 CFU ml^{-1}, and a Ag or Au concentration in the suspension of 10 to 180 μg ml^{-1}. A similar suspension without MCNP addition was used as a control. According to previous studies, Au-MCNPs (with similar size and preparation method as Ag-MCNPs) were found inert to inactivation of planktonic *E.coli* cells (Dror-Ehre et al., 2009). Thus it is assumed that Au-MCNPs will also have no effect on biofilm retardation. The suspensions of bacteria and MCNPs were well vortexed to allow the components to interact. Each sample was serially diluted in filtered deionized water,

plated and enumerated to determine the number of viable bacterial cells. Mean concentration (CFU ml^{-1}) of microorganisms in water without NPs was taken as the initial concentration, N_0, N being the arithmetic mean concentration per MCNP treatment. The log_{10} transformation of N_0/N was calculated as an indication of planktonic inactivation. In parallel, using the same suspensions, biofilm formation potential and quantification assays were conducted. All experiments were performed in triplicate.

The biofilm formation assay was performed in microtiter plates using a modification of previously reported protocols (Coico et al., 2006; O'Tool et al., 1998A). The microtiter plate assay is a useful screening method for assessing bacterial attachment and semi-quantitative assessment of biofilm formation. The limitations of this assay are that it does not allow differentiating between different stages of biofilm build-up and whether cells are dead or alive. The ability of bacteria to form biofilm was assessed by their ability to adhere to round-bottomed 96-well microtiter plates made of polystyrene (TC Microwell 96U, Nunc). Samples of *P. aeruginosa* were prepared in 10-fold diluted LB medium in the presence or absence of MCNPs. The experiments showed that the supplemented LB was sufficient to sustain cell growth. A 200-µl aliquot of each sample was placed in each well of the 96-well plate in 6 to 8 replicates, and the plates were incubated at 37°C without shaking for different times (12-160 h). After a predefined incubation time, the supernatant was gently removed and the wells were rinsed with phosphate buffer (PBS), leaving only adherent bacteria in the wells. For fixation of the biofilm, 99% ethanol was added and the plates were allowed to air-dry. Then, the plates were stained and incubated at room temperature with 0.4% (v/v) Gentian Violet (GV) solution. The unbound GV was removed by rinsing the plates under running tap water. GV-stained biofilm was extracted with 1% (v/v) SDS and incubated at room temperature for 15 min to allow all of the biofilm-associated dye to re-elute. Finally, 100 µl from each well was transferred to a new polystyrene plate, and absorbance was determined with a plate reader at 595 nm. Baseline biofilm formation (termed relative biomass) was defined as that for the untreated sample that contained ~10^7 CFU ml^{-1} of *P. aeruginosa* (without MCNPs) and was set as 100%. The relative percentage of biomass for the other samples was calculated relative to that baseline mass. All samples were incubated together in the same plate and under the same conditions.

CLSM was used to determine the effect of pretreatment with MCNPs on the viability of the adherent biofilm and the production of EPSs. Biofilm viability was determined using a double live/dead staining kit (BacLight Bacterial Viability Kits, Invitrogen Molecular Probes) containing nucleic acid stains SYTO 9 and propidium iodide (PI). In addition, lectin concanavalin A-conjugated Alexa Fluor 647 (Con A) (Invitrogen Molecular Probes) was used to stain glycoconjugates in the biofilm communities as an indication of EPSs (Lawrence et al., 2003; Neu et al., 2001). The sample mixtures were prepared of *P. aeruginosa* cultured in LB that was diluted 1:10 with filtered deionized water in the presence or absence of 45 µg ml^{-1} MCNPs was prepared and 5 ml of each of these mixtures was added into a 50-mm Petri dish containing a glass coverslip. The Petri dishes were incubated at 37°C without shaking for 22 and 46 h. After incubation, the coverslips were gently removed and rinsed by immersing in filtered water, leaving only the adhered bacteria. The

coverslips were then triple-stained according to the manufacturers' instructions with SYTO 9, PI and Con A by incubating in the staining mixture for 15 min. Stained samples were visualized by CLSM (Zeiss, LSM 510), with the following excitation/emission detectors and filter sets: for Con A, 555/580, for SYTO 9, 480/500 and for PI, 490/635.

The impact of treatment with MCNPs on *P. aeruginosa* cells and the fate of the particles in those cells were elucidated by high-pressure freezing (HPF) and freeze substitution followed by TEM observation. The benefit of the HPF/freeze substitution method over conventional chemical fixation is that the samples can be screened without fixation artifacts. Samples were prepared for TEM observation using *P. aeruginosa* centrifuged at 4000 rpm for 10 min and then mixed with 5 ml of 100 μg ml^{-1} Au- or Ag-MCNPs. To remove unbound MCNPs, several samples were rinsed with filtered water by two cycles of water addition and centrifugation. Cells were then concentrated by centrifugation and the pellet was mounted on an aluminum disc with a depth of 100 μm (Engineering Office, M. Wohlwend GmbH, Switzerland) and covered with a flat disc. The sandwiched sample was frozen in a HPM010 high-pressure freezing machine (Bal-Tec, Balzers, Liechtenstein). Cells were then freeze-substituted in an AFS2 freeze-substitution device (Leica Microsystems, Vienna, Austria) in anhydrous acetone containing 2% (w/v) osmium tetroxide for 3 days at -90ºC and then warmed up to -30ºC over 24 h. Samples were washed twice with acetone and infiltrated for 5 to 7 days at room temperature in a series of increasing concentrations of Epon in acetone. After polymerization at 60ºC, 60- to 80 nm sections were stained with uranyl acetate and lead citrate and examined in a Tecnai T12 electron microscope (FEI) operating at 120 kV, utilizing a 2k by 2k Eagle CCD camera (FEI).

IV-2.2.4 Characterization of Alginate-Like Exopolysaccharide Isolated from Aerobic Granular Sludge

To assess the methodology, larger masses of biofilms were necessary. Alginate-like exopolysaccharide was extracted from aerobic granular sludge according to Lin et al. (2008), with modifications. The biogranules were sampled from the Nereda® pilot plant, operated by DHV at the wastewater treatment plant Epe, The Netherlands. The reactor was fed with municipal sewage. The influent consisted of approximately 25% of slaughterhouse wastewater, which was discharged in the sewage. Raw influent was fed from the bottom of the reactor after passing an aerated sand and fat remover and a 6 mm screen. The reactor was operated in Sequencing Batch (SBR) mode in successive cycles of anaerobic feeding and simultaneous effluent extraction (60–120min), a reaction period (225–285 min), and a settling/sludge drain period (15 min). The reactors were 6 meters high and 60 cm wide, with a maximum hydraulic capacity of 5 m^3/day, with an average COD loading rate of 0.1-0.15 kg COD/(kg TSS per day). After start-up, biomass concentration in the reactor was maintained around 8 to 10 g TSS/l. Oxygen in the reactor was controlled between 2 and 3 mg/l during aeration. Temperature and pH were not controlled in this system and depended on the incoming sewage.

Aerobic granular sludge were collected during steady operation of the reactor and sieved, those granules with the size >2mm were analyzed as for this research.

Aerobic granular sludge were collected during steady operation of the reactor and sieved, those granules with the size >2mm were analyzed as for this research.

0.5 g dried biomass was homogenized and extracted in 80 ml 0.2 M sodium carbonate at 80°C for one hour. After centrifuging at 15,000 rpm for 20 min, the pellet was discarded. The supernatant pH was adjusted to 2 by adding 0.1 M HCl. The precipitate was collected by centrifugation (15,000 rpm), washed by di-deionized water until effluent pH reached 7, and dissolved in 0.1 M NaOH. The ALE in the supernatant was precipitated by the addition of cold absolute ethanol to a final concentration of 80% (vol/vol). The precipitate was collected by centrifugation (15,000 rpm), washed three times in absolute ethanol and lyophilized. Ash content of the extracted ALE was measured according to the standard method (APHA).

ALE chemical identification was performed according to FAO/WHO (1997).

Total carbohydrate content was determined by a phenol-sulfuric acid assay(Dubois et al., 1956) with both D-glucose (Merck, Germany) and sodium alginic acid from seaweed (Sigma, USA) (seaweed alginate) used as standard. Proteins content was measured by the Bradford assay with bovine serum albumin used as a standard (Bradford, 1976).

To test ALE's gel formation property in $CaCl_2$, 2% (w/v) ALE di-deionized water solution was extruded into 2% $CaCl_2$ solution through Pasteur pipettes. The gel beads formed were stained with ruthenium red according to Waller et al. (2004), cut into ultra-thin sections and studied by the transmission electron microscopy (TEM, Jeol JEM 2000FX, Japan).

ALE was fractionated according to Leal et al. (2008). 0.250g ALE was dissolved into 9 ml di-deionized water. After the addition of 1ml 3.0 M HCl, it was heated at 100°C for 0.5h. After cooling, the mixture was centrifuged (15,000 rpm) and the supernatant solution was neutralized with 1.0M NaOH and poured over 80 ml of ethanol, yielding a precipitate that was dissolved in di-deionized water and freeze-dried (Fraction 1). The insoluble material was dissolved in 1.0 M NaOH; the pH was decreased to 2.85 by the addition of 1.0M HCl. The soluble fraction was neutralized with 1.0M NaOH and precipitated by the addition of ethanol to a final concentration of 80% (vol/vol) and freeze-dried (Fraction 2). The insoluble fraction was dissolved by neutralization with 1.0 M NaOH, precipitated by ethanol and freeze-dried (Fraction 3).

Possible DNA and proteins contamination in ALE were detected by recording its spectra on the UV-visible spectrophotometer (UV-2550, Shimadzu, Japan) with its concentration of 28 mg/l. Spectrum of seaweed alginate (28mg/L) was also recorded as comparison.

MALDI-TOF MS spectra of both O-deacetylated ALE and seaweed alginate were also analyzed according to Leone et al. (2006) with a Bruker Biflex III mass spectrometer (Bruker Daltonics, USA).

The FT-IR spectra of the dried grinded granules and ALE in KBr pellets (98mg KBr + 2mg sample) were recorded in the 4000-400 cm^{-1} region using a Nicolet 670 instrument (Thermo, USA). Data derivation was performed with Origin 8.0 software.

Triplicates were made for each measurement above.

ALE sodium dodecyl sulfate-polyacrylamide gel electrophoresis was carried out according to Pedersen et al. (1989). ALE and seaweed alginate with concentrations of 7ug/ul respectively were run in 5% stacking and 14% separating gels. Separate gels were stained with Coomassie brilliant blue G-250 for proteins and Toluidine blue O for acid polysaccharides and distained in acetic acid and di-deionized water respectively.

IV-2.3 RESULTS AND DISCUSSION

IV-2.3.1 A Hybrid System of Constructed Wetland, Electroflocculation, Granular Filtration and Membrane Filtration for Upgrading Secondary Effluent.

QUALITY OF SECONDARY EFFLUENT AFTER UPGRADING

Shafdan's secondary effluents characteristics: turbidity–1.79 NTU, phosphate–0.99 mg/l as P, TOC 12mg/l, pH 7.35. After the treatment of constructed wetland, the characteristics changed to: turbidity–1.49 NTU, phosphate–1.13 mg/l as P, TOC 10mg/l, pH 7.35. After passing through the polishing pond, the characteristics changed to: turbidity–1.89 NTU, phosphate–1.06 mg/l as P, TOC 10mg/l, pH 7.35.

Characteristic parameters as turbidity, phosphate-P and TOC of secondary effluent are lower than those annual average values. After EF-UF/MF treatments, water quality was significantly improved. Both turbidity and phosphate-P values were decreased (Table 1 and 2), the lowest turbidity reached 0.431NTU and the lowest phosphate-P 0.17 mg/l. Membrane filtration combined with EF removed turbidity more efficiently than only membrane filtration alone. EF-UF obtained better results than MF-EF; and the lower the MWCO of the UF membrane, the better the water quality was improved. On the other hand, as extending EF working time increases iron dosage; the final turbidity and phosphate-P were declined as EF working time increased from 1 minute to 4 minutes.

Since the secondary effluent has better quality than the annual average value, CW treatment only got rid of 17% of TOC and 17% of turbidity. After EF-UF/MF treatments, water quality was significantly improved. Both turbidity and phosphate-P values were decreased (Table 17 and 18), the lowest turbidity reached 0.28NTU and the lowest phosphate-P 0.16 mg/l. Membrane filtration combined with EF removed turbidity more efficiently than only membrane filtration alone. EF-UF obtained better results than MF-EF; and the lower the MWCO of the UF membrane, the better the water quality was improved. On the other hand, as extending EF working time increases iron dosage; the final turbidity and phosphate-P were declined as EF working time increased from 1 minute to 4 minutes.

As biofilm grew in the collecting well of secondary effluent after CW-Polishing pond treatment, it slightly increased turbidity and phosphate-P. However, the water quality was quite improved after CW-polishing pond-EF-UF/MF hybrid treatment. The lowest turbidity reached 0.286 NTU and the lowest phosphate-P 0.15 mg/l. All the turbidity and phosphate-p values after membrane filtration of various combination of EF-UF/MF treatment were lower than those above if polishing pond was utilized. This indicated that polishing pond changed characteristics of particles, improved turbidity and phosphate-P removal capability of the hybrid system.

Table 17 Turbidity of secondary effluent after various treatments (NTU)

	EF treatment time, min											
	0	**1**	**2**	**4**	**0**	**1**	**2**	**4**	**0**	**1**	**2**	**4**
	Membrane filtration											
	10KD	**10KD**	**10KD**	**10KD**	**100KD**	**100KD**	**100KD**	**100KD**	**MF**	**MF**	**MF**	**MF**
Secondary effluent	0.447	0.442	0.438	0.431	0.487	0.464	0.458	0.443	0.597	0.492	0.498	0.419
Wetland outlet	0.421	0.305	0.293	0.282	0.489	0.362	0.358	0.323	0.562	0.394	0.385	0.369
Polishing pond outlet	0.347	0.359	0.286	0.284	0.410	0.375	0.363	0.352	0.465	0.384	0.372	0.367

Table 18 Phosphate-P of secondary effluent after various treatments (mg/l)

	EF treatment time, min											
	0	**1**	**2**	**4**	**0**	**1**	**2**	**4**	**0**	**1**	**2**	**4**
	Membrane filtration											
	10KD	**10KD**	**10KD**	**10KD**	**100KD**	**100KD**	**100KD**	**100KD**	**MF**	**MF**	**MF**	**MF**
Secondary effluent	0.73	0.17	0.17	0.19	0.79	0.24	0.24	0.19	0.72	0.36	0.36	0.37
Wetland outlet	0.82	0.16	0.16	0.17	0.85	0.31	0.31	0.32	0.88	0.33	0.34	0.33
Polishing pond outlet	0.75	0.15	0.15	0.15	0.79	0.25	0.26	0.25	0.79	0.26	0.26	0.26

Turbidity Removal

Turbidity removal rate are demonstrated in Figs. 95–97. For the secondary effluent, combination with EF did not increase greatly turbidity removal rate for UF with membrane MWCO of 10KD. It worked efficiently for MF. With MF alone, the turbidity removal rate was only 60%, while if EF was combined, turbidity removal increased to 75%.The longer the EF working time, the higher the removal rate. This can be explained that, as EF working time increased, more iron ions went into solution, at pH 7-8, those Fe(III) hydrolysis products combined with particles, drag them out from solution phase to solid phase, and finally was stopped by the membrane.

In contrast, addition of EF resulted in higher turbidity removal rate of CW outlet and polishing pond outlet. Without EF, turbidity removal rates were 72% for 10KD membrane, 67% for 100KD membrane and 62% for MF membrane; with EF, the removal rates may reach to 80% for 10KD, 78% for 100KD and 75% for MF. This displayed that after CW and polishing pond treatment, particle characteristics were changed, which resulted in easier absorption on Fe(III) hydrolysis products.

In addition, it can be found that the combination of EF-MF is capable of improving water quality than UF alone.

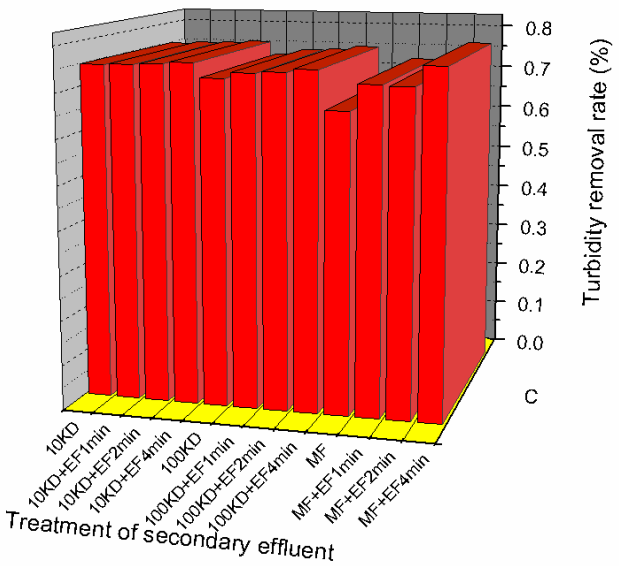

Fig. 95 Turbidity removal rate of secondary effluent after EF –UF/MF treatments.

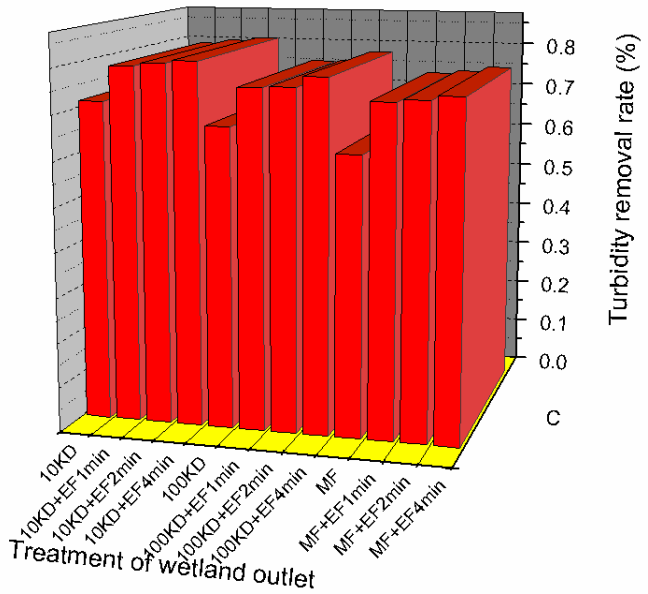

Fig. 96 Turbidity removal rate of secondary effluent after CW-EF-UF/MF treatments.

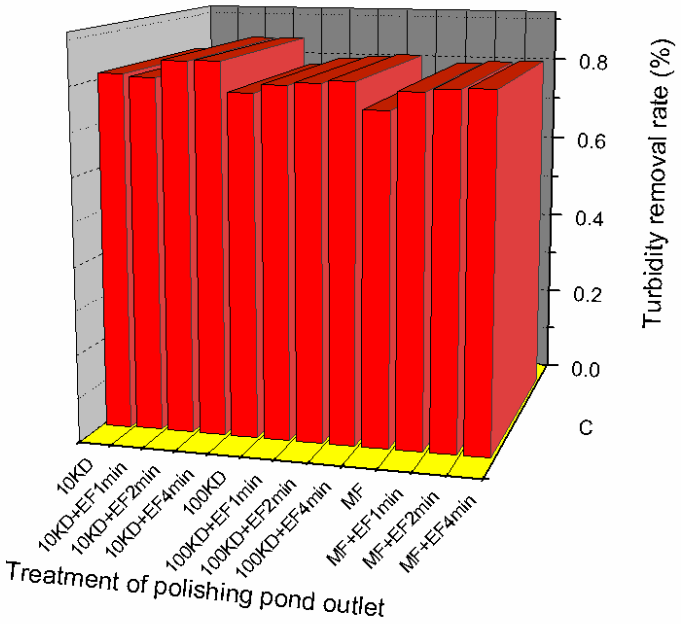

Fig. 97 Turbidity removal rate of secondary effluent after CW-polishing pond-EF-UF/MF treatments.

Phosphate Removal Rate

Phosphate, pyrophosphate, triphosphate and higher polyphosphate anions are known to form complexes, chelates and insoluble salts with number of metal ions such as iron. Some of the complexes such as $FePO_4$ have low solubility that lead to solid formation which have easier removal procedure. Phosphate anions are also sorption onto iron-hydroxide amorphous solids that formed when the sweep flocculation mechanism is operating. Both the iron-phosphate complex reactions, the solubility of those complexes and the sorption rate of phosphate anions to the iron-hydroxides are highly dependent on the pH value, iron and phosphate concentration.

As shown in Figs. 98–100, membrane filtration could not remove phosphate effectively due to its high solubility. The addition of EF not only causes the production of complexes such as $FePO_4$ with low solubility, but also provides phosphate possibility of sorption onto iron-hydroxide amorphous solids, resulting in greatly increased phosphate removal rate. The maximum phosphate removal rate was lower than 20% if EF was not included, however, it reached to 86% with the addition of EF.

In addition, CW and polishing pond treatments increased the final phosphate removal rate. The combination of EF-MF highly improved phosphate removal capability of the system, making it much more competitive than UF alone.

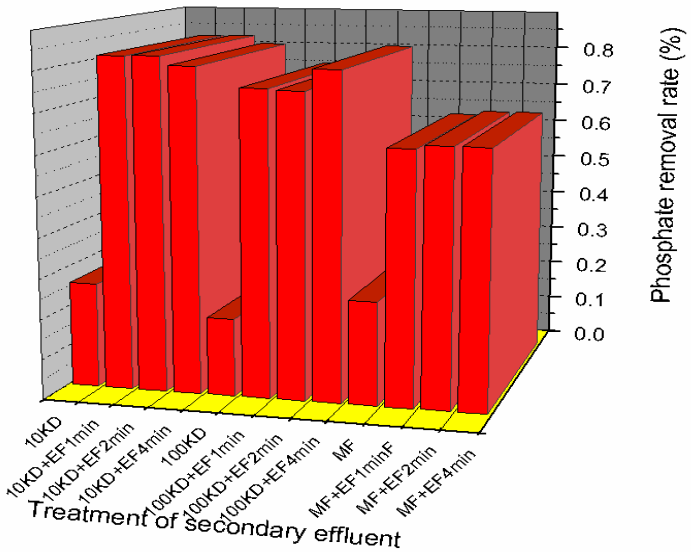

Fig. 98 Phosphate removal rate of secondary effluent after EF –UF/MF treatments.

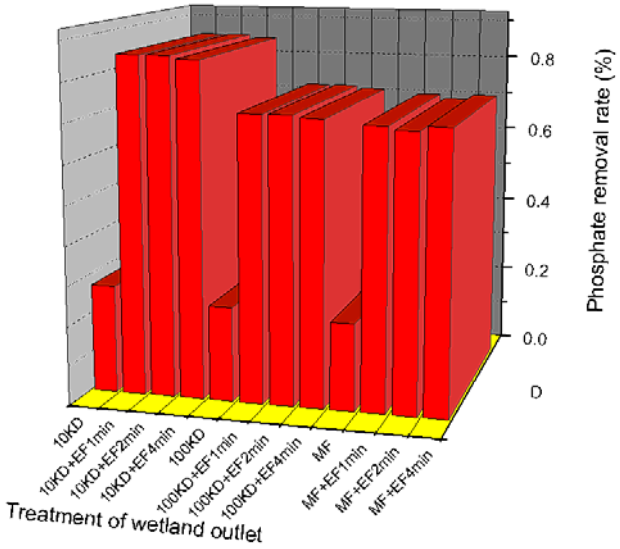

Fig. 99 Phosphate removal rate of secondary effluent after CW-EF-UF/MF treatments.

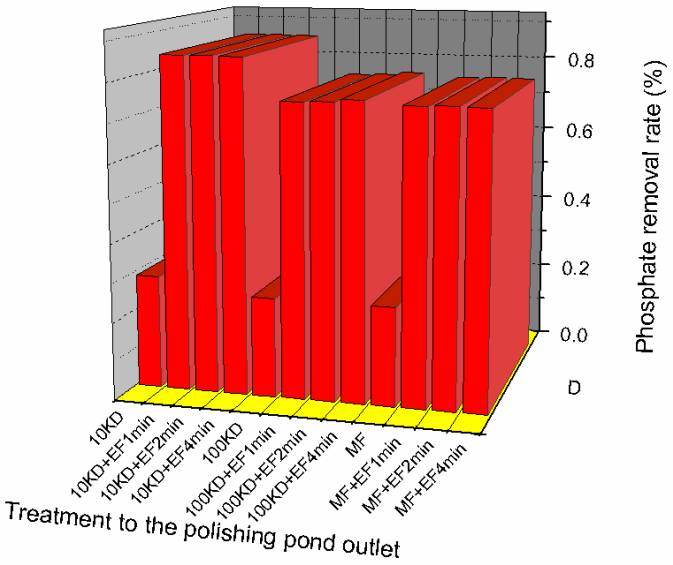

Fig. 100 Phosphate removal rate of secondary effluent of secondary effluent after CW-polishing pond-EF-UF/MF treatments.

EF Influence on Membrane Flux

During filtration, internal clogging and /or cake formation causes flux decrease in comparing with the initial flux. The addition of EF as pretreatment of membrane filtration greatly improved the filtration curve. For the secondary effluent, without EF, J/J_0 for 10KD UF membrane was 0.1 at quasi steady date, while the addition of EF increased J/J_0 to 0.4 (Fig. 101). As CW and polishing pond changed particle characteristics in the secondary effluent, without EF, J/J_0 was 0.7 and 0.5 for CW outlet and polishing pond outlet respectively. With EF, J/J0 could increase to 0.85 (Figs. 102, 103). Thus, CW and polishing pond not only improved the water quality, but also changed particles property (Fig. 104), decreased filtration resistance. The addition of EF as the pretreatment of membrane filtration mitigate fouling reduced the difference between J and the initial flux. The EF effects were different for the internal and external fouling mechanisms. In the internal fouling, the iron-hydroxide layer that formed on the membrane surface filtered out the small particle and prevented them to penetrate the pores of the membrane. In the external fouling the EF changed the composition of the cake and reduced its hydraulic resistance.

EF effects on fouling can be observed by SEM analysis (Fig. 105). It can be clearly seen that iron-hydroxide formed a layer with enlarged pore size than the cake formed without EF pretreatment.

Filtration Time

All the filtration experiments ended after 750ml of wastewater were filtered. Filtration time was shown in Figs. 106–108. Ultrafiltration (UF) and microfiltration (MF) can highly polish secondary effluents, but colloidal fouling i.e., the accumulation of the retain particles on the surface or inside the pores of the membrane, lead to hundreds percents increase of the consumed energy and to higher operational costs of the filtration process.

It is demonstrated that EF pretreatment mitigated fouling, reduced filtration resistance, decreased the time for filtering 750ml wastewater. By this means, electroflocculation greatly decreased the energy and thereafter the operation costs required for filtration system.

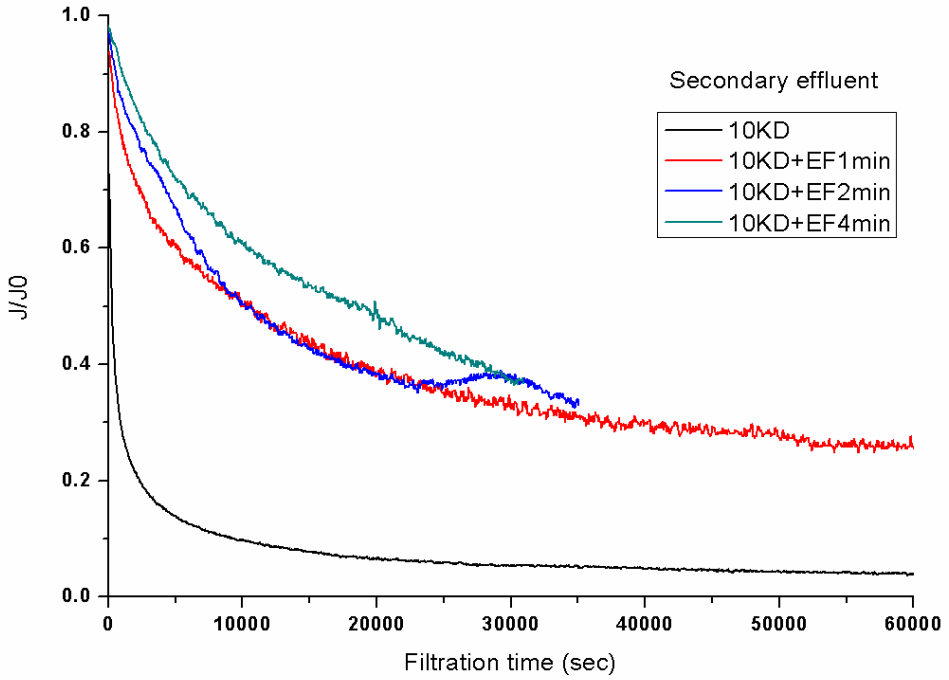
Secondary effluent
10KD
10KD+EF1min
10KD+EF2min
10KD+EF4min
J/J0
Filtration time (sec)
0.0
0.2
0.4
0.6
0.8
1.0
0
10000
20000
30000
40000
50000
60000

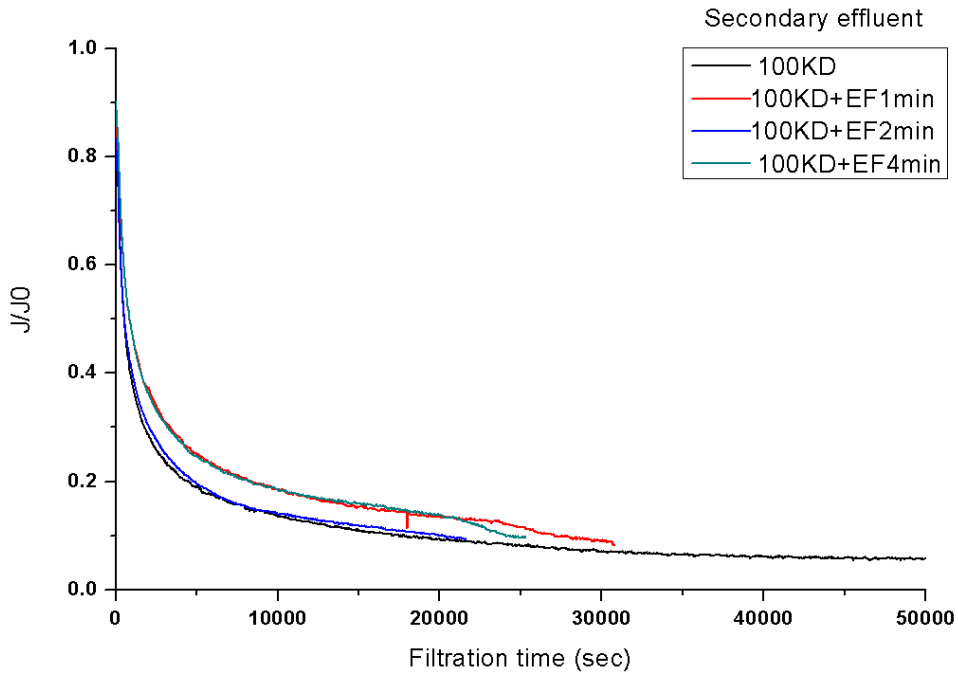
Secondary effluent
100KD
100KD+EF1min
100KD+EF2min
100KD+EF4min
J/J0
Filtration time (sec)
0.0
0.2
0.4
0.6
0.8
1.0
0
10000
20000
30000
40000
50000

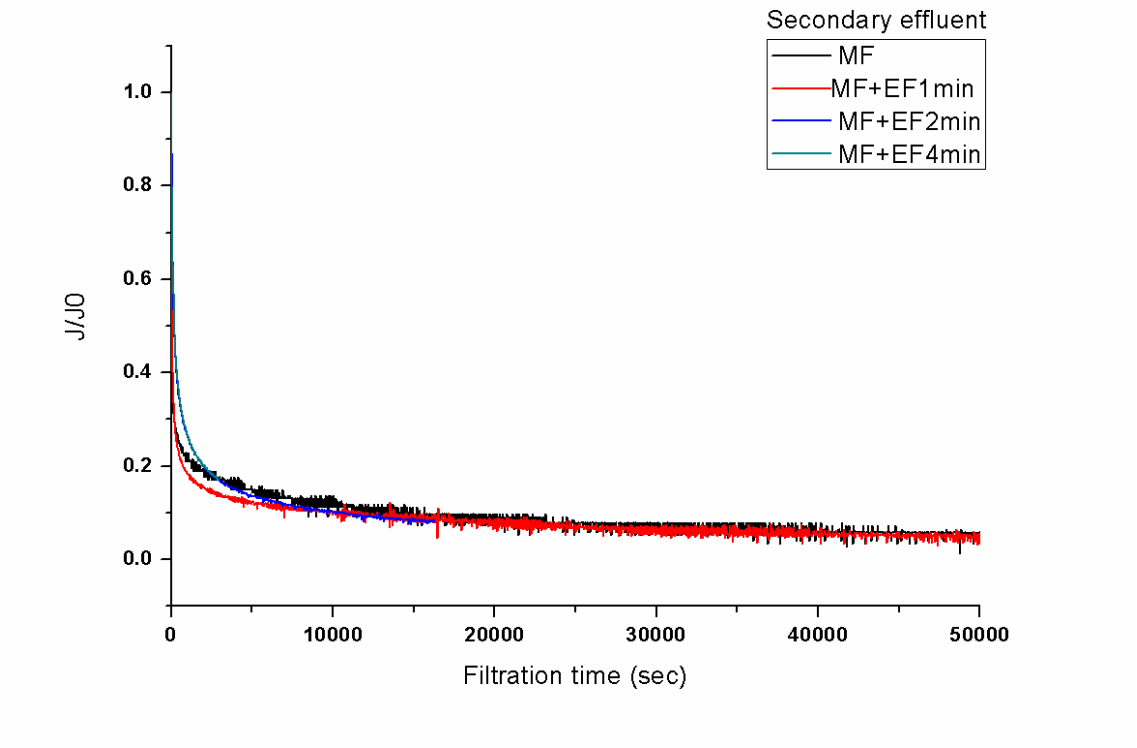

Fig. 101 Filtration curve of secondary effluent with and without EF pretreatment.

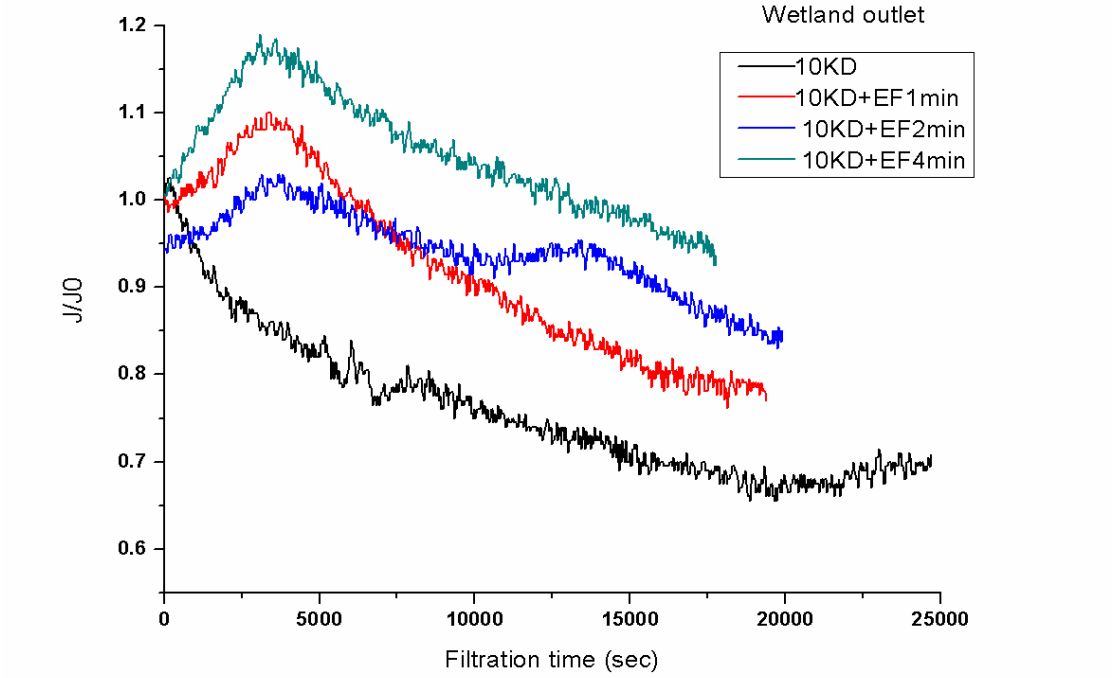

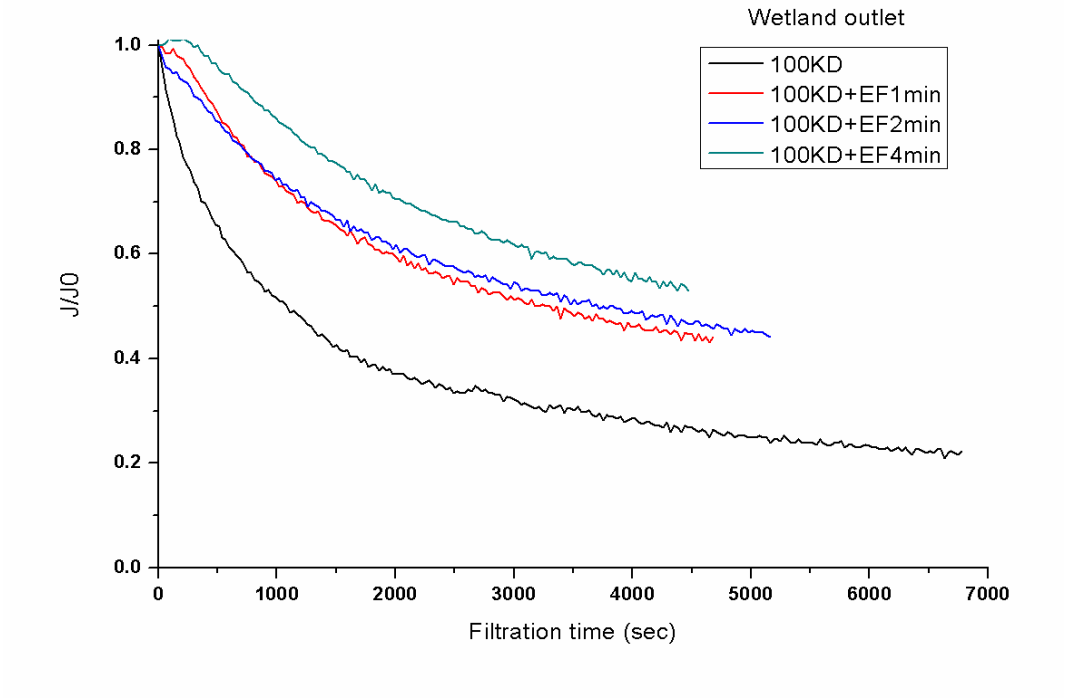

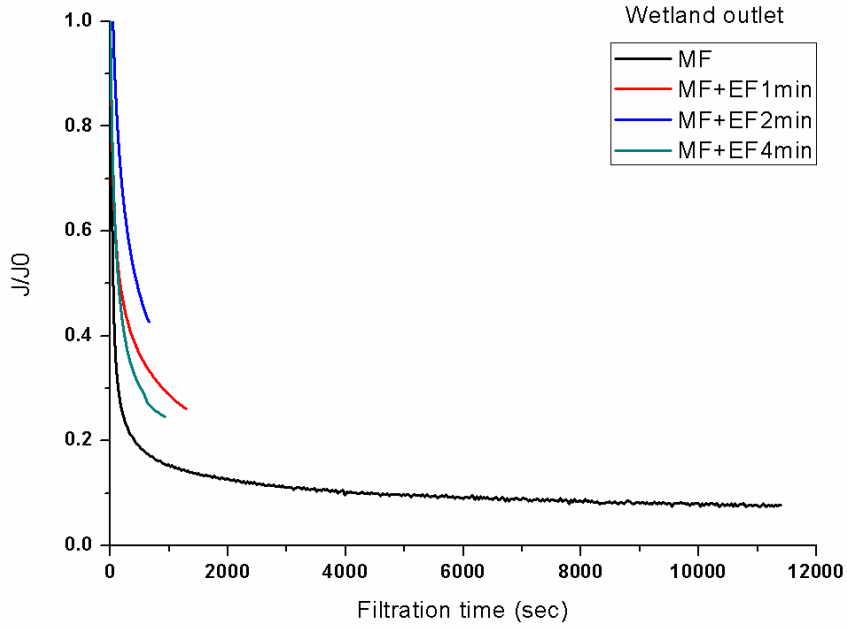

Fig. 102 . Filtration curve of secondary effluent with CW-EF pretreatment.

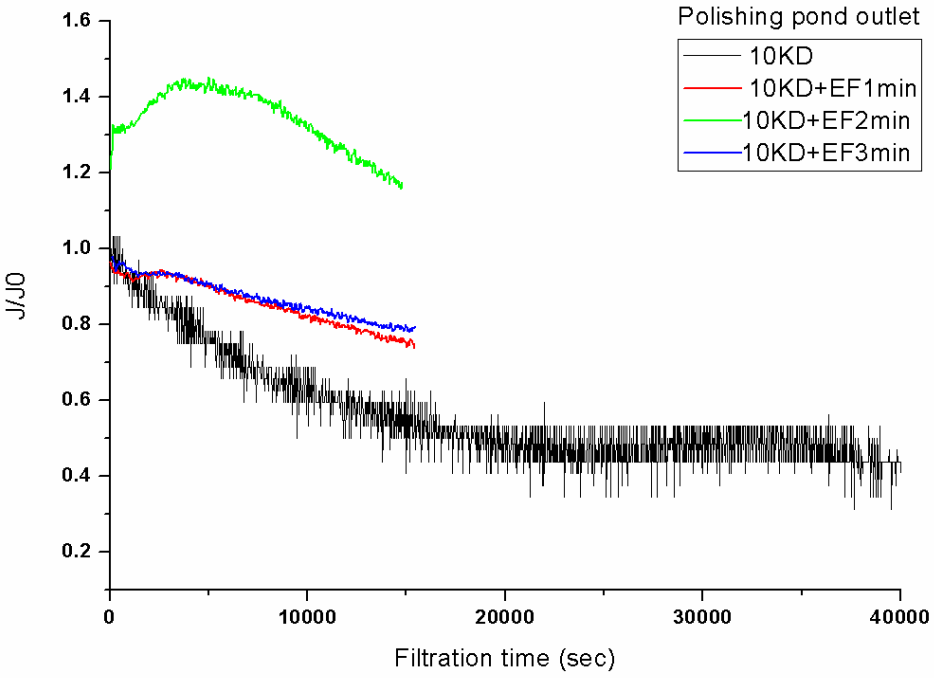
Polishing pond outlet
10KD
10KD+EF1min
10KD+EF2min
10KD+EF3min
J/J0
Filtration time (sec)
1.6
1.4
1.2
1.0
0.8
0.6
0.4
0.2
0
10000
20000
30000
40000

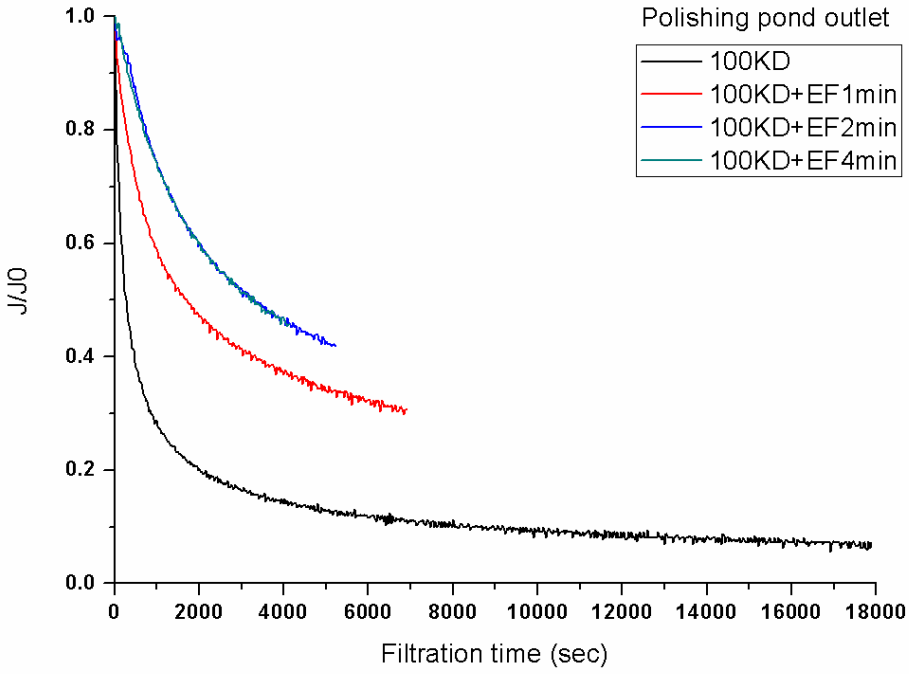
Polishing pond outlet
100KD
100KD+EF1min
100KD+EF2min
100KD+EF4min
J/J0
Filtration time (sec)
1.0
0.8
0.6
0.4
0.2
0.0
0
2000
4000
6000
8000
10000
12000
14000
16000
18000

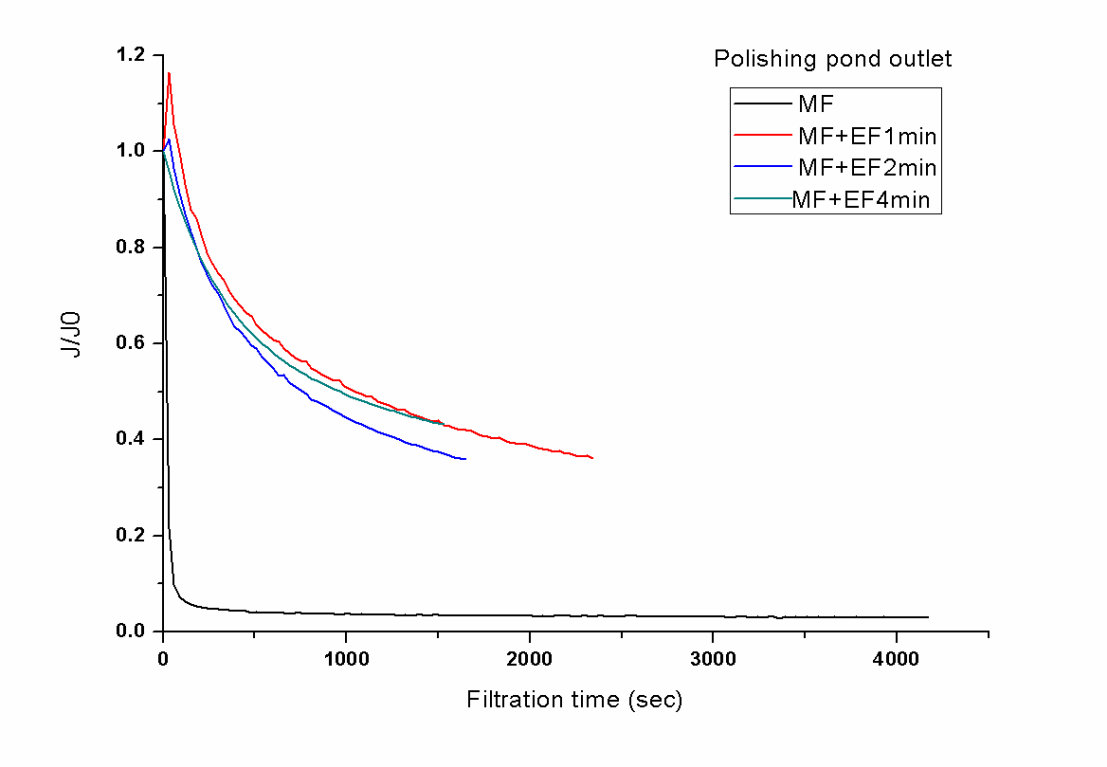

Fig. 103 Filtration curve of secondary effluent with CW-polishing pond-EF pretreatment.

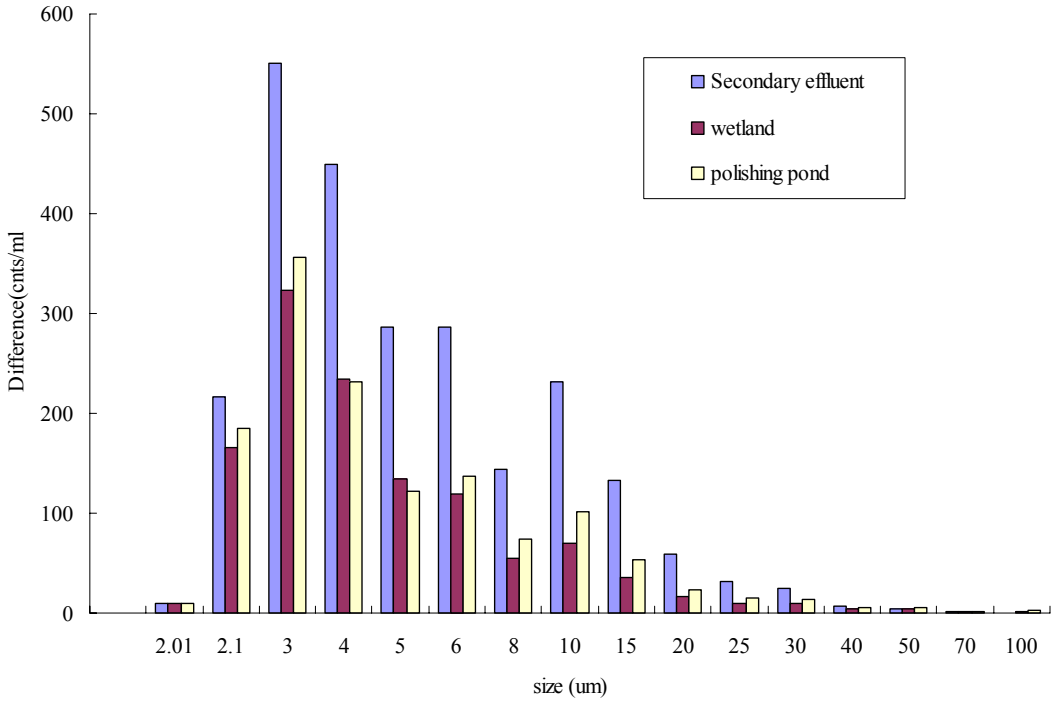

Fig. 104 Particle size distributions of secondary effluent, wetland outlet and polishing pond outlet.

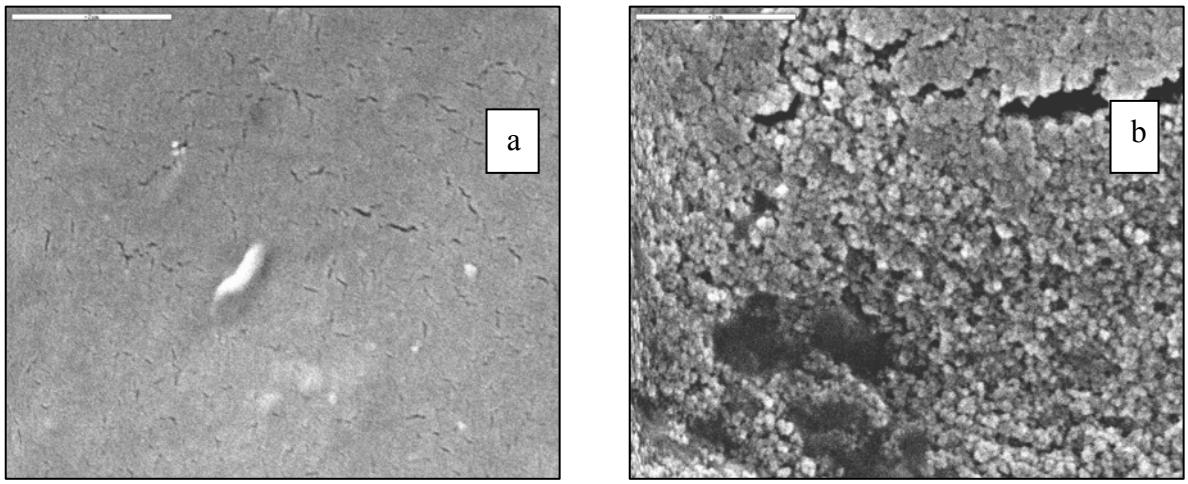

Fig. 105 SEM analysis of fouling layer with and without EF. The bar is 1um. a: without electroflocculation; b: with electroflocculation

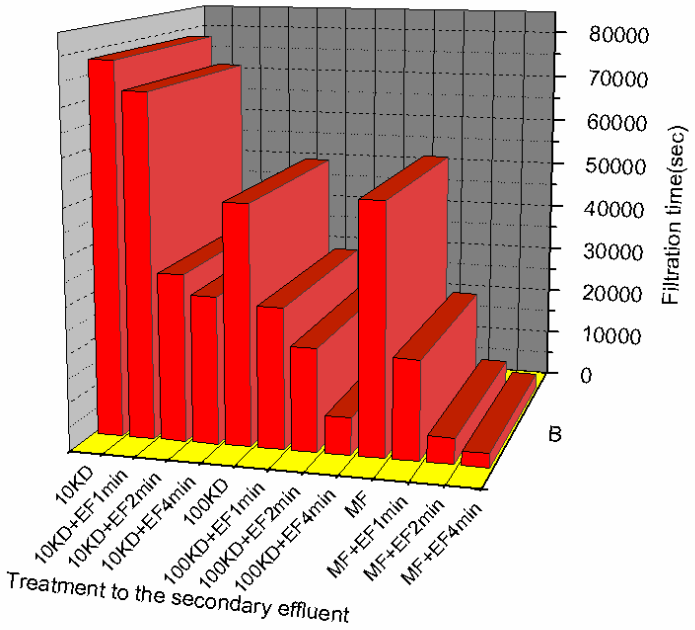

Fig. 106 Filtration time for 750ml secondary effluent with and without EF pretreatment

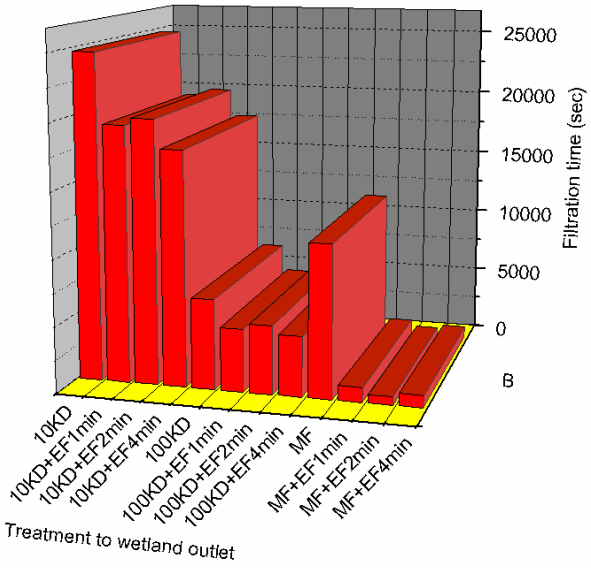

Fig. 107 Filtration time for 750ml secondary effluent with CW- EF pretreatment

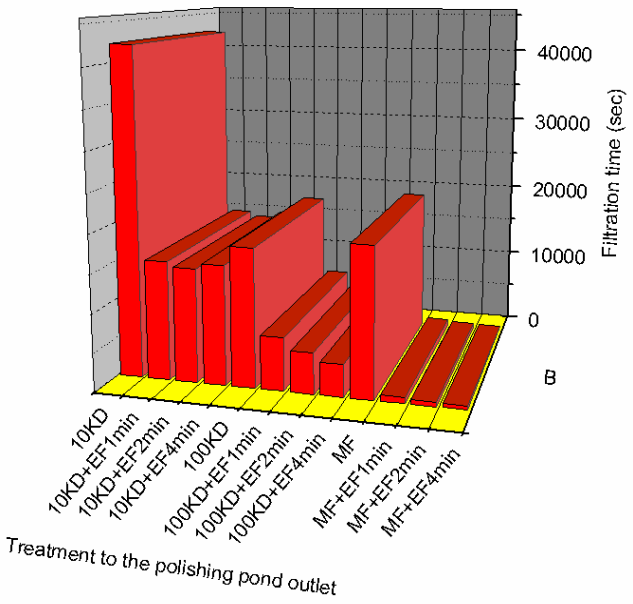

Fig. 108 Filtration time for 750ml secondary effluent with CW–polishing pond–EF pretreatment

POLLUTANTS REMOVAL BY CW– EF–GF CONFIGURATION TREATMENT

Turbidity

Fig. 109 shows turbidity removal capabilities of different treatments. Shafdan' secondary effluent turbidity was stable at 1.8–3.9NTU, with flow rate of 1.2–1.5 m^3/h and pH level of 7.7–-7.8 for all treatments. Turbidity removal was best by CW alone, reaching a constant of more then 60% removal wuth 0.56–1.5 residual turbidity.

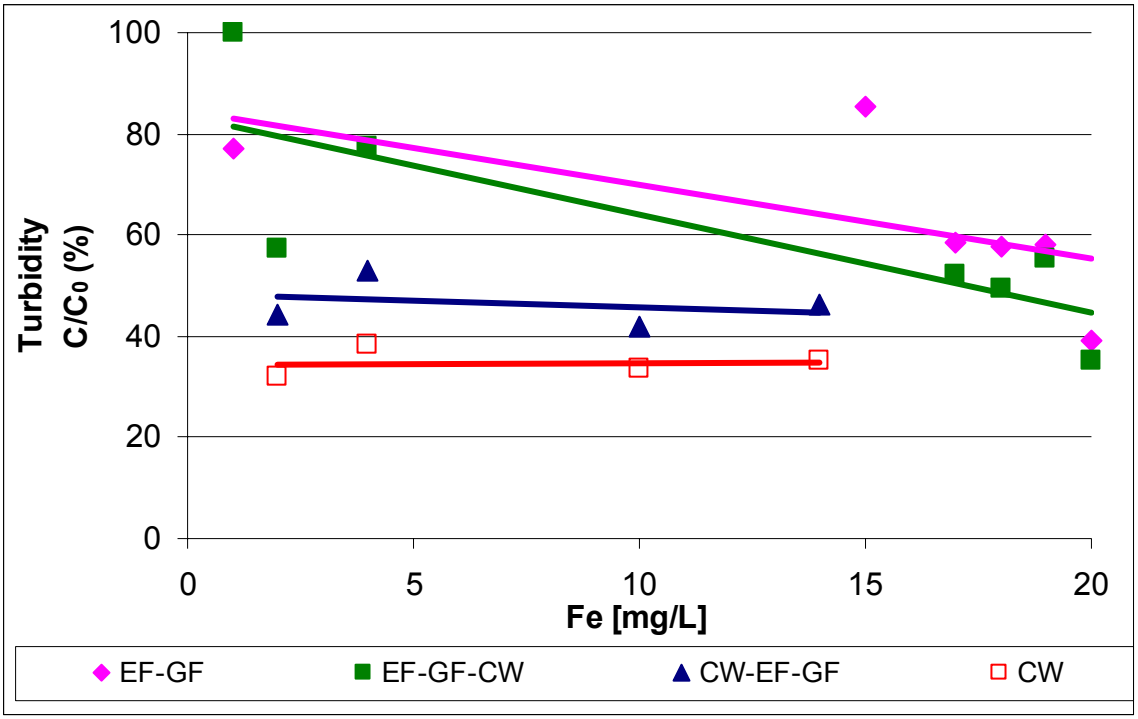

Fig. 109 Residual turbidity in 'Shafdan' secondary effluent for different treatments. C_0=1.8–4.5 NTU. Flow rate 1.5 m^3/h.

When CW preceded the electroflocculation unit, turbidity removal was around 47–58%, with lowest residual turbidity of 0.88 NTU. In this configuration, the constructed wetland reduced turbidity levels in 'Shafdan' secondary effluent from 1.8–3.9 NTU to a best level of 0.5 NTU. These low turbidity water continues through the EF system which adds iron ions to the effluent, at different concentrations (depending on current intensity), reaching turbidity levels of 10–50 NTU. After the effluent passes through the EFector, it continues through a double sand filter. This configuration yields turbidity levels similar to those reached by the CW alone.

Phosphorous removal

Fig.110 shows phosphorus removal of different treatment with changing coagulant dose of 1-20 mg/L Fe. P concentration in 'Shafdan' secondary effluent was 1-3 mg/L P total with Fe concentration below 0.1 mg/L (ICP measuring limit). Initial turbidity levels were 2–4 NTU with pH 7.6–7.8. For CW alone configuration there was no Fe addition.

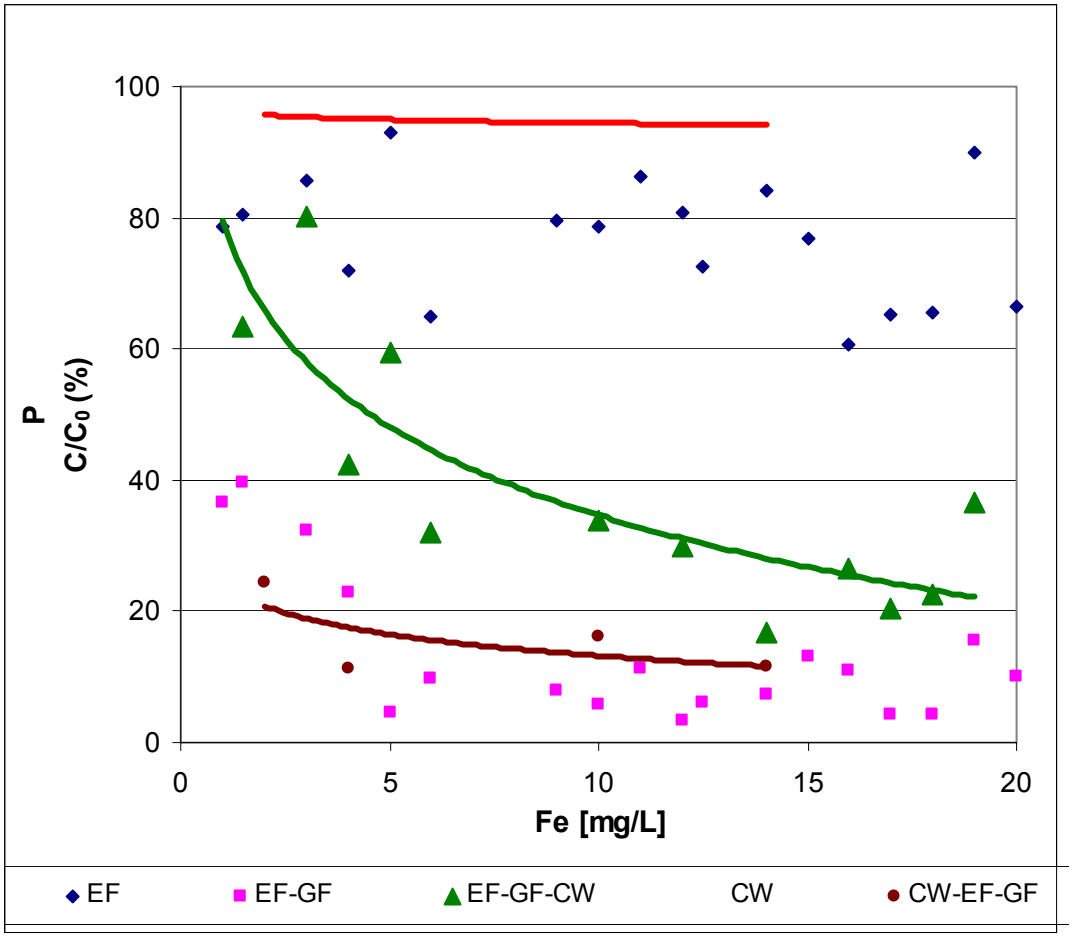

Fig. 110 Residual phosphorus in 'Shafdan' secondary effluent for different treatments. C_0=1-3 mg/L TP. Flow rate 1.5 m^3/hr.

Passing through the constructed wetlands did not alter phosphoroue concentration in the effluent, therefore removal capabilities was similar to those reached by the EF–GF configuration, at 85–90% P removal. Fig. 111 shows that passing through the CW did not effect P removal when GF preceded the system. Therefore, when CW was the last system component, it consistently contributed additional phosphorous to the effluent; that could be explained by formation of a phosphorous 'reservoir' supplied by (a) Shafdan's secondary effluent between EF treatments, and (2) plants decay, and released by water of lesser concentration. This contribution is eliminated by the proceeding EF–GF treatment.

Particles removal

Particles removal capabilities of different treatments were analyzed by two parameters (other then turbidity): Total Suspended Solids (TSS) on particle distribution (cumulative and differential). Shafdan' secondary effluent TSS concentration was variable between 1.7–10 mg/L with average concentration of 4.9 ± 2.6 mg/L.

Once the EF–GF treatment preceded the CW, TSS removal was similar and at times even better then CW alone. CW-EF-GF configuration showed TSS removal of 67–-87% (Fig.112) with low TSS concentration of 0.33 mg/L and an average of 0.64±0.24 mg/L. The EF-GF system was supplied with low TSS effluent from the CW hence, the CW-EF-GF configuration reached similar results to the CW alone, despite adding Fe particles to the effluent.

Fig.112 shows cumulative particles removal (>2μm) by the CW-EF-GF treatment for different Fe concentrations and by CW alone relatively to 'Shafdan' secondary effluent. It is shown that CW alone removes most of the particles from the effluent. Removal is slightly improve when adding the EF-GF system, specially at the low Fe concentrations. It is also shown that when the electroflocculation system is not polished by the CW, high Fe concentration of 17 mg/L added particles to the effluent in relation to the CW alone (since effluent flow through the CW system and onto the EF-GF system and samples were taken for the same incoming effluent, exiting CW and exiting GF).

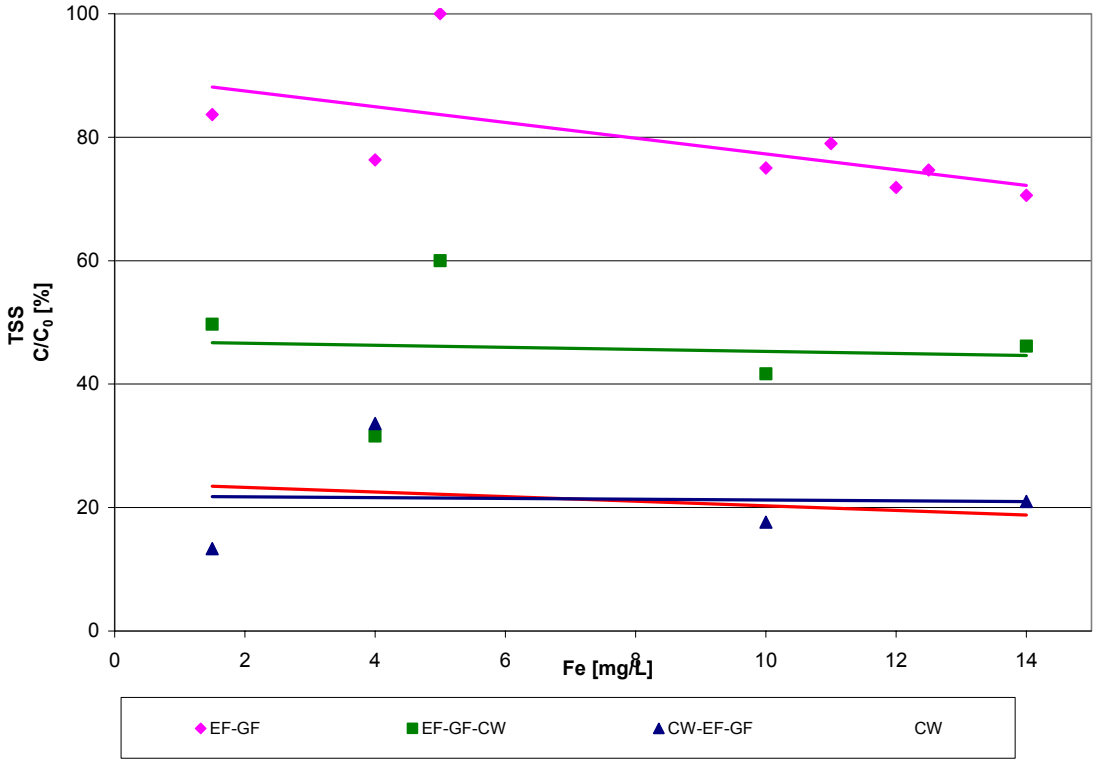

Fig. 111 TSS removal from 'Shafdan' secondary effluent for different treatments. C_0=1.7–-10 mg/L. Flow rate 1.5 m^3/hr.

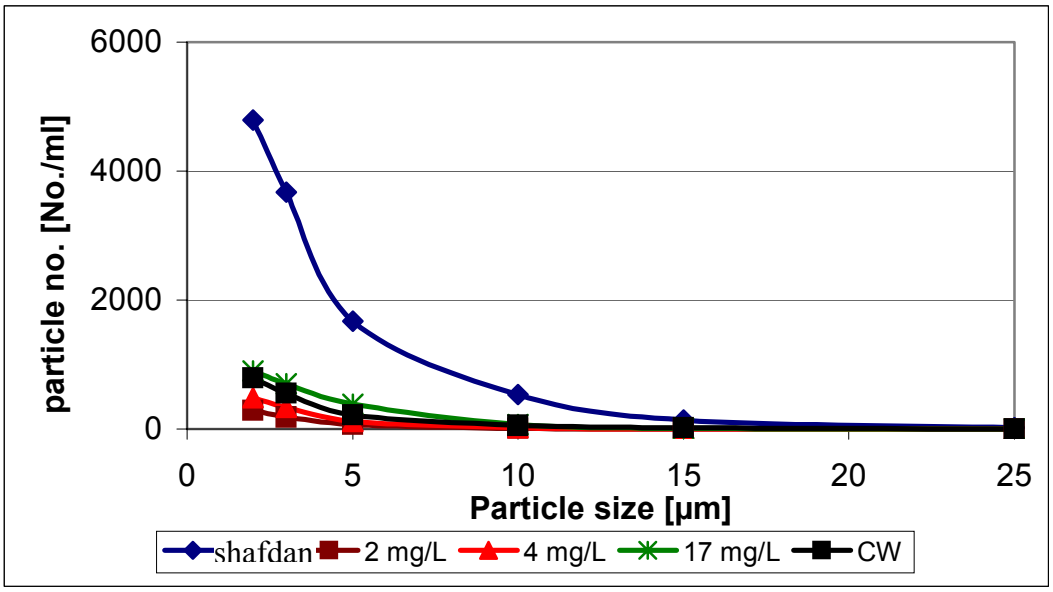

Fig. 112 Cumulative particles removal from 'Shafdan' secondary effluent by CW-EF-GF treatment for different Fe concentrations.

Examining differential particle removal (Fig.113) shows over 80% removal for all particle size and 99% removal of particle size >25µm for Fe concentration 2 and 4 mg/L. It is hypnotized that at low Fe concentrations not many large particles are created, thus particle removal is high tough turbidity and P removal are low.

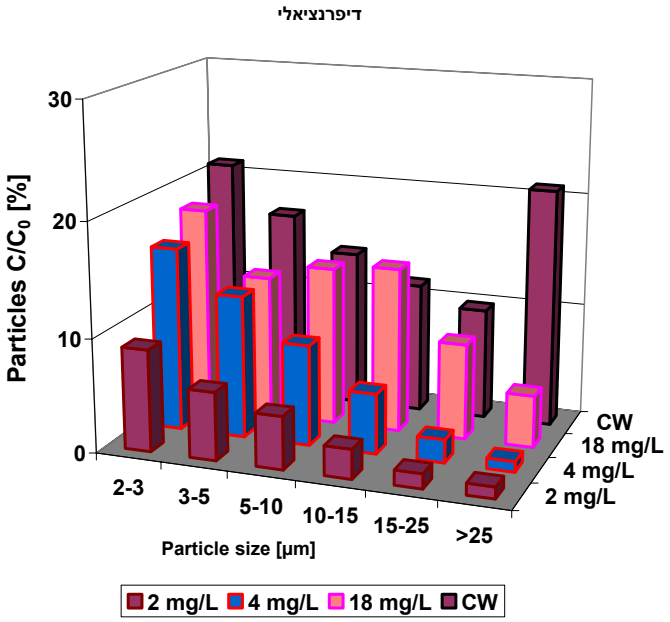

Fig. 113 Differential particles removal from 'Shafdan' secondary effluent by CW-EF-GF treatment for different Fe concentrations.

Organic matter removal

Organic matter removal was analyzed by two parameters: Total Organic Carbon (TOC) and Dissolved Organic Carbon (DOC). Fe concentration in 'Shafdan' secondary effluent was <0.1 mg/L (ICP measuring limit) with pH of 7.6-7.8. Organic matter removal by CW alone was tested with no added iron. Figure 114 Show TOC removal by different treatments for different quagulant dose of 1-15 mg/L. TOC concentration in 'Shafdan' secondary effluent was 8.85-18.80 mg/L with an average of 12.22±2.33 mg/L.

Figure 115 shows DOC removal by different treatments. DOC concentration in 'Shafdan' secondary effluent was 8.3–17.3 mg/L with an average of 11.69±2.56 mg/L.

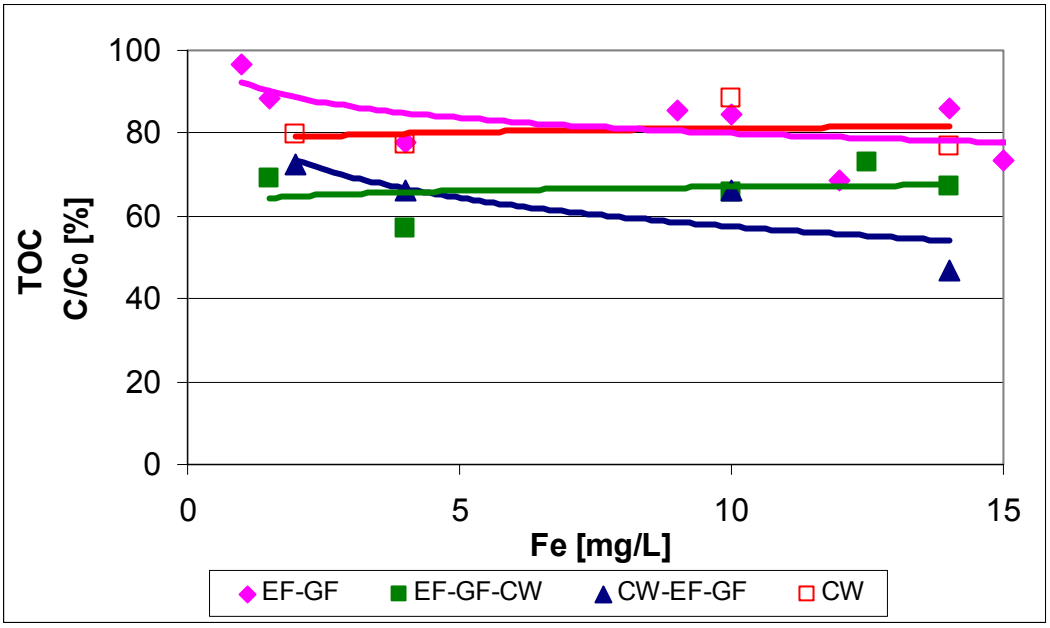

Fig. 114 Residual organic matter in 'Shafdan' secondary effluent for different treatments. C_0 =9-19 mg/L.

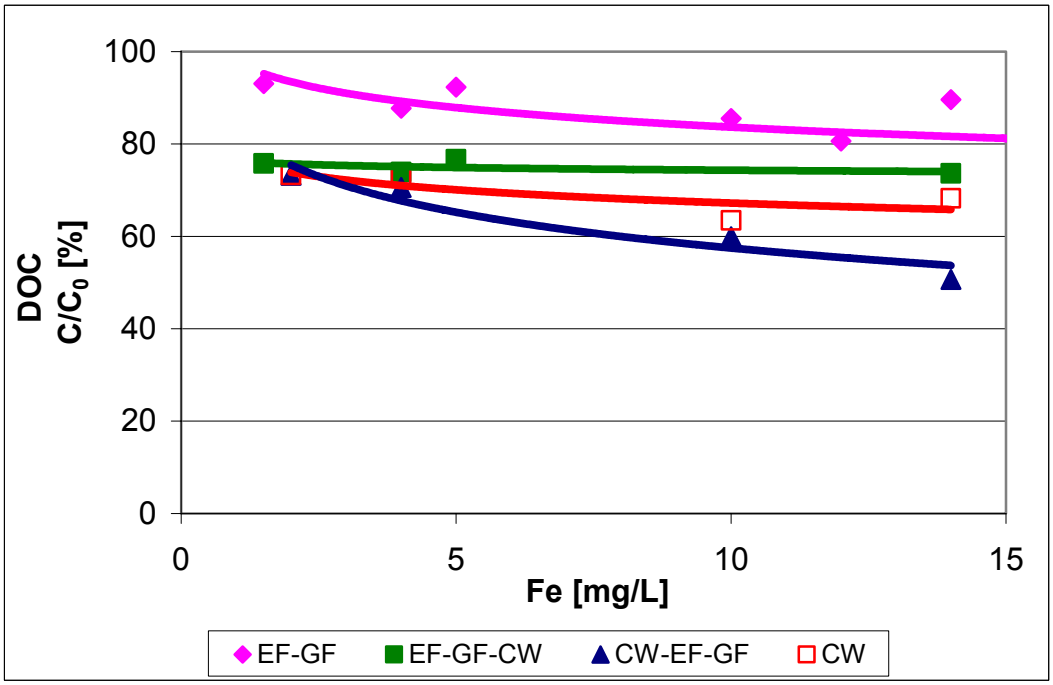

Fig. 115 Residual dissolved organic matter in 'Shafdan' secondary effluent for different treatments. C_0 =8-17 mg/L.

TOC removal by CW-EF-GF configuration was slightly better then the EF-GF-CW treatment, though results was similar with about 40% removal. DOC removal was at best at the CW-EF-GF configuration. As shown in Fig. 114, TOC removal by CW alone is poor at 20% removal. When proceeded by the EF–GF treatment, TOC and DOC removal reached an optimum of 50% removal, for Fe concentration of 14 mg/L. This configuration reached 28-53% TOC removal with an average of 37%±11.1% and 27–-49% DOC removal with an average of 36.4%±10.34%.

Overall, all different treatments showed similar results for organic matter removal. None of the treatments reached TOC or DOC removal of over 50% with an average of 35% removal. TOC removal was at best when combining the CW and the EF–GF systems. DOC removal was similar for CW alone and when proceeded by EF–GF treatment. The latter configuration showed best results though it highly depended on a well designed sand filtration following the EFector.

IV-2.3.2 The Effects of Electroflocculation Pretreatment on Fouling Mechanisms, Filtration Energy and Contaminants Removal Rates in Microfiltration

IV-2.3.2.1 Aluminum anode

The filtration curves for the internal fouling experiments with different EF operation times at different pH are presented in Fig. 116. The EF process had a dramatic effect on filtration performance. At pH 6.5, without EF pretreatment, the filtration time was more than 20,000 s (about 5.5 h), while a very short (0.5-1 min) EF pretreatment reduced the filtration time to 2000 s (35 min). A weaker, but still dramatic change was observed at pH 7.5: without EF pretreatment the filtration time was 23,000 s (over 6 h) whereas with an EF pretreatment of 6 min, filtration time decreased to 4300 s (about 1.2 h).

A dramatic effect of EF pretreatment, albeit less pronounced than in the internal fouling tests, was also observed in the external fouling experiments (Fig. 117). An EF operation time of 2 min at pH 6.5 reduced the filtration time from 11,000 s (about 3 h) to 2130 s (about 40 min). At pH 7.5, without EF pretreatment, the filtration time was more then 11,000 s while an EF operation time of 6 min reduced the filtration time to 3400 s.

The energy ratios (E_{ratio}) for the different pH values and EF operation times are shown in Fig. 118. This ratio shows the amount by which the experimental filtration energy needs to be multiplied so that the raw suspension (without EF treatment) will be filtered for the same amount of time as the EF-treated suspension. Thus, this ratio also represents the ratio between the filtration energy of the examined EF pretreatment and the raw suspension filtration energy. For the internal fouling

experiments, the calculated energy ratio was very high, reaching a maximum of almost 10 at pH 6 and 6.5 at EF operation times of 0.5 and 1 min, respectively. These values indicate a possible 90% energy saving resulted from EF treatment. In the external fouling experiments, the ratio was lower, peaking at 4.5 and 3.5 at EF operation times of 0.5 and 2 min at pH 6 and 6.5, respectively.

Table 19 presents restoration as percent of initial flux after physical cleaning by washing the membrane surface. With the EF pretreatment, the restoration rates were between 90 and 100% independent of the fouling type. Without EF pretreatment, restoration rates were negligible for the internal fouling and moderate for the external fouling.

Aluminum concentrations dissolved from the anode at different pH values and EF operation times are depicted in Fig. 119. The results showed good agreement with Faraday's law. The aluminum dissolution rates were found to be independent of pH value.

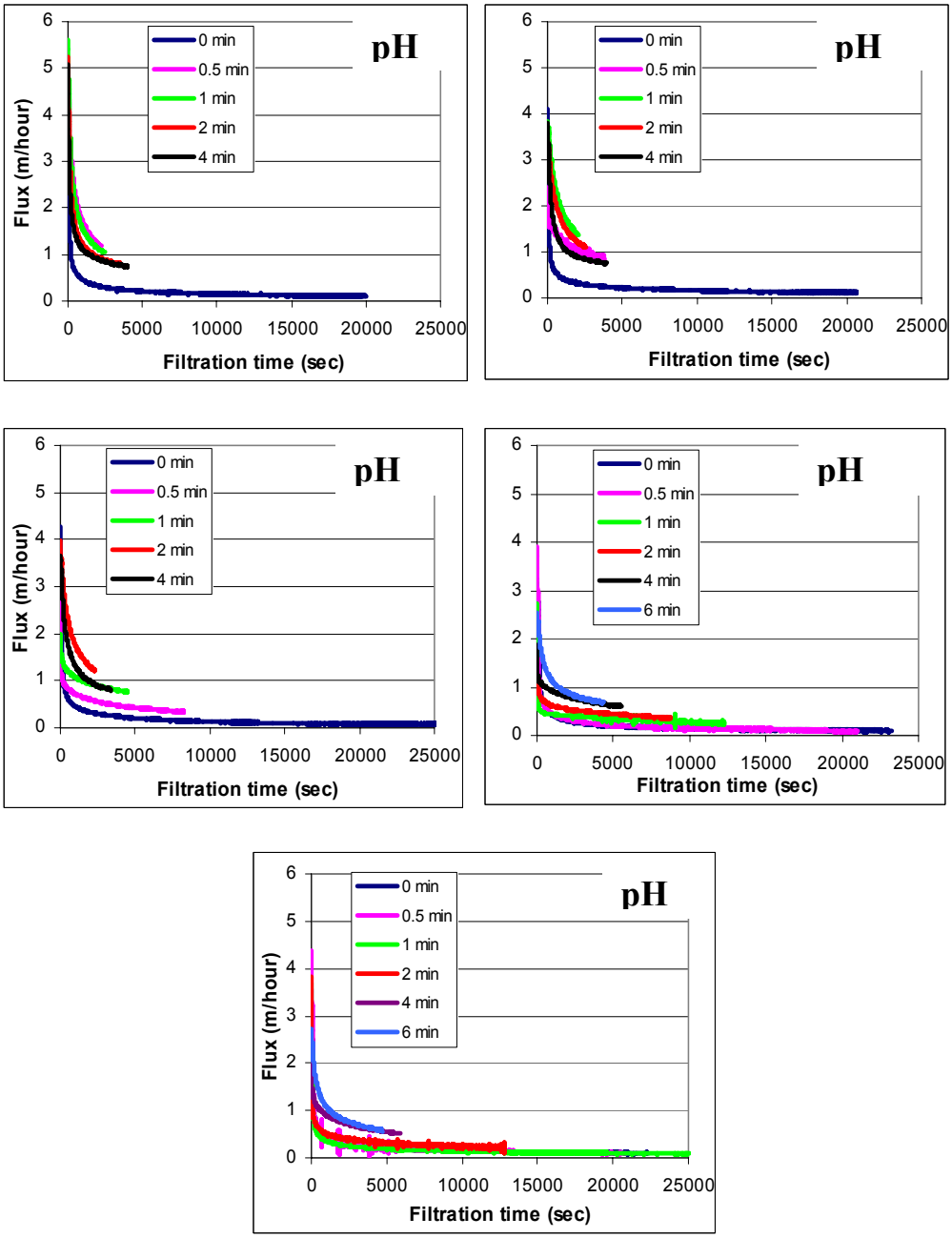

Fig. 116 Effect of EF operation time on flux performance at different pH at the internal fouling experiments.

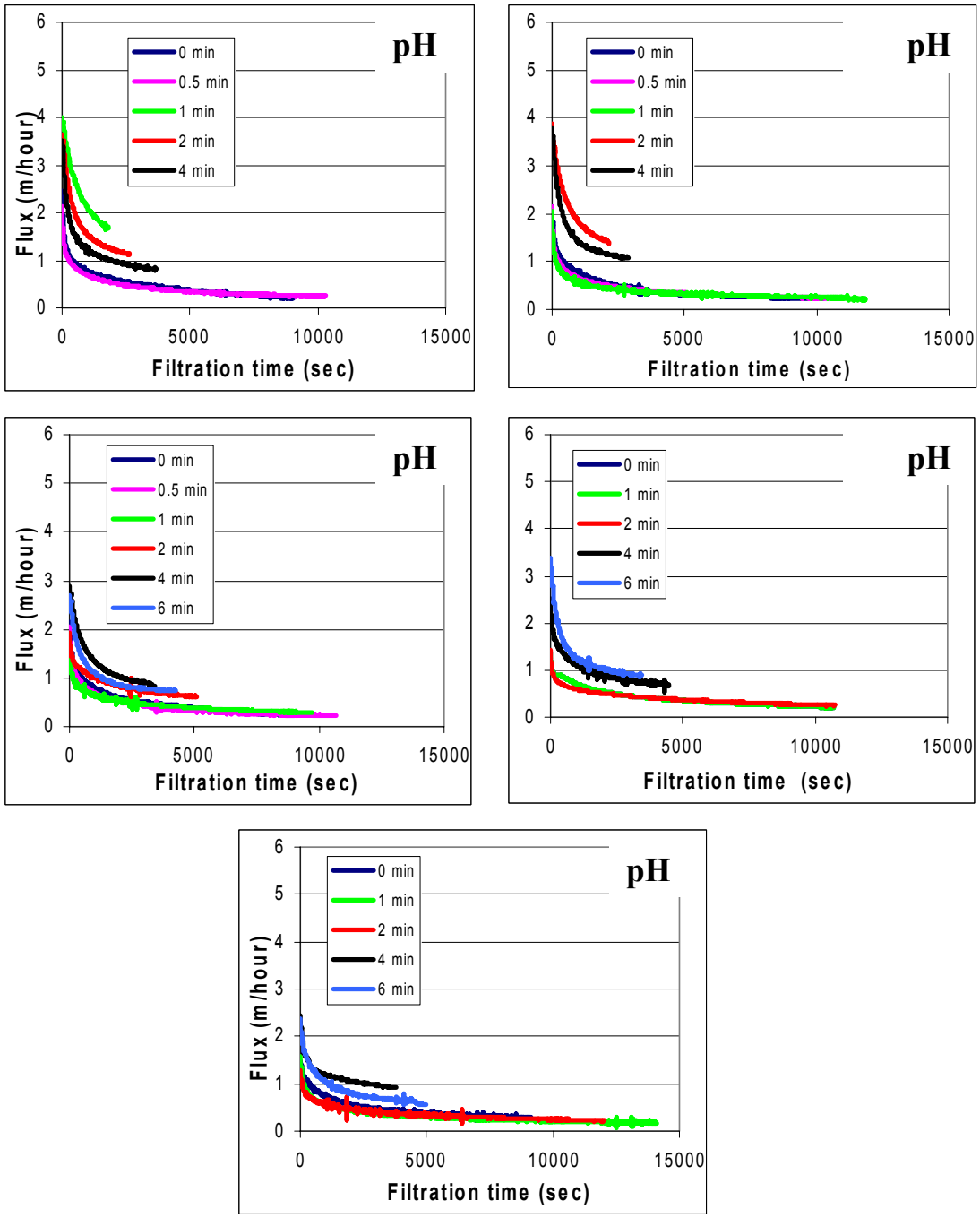

Fig. 117 Effect of EF operation time on flux performance at different pH at the external fouling experiments. ΔP = 2 bar, V = 1.9 l

Table 19 Recovery rates of the initial flux after physically washing the membrane surface, with and without EF pretreatment. EF operation time: 2 min (internal fouling) and 4 min (external fouling).

	pH 6.5		pH 7.5,	
	without EF	with EF	without EF	with EF
Internal fouling experiments	5.4	93	1	102
External fouling experiments	33	91	59	100

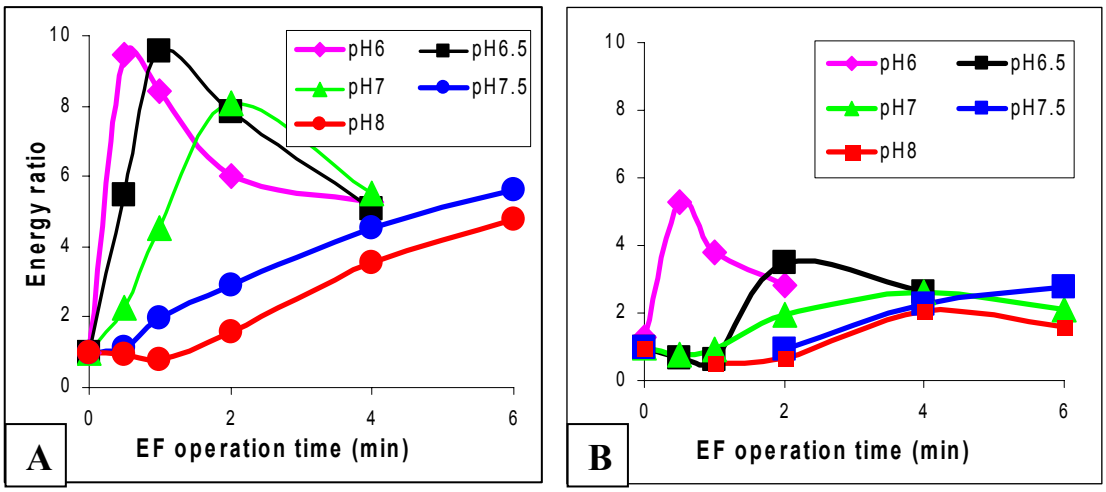

Fig. 118 Energy ratio for different pH values and EF operation times. (a) Internal fouling experiments, (b) external fouling experiments.

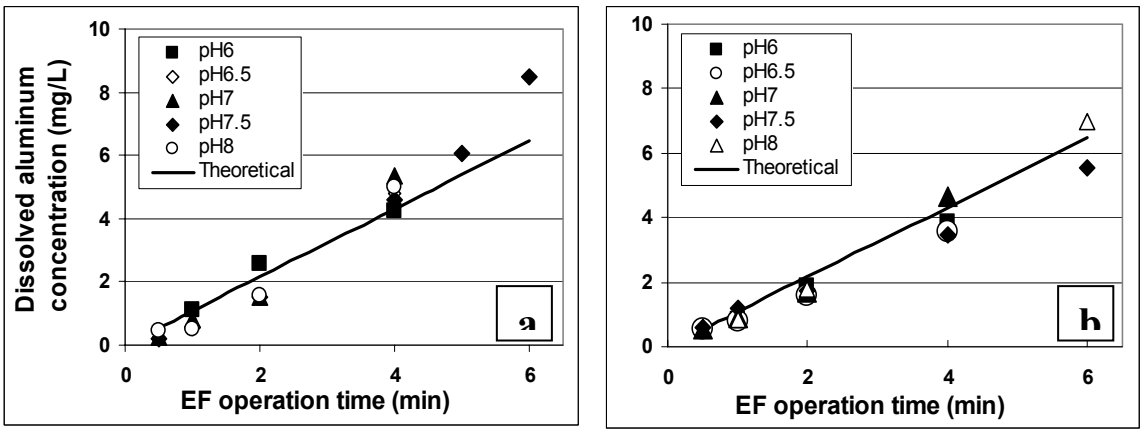

Fig. 119 Concentration of dissolved aluminum (anode) in the EF process for (a) internal fouling experiments, (b) external fouling experiments. The line represents the expected dissolved aluminum calculated by Faraday's Law

Average residual aluminum and silica concentrations for each pH value are depicted in Fig. 120. It can be concluded from the low standard deviation (except for pH 8) that these concentrations were independent of EF operation time. Residual silica concentrations were independent of pH, whereas higher concentrations of residual aluminum were observed at higher pH values. Concentrations of both residual silica and residual aluminum depended on experiment type, with lower residual concentrations observed in the internal fouling vs. external fouling experiments.

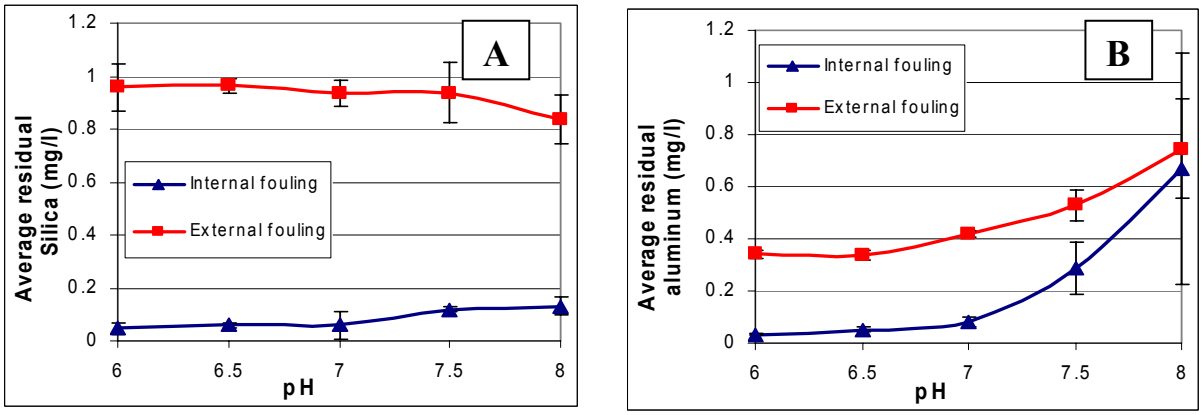

Fig. 120 Average concentration of (a) residual silica and (b) residual aluminum for different pH values at the internal and external fouling experiments.

Fig. 121shows SEM pictures of the fouled membrane and the cake, following suspension filtration at pH 6.5. After natural drying, the formed cake cracked and fell off, affording the

opportunity to observe both the membrane surface and the formed cake. The pictures from the internal fouling experiments showed large differences between the EF-pretreated and non-treated suspensions. Without EF pretreatment, the membrane surface was covered with a very thin and dense layer of silica particles with only a small number of open pores, leading to the severe fouling observed in the filtration experiments. With EF pretreatment, a thick layer was formed on the membrane due to solid aluminum hydroxide deposition. This layer protected the pores from plugging, keeping them clean and open for flow, as can be seen by visual observation of the exposed membrane surface. The pictures from the external fouling experiment did not show any marked visual differences between EF-pretreated and non-treated suspensions.

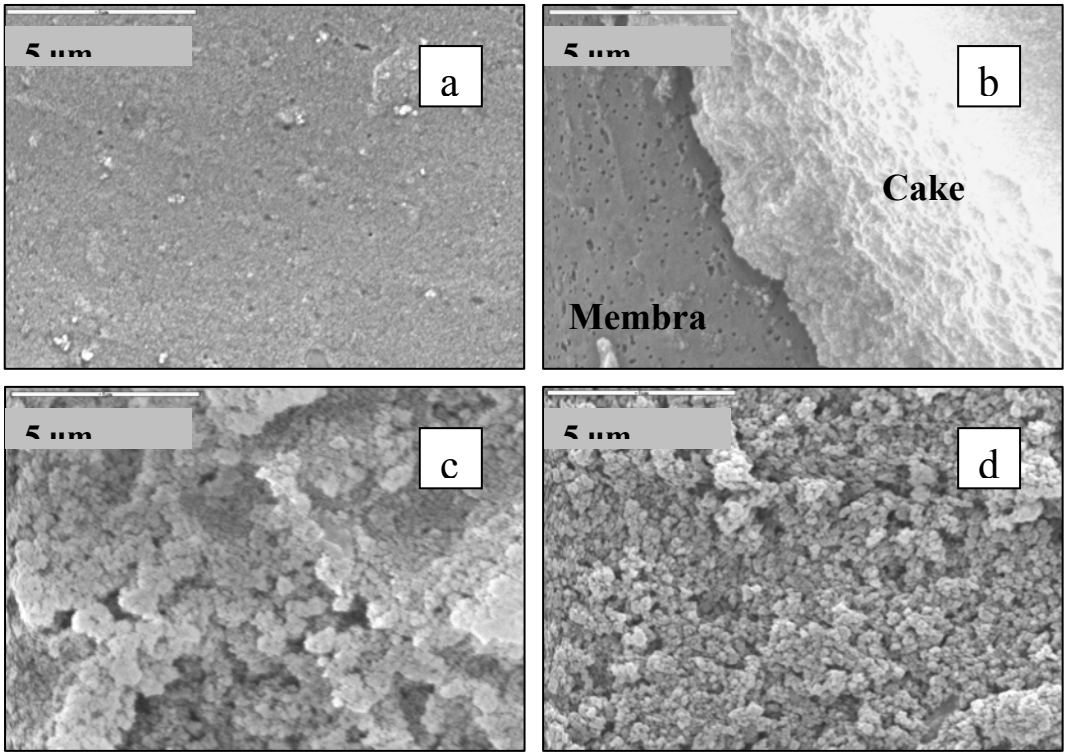

Fig. 121. SEM pictures of fouled membrane and the formed cake. (a) Internal fouling with no EF pretreatment, (b) internal fouling with 1 min EF treatment, (c) external fouling with no EF pretreatment, (d) external fouling with 4 min EF treatment. All suspensions were at pH 6.5.

Fig. 122 depicts the filtration-energy ratio between two suspensions — one pretreated by EF for 1 min and the other non-treated — as a function of duration of the EF slow mixing step. The suspensions were of the internal fouling type at the pH 6.5. Even without the slow mixing step (0 min slow mixing), a significant improvement in filtration energy was observed as reflected by an energy ratio value of 5. The longer the duration of the slow mixing, the higher the improvement in filtration energy, with maximal improvement occurring at 30 min.

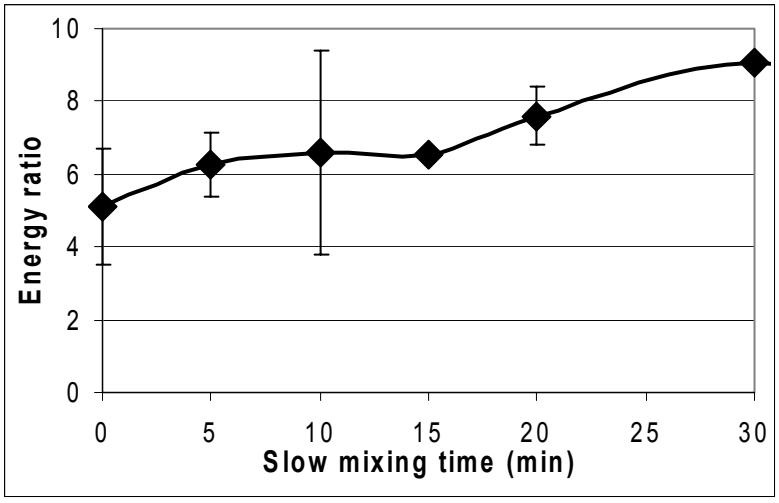

Fig. 122 Energy ratio for different durations of the slow mixing EF step following 1 min of the electrochemical dissolution, at the internal fouling experiments at pH 6.5.

IV-2.3.2.2 Iron Anode

The same set of experiments has been done when iron electrode has been used as an anode at electroflocculation process.

At an EF operation time $\leq$4 min at all pH, large amounts of iron-hydroxide deposits sank in the supply chamber and were not transferred with the flow to the membrane cell.

Internal fouling filtration curves for different EF operation times at different pH are presented in Fig. 123, where a dramatic effect of EF on filtration performance can clearly be seen. At pH 6.5, without EF pretreatment, it took more than 20,000 s (about 5.5 h) to filter 1.9 L of suspension, while a very short (2 min) pretreatment by EF reduced the filtration time to 1430 s (less than 25 min) for the same filtered volume (ΔP=2 bar). A similar improvement in filtration performance was also observed at pH 7.5: without EF the filtration time was 23,000 s (over 6 h), while 2 min of EF reduced the filtration time to 2170 s (about 35 min). The differences between the two pH values were found mostly at lower EF operation times: 0.5 min of EF treatment reduced the filtration time to 8800 s at pH 6.5 and to 3140 s at pH 7.5.

A significant improvement following EF pretreatment, albeit weaker than in the internal fouling experiments, was observed in the external fouling experiments (Fig. 124). At pH 6.5, 6 min of EF reduced the filtration time of 1.9 L from 17,200 s (more than 4.5 h) to 2300 s (about 40 min). At pH 7.5, without EF pretreatment the filtration time for 1.9 L was more than 18,000 s, while 6 min

EF pretreatment reduced the filtration time to only 1840 s. With the short EF operation time of 0.5 min, the filtration time decreased to 8900 s at pH 6.5 and to 5400 s at pH 7.5.

As previously determined, the energy ratio (E_{ratio}) represents the value by which the experimental filtration energy must be multiplied so that a raw suspension (without EF pretreatment) will be filtered at the same time as a suspension pretreated by EF. Thus, this ratio also represents the ratio between the filtration energies of EF-treated and untreated suspensions. The energy ratios for the external and internal experimental sets for different pH values and different EF operation times are depicted in Fig. 125. For the internal fouling experiments, the calculated energy ratio was very high, reaching a maximum of over 10 at all pH values examined for an EF operation time of 6 min. An energy ratio of 10 indicates a 90% savings in filtration energy by using the EF pretreatment. At the short EF operation time (0.5 min), lower energy ratios were observed at pH 6 and 6.5 relative to the higher pH values. With the exception of pH 6.5 and EF operation times below 4 min, longer EF operation times led to higher energy ratios. At EF operation time $\geq$ 4 min, the energy ratio was independent of operation time. At the short EF operation time (0.5 min), the energy ratio at pH 6 and 6.5 was significantly lower than at higher pH values. The observed maximum energy ratio at pH 6.5 with 2 min of EF was confirmed by repeating the experiment three times.

In the external fouling experiments, the energy ratio was lower than in the internal experiments, reaching a maximum of 7.5 at pH values of 7 and 7.5 with 6 min of EF. The longer the EF operation time, the higher the energy ratio was. Here again, lower energy ratios were observed at pH 6 for short EF operation times (0.5 and 1 min) relative to the higher pH values.

Initial-flux recovery ratios after physically washing the membrane surface with tap water are shown in Table 20. When the suspension was pretreated by EF, the recovery rates were 90 to 100%, independent of the fouling type. When the EF process was not operated, the recovery rates were negligible for the internal fouling and moderate for the external fouling.

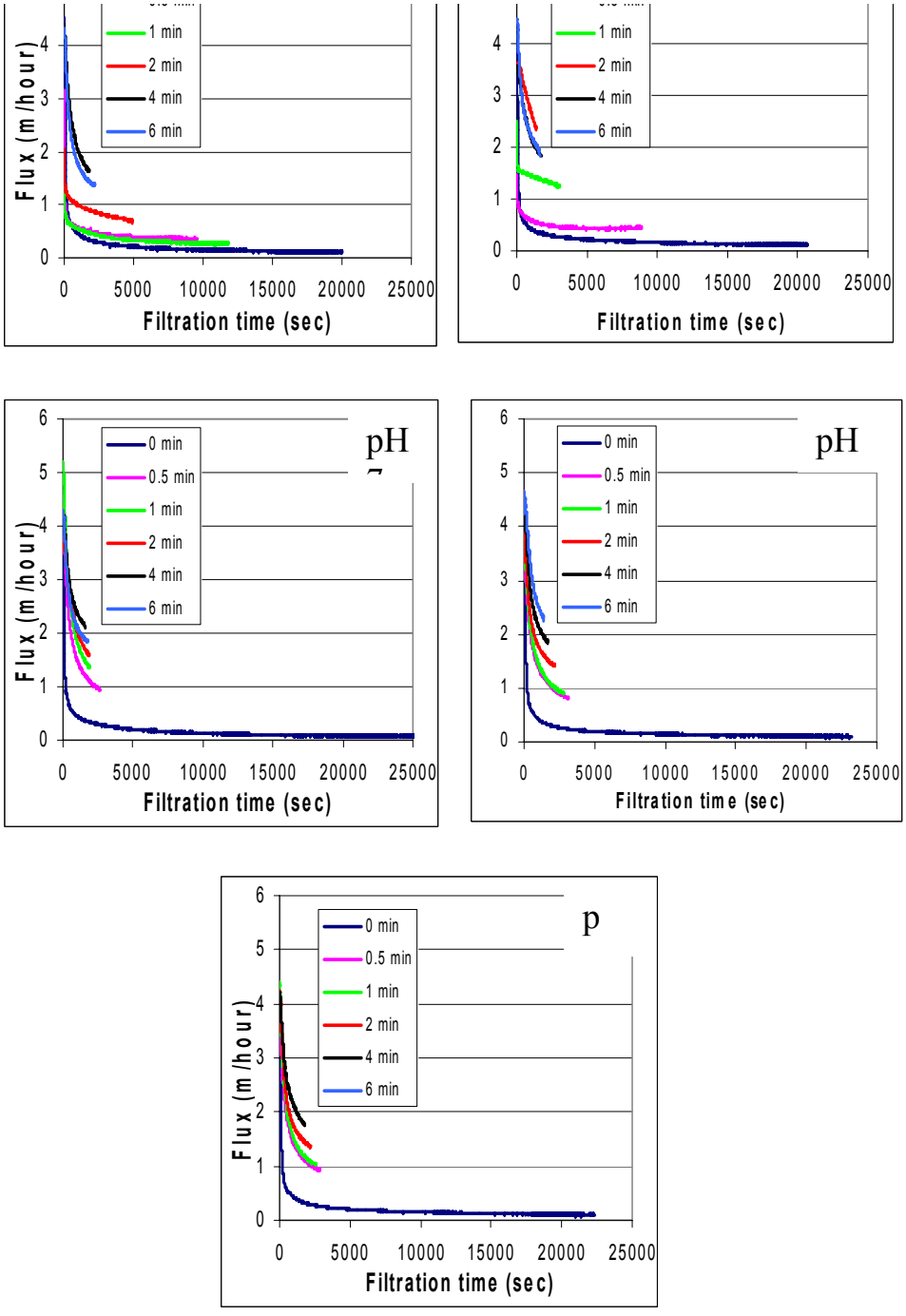

Fig. 123 Effect of EF operation time on flux performance at different pH at the internal fouling experiments.

Table 20 Recovery rates of the initial flux after physically washing the membrane surface, with and without EF pretreatment. EF operation time: 2 min (internal fouling) and 4 min (external fouling).

	pH 6.5		pH 7.5,	
	without EF	with EF	without EF	with EF
Internal fouling experiments	6.5	97	1	96
External fouling experiments	33	91	59	93

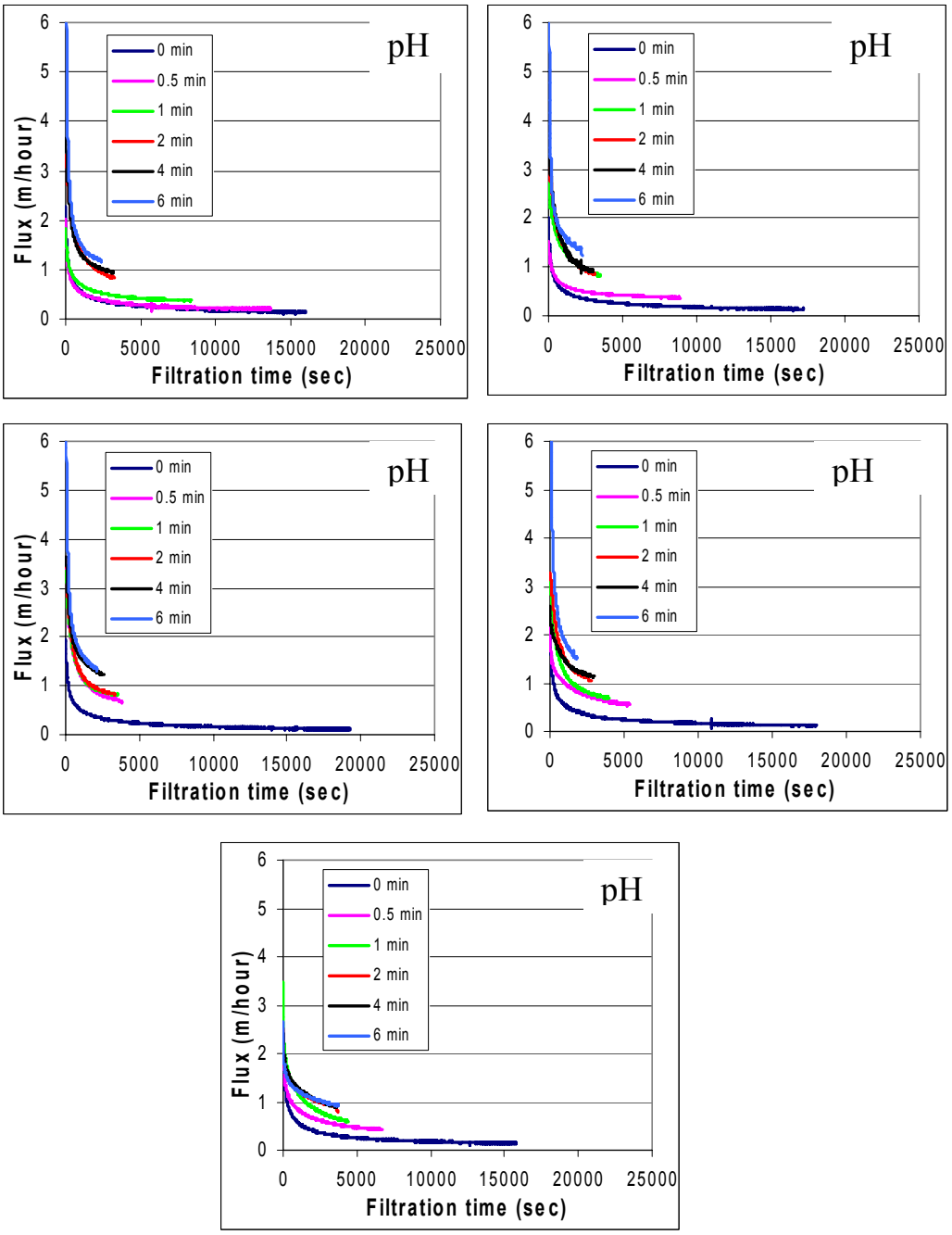

Fig. 124 Effect of EF operation time on flux performance at different pH at the external fouling experiments.

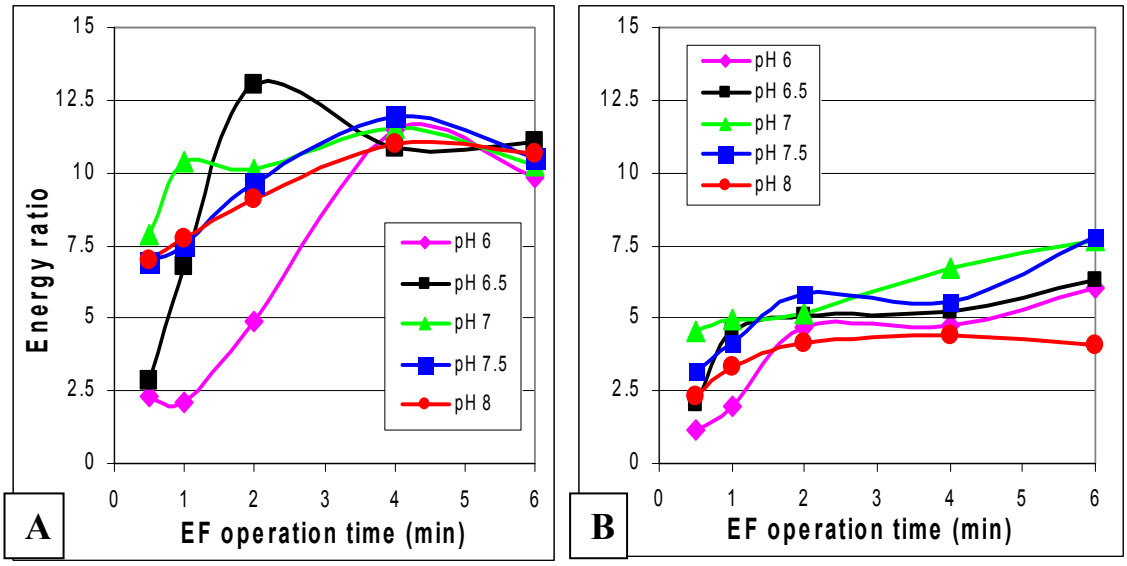

Fig. 125 Energy ratio for different pH values and EF operation times. (a) Internal fouling experiments, (b) external fouling experiments.

Average residual iron and silica concentrations for each pH value are presented in Fig. 126. The relatively low standard deviations in the residual silica data indicate low dependence on EF operation time. Residual silica concentrations appeared to be relatively high as compared to the residual silica results in the case of aluminum-based EF. Nevertheless, the rates were still quite high—50% and about 95% in the internal and external fouling experiments, respectively. Residual iron concentrations at high pH values (7, 7.5, and 8) were below detection limits (0.1 µg l^{-1}). Higher residual iron concentrations were observed at pH 6 versus pH 6.5, where the suspension turned yellow. The longer the EF operation time, the higher the residual iron concentrations were, in both the external and internal fouling experiments.

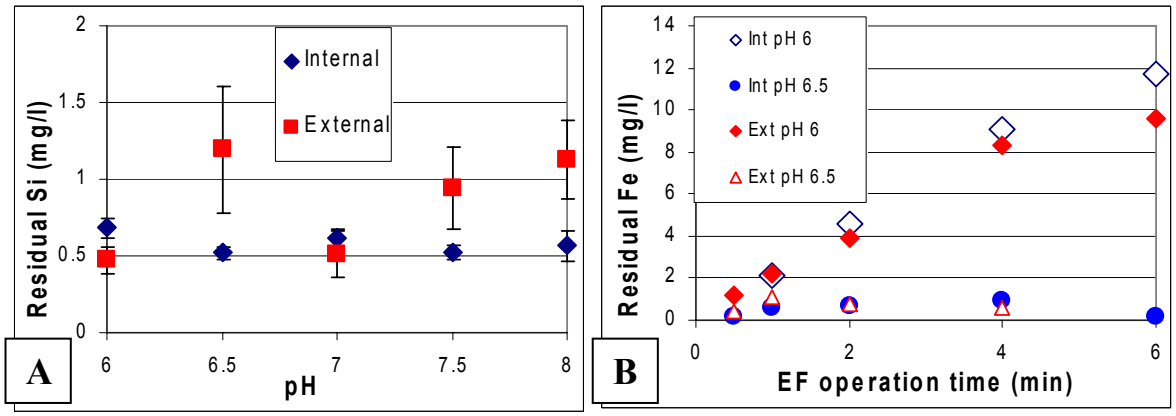

Fig. 126 Average concentration of (a) residual silica and (b) residual iron for different pH values at the internal and external fouling experiments.

Fig. 127 presents SEM pictures of the fouled membrane and the cake following filtration of 1.9 l of suspension at pH 6.5. After natural drying, the formed cake cracked and fell, providing an opportunity to observe both the membrane surface and the formed cake. The pictures from the internal fouling experiments show a large difference between EF-treated and untreated suspensions. Without EF pretreatment, the membrane surface was covered with a very thin and dense layer and had only a small number of open pores, indicating severe fouling occurrence in agreement with the filtration curves 3. With EF pretreatment, a thick layer formed on the membrane due to solid iron-hydroxide deposition. This layer protected the pores from plugging, keeping them clean and open to flow as observed on the exposed membrane surface (Fig. 127b). In the external fouling experiment, there were no significant visual differences between suspensions which had been treated, or not, by EF.

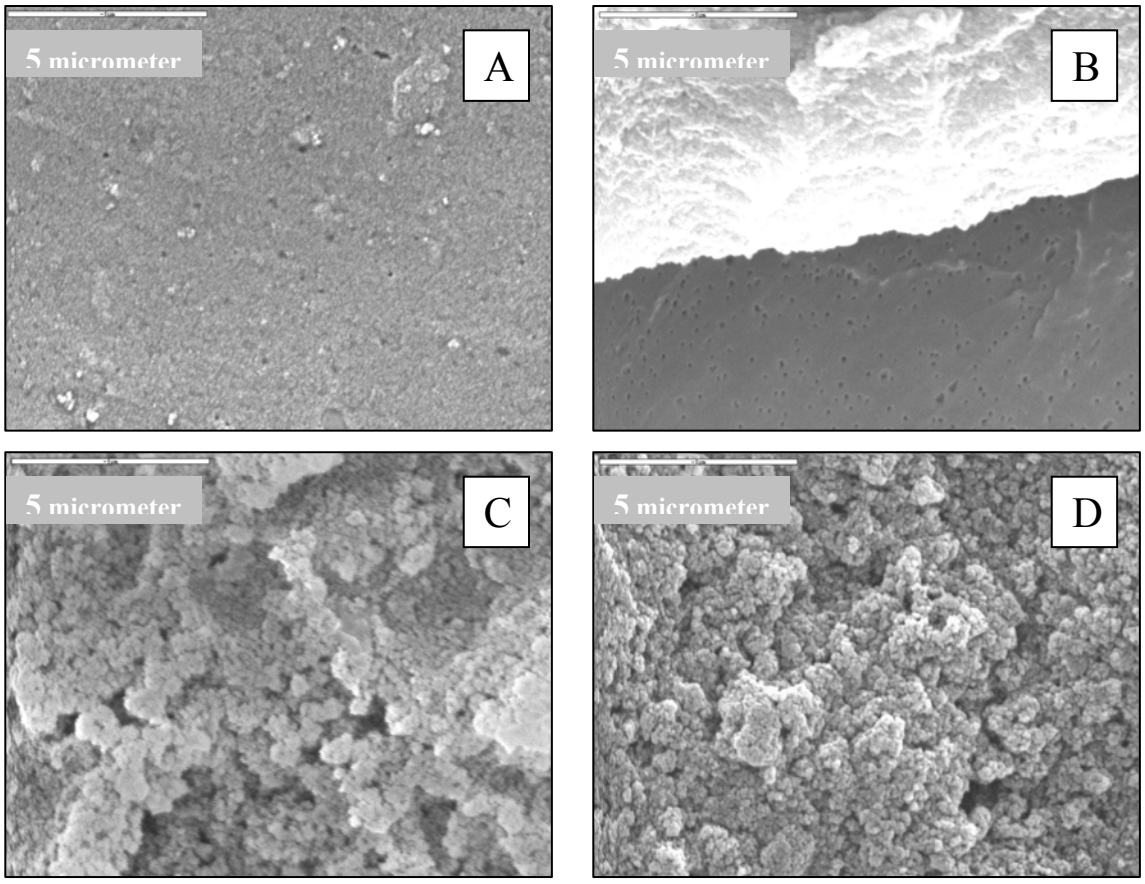

Fig. 127 SEM pictures of fouled membrane and the formed cake. (a) Internal fouling with no EF pretreatment, (b) internal fouling with EF treatment, (c) external fouling with no EF pretreatment, (d) external fouling with EF treatment. All suspensions were at pH 6.5.

Fig. 128 depicts the filtration energy ratio between a suspension that was pretreated by EF for 2 min followed by slow mixing and an untreated suspension, as a function of slow-mixing time. The suspensions were of the internal fouling type and the pH was 7. High energy ratios were observed in all cases, even without the slow mixing. Longer slow-mixing times barely increased the energy ratio. At long slow-mixing times (15, 20 min), the energy ratio was even a little lower than that with no slow mixing.

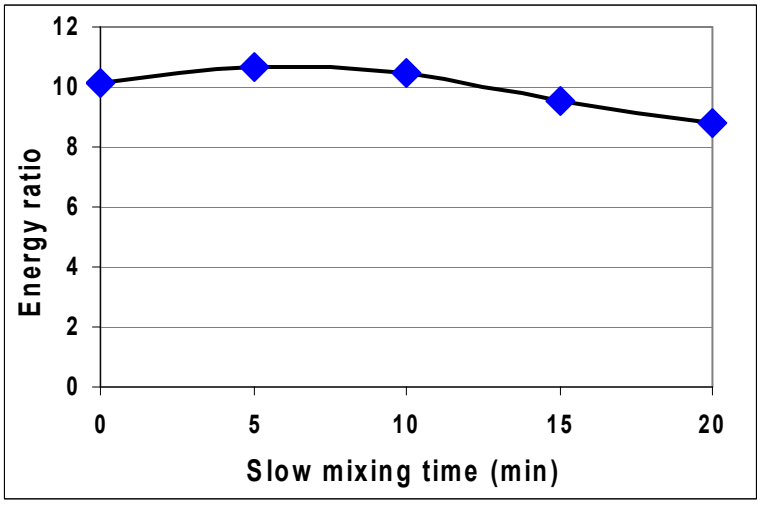

Fig. 128 Energy ratio for different durations of the slow mixing EF step following 2 min of the electrochemical dissolution, at the internal fouling experiments at pH 6.5.

IV-2.3.2.3 Organic Matter Contaminates Removal

Another set of experiments was designed to study the effects of EF pretreatment to MF on organic matter contaminates removal rates. Synthetic solutions of dissolved organic matter were pretreatment by different operation times of iron and aluminum based EF (0 to 12 min, constant electric current of 0.3 A) followed by MF. At all experiments 750 ml of solution of 15 mg/l (10 mg/l DOC) of humic acid (IHSS Leonardite, Humic Acid Standard, 1S104H-5) has been used. The pressure of 2 bar was applied on MF and 3 bar on UF process.

The removal of organic dissolved matter at different treatment processes are shown in Figs. 129 (aluminum anode) and 130 (iron).

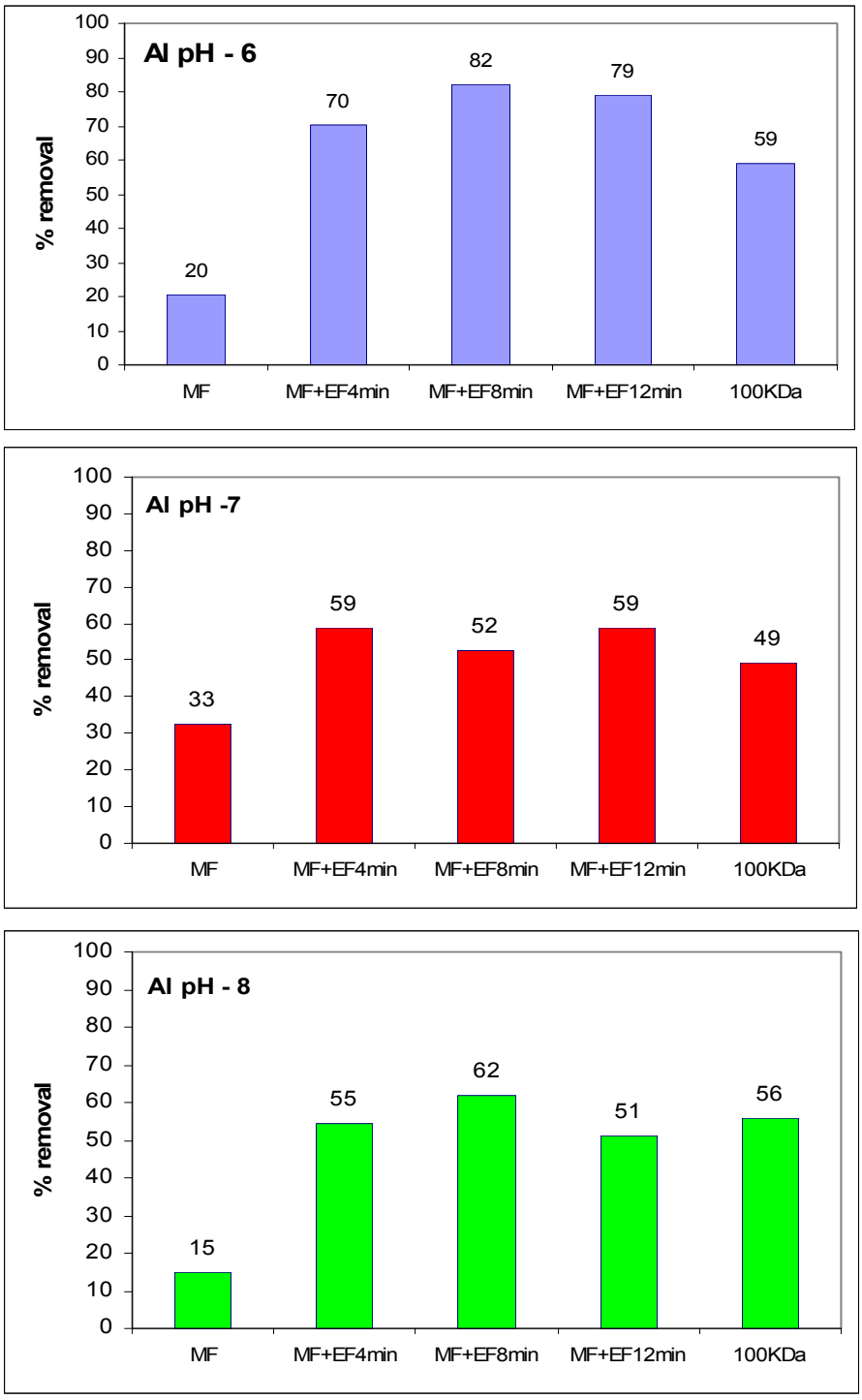

Fig. 129 Removal of organic dissolved matter at different treatment processes (aluminum anode)

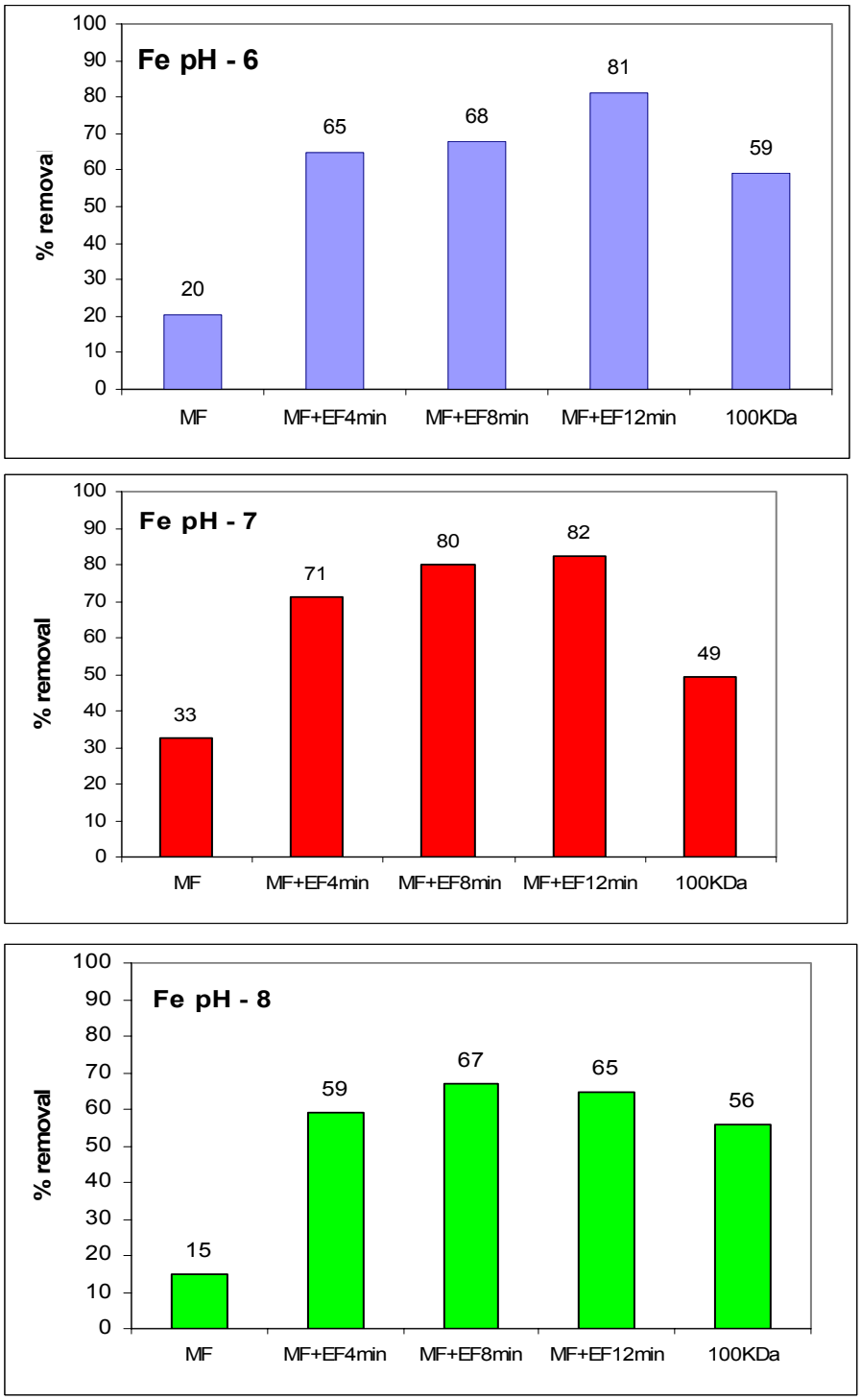

Fig. 130 Removal of organic dissolved matter at different treatment processes (iron anode)

The filtration time of 750 ml solution at different treatment processes are shown in Fig. 131

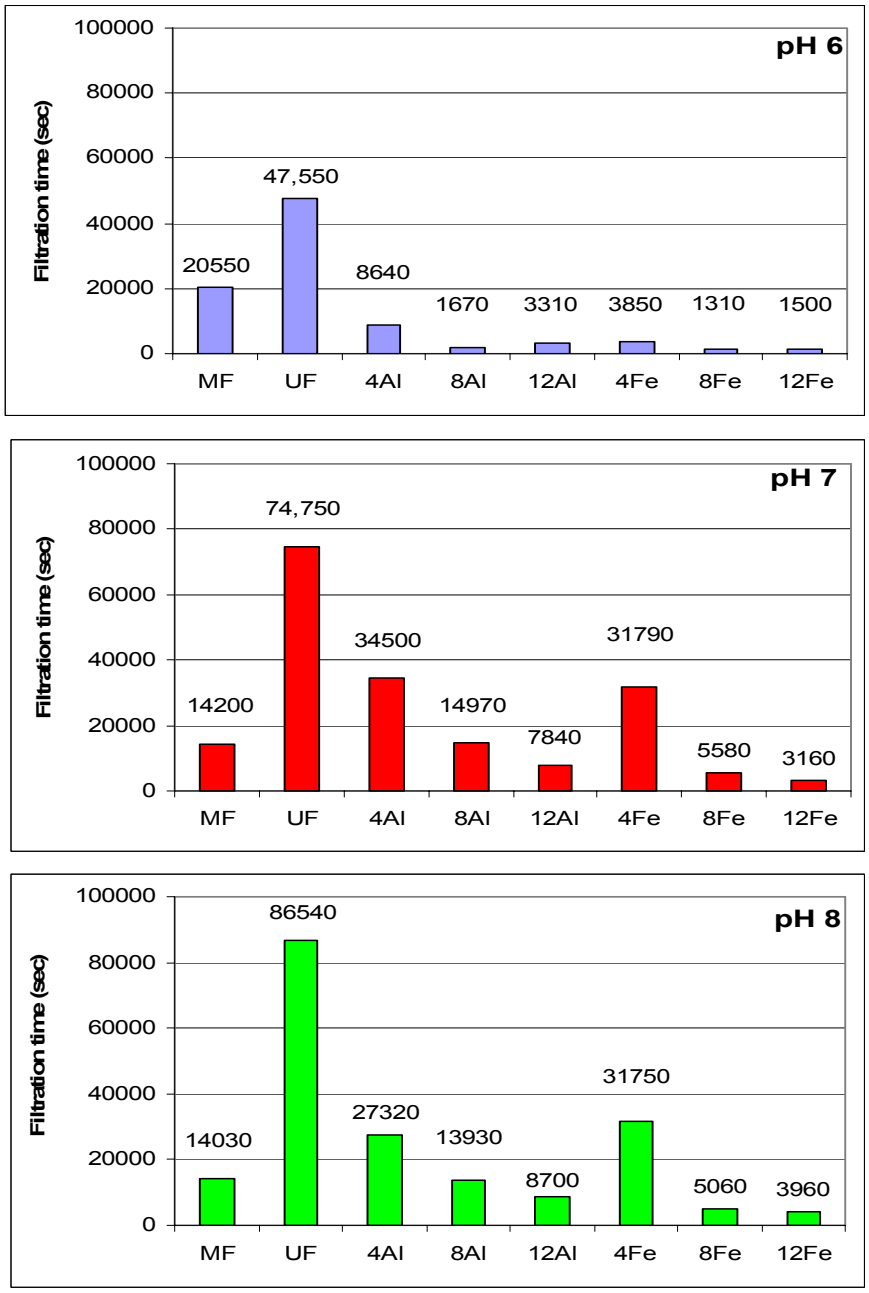

Fig. 131 750 ml solution filtration time at different treatment processes

As it seen from the results, EF pretreatment improves the removal of organic matter by MF, moreover, the EF-MF treatment gave better results than UF-100 KDa (it was impossible to use UF 10KDa treatment; only 340 ml of solution were filter during a week–600,000 sec). The EF-MF combination also saves the filtration time, i.e., energy.

IV-2.3.3 Using Silver Nanoparticles as a Method to Minimize the Formation of Biofouling in Membrane Filtration Systems.

IV-2.3.3.1 Characterization of MCNPs.

The Ag- and Au-MCNPs formed stable dispersions and had a roughly spherical shape with a relatively narrow size distribution. Fig. 132 shows the size-distribution histograms of Ag-MCNPs evaluated by analyzing the TEM micrographs. The inset is a representative TEM micrograph of Ag-MCNPs which appear well-dispersed, with a mean size of 8 ± 2.6 nm. The mean size of 207 sampled Au-MCNPs was 5 ± 1.7 nm.

Thus, while the Ag- and Au-MCNPs were of the same size scale, the Au-MCNPs used as controls were smaller, with a narrower size distribution. Ag-MCNP inactivation of planktonic *E. coli* has been found to be associated with particle size (Baker et al., 2005; Morones et al., 2005). However, since smaller particles are generally more active and the <10 nm fraction has been shown to exhibit a direct interaction with several bacterial strains, including *E. coli* and *P. aeruginosa* (Morones et al., 2005), the minor size difference between our two particles was considered negligible.

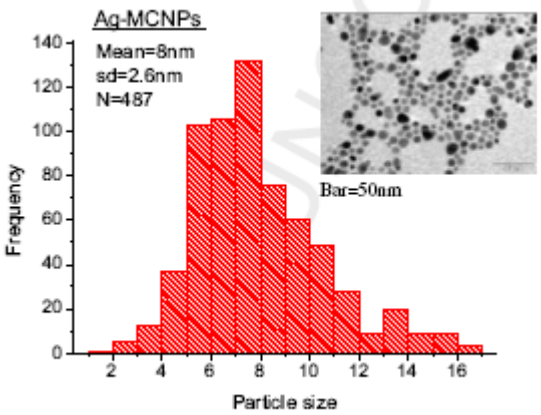

Fig. 132 Particle-size-distribution histogram of Ag-MCNPs; sd - standard deviation, N - number of particles sampled for averaging.

IV-2.3.3.2 Effect of MCNPs on Biofilm Formation.

One of the goals of this research was to determine whether the extent of planktonic inactivation of the model microorganism by Ag-MCNPs is associated with biofilm prevention. To address this issue, the inactivation of planktonic *P. aeruginosa*, determined by microbial count, was compared to biofilm formation as determined by biofilm formation assay and presented as relative biomass. The term "microbial count" corresponds to log inactivation values and describes the concentration of colony-forming bacteria after pretreatment with MCNPs and before the incubation step used to determine biofilm formation. For example, a control sample consisting of 10^7 CFU mlL^{-1} bacteria which was pretreated with MCNPs showed 2-log inactivation, corresponding to a microbial count of 10^5 CFU ml^{-1}. Then, the treated samples with a microbial count of 10^5 CFU ml^{-1} were incubated and biofilm formation was quantified. The relative effectiveness of each Ag-MCNP concentration in preventing biofilm formation was examined using the modified microtiter plate assay and quantified using the GV technique (detailed in Materials and Methods). Again, biofilm formation presented as relative biomass was calculated and compared to a control sample of 10^7 CFU ml^{-1} of non-treated bacteria, set at 100%. A reasonable although not maximum value of ~0.8 OD_{595} according to the biofilm formation and quantification assay was measured for control samples. The biofilm formation assay as it was implemented in this study, measured presumably all the adherent cells and initial stage of the biofilm formation.

Fig. 133 presents relative biomass and % of *P. aeruginosa* cells that survived the treatment, at different Ag-MCNP concentrations in the range of 10 to 180 μg ml^{-1}. Results obtained after 39 hours of incubation using LB medium at 37°C showed that Ag-MCNPs retarded biofilm formation, even at high percentage of ~10-50% surviving cells (0.3-1.42 log inactivation). Obviously, biofilm formation follows similar pace as the surviving cells at various MCNPs concentrations and both reached threshold levels. The threshold of the biofilm formation assay was chosen at about 5% based on blank samples containing pure LB medium and water.

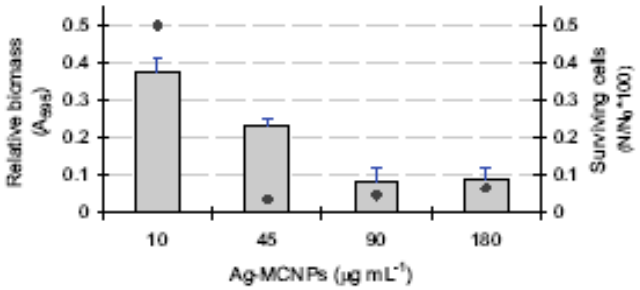

Fig. 133 Relative biomass formed by *P. aeruginosa* (bars) and percentage of surviving cells (points) at various Ag-MCNP concentrations.

Exposure of *P. aeruginosa* to increasing Ag-MCNP concentration in the planktonic phase resulted in a decrease in surviving colony forming cells which reached a value of ~10% survival (1.2- to 1.4-log inactivation) in the range of 45 to 180 µg ml^{-1} Ag-MCNPs. A reduction of more than 60% in biomass formation was achieved at about 50% surviving cells and it reached a threshold of 90% biomass formation at 90 µg ml^{-1} Ag-MCNPs.

Biofilm prevention of *P. aeruginosa* is expected to be directly related to planktonic inactivation, as well as to the concentration of Ag-MCNPs. Biofilm control appeared to improve with increasing Ag-MCNP concentration and increasing planktonic inactivation, but the tests for both inactivation and biofilm formation reached threshold levels. This may indicate that increasing the Ag-MCNP concentration up to a certain value enhances the reduction in biofilm formation, but its increase beyond that value will not improve treatment. Nevertheless, the limitation of the assay threshold measurement needs to be taken into account before drawing this conclusion. At this stage of research we did not attempt to find detailed correlation between the concentration of NPs, inactivation of planktonic cells and biofilm formation, but to observe the phenomena related to the impact of Ag-MCNPs on biofilm formation using a high throughput screening method. Under the experimental conditions, an Ag-MCNP concentration of 45 µg mL^{-1} resulted in both moderate inactivation of planktonic cells and a moderate ability to retard biofilm formation above the threshold. This concentration was thus chosen as the optimal concentration for further studies. A control study using Au-MCNPs under similar experimental conditions (surfactant, MCNP concentration of 45µg ml^{-1}, incubation time, etc.) showed a relative biomass of 80 to 100%, indicating these NPs' inferior ability to retard biofilm formation compared to Ag-MCNPs (data not shown).

Another goal of this study was to determine differences between biofilm formation following pretreatment with either Ag- or Au-MCNPs and biofilm formation produced by the same

microbial counts of control bacteria (without NP addition). Fig. 134 illustrates relative biomass as a function of initial cells concentration and incubation time. An aqueous suspension of non-treated *P. aeruginosa* at concentrations of ~10^7 was termed the 100% control and is the reference for other samples. The non-treated samples of ~10^6, ~10^5 and ~10^4 CFU ml^{-1} were achieved by dilution (termed as control-diluted). The treatment (of *P. aeruginosa* at initial concentration of ~10^7 CFU mL^{-1}) with Ag-MCNPs at 45µg mlL^{-1} results in 1.4 log inactivation meaning its cells' concentration in the microtiter wells was between 10^5 to 10^6 CFU ml^{-1}. The samples treated with Au-MCNPs corresponded to 0-log inactivation value, meaning its cells concentration in the microtiter wells was ~10^7 CFU ml^{-1}. All samples were incubated at 37°C for 39 and 100 hours, representing short and long incubation times, respectively. The surviving colony forming cells that were exposed to Ag-MCNPs (at a fixed NP concentration) resulted in either similar or lower biofilm formation compared to non-exposed cells at the same colony forming cells count, depending on incubation time of 39 and 100 hours, respectively.

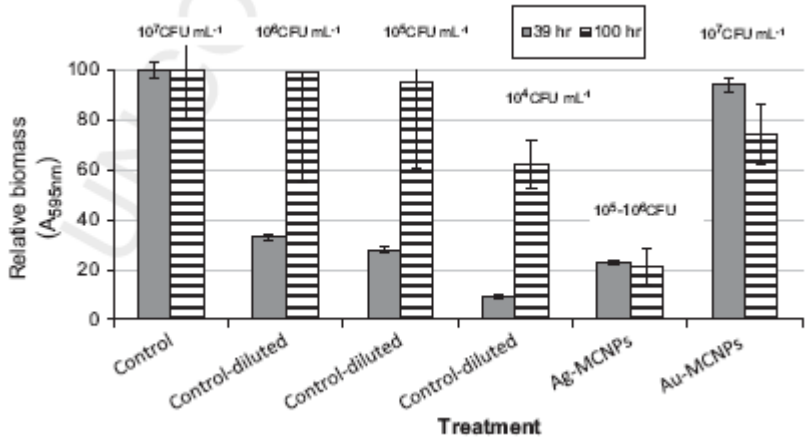

Fig. 134 Relative biomass in MCNP-treated vs. control samples at incubation times of 39 and 100 h; MCNP concentration was held constant at 45 µg ml^{-1} (Ag-MCNP- and Au-MCNP-treated samples correspond to ~10^5 and 10^7 CFU ml^{-1}, respectively).

Other experiments were performed to elucidate the effect of incubation time on biofilm formation by treated bacteria. Fig. 135 presents the relative biomass produced by *P. aeruginosa* at various incubation times, in the range of 12 to 162 h at 37°C, pretreated with 45µg ml^{-1} MCNPs and at an initial cell count of ~10^7 CFU ml^{-1}.

The ability of Ag-MCNPs to control biofilm formation was retained at all incubation times, with a relative biomass of between 10 and 37%. Similarly, the inferior activity of Au-MCNPs was retained, with a relative biomass between 80 and 100%. Under the same experimental conditions,

but using MCNPs at 90μg ml^{-1}, Ag-MCNPs showed 9 to 23% relative biomass while Au-MCNPs showed 70 to 100% (data not shown).

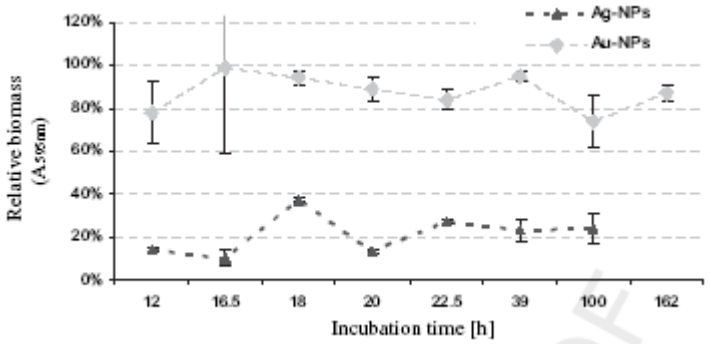

Fig. 135 Relative biomass formed vs. incubation time, at a constant concentration of 45 μg ml^{-1} Au- or Ag-MCNPs.

Figures 134 and 135 show that stable value of relative biomass have been formed in the presence of Ag-MCNP. This could be associated not only with inactivation of planktonic cells, but also with many other factors such as physiological changes in cells, impact on molecular mechanisms related to biofilm formation and continuous release of silver ions (Morones et al., 2005). However, these factors were not examined in this study.

To determine whether the phenomenon of biofilm retardation is unique to *P. aeruginosa*, a few experiments were performed with *E. coli*, another gram-negative bacterium. The two bacteria were suspended at about 10^8 and 10^7 CFU ml^{-1} for *E. coli* and *P. aeruginosa*, respectively, and incubated with 45 μg mll^{-1} MCNPs in microtiter wells at 37°C for 22.5 h. Fig. 136 presents the effect of pretreatment with MCNPs on the formation of relative biomass for the two bacteria. Results show similar relative biomass in both microorganisms with each MCNP.

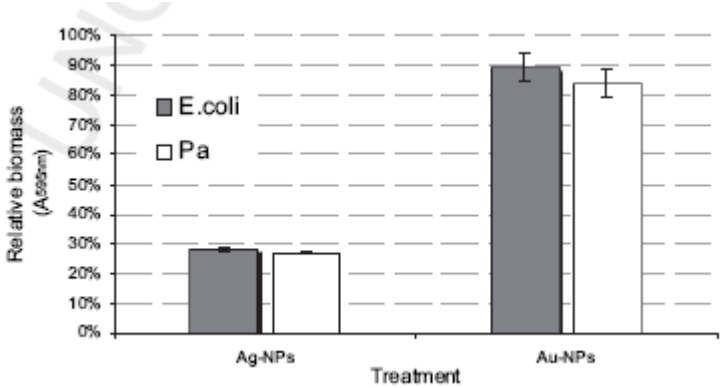

Fig. 136 Effect of pretreatment with 45 μg ml^{-1} MCNPs on relative biomass formation by *E. coli* and *P. aeruginosa* (Pa).

IV-2.3.3.3 Microscopic Observation of MCNP-Microbial Cell Interaction.

TEM of HPF/freeze-substituted samples was applied to visually elucidate the outcome of the interaction of MCNPs with *P. aeruginosa* cells. Fig. 137 shows TEM micrographs of *P. aeruginosa* cells after pretreatment with Ag-MCNPs (column A) and Au-MCNPs (column B). About 10^9 CFU ml^{-1} of bacteria were mixed with 2 x 10^{14} Ag-NPs or 4 x 10^{14} Au-NPs. The numerical density of the particles was estimated based on metal density and solution concentration (Dror-Ehre et al., 2009). The biofilm-formation potential and planktonic inactivation of these same samples were estimated before freezing, using the biofilm formation assay and enumeration of viable bacteria. As detailed in Materials and Methods, some of the samples were rinsed after interaction and before freezing to remove the unattached particles; the presented silver specimen was not rinsed while the gold one was. However, on the micrographs, virtually no silver or gold NPs were observed on or inside the cell envelope, even though their mean size was in the range of 1 to 10 nm, which can penetrate the cell (Morones et al., 2005), and many particles were present in the samples. The bacterial cells in both TEM micrographs look well preserved and undamaged, even though the relative biomass under the test conditions was about 40% in the presence of Ag-MCNPs (regardless of rinsing). No impact on the planktonic cells was seen. Choi et al. (2008) also found no evidence of changes in membrane integrity or leakage caused by AgNPs at 1 mg ml^{-1}. This is in contrast to Sondi and Salopek-Sondi (2004), who assumed that Ag-NPs cause pitting in the membrane that leads to leakage of internal material and cell death. The intra cellular material appeared to be evenly dispersed in all of the cells, but there was a slightly higher number of cells whose ribosome (blackish dots on the micrograph) seemed to be pushed towards the peripheral parts of the cell in the presence of Ag-MCNPs. Crystallization of vital intercellular components is mentioned as a survival strategy to severe or prolonged stress as it physically sequestered and protected these components from their surrounding (Minsky et al., 2002). The non-uniform distribution pattern observed in Fig. 6 column A indicates that the DNA is condensing and this could be a survival strategy to the presence of Ag-MCNPs. This phenomenon has also been observed by Feng et al. (2000), who found condensation of DNA molecules in the center of *E. coli* and *Staphylococcus aureus* cells after treatment with silver ions in comparison to their random distribution in control samples.

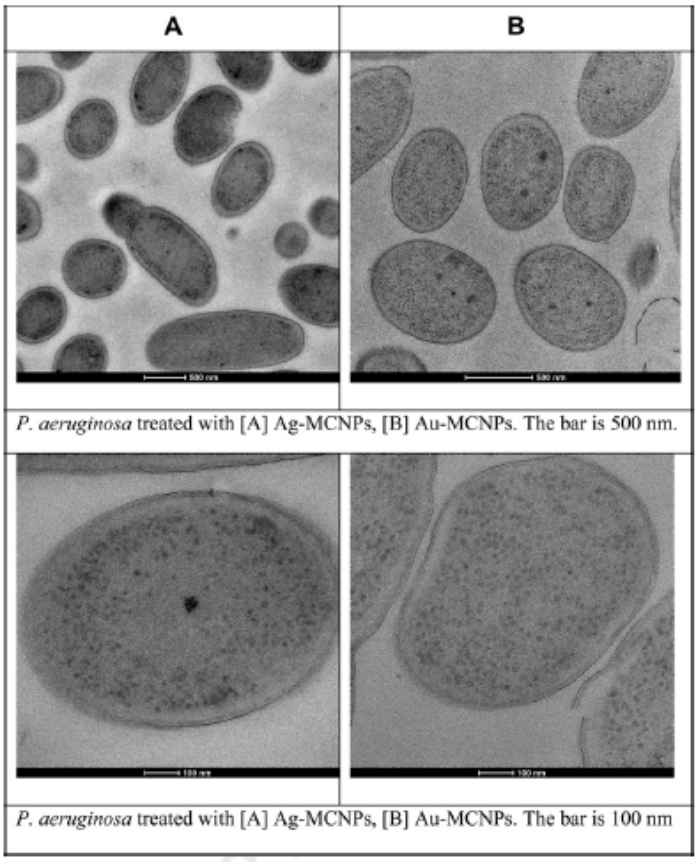

Fig. 137 TEM micrographs of *P. aeruginosa* pretreated with Ag- or Au-MCNPs.

IV-2.3.3.4 Microscopic Observation of the Adherent Biofilm and its Components.

The ability of *P. aeruginosa* to form an adherent biofilm after pretreatment with MCNPs, the viability of the formed biofilm cells and the production of EPS were assessed by CLSM using double live/dead staining with the addition of Con A as a third stain. The biofilm were grown on glass coverslips that were placed in petri dishes containing aqueous suspensions of ~10^7 CFU ml^{-1} non-treated (control) or Ag-MCNPs pretreated *P. aeruginosa* cells. Fig. 138 shows representative CLSM images.

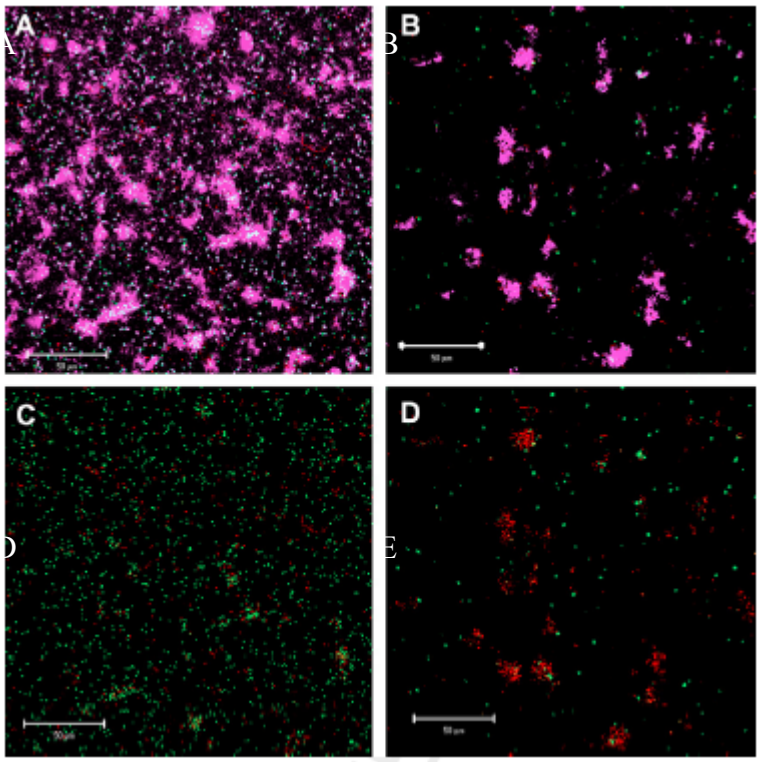

Fig. 138 CLSM micrographs of *P. aeruginosa* cells. [A] Non-treated cells on glass coverslip stained with SYTO 9 (green) for live cells, PI (red) for dead cells and ConA (violet) for EPS, 46 h incubation, bar = 50 nm; [B] cells on glass coverslip pretreated with 45 μg ml^{-1} Ag-MCNPs and stained with SYTO 9, PI and ConA, 46 h incubation, bar = 50 nm; [C] non-treated cells on glass coverslip stained with SYTO 9 and PI, 46 h incubation, bar = 50 nm; [D] cells on glass coverslip pretreated with 45 μg mL^{-1} Ag-MCNPs and stained with SYTO 9 and PI, 46 h incubation, bar = 50 nm

Most of the adherent non-treated control bacteria were alive and evenly dispersed across the slide (Fig.138C), and EPS was produced and was also evenly dispersed (Fig. 138A). Less EPS was produced or attached to the slide in the suspension that was pretreated with Ag-MCNPs (Fig. 138B) and only a few bacteria were attached to the glass slides (Fig. 138D).

In parallel to preparing the CLSM specimens, the same suspensions were grown in microtiter plates under the same conditions (46 h incubation at 37^{o}C) for an assessment of relative biomass. The relative biomass for the suspension pretreated with Ag-MCNPs (Fig. 138B, E) was 9%. Fig. 138B shows that Ag-MCNPs pretreated cells were able to produce EPS although they succeeded to form relatively low adherent biofilm. Moreover, not all the possible EPSs' compound may be recognized by staining with ConA since Con A binds to α-manopyranosyl and α-glucopyranosyl sugar residues (Chen et al., 2006); which means that perhaps other EPS compounds were produced but not stained.

The initial attachment of bacteria to surfaces is a crucial stage in the process of biofilm growth into a mature biofilm, and it is controlled by, among other things, bacterial factors, including gene expression for functions such as adhesion, motility organelles or surface proteins (Hoffman et al., 2005; O'Toole and Kolter, 1998). Stress conditions may lead to the postponement of cellular pools of high-energy functional compounds (Minsky et al., 2002). Furthermore, the antimicrobial ability of silver has been related to its disruption of energy metabolism (Roe et al., 2008). Thus, it is inferred that the presence of Ag-MCNPs results in stress and a change in the energy balance

To summarize, this study presented the use of Ag-MCNPs as a strategy for retardation of biofilm formation that could be implemented to control biofouling in water membrane filtration systems. However, to fully understand the limitations and possibilities associated with the use of Ag-MCNPs, further research is needed to identify the impact of Ag-MCNPs on molecular mechanisms related to biofilm formation such as gene expression. Other interesting aspects that might be examined are the differentiation between initial adhesion to surfaces of the cells after treatment from the subsequent steps that include development of micro-colonies and mature biofilm. Additionally, further research will study the impact of Ag-MCNPs treatment on biofouling using indigenous microorganisms in natural waters.

IV-2.3.4 Characterization of Alginate-Like Exopolysaccharide Isolated from Aerobic Granular Sludge

IV-2.3.4.1 Alginate-Like Exopolysaccharide (ALE) Yield and its Identification

The extracted ALE had the same dark brown color as the aerobic granules. Its yield was (147±6) mg/g SS with ash content of (9.39± 0.46) %.

Precipitate was formed when ALE solution was mixed with $CaCl_2$ solution, and no precipitate appeared when ALE solution reacted with saturated $(NH_4)_2SO_4$ solution. The positive results of these two identification tests confirm that ALE contains a large quantity of alginate (FAO/WHO, 1997).

According to FAO/WHO alginates identification tests, besides the specific reaction with $CaCl_2$ and saturated $(NH_4)_2SO_4$, alginates should manifest cherry red color after their solutions mix with acid ferric sulfate (FAO/WHO, 1997). It was discovered that ALE present a kind of cherry red color in the reaction after partial decolouration by the activated carbon for 1 hour (Fig. 139). However, this color is dissimilar with that of seaweed alginate. An explanation for this difference could be that ALE is produced by bacteria; the significant difference between bacterial alginates

and seaweed alginates is that bacterial alginates are O-acetylated while seaweed alginates are lack of O-acetyl group. The properties of polysaccharides highly depend on their chemical structures: slight changes as the degree of acetylation may cause considerable differences (Sutherland, 2001).

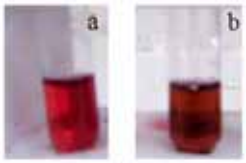

Fig. 139 Acid ferric sulfate identification test results of seaweed alginate (a) and alginate-like exopolysacharide from granular sludge (b).

IV-2.3.4.2 Alginate-Like Exopolysaccharide (ALE) Characterization

Chemical analyses

Total carbohydrate determination

ALE had maximum absorbance at 485 nm (A_{485}) in the phenol-sulfuric acid assay, indicating that uronic acid is its main carbohydrate component (Pedersen et al., 1989). A_{485} was proportional to its concentration over a wide range, presenting a linear relationship with low slope (Fig. 140).

The two sugar standards, D-glucose and seaweed alginate showed absorbance maxima at 490 nm (A_{490}) and 485 nm respectively. As their concentration increased, A_{490} of D-glucose sharply grew, while A_{485} of seaweed alginate slowly rose. Significantly different linear curves were followed between these two sugar standards. If D-glucose was used as the internal standard, the carbohydrate content of seaweed alginate would be underestimated by 62.6%.

Regarding ALE's carbohydrate content determination, the value obtained by choosing seaweed alginate as the standard was at least three times higher than if D-glucose was selected (Table 21). Thus, ALE's total carbohydrate content determined by the phenol-sulfuric acid assay was greatly dependent on the selection of the standard. Likewise, Handa (1966) checked the total carbohydrate content of one sea water sample with 8 different kinds of sugar as the standards respectively; the absorbance widely diverged from 100% for D-xylose to 35% of L-fucose. As ALE demonstrated clear alginate characteristics in the identification tests, seaweed alginate was selected as the internal standard to quantify ALE's carbohydrate content. The equivalent value is (486.2±22.3) mg sugar/g ALE. It is noted that even seaweed alginate concentration-absorbance curve is greatly indifferent from that of ALE. Predicted from ALE's positive results in the

identification tests, the seaweed alginate equivalent value might still underestimate ALE's real carbohydrate content.

Table 21 Granular sludge alginate like exopolysaccharide total carbohydrate content estimated by selecting D-glucose and seaweed alginate as internal standard

ALE concentration (mg/L)	Absorbance	Total carbohydrate content(mg/g)	
		seaweed alginates equivalent y=0.0017x +0.0039	D-glucose equivalent y=0.0057x+0.0313
800	0.652	476.5	136.1
400	0.331	481.0	131.4
200	0.171	491.4	122.5
80	0.075	522.8	95.8

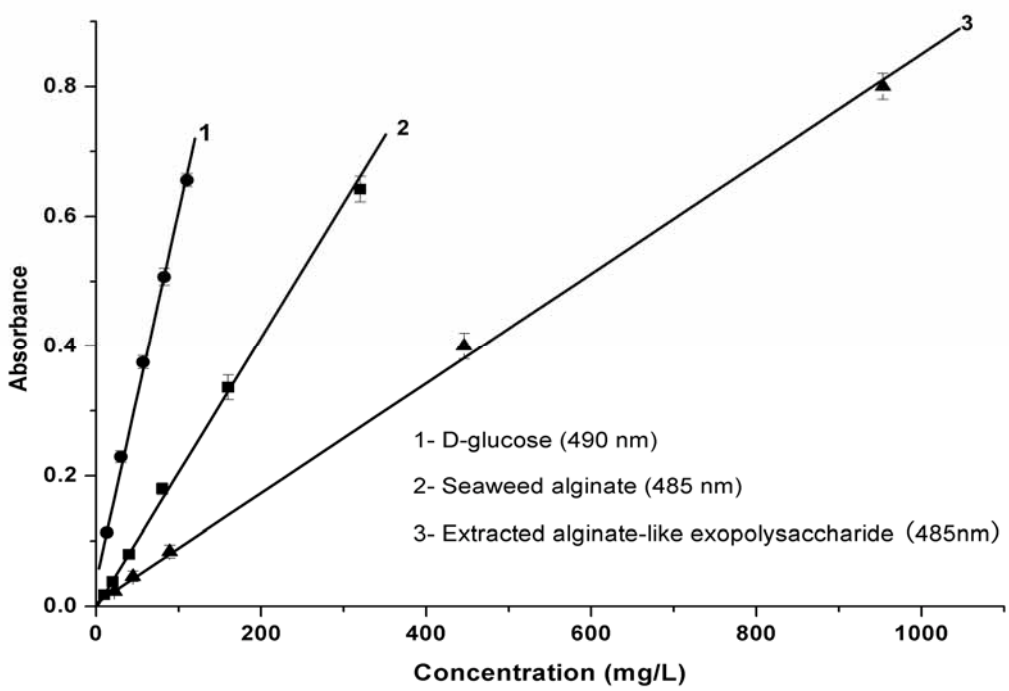

Fig. 140 Concentration-absorbance curves of D-glucose, seaweed alginate and alginate-like exopolysaccharide from granular sludge in phenol-sulfuric acid assay for total carbohydrate determination

Protein determination

ALE protein content was measured by the Bradford assay. Without the addition of ALE sample or protein standard, spectrum of the Coomassie brilliant blue G250 dye (blank) presented absorbance maxima at 466 and 645 nm respectively (Fig. 141). After the addition of bovine serum albumin, the absorbance curve was totally changed. Intense absorbance appeared at 595nm, while the absorbance at 466 nm was completely disappeared. In contrast, when ALE mixed with the dye, precipitation formed as ALE concentration was higher than 500 mg/L. This was due to the formation of alginic acid at the acidic pH of the assay (pH=1.1). As ALE concentration was lower than 500 mg/L, the spectrum after reaction was similar with that of the blank. Although the curve had significant absorbance at 595 nm, it was still the typical absorbing spectrum of Coomassie brilliant blue G250 dye at pH 1.1, but not the specific one of dye-protein complex. No linear relationship was followed between ALE's concentration and the absorbance. Hence, ALE's protein content is under detection limit by the Bradford assay.

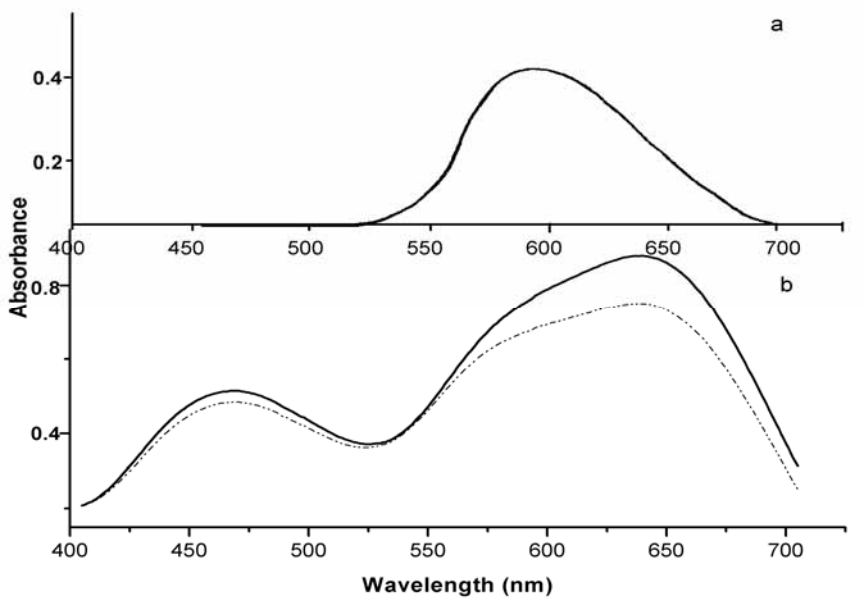

Fig. 141 Spectra of dye-protein complex, blank and alginate-like exopolysaccharides from granular sludge in the Bradford assay. a:100 mg/L bovine serum albumin;b: blank (solid line) and 400 mg/L alginate-like exopolysaccharide from granular sludge (dash line)

Gel formation property

As 2% ALE solution was dropped into 2% $CaCl_2$ through Pasteur pipette, self-standing gel beads with good mechanical stability immediately produced (Fig.142a). Clearly, ALE displayed perfect

gel formation property when it interacted with Ca^{2+}. Its gelation process is dissimilar with proteins', which requires preliminary denaturation by heating, applying high pressure, or chemical treatment, before gelling with divalent cations (e.g., Ca^{2+}) (Totosaus et al., 2002). It is also distinguished from some polysaccharides like agar, glucuronan, pectin and so on, which only gel at specific temperatures (Braccini et al., 1999). ALE totally demonstrated alginates' unique gelation property with divalent cations, i.e. forming heat irreversible gels in a wide range of temperatures and pHs (Sobeck and Higgins, 2002).

Aerobic granular sludge can be characterized as a kind of hydrogel. ALE's perfect gelation capability implies that it should play an important role in the formation and stability sustaining of aerobic granules.

The gel beads micro-structure was revealed by introducing ruthenium red staining in TEM ultra-thin section (Fig. 143b). Alginates are composed of uronic acid residues; each residue contains one COO^- group. Ruthenium red can form precipitate on COO^- groups, helping increase electronic density in TEM (Waller et al., 2004). It was discovered that the gel bead was able to be heavily stained by ruthenium red, indicating the existence of great numbers of COO^- groups in ALE. The gel bead was structurally homogeneous. Electron denser rods with various sizes and extended fine fibers became two main components. Those fine fibers connected the rods, aiding in establishing a well organized network.

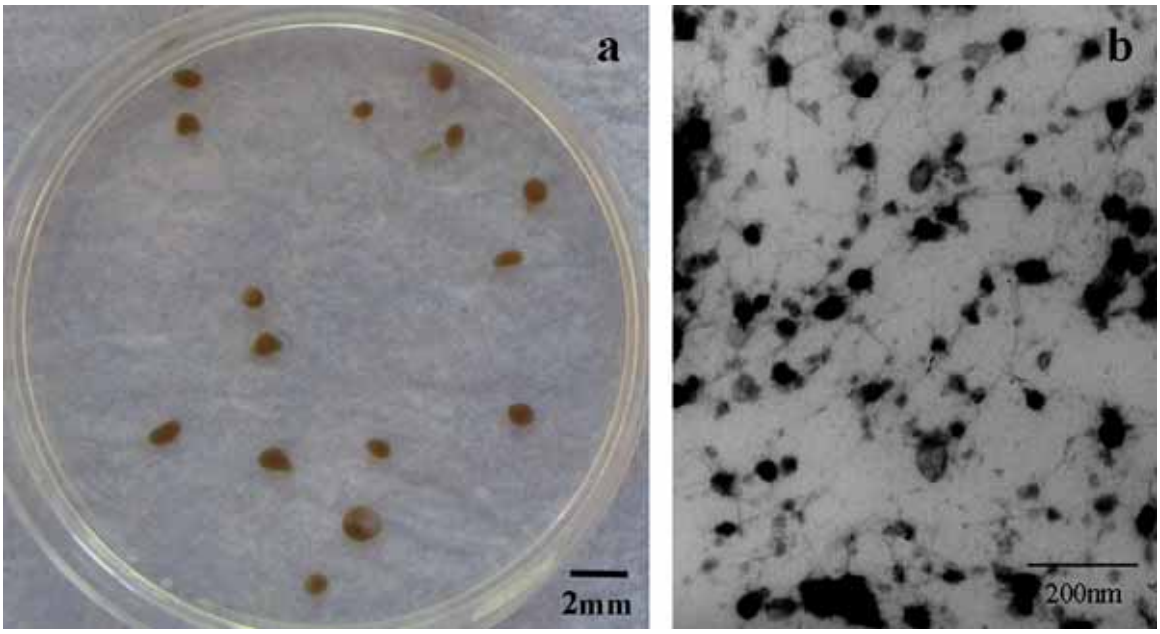

Fig. 142 Gel spheres formed after 2% alginate-like exopolysaccharide solution was extruded into 2% $CaCl_2$ (a), and the microstructure of the gel bead observed by TEM after ruthenium red staining (b)

Blocks fractionation

Alginates are composed of mannuronic acid (M) and guluronic acid (G) residues. These two uronic acid residues can be arranged in homopolymeric blocks [poly(mannuronic acid) (MM) and poly(guluronic acid) (GG)] or heteropolymeric blocks (MG), distributing randomly in alginate molecules (Davis et al., 2003). Their proportion, distribution and length, determine the chemical and physical properties of alginate molecules. In general, GG blocks provide gel-forming capacity, MM and MG blocks provide flexibility to the chains (Melvik and Dornish, 2004).

According to Leal et al. (2008), fraction 1 obtained by partial hydrolysis with 0.3 M HCl is mainly composed of heteropolymeric blocks (MG block), fraction 2 soluble at pH 2.85 is enriched in MM block, and fraction 3 insoluble at pH 2.85 is enriched in GG block. The recovery yield after ALE fractionation was (85.39±7.22)%, with MG fraction (14.57±2.25)%, MM fraction (2.10±1.43)%, and GG fraction (69.07±8.95)%.

Alginates' gel forming capacity is decided by the presence of GG blocks (Leal et al., 2008). ALE's GG fraction reached (69.07±8.95)%, such high percentage elucidated ALE's perfect gel formation capacity with Ca^{2+}. On the other hand, the presence of MM and MG fractions is also necessary. They provide flexibility to the chains, connect GG blocks and aid in establishing network structure during gelation. As GG blocks were found to have rod-like structure (Sadoff, 1975), it can be predicted that those electron condensed rods observed by TEM (Figure 143b) are rich in GG blocks, while those fine fibers are rich in MG and/or MM blocks.

Spectroscopic analysis

UV-visible spectroscopy

ALE displayed similar UV-visible spectrum with seaweed alginate (Fig. 143). Within the wavelength range of 190-800nm, both spectra had absorbance maxima at 193nm; no clear peaks appeared at 260nm and 280nm, which are considered as the typical peaks of DNA and proteins, respectively. Therefore, DNA and proteins are under detectable range by UV-visible spectroscopy.

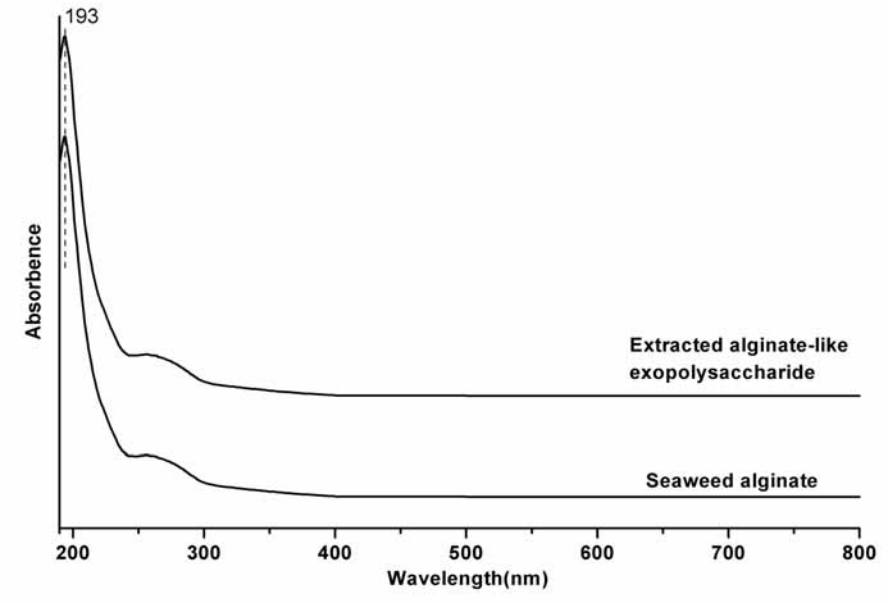

Fig. 143 UV-visible spectra of alginate-like exopolysaccharide from granular sludge and seaweed alginate.

MALDI-TOF MS

Similar MALDI-TOF MS spectra were also presented between O-deacetylated product of ALE and seaweed alginate (Fig. 144). The interval between peaks is 176, which happens to be the molecular mass of uronic acid monomer ($C_6H_8O_6$). Those peaks detected are oligosaccharides debris of sodium alginic acid (monosaccharide, disaccharide, trisaccharide and so on, $(C_6H_8O_6)_nNa^+$).

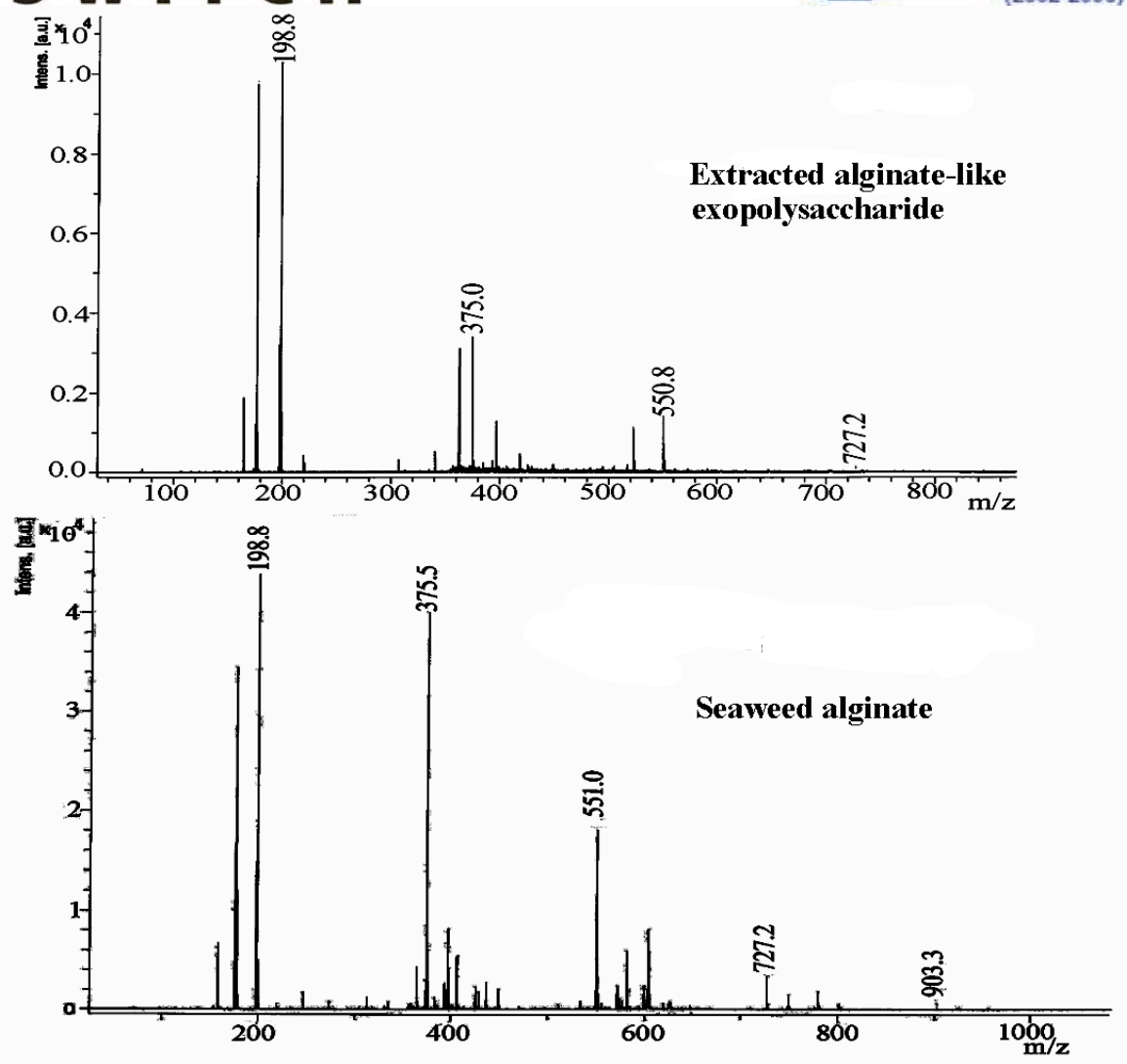
Intens. [a.u.]
×10⁴
1.0
0.8
0.6
0.4
0.2
0.0
198.8
375.0
550.8
727.2
100
200
300
400
500
600
700
800
m/z
Extracted alginate-like exopolysaccharide
Intens. [a.u.]
×10⁴
4
3
2
1
0
198.8
375.5
551.0
727.2
903.3
200
400
600
800
1000
m/z
Seaweed alginate

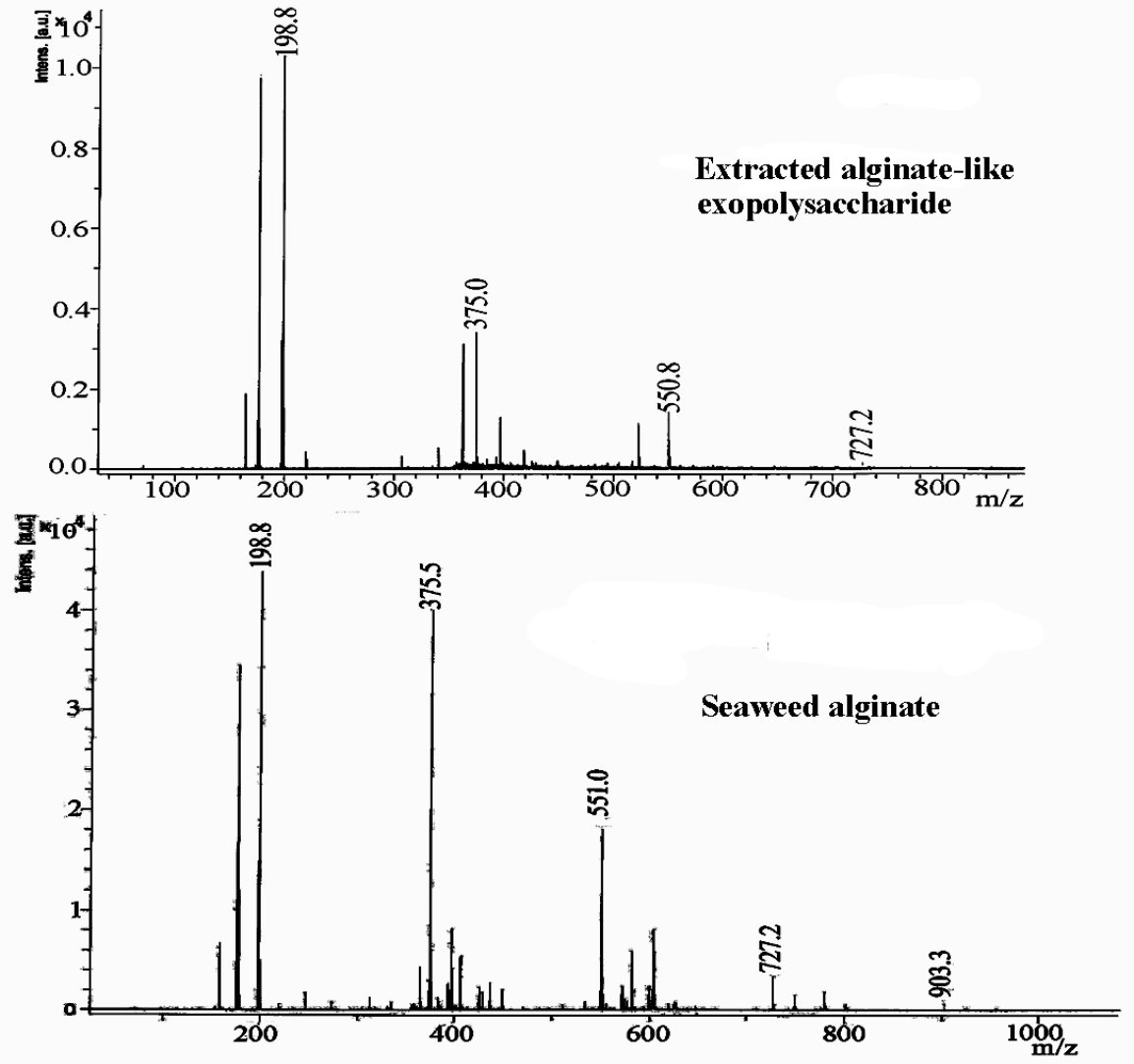

Fig. 144 MALDI-TOF spectra of alginate-like exopolysaccharide from granular sludge and seaweed alginate.

FT-IR and the second-derivative spectra

FT-IR spectroscopy has been a useful tool in monitoring structural changes in biopolymers. The FT-IR spectra of the aerobic granules and ALE were given in Fig. 145. Both of them demonstrate typical bands of polysaccharides: a broad rounded absorption band above wavenumber 3000 cm^{-1} assigned to O-H stretching vibrations, a weak C–H stretching peak at 2927 cm^{-1} and a strong and broad stretch of C–O–C, C–O at 1000–1200 cm^{-1} (Bramhachari et al., 2007).

Mannuronic and guluronic acid residues are the repeating units in alginate molecules; each of them contains one $–COO^-$ group (Figure 146). The bands at 1654cm^{-1} and 1400 cm^{-1} in the spectrum of ALE correspond to the asymmetric and symmetric stretching of carboxylate O-C-O vibration respectively (Silverstein et al., 1991). The band at 1539 cm^{-1} is assigned to the C=C in pyronose ring, which may be caused by the β-elimination effect of alginate lyases. The band at 1240cm^{-1} is assigned to the presence of O-acetyl ester for bacterial alginates (Kazy et al., 2002).

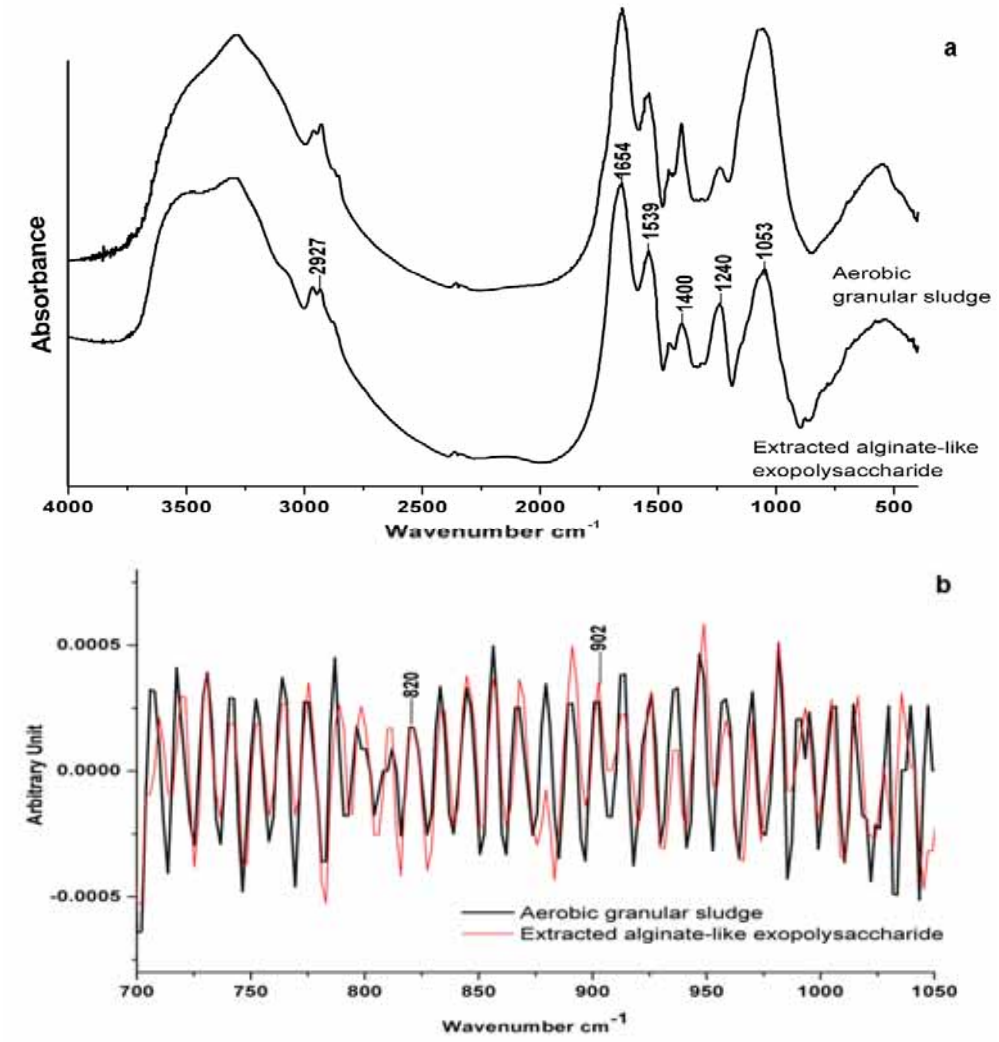

Fig. 145 FT-IR spectra of aerobic granular sludge and alginate-like exopolysaccharide from granular sludge (a: normal FT-IR spectra; b: secondary derivative spectra at fingerprint region for carbohydrate)

The spectrum of aerobic granular sludge is surprisingly similar with that of ALE, implying that ALE is distributed widely in the granules. The amide III, II, I and A vibrational modes of proteins, which have infrared absorption around 1200 cm^{-1}, 1500 cm^{-1}, 1700 cm^{-1}, and 3500 cm^{-1} respectively (Hayashi and Mukamel, 2008), could not be clearly seen in the spectrum of the granules. They are probably mixed or shielded by ALE's bands of O-acetyl group, C=C in pyronose ring, $–COO^-$, and –OH around these wavenumbers. The bands at 1400 and 1053 cm^{-1} show higher density in the spectrum of aerobic granular sludge, which may be caused by the existence of proteins and other kinds of polysaccharides.

The 950-750 cm^{-1} region is the fingerprint (or anomeric) region of carbohydrate; the second-derivative spectrum in this region is proved to give more information (Oust et al., 2006). Both aerobic granular sludge and ALE's second-derivative spectra presented more bands than the normal spectrum in this region and great similarities were shown between them. The band at 820 cm^{-1} is assigned to the C1-H deformation vibration of β-mannuronic acid residues. The band at 902 cm^{-1} is due to anomeric C-H deformation vibration of α-L-guluronic acid residues (Chandía et al., 2001).

Given the resemblance between aerobic granular sludge and ALE in FT-IR spectrum, it can be estimated that a large proportion of the dry weight of aerobic ranules is ALE, and thus could be concluded that ALE is one of the dominant exopolysaccharides in aerobic granular sludge.

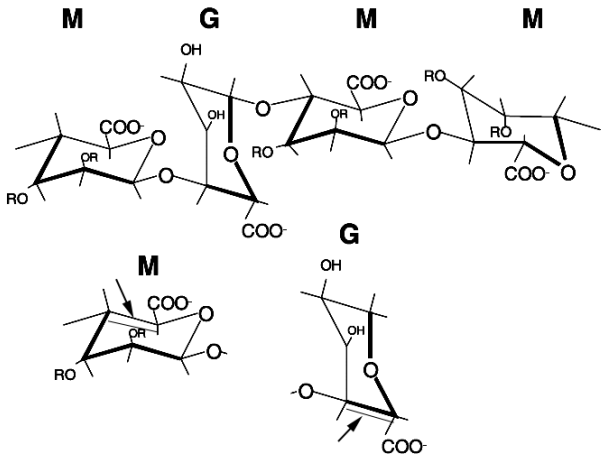

Fig. 146 Bacterial alginate monomers (M: mannuronic acid residue, G: guluronic acid residues, R= H or $–COCH_3$, the arrows indicate the possible positions of C=C) (based on Donali and Paoletti, 2009)

Electrophoresis analysis

Results of ALE electrophoresis are demonstrated in Fig. 147. Lane 1 and 2 are ALE and seaweed alginate stained by Coomassie brilliant blue G250 for proteins respectively; lane 3 and 4 are ALE and seaweed alginate stained by Toluidine blue O for acid polysaccharides respectively (Fig. 150).

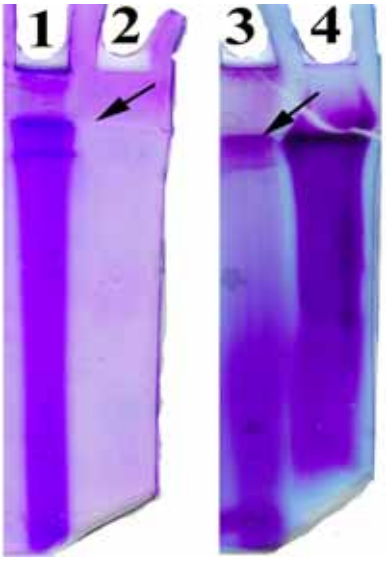

Fig. 147 Electrophoresis gels of ALE and seaweed alginate (Sigma). Lane 1 and 2: ALE and seaweed alginate (7ug/ul) stained by Coomassie brilliant blue G250 for protein detection respectively. Lane 3 and 4: ALE and seaweed alginate (7μg/μl) stained by Toluidine blue O for acid polysaccharides detection respectively. The arrow indicates the boundary between the stacking and running gels.

It was found that ALE retained the colour of Coomassie brilliant blue G250, but no protein bands formed (lane1). In contrast, the seaweed alginate did not retain the colour at all (lane 2). Likewise, Pedersen et al. (1989) observed that bacterial alginates produced by *Pseudomonas aeruginosa* were able to be stained by Coomassie brilliant blue, while calcium alginic acid instead of sodium alginic acid from seaweed showed such phenomenon. As alginate dose not retard the migration of proteins in gels (Pedersen et al., 1989), no protein band observed displays that ALE's protein content is less than the lower detection level. This result is in agreement with what has been discovered through UV-visible spectroscopic analysis and Bradford assay: ALE's protein content is undetectable.

The gel for polysaccharides staining was positively stained by Toluidine blue O (lane 3 and 4), manifesting that both ALE and seaweed alginate contain acid polysaccharides.

Thus, ALE was able to retain the color of Coomassie brilliant blue G250; it mainly demonstrated acid polysaccharide's property in electrophoresis.

IV-2.3.4.3 Exopolysaccharides Investigation Based on Specific Extraction Method

Alginate enriched exopolysacchairde was extracted from aerobic granular sludge cultivated in pilot plant treating municipal wastewater. The dry weight of the aerobic granules contained more than 10% ALE. It is noted that ALE is only one component of total exopolysaccharides in the granules, but its proportion is even higher than the total exopolysaccharides content reported in some literature. This is probably due to the fact that ALE extraction was based on the specific method for alginate extracting, while those extraction methods employed in literature took exopolysaccharides as a whole target, they are likely to underestimate the amount of alginate-like exopolysaccharide.

In effect, aerobic granular sludge is a complex microbial consortium, in which various kinds of exopolysaccharides can be synthesized. Some of them are neutral, some are polyanionic and others are polycationic macromolecules (Sutherland, 2001). These exopolysaccharides do not exist alone, but may interact with a wide range of other molecular species, including proteins, lipids, metal ions as well as other exopolysaccharides through electrostatic forces, hydrogen bonds and/or biochemical reactions (Rickard, 2000). This leads to a dense and compact tertiary network structure, making it almost impossible to extract all the exopolysaccharides by one method. Regarding this situation, specific extracting methods may help collecting more material due to its enrichment of the specific target. Furthermore, as polysaccharides properties highly depend on their chemical structures (Villain-Simonnet, 2000), isolation of specific exopolysaccharides provides the opportunity for further structure-function investigation.

IV-2.3.4.4 Alginate-Like Exopolysaccharide's Characteristics and Role in Aerobic Granular Sludge

Following the method of alginate extraction from seaweed, the exopolysaccharide extracted from aerobic granules resembled seaweed alginate in the reactions with $CaCl_2$ and saturated $(NH_4)_2SO_4$, perfect gel formation property with Ca^{2+}, UV-visible and MALDI-TOF MS spectra. On the other hand, it was dissimilar with seaweed alginate in the reactions with acid ferric sulfate, phenol-sulfuric acid and Coomassie brilliant blue G250, which may be attributed to the O-acetylation of bacterial alginates.

The quantity of alginate-like exopolysaccharide extractable from aerobic granular sludge reached (147±6) mg/g SS with an ash content of (9.39±0.46) %. The great similarities between aerobic granular sludge and alginate-like exopolysaccharide in their FT-IR and second-derivative spectra indicates that ALE is distributed throughout the whole sludge granule and located to a few micro-environments.

The wide distribution of ALE may benefit the aerobic granules in maintaining their stability and integrity. Alginates readily form rigid, non-deformable gels due to their highly specific interaction with divalent cations. This property has been widely used in immobilization of cells and enzymes (Melvik and Dornish, 2004). Alginate gel is unique that it can be formed in a broad temperature and pH range, while most of polysaccharides and proteins have special requirements on these two parameters to form gel (Braccini et al., 1999). Hence, the naturally formed ALE gel undoubtedly contributes to the strong physical structure of aerobic granules and offers microorganisms the same inhabitancy and protection as the manmade alginate immobilization carriers do. It may also entrap proteins, lipids, metal ions as well as other exopolysaccharides through chemical and/or physical interactions, aiding in establishing dense and compact tertiary network structure in aerobic granular sludge.

IV-2.3.4.5 Structure–Function Relationship Of Alginate-Like Exopolysaccharide

Alginates consist of heteropolymeric and homopolymeric blocks as MG, MM and GG blocks. They contribute unequally to alginates' property due to their substantially different geometries. Especially, GG blocks are buckled. If two GG blocks are aligned side by side, diamond shaped holes result. Their dimensions are ideal for the crosslink with divalent cations (especially Ca^{2+}). This is the so-called "egg-box" model (Christensen et al., 1990) (Fig. 148). Hence, the gel-forming capacity of alginates depends on the presence of GG blocks. MM and MG blocks do not contribute to the crosslink of divalent ions; they decide the flexibility of alginate chains (Melvik and Dornish, 2004).

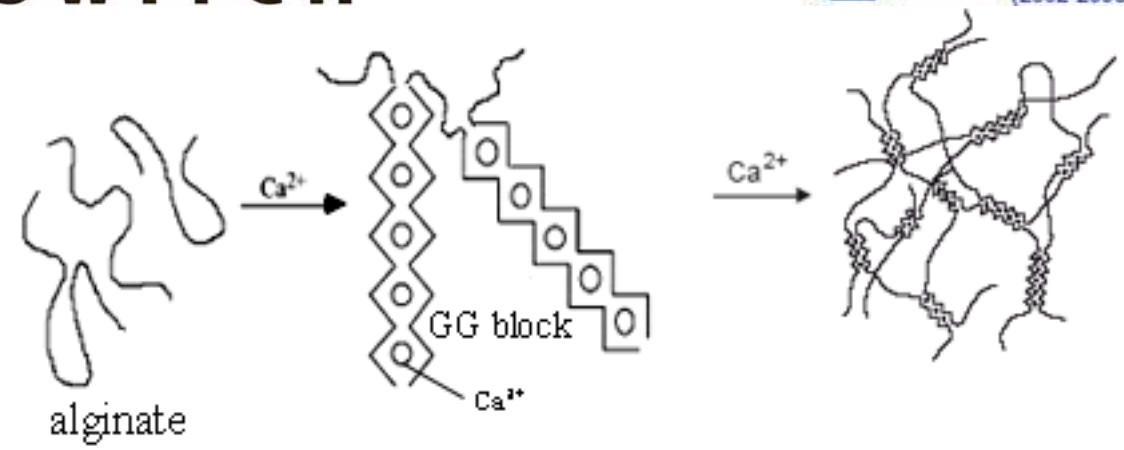

Fig. 148 "Egg-box" model of the GG blocks in alginate

ALE in aerobic granular sludge was found to have an MG fraction of (14.57±2.25)%, an MM fraction of (2.10±1.43)%, and a GG fraction of (69.07±8.95)%. This chemical structure of ALE highly involves in raising the hydrophobicity, strength and flexibility of aerobic granular sludge. Once ALE crosslinks with Ca^{2+} in wastewater, the GG-Ca segments turn to insoluble (Jiang et al., 2006) and become the hydrophobic regions of ALE thereafter, while MM and MG blocks are the hydrophilic regions. The high percentage of GG blocks of ALE may contribute to the frequently claimed hydrophobicity of aerobic granular sludge as described in previous studies (Zhang et al., 2007). Contributions to hydrophobicity were normally considered to originate from extracellular proteins (Zhang et al., 2007). However, it should not be forgotten that besides proteins, a few exopolysaccharides might also be hydrophobic or possess hydrophobic regions (as alginates), because of their composition and tertiary structure (Neu and Poralla, 1988).

Selection by settling velocity and applied shear stress are two of the factors responsible for the formation and stability of aerobic granular sludge (Beun et al., 2000). The high proportion of GG blocks enables ALE to crosslink with more divalent cations, to form a compact and strong gel. It might well be that bacteria producing weaker exopolymeric matrix are washed out of the system since they cannot form a stable structure under these conditions. Consequently, this ALE gel may play a significant role in increasing the settling ability of the granules by maintaining the integrity of the structure in the mixed reactors, but also because the density will be higher than a normal exopolymeric matrix. Applying a selection pressure for rapid settling granules during start up, might enhance or select also for the GG block formation. However, this should be further investigated by analyzing the biomass during start-up of an aerobic granular sludge reactor.

As the flexibilities increase in the order of GG<MM<MG (Melvik and Dornish, 2004), the higher percentage of MG blocks than MM blocks endows ALE with good flexibility, increases

the elasticity of ALE gel, and eventually could enhance the capability of the aerobic granules to be stable in the strong shear stress in the reactor.

IV-2.3.4.6 Bacterial Alginates in the Mixed Consortium

ALE is produced by bacteria. High proportion of GG blocks is one of its important characteristics. So far, the two bacterial genera *Pseudomonas* and *Azotobacter* have been described to produce alginate (Remminghorst and Rehm, 2006). In contrast to ALE, alginate produced by P. *aeruginosa* totally lack GG blocks. Only alginate in the outer layer of *Azotobacter vinelandii*'s cyst highly enriched in GG blocks (Rehm et al. 1996).

It is worth pointing out that alginate consists of M and G residues. These two residues are epimers. The biosynthesis of G residue is a postepimerization process. *Azotobacter* additionally modifies its alginates by extracellular epimerases (Rehm et al. 1996), i.e. G residues and consequently MG and GG blocks are produced extracellularly. In a mixed consortium as exists in aerobic granular sludge, possibilities may exist that alginates produced by both *Pseudomonas* and *Azotobacter* or other bacteria are exposed to those extracellular epimerases simultaneously, resulting in ALE with a high proportion of GG blocks.

Biofilms play a detrimental part in biofouling, causing significant problems in membrane filtration processes and water distribution systems. Within various kinds of biofilms, aerobic granular sludge is considered as a special case. It is the collection of cells self-immobilized through EPS into a spherical form, without any involvement of carrier material.

The major problem for studying exopolysacchairdes in biofilms is the small exopolysaccharides quantity derived from the real biofilm, which hinders further fine structure analysis. Aerobic granular sludge is a special case of biofilm, they definitely have common exopolysaccharides characteristics with the normal biofilms. Methods established in aerobic granular sludge, as specific isolation for functional gel-forming exopolysaccharides, blocks fractionation for chemical structure identification, and integrated methods (UV-visible spectroscopy, FT-IR spectroscopy and Mass spectrometry) for isolated exopolysaccharides characterization may be extrapolated or being referenced to normal biofilms.

Gel-forming exopolysacchairdes investigation in aerobic granular sludge may further contribute to better understanding biofouling, and establishing strategies for biofouling control, e.g., by finding the appropriate methods to destroy the gel network structure in biofouling, which is the basic structure for biofouling formation.

IV-2.4 CONCLUSIONS

- EF-UF/MF effectively removed phosphate and suspended particles, greatly increased phosphate and turbidity removal rate. The addition of EF as a pretreatment of membrane filtration significantly improved the filtration curve and reduced the filtration energy requirement. Constructed wetland and polishing pond not only improved water quality but also changed particle property. Combination of both units would multiply their treating abilities.
- There is a slight improvement of the overall process of CW-EF-GF configuration over EF-GF-CW configuration reported last year. The comprehensive reporting on this innovative topic including process optimization, which is in the framework of MS thesis, is in advanced stages and expected to be ready by the end of the current academic year.
- Constructed wetland–electroflocculation–-membrane filtration system implies shorter residence time and better water quality, thus reduces land, construction and maintenance costs as well as water loss. The system can be optimized for different treatment plants for phosphorous removal primarily by controlling EF working time, which actually represents coagulant dose.
- Pretreatment by both aluminum-based and iron-based EF can significantly decrease (up to 90%) filtration-energy consumption in dead-end microfiltration. The aluminum-hydroxide amorphous solids formed during sweep coagulation are responsible for the mitigation of both internal and external fouling. The cake built up by those amorphous solids forms a secondary membrane that filters out the primary particles and prevents them from penetrating the membrane pores, consequently decreasing internal fouling intensity. The amorphous solids also decrease the hydraulic resistance of the cake when external fouling serves as the dominant fouling mechanism.
- Longer EF operation times lead to the formation of a larger number of aluminum-hydroxide particles and to a higher cake-accumulation rate, which increases the external fouling intensity. Superposition of the positive and negative effects of EF will dictate the optimal EF operation time for each suspension, i.e. that at which the lowest energy consumption is achieved.
- The optimum pH value for aluminum-based EF pretreatment operation ranges from 6 to 6.5. The optimum pH value for iron operation is >7, where rapid oxidation rates of Fe^{2+}

to Fe^{3+} exist. At lower pH values, a detectable residual iron concentration may lead to visual, odor and taste problems. Working at the optimum pH provides (a) the lowest optimum EF operation time, (b) the strongest minimization of filtration energy and (c) the lowest concentration of residual aluminum. This can be explained by the minimal solubility of the metal and the pH dependency of its hydroxide's surface charge and structure. The primary particles and the mettalic-hydroxide particles transfer to and accumulate on the membrane surface where they contact each other and agglomerate, thus even without slow mixing, pronounced filtration-energy minimization can be achieved.

- Applying EF has an advantage of almost complete restoration of initial flux rates by simple physical washing of the membrane surface with tap water. This lowers the energy and water consumed during the cleaning procedure and leads to a longer life expectancy for the membrane.
- It is suggested, that the effect of electroflocculation on fouling mitigation can be higher in microfiltration than in ultrafiltration as was observed. Considering theoretically only external fouling mechanism, clean membrane resistance is a very important factor that control the affects of colloidal fouling on the flux decay. For the same filtrated volume and solution, the higher the clean membrane resistance, the lower is the fouling effect. As results of that, the lower the clean membrane resistance the higher the fouling mitigation that can be achieve by using fouling mitigation methods. Further investigation is needed for understanding the effects of electroflocculation on the internal fouling in filtration of secondary effluent.

- Under specific conditions, Ag-MCNPs retarded biofilm formation, even when high percentage of planktonic *P. aeruginosa* cells survived the pre-treatment.
- Stable low values of relative biomass have been formed in the presence of Ag-MCNPs at various incubation times. Ag-MCNPs pretreated cells were able to produce EPS although they succeeded to form relatively low adherent biofilm.
- Ag-MCNPs pretreated cells appear well preserved and undamaged under TEM HPH/freeze micrographs, yet the intra cellular material seem to be pushed towards the peripheral parts of the cell, possibly indicating a survival strategy to the presence of Ag-MCNPs.

- The yield of extractable alginate-like exopolysaccharide reached 147±6 mg/g dry mass with an ash content of (9.39±0.46) %. It resembled seaweed alginate in the reactions with $CaCl_2$ and saturated $(NH_4)_2SO_4$, perfect gel formation property with Ca^{2+}, UV-visible and MALDI-TOF MS spectra. It distinguished from seaweed alginate in the reactions with acid ferric sulfate, phenol-sulfuric acid and Coomassie brilliant blue G250.
- Alginate-like exopolysaccharide is one of the dominant exopolysaccharides in aerobic granular sludge, it is distributed throughout the whole granule. It is one of the functional exopolysaccharides in maintaining aerobic granular sludge integrity.
- The fraction of blocks in the extracted alginate-like exopolysaccharides were: MG fraction (14.57±2.25)%, MM fraction (2.10±1.43)%, and GG fraction (69.07±8.95)%. This special characteristic plays an important role in providing aerobic granular sludge high hydrophobicity and a compact, strong and elastic structure.
- Gel-forming exopolysacchairdes investigation in aerobic granular sludge may further contribute to better understanding biofouling, and establishing strategies for biofouling control, e.g. by finding the appropriate methods to destroy the gel network structure in biofouling, which is the basic structure for biofouling formation.

REFERENCES

Abuzaid N.S., Bukhari A. and Al-Hamouz Z.M. (2002). Ground water coagulation using soluble stainless steel. *Adv. Environm. Res*. (6): pp. 325-333.

Adav, S.S. and Lee, D.J. Extraction of extracellular polymeric substances from aerobic granule with compact interior structure. J Hazard Mater. 154(1-3), (2008) 1120-1126

Adin, A. (1999) Particle characteristics: A key factor in effluent treatment and reuse. *Water Res*., 40: 67.

Adin, A. and Elimelech, M. (1989) Particle filtration for waste-water irrigation. *J. Irrig. Drain E-ASCE*., 115: 474.

Adin, A., and Sacks, M. (1991) Dripper clogging factors in wastewater irrigation. *J. Irrig. Drain E-ASCE.*, 117: 813.

Aguilar, M.I., Saez, J., Llorens, M, Soler, A. and Ortuno, J.F. (2003) Microscopic observation of particle reduction in slaughterhouse wastewater by coagulation-flocculation using ferric sulphate as coagulant and different coagulant aids. *Water Res.*, 37: 2233.

Al-Malack M. H., Abuzaid N. S., El-Mubarak A. H., Coagulation of polymeric wastewater discharged by chemical factory, Water Research, 33 (1999) 521-529.

Al-Malack M. H., Anderson G. K., Coagulation-crossflow microfiltration of domestic wastewater, J. Membrane Science, 121 (1996) 59-70.

Al-Malack M. H., Bukhari A. A., Abuzaid N. S., Crossflow microfiltration of electrocoagulation kaolin suspension: fouling mechanism, J. Membrane Science, 243 (2004) 143-153.

Al-Malack M. H., Bukhari A. A., Abuzaid N. S., Crossflow microfiltration of electrocoagulated kaolin suspension: fouling mechanism, J Membrane Science, 243 (2004) 143-153.

Amirtharajah, A. & Mills, K.M. (1982) Rapid-mix design for mechanisms of alum coagulation. Research & Technology, pp: 210-216.

Amirtharajah, A., (1988) Some Theoretical and Conceptual Views of Filtration, *J. Am. Water Works Ass*., 80: 6.

Annual Report 2008. Advanced water management centre, the Queensland University

APHA 1998. Standard Methods for the Examination of Water and Wastewater, 20th edn.; American Public Health Association: Washington, DC

Arora N., Davis R. H., Yeast cake layers as secondary membranes in dead-end microfiltration of bovine serum albumin, J Membrane Science, 92 (1994) 247-256.

Bagga A., Chellam S., Clifford D. A., Evaluation of iron chemical coagulation and electrocoagulation pretreatment for surface water microfiltration, J Membrane Science, 309 (2008) 82-93.

Baker, C., Pradhan, A., Pakstis, L., Pochan, D.J. and Shah, S.I. Synthesis and antibacterial properties of silver nanoparticles. J Nanoscience and Nanotechnology 5(2), (2005) 244-249.

Bektas, N., Akbulut, H., Inan, H., Dimoglo, A. (2004) Removal of phosphate from aqueous solutions by electro-coagulation. Journal of Hazardous Materials, (B106) pp: 101-105.

Ben-Sasson M., Adin A., Fouling mechanisms and energy appraisal in microfiltration pretreated by aluminum based electroflocculation, Journal of Membrane Science, 352(1), 86-94 (2010)

Ben-Sasson M., Adin A., Fouling mitigation by iron-based electroflocculation in microfiltration: mechanisms and energy minimization, Water Research, 44(13), 3973-3981 (2010).

Ben-Sasson M., Calmano W., Adin A., Iron oxidation processes in electroflocculation (electrocoagulation) cell, Journal of Hazardous Materials, 171 (2009) 704-709.

Beun, J.J., van Loosdrecht, M.C.M. and Heijnen J.J. Aerobic granulation. Water Science and Technology. 41(4-5), (2000) 41-48

Bishop, P.L. The role of biofilms in water reclamation and reuse. Water Science and Technology 55(1-2), (2007)19-26.

Blankert B., Betlem B. H. L., Roffel B., Dynamic optimization of a dead-end filtration trajectory: Blocking filtration laws, J. Membrane Science, 285 (2006) 90-95.

Braccini, I., Grasso, R. P. and Perez, S. Conformational and configurational features of acidic polysaccharides and their interactions with calcium ions: a molecular modeling investigation. Carbohydrate Research. 317, (1999)119-130

Bradford, M.M. 1976. A rapid and sensitive method for quantitation of microgram quantities of protein utilizing the principle of protein-dye-binding. Anal Biochem. 72,248-54

Bramhachari, P.V., Kavikishor, P.B., Ramadevi, R., Kumar, R., Rao, B.R., and Dubey, S.K. Isolation and characterization of mucous exopolysaccharide (EPS) produced by Vibrio furnissii strain VB0S3 J. Microbiol. Biotechnol. 17, (2007) 14–51

Brix, H. Plant use in constructed wetland and their function. In Dias, V. and J. Vymazal (Eds.). The 1st international seminar on the use of aquatic macrophytes for wastewater treatment in constructed wetland, (2003) Portugal pp. 81-109

Brock, T.D., Madigan, M.T., Biology and Microorganisms, Prentice Hall, New Jersey, 1991, p. 47, 312.

Brooks, A. S., Rozenwald, M. N., Geohring, L. D., Lion, L. W., & Steenhuis, T.M. (2000) Phosphorus removal by wollastonite: A constructed wetland Substrate. Ecological engineering, (15) pp: 121-132.

Carmona M., Khamis M., Leclerc J.-P., Lapicque F., A simple model to predict the removal of oil suspensions from water using the elwctrocoagulation technique, Chemical Engineering Science, 61 (2006) 1237-1246.

Chandia, N.P., Matsuhiro, B. and Vasquez, A.E. Alginic acids in Lessonia trabeculata: characterization by formic acid hydrolysis and FT-IR spectroscopy, Carbohydrate Polymers. 46, (2001) 81–87.

Chavez, A., Jimenez, B. and Maya, C. (2004) Particle size distribution as a useful tool for microbial detection. *Water Sci. Technol*., 50: 179.

Chen D., Weavers L. K., Walker H. W., Lenhart J. J., Ultrasonic control of ceramic membrane fouling caused by natural organic matter and silica particles, Journal of Membrane Science, 276 (2006) 135-144.

Chen X., Chen G., Yue P. L., Investigation on the electrolysis voltage of electrocoagulation, *Chemical Engineering Science*, 57 (2002) 2449-2455.

Chen Y., Dong B. Z., Gao N. Y., Fan J. C., Effect of coagulation pretreatment on fouling of an ultrafiltration membrane, Desalination, 204 (2007) 181-188.

Chen, M.Y., Lee, D.J., Yang, Z., Peng, F., Lai, J.Y. Fluorescent staining for study of extracellular polymeric substances in membrane biofouling layers. Environmental Science and Technology 40(21), (2006) 6642-6646.

Cheng T.-W., Lin C.-T., A study on cross-flow ultrafiltration with various membrane orientations, Separation and Purification Technology, 39 (2004) 13-22.

Choi, O., Deng, K.K., Kim, N.J., Ross, L., Surampalli, R.Y. and Hu, Z.Q. (2008) The inhibitory effects of silver nanoparticles, silver ions, and silver chloride colloids on microbial growth. Water Research 42(12), 3066-3074.

Choksuchart P., Heran M., Grasmick A., Ultrafiltration enhanced by coagulation in an immersed membrane system, Desalination, 145 (2002) 265-272.

Chopra, I. . Journal of Antimicrobial Chemotherapy 59(4), (2007) 587-590.

Christensen, B.E., Indergaard, M. and Smidsrød O..Polysaccharide research in Trondheim. Carbohydrate Polymers. 13, (1990) 239–255.

Clancy, J.L. and McCuin, R.M. (2005) Use of microscopic fluidic imaging for identification and quantification of organisms in water. Am. Water Works Ass., WQTC Conference.

Clesceri L. S., Greenberg A. E., Trussell R. R., Standard Methods for the examination of water and wastewater, APHA-AWWA-WPCF, 17th edition (1989) 3,102-3.106.

Coico, R., Kowalik, T., Quarles, J.M., Stevenson, B. and Taylor, R.K. (2006) Current Protocols in Microbiology. John Wiley & Sons, Inc., New York, USA.

Darby, J.L., Attanasio, R.E. and Lawler, D.F. (1992) Filtration of heterodisperse suspensions – modeling of particle removal and headloss. *Water Res*., 26: 711.

Davis, T.A., Llanes, F., Volesky, B., Mucci, A., Metal selectivity of Sargassum spp. and their alginates in relation to their α-L-guluronic acid content and conformation. *Environ. Sci. Technol*., 37 (2003) 261-267.

Davis, T.A., Volesky, B. and Mucci, A. A review of the biochemistry of heavy metal biosorption by brown algae. Water Research. 37, (2003) 4311-4317

Day, P.R. (1965) *Particle fractionation and particle-size analysis* in *Methods of Soil Analysis, part I*, American Society of Agronomy and Soil Science Society of America, Madison, Wisconsin, USA.

de Prijck, K., Nelis, H. and Coenye, T. (2007) Efficacy of silver-releasing rubber for the prevention of Pseudomonas aeruginosa biofilm formation in water. Biofouling 23(6), 405-411.

Den W., Huang C., Ke H.-C., Mechanistic study on the continuous flow electrocoagulation of silica nanoparticles from polishing wastewater, *Industrial & Engineering Chemistry Research*, 45 (2006) 3644-3651.

Denkhaus, E., Meisen, S., Telgheder, U. and Wingender, J. Chemical and physical methods for characterization of biofilm. Microchimica Acta 158(1-2), (2007) 1-27.

Dibrov, P, .J. Dzioba, K.K. Gosink, C.C. Hase, *Antimicrob. Agents Chemother.* 46 (2002) 2668.

Donali, I., Paoletti, S., Material properties of alginates. In: Rehm, B.H.A. (ed.), Alginates: Biology and Applications, Springer-Verlag, Berlin Heidelberg, (2009) 1-54.

Doty, R.C., Tshikhudo, T.R., Brust, M., Fernig, D.G., *Chem Mater.* 5 (2005) 4630.

Douglas, I., Thomas, D., Guthmann, J., Russell, S. and Springthorpe, S. (2004) Dynamic particle analysis: A new technology for optimizing particle removal in a water treatment plant. Water Quality Technology Conference.

Dror-Ehre, A., Mamane, H., Belenkova, T., Markovich, G. and Adin, A. Silver nanoparticle-E. coli colloidal interaction in water and effect on E. coli survival. Journal of Colloid and Interface Science 339(2), (2009) 521-526.

Duan J. and Gregory J., Coagulation by hydrolyzing metal salts, Advances in Colloid and Interface Science, 100-102 (2003) 475-502.

Dubois, M., Gilles, K.A., Hamilton, J.K., Rebers, P.A. and Smith, F. Colorimetric method for determination of sugars and related substances. Anal. Chem. 28, (1956) 350-356

Eaton, A.D., Rice, E.W., Baird, R.B. (eds.), Standard Methods for the Examination of Water and Wastewater, APHA-AWWA-WEF, 2005, 21st edition

Egozy, Y. (1996). Water recirculation through biological filter for coastal streams rehabilitation in Israel. MSc thesis, The Hebrew University of Israel and Tel-Aviv University (in Hebrew).

EPA, (2000) Constructed wetlands treatment of municipal wastewater. EPA/625/R/99/010.

FAO ed., "Compendium of food additive specifications. Addendum 5". (FAO Food and Nutrition Paper-52 add.5) Joint FAO/WHO Expert Committee on Food Additives 49th session, Rome, 1997.

FAO/WHO. 1997. "Compendium of food additive specifications. Addendum 5". (FAO Food and Nutrition Paper-52 add. 5) Joint FAO/WHO Expert Committee on Food Additives 49th session, Rome.

Feng, C., Sugiura, N., Shimada, S. (2003) Development of a high performance electrochemical wastewater treatment system. *J. Hazardous Materials*, (B103) pp: 65- 78.

Feng, Q.L., Wu, J., Chen, G.O., Cui, F.Z., Kim, T.N., Kim, J.O. A mechanistic study of the antibacterial effect of silver ions on Escherichia coli and Staphylococcus aureus. Journal of Biomedical Materials Research 52(4), (2000) 662-668.

Fernandez, E.J., Garcia-Barrasa, J., Laguna , A., Lopez-de-Luzuriaga, J.M., Monge, M. and Torres, C. The preparation of highly active antimicrobial silver nanoparticles by an organometallic approach. Nanotechnology 19(18), (2008) 177-183.

Flemming, H.C. Biofouling in water systems - cases, causes and countermeasures. Applied Microbiology and Biotechnology 59(6), (2002) 629-640.

Ge, J., Qu, J., Lei, P., Liu, H. (2004) New bipolar electrocoagulation-electroflotation process for the treatment of laundry wastewater. Separation and Purification Technology, (36) pp: 33-39.

Gentry, H., Cope, S., *Nurs Stand* 19 (2005) 51.

Glasstone S., An introduction to electrochemistry, D. Van Nostrand Company, Inc. (1942) pp. 567.

Grant, G.T., Morris, E.R., Rees, D.A., Smith, P.J.C., and Thom, D. Biological interactions between polysaccharides and divalent cations: the egg-box model. Febs. Letters. 32, (1973) 195-197

Gregory, J. (1998) Turbidity and beyond. *Filtr. Separat.*, 35: 63.

Gregory,J., Particles in Water: Properties and Processes, Taylor & Francis, Boca Raton, FL, 2006, p. 93.

Guo W. S., Vigneswaran S., Ngo H. H., Effect of flocculation and/or adsorption as pretreatment on the critical flux of crossflow microfiltration, Desalination, 172 (2005) 53-62.

Haberl R., History of the use of constructed wetland. In Dias, V. and J. Vymazal (Eds.). The 1st international seminar on the use of aquatic macrophytes for wastewater treatment in constructed wetland, Portugal (2003) pp. 12.1-12.1

Halperin, R. (1999) Irrigation with effluents: Standards. Israel, Ministry of Health.

Hamouda, T., Baker, J., *J. Appl. Microbiol.* 89 (2000) 397.

Han B., Runnells T., Zimbron J., Wickramasinghe R., Arsenic removal from drinking water by flocculation and microfiltration, Desalination, 145 (2002) 293-298.

Handa, N. Examination on the applicability of the phenol sulfuric acid method to the determination of dissolved carbohydrate in seawater. J.Oceanographical Society of Japan. 22(3), (1966) 79-86

Harif T. and Adin A., Characteristics of aggregates formed by electroflocculation of a colloidal suspension, Water Research, 41 (2007) 2951-2961.

Harif T., Hai M., Adin A., Electroflocculation as potential pretreatment in colloid ultrafiltration, Water Supply, 6-1 (2006) 69-78.

Harrison, J.J., Ceri, H., Stermick, C.A. and Turner, R.J. Biofilm susceptibility to metal toxicity. Environmental Microbiology 6(12), (2004) 1220-1227.

Hatchett, .D.W., White, H.S., *J. Phys. Chem.* 100 (1996) 9854.

Hayashi, T. and Mukamel, S. Two-dimensional vibrational lineshapes of amide III, II, I and A bands in a helical peptide. Journal of Molecular Liquids, 141, (2008)149-154

Heidmann I., Calmano W., Removal of Cr(VI) from model wastewaters by electrocoagulation with Fe electrodes, Separation and Purification Technology 61 (2008) 15-21.

Heidmann I., Calmano W., Removal of Zn(II), Cu(II), Ni(II), Ag(I) and Cr(VI) present in aqueous solutions by aluminum electrocoagulation, J. Hazardous Materials, 152 (2008b) 934-941.

Heidmann, I., Calmano, W., Removal of Cr(VI) from Model Wastewaters by Electrocoagulation with Fe Electrodes. *Separation and Purification Technology*, 61 (2008) 15-21

Hentschel, M.L. and Page, N.W. (2003) Selection of descriptors for particle shape characterization. *Part. Part. Syst. Charact.*, 20: 25.

Hermia J., Costant pressure blocking filtration laws – Application to power-law non newtonian fluid, Transaction of the Institute of Chemical Engineers, 60 (1982) 183.

Hoffman, L.R., D'Argenio, D.A., MacCross, M.J., Zhang, Z., Jones, R.A. and Miller, S.I. Aminoglycoside antibiotics induce bacterial biofilm formation, Nature 436(3912), (2005) 1171-1175.

Holt, K.B., Bard, A.L., *Biochemistry* 44 (2005) 13214

http://wwwdep.state.pa.us/dep/deputate/watermgt/WSM/WSMTAO/InnovTech-Forum/InnovTechForum-IIB-Lindell.pdf

Hu C. Y., Lo S. L., Li C. M., Kuan W. H., Treating chemical mechanical polishing (CMP) wastewater by electro-coagulation-flotation process with surfactant, Journal of Hazardous Materials, A120 (2005) 15-20.

Irdemez S., Demiricioglu N., Yildiz Y. S., The effcts of pH on phosphate removal from wastewater by electroflocculation with iron plate electrodes, Journal of Hazardous Materials, 137 (2006) 1231-1235.

Irdenez S., Demircioglu N., Yildiz Y. S., Bingul Z., The effects of current density and phosphate concentration on phosphate removal from wastewater by electrocoagulation using aluminum and iron plate electrodes, Separation and Purification Technology, 52 (2006) 218-223.

Ives, K.J. (1982) *Fundamentals of filtration*. In Proceedings of the 21st European Federation of Chemical Engineering Event Symposium on Water Filtration, Antwerp, Belgium.

Jiang J. Q., Graham N., Andre C., Kelsall G. H., Brandon N., Laboratory study of electro-coagulation-flotation for water treatment, Water Research, 36 (2002) 4064-4078.

Jiang, M., Eisenberg, A., Liu, G.J., and Zhang, X. 2006. Macromolecular Selfassembly, 1st edn.; Science Publication: Beijing, China.

Judd S. J., Hillis P., Optimization of combined coagulation and microfiltration for water treatment, Water Research, 35 (2001) 2895-2904.

Kadlec, R.H. and Wallace, S.D. (2008). Treatment wetland, Second edition. CRC Press. INC, U.S.A.

Kadlec, R.H., Wallace, S.D., Treatment wetland, Second edition. CRC Press. (2008) INC, U.S.A.

Kaminski, I., Vescan, N. and Adin, A. (1997) Particle size distribution and wastewater filters performance, *Water Sci. Technol*., 36: 217.

Kassaee, M.Z., Akhavan, , Sheikh, N., Beteshobabrud, R., *Radiat. Phys. Chem.* 77 (2008) 1074.

Katsoufidou, K., Yiantsions, S.G., Karabelas, A.J., A study of ultrafiltration membrane fouling by humic acids and flux recovery by backwashing: experiments and modeling. *J. Membr. Sci.*, 266 (2005) 40-50.

Kazy, S K., Sar, P., Sen, A. K, Singh, S. P. and D'Souza, S.F. Extracellular polysaccharides of a copper-sensitive and a copper-resistant Psuedomonas aeruginosa strains: synthesis, chemical nature and copper binding. World J Microbiol Biotechnol. 18, (2002) 583-588

Khotimchenko, Y. S., Kovalev, V.V., Savchenko, O.V., Ziganshina, O.A., Physical-Chemical properties, physiological activity, and usage of alginates, the polysaccharides of brown algae. *Russian J. of Marine Biology*, 27 (2001) S53-S64.

Kierek-Pearson, K. and Karatan, E. (2005) Biofilm development in bacteria. Advances in Applied Microbiology 57, 79-111.

Kim, J., Cho, M., Oh, B., Choi, S. and Yoon, J. Control of bacterial growth in water using synthesized inorganic disinfectant. Chemosphere 55(5), (2004) 775-780.

Kim, J.S., Kuk, E., Yu, K.N., Kim, J.H., Park, S.H., Lee, H.J., Kim, S.H., *Nanomed-Nanothecnol*. 3 (2007) 95.

Konieczny K., Bodzek M., Rajca M., A coagulation-MF system for water treatment using ceramic membranes, Desalination, 198 (2006) 92-101.

Kramer, A., Guggenbichler, P., Heldt, P., Jünger, M., Ladwig, A., Thierbach, H., Weber, U. and Daeschlein, G. Hygienic relevance and risk assessment of antimicrobial-impregnated textiles. Current Problems in Dermatology 33, (2006) 78-109.

Kuberkar V. T., Davis R. H., Modeling of fouling reduction by secondary membranes, Journal of Membrane Science, 168 (2000) 243-258.

Lahoussine-Turcaud V., Wiesner M. R., Bottero J.-Y., Fouling in tangential-flow ultrafiltration: The effect of colloid size and coagulation pretreatment, Journal of Membrane Science, 52 (1990) 173-190.

Lawrence, J.R., Swerhone, G.G.W., Leppard, D.G., Araki, T., Zhang, X., West, M.M. and Hitchcock, A.P. Scanning transmission x-ray, laser scanning, and transmission electron microscopy mapping of the exopolymeric matrix of microbial biofilms. Applied and Environmental Microbiology 69(9), (2003) 5543-5554.

Leal, D., Matsuhiro, B., Rossi, M. and Caruso, F. FT-IR spectra of alginic acid block fractions in three species of brown seaweeds. Carbohydrate Research. 343, (2008) 308-316

Lee, S., Elimelech, M., Relating organic fouling to reverse osmosis membranes to intermolecular adhesion forces. *Environ. Sci. Technol*., 40 (2006) 980-987.

Lee, S.Y., Kim, H.J., Patel, R., Kim, S.J., Kim, J.H. and Min, B.R. (2007) Silver nanoparticles immobilized on thin film composite polyamide membrane: characterization, nanofiltration, antifouling properties. Polymers for Advanced Technologies 18(7), 562-568.

Leone, S., Molinaro, A., Alfieri, F., Cafaro, V., Lanzetta, R., Donato, A. D. and Parrilli, M. The biofilm matrix of Pseudomonas sp. OX1 grown on phenol is mainly constituted by alginate oligosaccharides. Carbohydrate Research. 341, (2006) 2456-2461

Li, P., Li, J., Wu, C.Z., Wu, Q.S., Li, J., *Nanotechnology* 16 (2005) 1912.

Lin, Y.M., Wang, L., Chi, Z.M. and Liu, X.Y. 2008. Bacterial alginate role in aerobic granular bio-particles formation and settleability improvement. Separation Science and Technology. 43(7), 1642-1652

Linares-Hernandez I., Barrera-Diaz C., Roa-Morales G., Bilyeu B., Urena-Nunez F., Influence of the anodic material on electrocoagulation performance, Chemical Engineering Journal,148 (2009) 97-105.

Lindell C., Decentralized wastewater treatment.

Lok, C.N., Ho, C.M., Chen, R., He, Q.Y., Yu, W.Y., Sun, H., Tam, P.K.H., Chiu, J.F., Che, C.M., *J. Biol Inorg Chem* 12 (2007) 527.

Lok, C.N., Ho, C.M., Chen, R., He, Q.Y., Yu, W.Y., Sun, H.Z., Tam, P.K.H., Chiu, J.F. and Che, C.M. Proteomic analysis of the mode of antibacterial action of silver nanoparticles. Proteome Research 5(4), (2006) 916-924.

Maleriat, J.P., Jaouen, P., Rossignol, N., Schlumpf, J.P., Quemeneur, F., Influence of alginates adsorption on properties of ultrafiltration and microfiltration organic membranes. *Rev. Sci. Eau* 13(3) (2000) 269-287.

Matteson M. J., Dobson R. L., Glenn R. W., Kukunoor N. S., Waits III W. H., Clayfield E. J., Electrocoagulation and separation of aqueous suspensions of ultra fine particles, *Colloids and Surfaces* A*: Physicochemical and Engineering Aspects*, 104 (1995) 101-109.

Mavrov V., Stamenov S., Todorova E., Chmiel H., Erwe T., New hybrid electrocoagulation membrane process for removing selenium from industrial wastewater, Desalination, 201 (2006) 290-296.

Mchugh, D.J., A guide to the seaweed industry. FAO Fisheries Technical Paper 441. FAO of the United Nations, Rome, 2003.

Melvik, J.E. and Dornish, M. 2004. Alginate as a carrier for cell immobilization. In: fundamentals of cell immobilization biotechnology. By: Nedovic V. and Willaert R. 2004, Kluwer Academic Publishers

Mietton M., Ben Aim R., Improvement of crossflow microfiltration performances with flocculation, Journal of Membrane Science, 68 (1992) 241-248.

Minsky, A., Shimoni, E. and Frenkiel-Krispin, D. Stress, order and survival. Nature Reviews Molecular Cell Biology 3(1), (2002) 50-60.

Mintz, D.M. (1966) Modern Theory of Filtration, International Water Supply Congress, Barcelona, International Water Supply Association, London.

Mollah M. Y. A., Schennach R., Parga J. R., Cocke D. L., Electrocoagulation (EC)-science and applications, Journal of Hazardous Materials B84 (2001) 29-41.

Mollah M., Morkovsky, Y. A., P., Gomes J. A. G., Kesmez M., Parga J., Cocke D. L., Fundamentals, present and future perspectives of electrocoagulation, *Journal of Hazardous Materials*, B114 (2004) 199-210.

Momba, M.N.B., Kfir, R., Venter, S.N. and Cloete T.E. An overview of biofilm formation in distribution systems and its impact on the deterioration of water quality. Water SA 26(1), (2000) 59-66.

Morgan B., and Lahav O., The effect of pH on the kinetics of spontaneous Fe (II) oxidation by O_2 in aqueous solution – basic principles and simple heuristic description, *Chemosphere*, 11 (2007) 2080-2084.

Morones, J.R., Elechiguerra, J.L., Camacho, A., Holt, K., Kouri, J., Ramirez, J.T. and Yacaman, M.J. The bactericidal effect of silver nanoparticles. Nanotechnology 16(10), (2005) 2346-2353.

Narkis, N., & Rebhun, M. (1997). Flocculation in presence of organic macromolecules of natural water and secondary effluents. Wat. Sci. Tech., (36: 4) pp: 85-91.

Nathaniel G., Barona B., Jun Cha B., Jung B., Negatively charged poly (vinylidene fluoride) microfiltration membranes by sulfonation, Journal of Membrane Science, 290 (2007) 46-54.

Nel, A., Xia, T., Madler, L. and Lin, N. Toxic potential of materials at the nanolevel. Science 311(5761), (2006) 622-627.

Neu, T., Swerhone, G.D. and Lawrence, J.R. Assessment of lectin-binding analysis for in situ detection of glycoconjugates in biofilm systems. Microbiology 147(2), (2001) 299-313.

Neu, T.M. and Poralla, K. An amphiphilic polysaccharide from an adhesive Rhodococcus strain. FEMS Microbiol Lett. 49, (1988) 389-392

O'Toole, G.A. and Kolter, R. Flagellar and twitching motility are necessary for Pseudomonas aeruginosa biofilm development. Molecular Microbiology 30, (1998B) 295-304.

Ofir E., Oren Y., Adin A., Electroflocculation: the effect of zeta-potential on particle size, *Desalination*, 204 (2007) 33-38.

O'Toole G A, Kotler R. Initiation of biofilm formation in Pseudomonas fluorescens WCS365 proceeds via multiple, convergent signalling pathways: a genetic analysis. Mol. Microbiol 28(3) (1998A) 449-61.

Oust, A., Moretro, T., Naterstad, K., Sockalingum, G., Adt, I., Manfait, M., Kohler, A. Analysis of co-variation patterns in gene expression data and FT-IR spectra. J. Microbiol. Methods. 65, (2006) 573-584

Pal, S., Tak, Y.K., Song, J.M., *Appl. Environ. Microbiol*. 73 (2007) 1712.

Panacek, A., Prucek, R., Kolar, M., Vecerova, R., Kvıtek, L., Pizurova, R.N., Nevecna, T., Zboril, V.K., *J. Phys. Chem*. B. 110 (2005) 16248.

Parashar, U.K., Saxena, P.S., Srivastava, A., *Digest. J. of Nanomater. Bioruct.* 3 (2008) 81.

Park P. K., Lee C.-H., Choi S.-J., Choo K.-H., Kim S.-H., Yoon C.-H., Effect of the removal of DOMs on the performance of a coagulation-UF membrane system for drinking water production, Desalination, 145 (2002) 237-245.

Pedersen, S.S., Espersen, F., Hoiby, N., and Shand G.H. Purification, Characterization, and immunological cross-reactivity of alginates produced by mucoid Pseudomonas aeruginosa from patients with cystic fibrosis. J. Clinical Microbiology. (1989) 691-699.

Pereira, L.,A. Sousa, H. Coelho, A. M. Amado, P. J. A. Ribeiro-Claro, Use of FTIR, FT-Raman and 13C NMR spectroscopy for identification of some seaweed phycocolloids. *Biomolecular Engineering*, 20 (2003) 223-227.

Picard T., Cathalifaud-Feuillade G., Mazet M. and Colette V., Cathodic dissolution in the electrocoagulation process using aluminum electrodes. *J. Environmental Monitoring*, 2 (2000) 77-80.

Picard T., Cathalifaud-Feuillade G., Mazet M., Vandensteendam C., Cathodic dissolution in the electrocoagulation process using aluminum electrodes, Journal of Environmental Monitoring, 2 (2000) 77-80.

Pikkarainer A. T., Judd S. J., Jokela J., Gilberg L., Pre-coagulation for microfiltration of an upland surface water, Water Research, 38 (2004) 455-465.

Poon, V.K., Burd, A., *Burns* 30 (2004) 140.

Pouet M.-F., Grasmick A., Electroflocculation and flotation: Applications in crossflow microfiltration, Filtration and Separation, 3 (1994) 269-272.

Rabanski, G. and King, F.D. (2002) Beyond turbidity – A quantifiable analysis of solids in drinking water. ICHW.

Rehm, B.H.A. The Azotobacter vinelandii gene algJ encodes an outer membrane protein presumably involved in export of alginate. Microbiology. 142, (1996) 873–880

Remminghorst, U. and Rehm, B.H.A. Bacterial alginates: from biosynthesis to applications. Biotechnol Lett. 28, (2006) 1701-1712

Rickard, A.H., Leach, S.A., Buswell, C.M., High, N.J. and Handley, P.S. Coaggregation between aquatic bacteria is mediated by specific growth phase dependent lectin saccharide interactions. Appl Environ Microbiol. 66, (2000) 431-434

Roe, D., Karandikar, B., Bonn-Savage, N., Gibbins, B. and Roullet, J.B. Antimicrobial surface functionalization of plastic catheters by silver nanoparticles. J.Antimicrobial Chemotherapy 61(4), (2008) 869-876.

Sadoff, H.L. Encystment and germination in Azotobacter vindelandii. Bacteriological Reviews. 39(4), (1975) 516-539

Sadovskaya, I., Vinogradov, E., Flahaut, S., Kogan, G., and Jabbouri, S. Extracellular carbohydrate-containing polymers of a model biofilm-producing strain, Staphylococcus epidermidis RP62A. Infect. Immun. 73,(2005) 3007-3017.

Salomonsen, T., Jensen, H.M., Stenbæk, D., Engelsen, S. B., Chemometric prediction of alginate monomer composition. A comparative spectroscopic study using IR, Raman, NIR and NMR. *Carbohydrate Polymers*. 2008, CARBPOL-D-07-00446

Sayiner G., Kandemirili F., Dimoglo A., Evaluation of boron removal by electrocoagulation using iron and aluminum electrodes, Desalination, 230 (2008) 205-212.

Sharp M. M., Escobar I. C., Effects of dynamic or secondary-layer coagulation on ultrafiltration, Desalination, 186 (2006) 239-249.

Shen F., Chen X., Gao P., Chen G., Electrochemical removal of fluoride ions from industrial wastewater, Chemical Engineering Science, 58 (2003) 987-993.

Shon H. K., Vigneswaran S., Ngo H. H., Ben Aim R., In semi-flocculation effective as pretreatment to ultrafiltration in wastewater treatment, Water Research, 39 (2005) 147-153.

Shrivastava, S., Bera, T., Roy, A., Singh, G., Ramachandrarao, P., Dash, D., *Nanotechnology* 18 (2007) 1.

Silver, S. Bacterial silver resistance: molecular biology and uses and misuses of silver compounds. FEMS Microbiology Reviews 27(2-3), (2003) 341-353.

Silverstein, R.M.; Clayton Bassier, G.; Morrill, T.C. 1991. Spectrometric Identification of Organic Compounds. Willey: New York.

Silvestry-Rodriguez, N., Bright, K.R., Slack, D.C., Uhlmann, D.R. and Gerba, C.P. Silver as a residual disinfectant to prevent biofilm formation in water distribution systems Applied and Environmental Microbiology 74(5), (2008) 1639-1641.

Silvestry-Rodriguez, N., Sicairos-Ruelas, E.E., Gerba, C.P, Bright, K.R., *Rev Environ Contam*. 191 (2007) 23.

Skafel, M.G. and Krishnappan, B.G. (1995) Deposition of tine-grained sediment under wave action, in Proceedings of the Canadian Coastal Conference, Dartrnouth, Nova Scotia, Canada.

Smalley R.E., Our energy challenge. http://smalley.rice.edu/ Presentations/ Columbia 09232003.ppt

Sobeck, D.C. and Higgins, M.J. Examination of three theories for mechanisms of cation-induced biofloculation. Water Research. 36, (2002) 527-531

Soffer Y., Ben Aim R., Adin A., Membrane for water reuse: effect of pre-coagulation on fouling and selectivity, Water Science and Technology, 42 (2000) 367-372.

Sommariva, C., Converti, A., Borghi, M.D., Increase in phosphate removal from wastewater by alternating aerobic and anaerobic conditions, Desalination (1996) 255–260.

Sondi, I, .D.V. Goia, E. Matijevic, *J. Colloid Interf Sci* 260 (2003)75.

Sondi, I. and Salopek-Sondi, B. Silver nanoparticles as antimicrobial agent: a case study on E. coli as a model for Gram-negative bacteria. Journal of Colloid and Interface Science 275(1), (2004) 177-182.

Song W., Ravindran V., Koel B. E., Pirbazari M., Nanofiltration of natural organic matter with H_2O_2/UV pretreatment: fouling mitigation and membrane surface characterization, Journal of Membrane Science, 241 (2004) 143-160.

Steinberger R.E. and Holden P.A. Extracellular DNA in Single- and Multiple-Species Unsaturated Biofilms. Applied and Environmental Microbiology 71(9), (2005) 5404–5410.

Stoimenov, P.K, Klinger, R.L., Marchin, G.L., Klabunde, K.J., *Langmuir* 18 (2002) 6679.

Stumm W., Morgan J. J., Aquatic Chemistry, An introduction emphasizing chemical equilibria in natural waters, John Wiley & sons, Inc., USA (1970).

Subramanyan V., Lakshmi J., Jayaraj J., Sozhan G., Remediation of phosphate-contaminated water by electroflocculation with aluminum, aluminum alloy and mild steel anodes, Journal of Hazardous Materials, 164 (2009) 1480-1486.

Sutherland, I.W. Biofilm exopolysaccharides: a strong and sticky framework. Microbiology. 147, (2001) 3-9

Tay, J. H., Liu, Q. S., Liu, Y., Microscopic observation of aerobic granulation in sequential aerobic sludge blanket reactor. *J Appl. Microbiol.*, 91 (2001) 168-175.

Thomas, D. and Moore, P. (2004) Water treatment plant particle characterization using digital imaging technology. Canadian Water Works Association Annual Conference.

Totosaus, A., Montejano, J.G., Salazar, J. A. and Guerrero, I. A review of physical and chemical protein-gel induction. International Journal of Food Science and Technology. 37, (2002) 589-601

Tysmans, D., Claeys, P., Deriemaeker, L., Maes, D., Finsy, R. and Van Molle, M. (2007) Size and shape analysis of sedimentary grains by automated dynamic image analysis. *Part. Syst. Charact.*, 23: 381.

Ugurlu, A., Salman, B., Phosphorus removal by fly ash, Environ. Int. 24 (1998) 911–918.

United Nations Environment Program, Challenges to International Waters; Regional Assessments in a Global Perspective, (2006) 120 pp.

USEPA (2000) Constructed wetlands treatment of municipal wastewater. EPA-625-R-99-010

Vasudevan S., Lakshmi J., Jayaraj J., Ganapathy S., Remediation of phosphate-contaminated water by electrocoagulation with aluminum, aluminum alloy and mild steel anodes, Journal of Hazardous Materials, 64 (2009) 1480-1486.

Villain-Simonnet, A., Milas, M. and Rinaudo, M. A new bacterial polysaccharide (YAS34). I. Characterization of the conformations and conformational transition. Int J Biol Macromol. 27, (2000) 65-75

Vymazal, J. Removal mechanisms in constructed wetland. In Dias, V. and J. Vymazal (Eds). The 1st international seminar on the use of aquatic macrophytes for wastewater treatment in constructed wetland, (2003).Portugal. pp: 219-263.

Waller, L.N., Fox, N., Fox, K.F., Fox, A. and Price, R.L. Ruthenium red staining for ultrastructural visualization of a glycoprotein layer surrounding the spore of Bacillus anthracis and Bacillus subtitles. J.Microbiological methods 58, (2004) 23-30

Wang, L. and Lin, Y.M. Spore detection in aerobic granules by different dipicolinic acid. Bioresour. Technol. 98, (2007) 3164-3167

Wang, Z.W., Li, Y., Zhou, J.Q. and Liu, Y. 2006. The influence of short-term starvation on aerobic granules. Process Biochemistry. 41, 2373-2378

Weng Y.-H., Li K.-C., Chang-Hsieh L. H., Huang C. P., Removal of humic substances (Hs) from water by electro-microfiltration (EMF), Water Research, 40 (2006) 1783-1794.

WHO World Health Organization (2004) Silver in drinking water, WHO /SDE/WSH /03.04/14

Wong, T. Y, Preston, L. A., Schiller, N. L., Alginate lyase: Review of major sources and enzyme characteristics, structure-function analysis, biological roles, and applications. *Annu. Rev. Microbiol.*, 54 (2000) 289-340.

Xu, X.H.N., Brownlow, W.J., Kyriacou, S.V. , Wan, Q., Viola, J.J., *Biochemistry* 43 (2004) 10400.

Y. Israel. MSc thesis, The Hebrew University of Israel and Tel-Aviv University (in Hebrew).

Yamanaka, M., Hara, K., Kudo, J., *Appl. Environ. Microbiol*. 71 (2005) 7589.

Yao, K. M., Habibian, M. T. and O`Melia, C.R. (1971) Water and Wastewater Filtration: Concepts and Applications. *J. Environ. Sci. Technol*., 5: 1105.

Ye, Y., Le Clech, P., Chen, V., Fance, A.G., Evolution of fouling during cross-flow filtration of model EPS solution. *J. Membr. Sci*., 264 (2005) 190-199.

Ye, Y., Le Clech, P., Chen, V., Fance, A.G., Jefferson, B., Fouling mechanisms of alginate solutions as model extracellular polymeric substances. *Desalination*, 175 (2005) 7-20.

Ye, Y., Le Clech, P., Chen, V., Fance, A.G., Modeling long-term subcritical filtration of model EPS solutions, *Desalination*, 191 (2006) 318-327.

Yoon, K.Y., Byeon, J.H., Park, J.H., Hwang. J., *Sc. of Total Environ.* 373 (2007) 572.

Zhang, L.L., Feng, S.S., Zhu, N. W., Chen, J.M. Role of extracellular protein in the formation and stability of aerobic granules. Enzyme and Microbial Technology. 41, (2007) 551-557

Zhao G., and Stevens, S.E., *BioMetals*. 11 (1998) 27.

Zhu B., Clifford D., Chellam S., Comparison of electrocoagulation and chemical coagulation pretreatment for enhanced virus removal using microfiltration membranes, Water research, 39 (2005b) 3098-3108

Zhu B., Clifford D., Chellam S., Virus removal by iron coagulation-microfiltration, Water research, 39 (2005a) 5153-5161

Zodrow, K., Brunet, L., Mahendra, S., Li, D., Zhang, A., Li, Q. and Alvarez, P.J.J. Polysulfone ultrafiltration membranes impregnated with silver nanoparticles show improved biofouling resistance and virus removal. Water Research 43(3), (2009) 715-723

HUJI Publications originated in SWITCH

Harif, T., and Adin, A. Characteristics of aggregates formed by electroflocculation of a colloidal suspension. Water Research, 41(13):2951-61 (2007).

Mamane, H., Kohn, C. and Adin, A. Characterizing shape of effluent particles by image analysis. Separation Science and Technology, 43 (7):1737-1753 (2008).

Sun, L., Miznikov, E., Wang, L., and Adin, A. Nickel removal from wastewater by electroflocculation-filtration hybridization. Desalination, 249 (2):832-836 (2009).

Dror-Ehre, A., Mamane, H., Belenkov, T.,. Markovich, G, and Adin, A. Silver nanoparticle-*E. coli* colloidal interaction in water and effect on *E. coli* survival. Journal of Colloid and Interface Science, 339 (2): 275-550 (2009).

Lin, Y., Zhang, H. and Adin, A. Characterization of bacterial alginate extracted from biofilm matrix. Desalination and Water Treatment, 8:250-256 (2009).

Ben-Sasson M., Calmano W., Adin A., Iron oxidation processes in electroflocculation (electrocoagulation) cell, Journal of Hazardous Materials, 171, 704-709 (2009).

A. Adin, A. Barash, K. Ozer, D. Milstein And A. Gasith, Electroflocculation – Constructed Wetland Hybrid For Improved Phosphate Removal In Effluent ReUse. International Workshop, Reuse09 In Brisbane, Australia, 25 September 2009

Ben-Sasson M., Adin A., Fouling mechanisms and energy appraisal in microfiltration pretreated by aluminum based electroflocculation, Journal of Membrane Science, 352(1), 86-94 (2010)

Dror-Ehre, A., Adin A., Markovich, G. Mamane H. Control of biofilm formation in water using molecularly capped silver nanoparticles. Water Research, 44(8), 2601-9 (2010).

Lin Y.M., de Kreuk M., van Loosdrecht M.C.M. and Adin A. Characterization of alginate-like exopolysaccharides isolated from aerobic granular sludge in pilot plant. Water Research, 44(11), 3355-64 (2010).

Ben-Sasson M., Adin A., Fouling mitigation by iron-based electroflocculation in microfiltration: mechanisms and energy minimization. Water Research, 44(13), 3973-3981 (2010).